Understanding and Targeting Coronaviruses: exploring advanced cell culture models and host-directed antiviral strategies

Thaler, M.

UNDERSTANDING AND TARGETING CORONAVIRUSES

Exploring advanced cell culture models and host-directed antiviral strategies

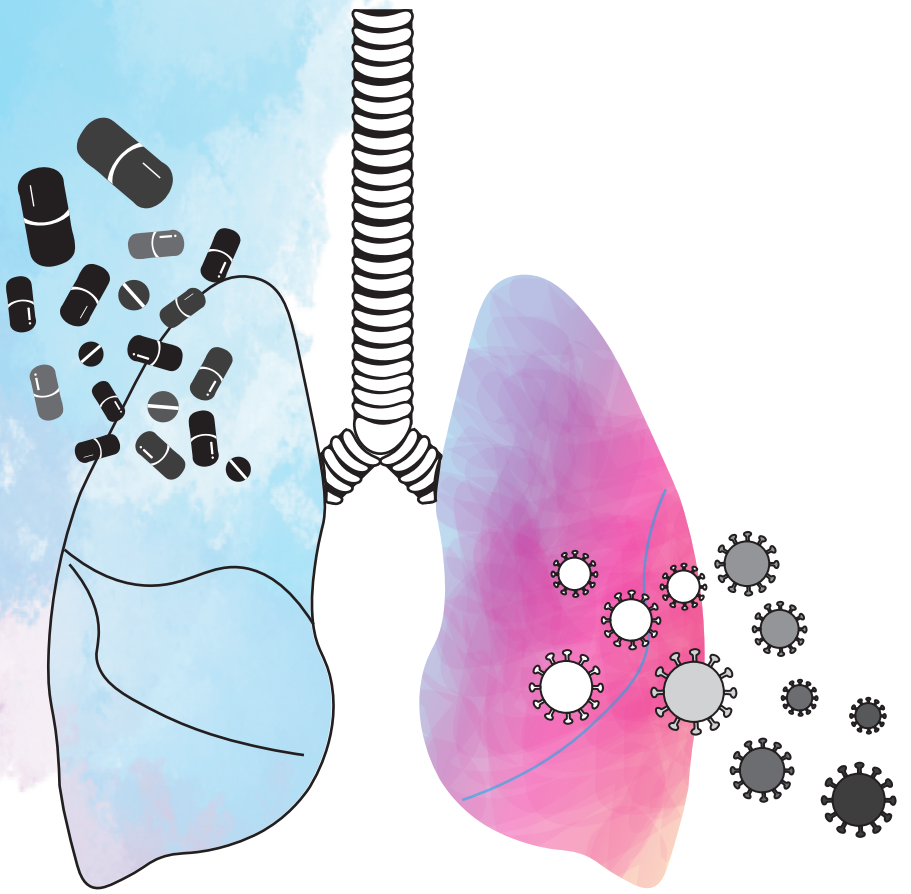

Melissa Thaler

Understanding and targeting coronaviruses

Exploring advanced cell culture models and host-directed antiviral strategies

Melissa Thaler

PhD Thesis Melissa Thaler

The research described in this thesis was performed at Leiden University Medical Center, Department of Medical Microbiology (now LUCID), Leiden, The Netherlands

Funding The work presented in this thesis was supported in part by a COVID-19 MKMD grant from the Netherlands Organization for Health Research and Development (ZonMw), the Dutch Society for the Replacement of Animal Testing (Stichting Proefdiervrij) (grant #114025007), the Leiden University Fund (LUF), the Bontius Foundation, donations from the crowdfunding initiative “wake up to corona”, the European Union’s Horizon 2020 research and Innovation program under grant No 10100362 (the SCORE project), the RSEOH-CAG Rapid Response Research Initiative and RSEOH-CAG 2021 Extension Grant, the Deutsche Forschungsgemeinschaft (DFG) (Ta 275/7-1 and Ta 275/8-1); the coordination for the Improvement of Higher Educational Personnel (CAPES) (process no. 88881.171440/2018-01), Ministry of Education Brazil.

Layout Melissa Thaler
Cover Melissa Thaler
Print Gildeprint, www.gildeprint.nl

Understanding and targeting coronaviruses

Exploring advanced cell culture models and host-directed antiviral strategies

Proefschrift

ter verkrijging van

de graad van doctor aan de Universiteit Leiden,

op gezag van rector magnificus prof. dr. ir. H. Bijl,

volgens besluit van het college voor promoties

te verdedigen op dinsdag 2 juli 2024

klokke 13.45 uur

door

Melissa Thaler

Geboren te Klagenfurt am Wörthersee, Oostenrijk

in 1994

Promotor: Prof. dr. E. J. Snijder

Co-promotor: Dr. M.J. van Hemert

Leden van de promotiecommissie:

Prof. dr. P.S. Hiemstra
Dr. J.J.C. de Vries
Prof. dr. R. van Rij (Radboud Universiteit Nijmegen, Nederland)
Prof. dr. L. Delang (Katholieke Universiteit Leuven, België)

“Somewhere something incredible is waiting to be known”.

(Carl Sagan)

Table of Contents

Chapter 1

General Introduction
and
Outline of the Thesis

Introduction

Viruses are biological entities that can infect host organisms from all domains of life, from prokaryotic microorganisms, such as bacteria and archaea, to plants, animals, and humans. Their replication occurs intracellularly and is dependent on the infrastructure and metabolism of the host cell. Viruses have been evolving alongside (in other animal hosts) or with humans since the dawn of humanity. As ancient as viruses are, they are subject to rapid evolution, especially when we look at viruses with an RNA genome, which have high mutation rates and great genetic diversity (1). These viruses continuously adapt to changing environments through changes in their tropism, transmission, replication, pathogenicity, or immune evasion. Escape from neutralizing antibodies or antiviral drug treatment is also driven by their potential for rapid evolution, resulting in antibody or drug resistance of an adapted virus population. To combat viruses we need vaccine and antiviral drug strategies, and to develop such it is crucial to study and understand viruses in detail. Coronaviruses in particular, besides other respiratory virus groups, are endemic in the human population as common cold viruses, which are low pathogenic viruses that usually cause minor symptoms in the upper respiratory tract of healthy individuals. However, coronaviruses, like many other virus groups, also have a great zoonotic potential (2), which has led to three outbreaks in humans since the beginning of the 21st century. In the past two decades, severe acute respiratory syndrome coronavirus (SARS-CoV), Middle East respiratory syndrome coronavirus (MERS-CoV), and most recently SARS-CoV-2, the causative agent of COVID-19, have crossed the species barrier. The zoonotic potential of coronaviruses, as well as the continuously evolving variants of SARS-CoV-2, underscore the risk of new pandemics. Enhancing our understanding of how a virus can cause a pandemic and studying antiviral approaches against a broad-spectrum of viruses can help to prepare us for future viral threats.

In this thesis, I will describe our efforts to add to this understanding by studying coronavirus infection and host responses to infection using an advanced human cell culture model. Moreover, I demonstrate how coronavirus replication in cell culture models can be inhibited by targeting the host cell with small-molecule compounds. Given the SARS-CoV-2 outbreak in late 2019, this pandemic virus was the main focus of my research project.

Coronaviruses

Coronaviruses (CoVs) belong to the subfamily *Orthocoronavirinae* (family *Coronaviridae)* of the order of *Nidovirales*, and are enveloped, positive-sense single-stranded RNA viruses that

infect mammalian and avian species (3, 4). *Orthocoronavirinae* are classified into four genera: *Alphacoronavirus, Betacoronavirus, Gammacoronavirus,* and *Deltacoronavirus (4)*. *Gamma-* and *deltacoronaviruses* mainly infect birds (5). The *alpha-* and *betacoronavirus* genera comprise, besides others, the seven coronaviruses that infect humans and are known to date (**Figure 1**). The human alphacoronaviruses 229E and NL63 as well as the human betacoronaviruses HKU1 and OC43 circulate in the human population as common cold viruses, and in healthy individuals they only cause mild upper respiratory tract symptoms (6). However, the other three coronaviruses that can infect humans can cause severe clinical symptoms: SARS-CoV, MERS-CoV, and SARS-CoV-2; all three belong to the *Betacoronavirus* genus. Due to their zoonotic emergence in the past two decades, they have gained global public health attention. The first epidemic outbreak of a highly pathogenic coronavirus in the 21st century started in 2002 and was caused by SARS-CoV (7), which spread mostly in Southeast Asia, where it could be contained within a year. MERS-CoV, which was first identified in 2012 in Saudi Arabia (8), is still causing small outbreaks in the Middle East. Both viruses likely originated in bats, but transmission to humans is thought to have occurred through intermediate hosts, like civet cats for SARS-CoV and dromedary camels for MERS-CoV (9). Recent studies in the human population have shown that there is also transmission of MERS-CoV from dromedary camels to humans in Africa (10). Furthermore, numerous coronaviruses are now known to circulate in a range of bat species, highlighting the risk of new zoonotic outbreaks (9, 11). Most recently, at the end of 2019, SARS-CoV-2 caught the world off guard and caused a pandemic of unprecedented impact on health care systems, societies, and economies worldwide (12). In contrast to SARS-CoV and MERS-CoV, this new virus spread quickly across the world. SARS-CoV-2 was first reported in Wuhan, China, and is suspected to be of zoonotic origin, as closely related viruses were found in bats and pangolins (13, 14). SARS-CoV-2 is closely related to SARS-CoV, as they share 79.6% nucleotide identity in their genomic sequences (15) and belong to the same phylogenetic subgenus classification, *Sarbecovirus.*

Although the emergence of SARS-CoV and MERS-CoV had put coronaviruses on the map as potentially lethal agents for humans, and coronavirus research had spiked since then, still the world was not prepared for SARS-CoV-2, as there were no approved vaccines or antiviral drugs available. While it seemed the world was brought to a halt in order to stop the spread of the pandemic, health care personnel and scientists raced to understand the new virus and the disease it can cause and tried to identify or develop vaccines and drugs. Consequently, in 2020, coronavirus research output increased by a hundredfold (in the first pandemic year, in PubMed the number of publications on coronaviruses increased from about 800 in 2019 to 80,000 in 2020).

Over the past 4 years, SARS-CoV-2 has evolved and different variant strains have been circulating. Through variant classification, the World Health Organization (WHO) and the European Center for Disease Control (ECDC) keep track of so-called variants under monitoring (VUM), variants of interest (VOI) and variants of concern (VOC). In particular the latter have predominantly circulated across the world and are known as the Alpha, Beta, Gamma, Delta, and Omicron variants of SARS-CoV-2. Since March 2023, there have been no new SARS-CoV-2 variants reported that meet the VOC criteria, although monitoring shows that SARS-CoV-2 is undoubtedly still circulating in the human population. In May 2023 the WHO declared that COVID-19 no longer constitutes a public health emergency of international concern, but instead has become an established and ongoing health issue (16). Descendants of the Omicron variant continue to prevail and evolve into new subvariants. Most recently, the variant of interest (VOI) that is steadily spreading is JN.1, an Omicron BA.2.86-like lineage, which is slowly replacing the XBB descendant lineages (17). Although the WHO no longer considers the SARS-CoV-2 pandemic a public health emergency, the number of cases in the winter of 2023-2024 illustrates that this virus is here to stay and for now continues to require management and surveillance on a daily basis.

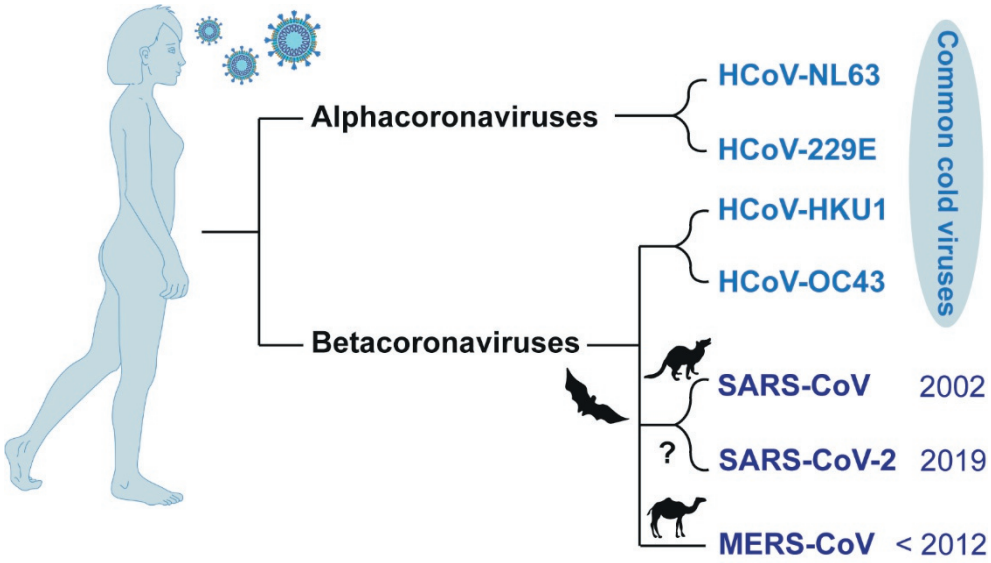

Figure 1: Seven coronaviruses are known to date that infect humans: The low pathogenic coronaviruses that cause the common cold are the alphacoronaviruses NL63 and 229E, and the betacoronaviruses HKU1 and OC43. The possibly highly pathogenic coronaviruses are all betacoronaviruses, comprising SARS-CoV and SARS-CoV-2 and MERS-CoV. The figure was partly generated using Servier Medical Art, provided by Servier, licensed under a Creative Commons Attribution 3.0 Unported License.

Coronavirus replication

Coronaviruses are spherical virions with a diameter of around 100 nm (18). They are enveloped viruses with a lipid membrane containing three structural proteins: membrane (M), envelope (E), and spike (S) protein (19). The virion core (nucleocapsid) consists of a 30-kilobase long positive-sense single-stranded RNA molecule, containing a 5' cap structure and a 3' poly (A) tail, which is encapsidated by the nucleocapsid (N) protein. The S protein is present on the virion surface as a homotrimer and is the most prominent envelope protein, as it is studied in detail for its role in infectivity and host immunity. It orchestrates host cell attachment and virus entry, is the main target of neutralizing antibodies and undergoes significant changes during SARS-CoV-2 variant evolution (20, 21). The S proteins that protrude from the surface of coronaviruses are seen as a crown, or "*corona*" in Latin, when using an electron microscope, which was the basis for the name of the coronavirus family (22). The S protein consists of two subunits, S1, which is responsible for attachment, and S2, which enables the fusion of the viral and host cell membrane (23). The S1 subunit contains the receptor-binding domain (RBD), which is the point of contact for the host receptor as well as the main target of neutralizing antibodies (24). Via the RBD, SARS-CoV and SARS-CoV-2 bind predominantly to the angiotensin-converting enzyme 2 (ACE2) receptor (25, 26), while MERS-CoV binds to dipeptidyl peptidase 4 (DPP4) receptor (27). HCoV-NL63 also binds to ACE2 (28). In turn, the other common-cold coronaviruses again utilize different host receptors, with HCoV-229E binding to human aminopeptidase (hAPN), and OC43 and HKU1 to 9-*O*-acetylsialic acids (29, 30). For variants of SARS-CoV-2, like the delta variant, amino acid changes in the S1 subunit have been reported to enhance binding to ACE2 and increase replication and transmissibility (31). Essential for SARS-CoV-2 entry into the host cell is a cleavage site for the host cell protease furin at the S1/S2 boundary (32). Following production and maturation of the S protein in the host cell, furin cleavage at the S1/S2 site in the Golgi apparatus results in the two subunits being non-covalently associated to perform the different functions of attachment and virus-membrane fusion (**Figure 2**). Furin proteases are ubiquitously expressed in humans, resulting in enhanced tissue tropism and pathogenesis for SARS-CoV-2 (33). Another cleavage event occurs at the target host cell. Upon receptor binding through S1 and conformational changes, a S2' cleavage site within the S2 subunit becomes accessible for cleavage at the membrane of an infected cell (**Figure 2**). Cleavage of the S2' site by cellular proteases is a pre-requisite for entering host cells as it exposes the fusion peptide and initiates membrane fusion. The type II transmembrane serine protease (TMPRSS2) is the main host protease to prime the S protein for cell entry by cleaving the S2' site (34). Mediated by conformational changes of the S protein, the exposed fusion loop is inserted into the host cell membrane and the viral

and cellular plasma membrane fuse, through which the RNA-containing nucleocapsid complex enters the host cell (23, 35). Besides SARS-CoV-2, also MERS-CoV and HCoV-OC43 have a S1/S2 furin cleavage site, however, other coronaviruses, including SARS-CoV, lack such a site (36). These coronaviruses, however, harbor other sequences that can be cleaved by the proteases at the target host cell (37-39). Studies have shown that additionally to using TMPRSS2-mediated fusion at the cell membrane, some coronaviruses, including SARS-CoV as well as SARS-CoV-2, can also employ the endosomal route for entry, which is dependent on the host cell protease cathepsin L (CTSL), which performs cleavage at the S2' site in the endosome (40, 41). In that case, upon ACE2 receptor binding, the virus is first internalized through the endosome and fusion occurs between the virus membrane and the endosomal membrane (23). Omicron variants were even reported to have a higher dependence on the endosomal route for entry (42). Many other cofactors for viral entry were also identified, like for example neuropilin-1 or c-type lectins (43, 44). Likewise, studies have reported alternative receptors for SARS-CoV-2 attachment (45, 46).

Once coronaviruses have entered the host cell, they express the non-structural proteins (nsps) necessary to form the enzymatic complex for viral replication and transcription (**Figure 2**). From two large open reading frames (ORF1a and ORF1b) covering the 5' two-thirds of the coronavirus genome, first, two polyproteins are translated: pp1a (includes nsp 1-11) or pp1ab (includes nsp 1-16) (47). To generate the individual nsps, the polyproteins are proteolytically processed by the two internal viral proteases, located in nsp3 (48) and nsp5 (49). Nsp5, the main protease (Mpro) or chymotrypsin-like cysteine protease (3CLpro), releases all nsps downstream of nsp4. The replication-transcription complex that is formed, includes a helicase (nsp13), a RNA-dependent RNA polymerase (RdRp) (nsp12), processivity factors (nsp7 and 8), a single-strand binding protein (nsp9), a proofreading exonuclease and N7-methyltransferase (nsp14), and a 2'-O-methyltransferase (nsp16), and other cofactors (e.g. nsp10) (47). Recently, the mechanism of viral RNA capping, which is important for efficient translation and hiding the viral RNA from host detection, was elucidated in more detail (50). Mediated by the nidovirus RdRp-associated nucleotidyltransferase (NiRAN) domain of nsp12, nsp9 forms a covalent RNA-protein complex with the nascent RNA, a mechanism termed RNAylation, which enables further capping of the RNA.

From the virus genome, full-length negative-sense RNA is produced as a template for new positive-sense RNA, which is then used for translation, packaging into newly formed virus particles or further genomic RNA replication. Replication of new viral RNA is thought to happen inside double-membrane vesicles (DMVs), which arise by the transformation of endoplasmic reticulum (ER) membranes, and were shown to be induced by expression of nsp3, nsp4 and nsp6 (51-54). Although many details of coronaviral RNA synthesis inside DMVs remain to be elucidated, recently, molecular pores in the DMV membranes were

found, which could enable the trafficking of newly synthesized RNA to the cytosol for translation and incorporation into viral particles (55). Structural and accessory proteins are translated manifold from a nested set of subgenomic mRNAs. These subgenomic mRNAs derive from the 3'-proximal third of the positive-sense genome through a mechanism where minus-strand synthesis is discontinuous (47, 56, 57). Following the translation of structural proteins in the cytosol, the envelope proteins S, M and E are processed into their mature form in the ER and trafficked to the ER-Golgi intermediate compartment (ERGIC). The S protein is for example heavily glycosylated, which has implications for antibody recognition and infectivity, as the glycans on the S surface were shown to be necessary for efficient binding of S to the host receptor ACE2 (58-60). The envelope proteins, together with N-encapsidated genomic RNA, assemble into new virions at the ERGIC. The assembled virions then traffic to the Golgi apparatus, where furin-mediated S protein cleavage occurs (as described above for some coronaviruses like SARS-CoV-2). Finally, coronaviruses then exit the cell through exocytosis through the secretory pathway or lysosomal egress (61).

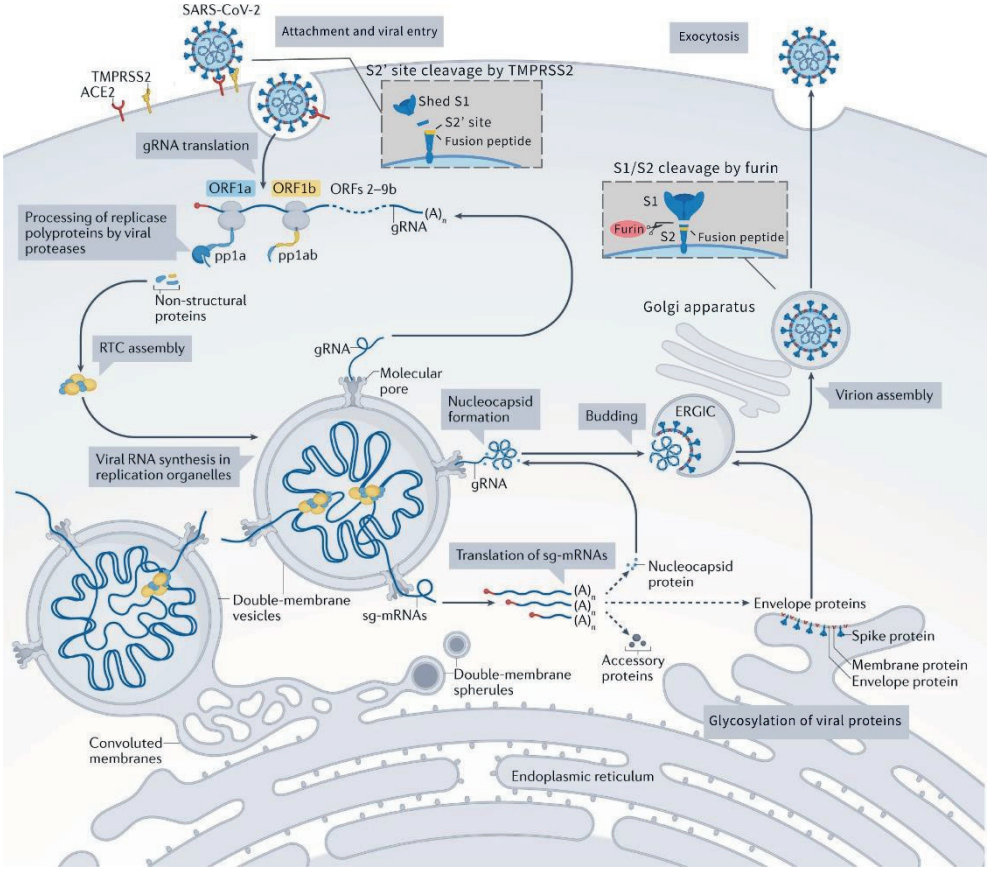

Figure 2: Schematic representation of the coronavirus replication cycle. Following receptor binding and virus entry into the host cell, the positive-sense genomic RNA is translated and processed to produce the non-structural proteins necessary for the replication-transcription complex (RTC). The figure shows the proposed model of RNA replication inside DMVs and the export of newly-made viral RNA into the cytosol through DMV membrane pores. Following the translation of subgenomic mRNAs in the cytosol, virus particles are assembled at the ERGIC. In the case of SARS-CoV-2, the S protein is pre-cleaved by the host protease furin in the Golgi apparatus. Adapted from (47) and (23) and reproduced with permission from Springer Nature. TMPRSS2: Transmembrane protease serine subtype 2, ACE2: Angiotensin-converting enzyme 2, pp1: polypeptide 1, gRNA: genomic RNA, sgRNA: subgenomic RNA.

Lung epithelium and coronavirus infection

The human respiratory tract is the point of entry for respiratory viruses like coronaviruses and spans from the nasal cavity to the lung alveoli. It is lined by the airway epithelium, which is composed of varying cell types depending on the anatomical location (62, 63). The airway epithelium is not only a physical barrier against invading pathogens, but the cell types also differ in their functions. In the tracheae and bronchi of the upper airway, the epithelium mainly includes ciliated cells, secretory goblet cells, club cells, and basal cells. Also other cell types, like ionocytes, tuft cells, and neuroendocrine cells, were described, which are less abundant (64). In the most distal area of the lung are the alveoli, where the exchange of oxygen and carbon dioxide happens. The alveolar epithelium is composed of alveolar epithelial type I cells (AEC1), which perform gas exchange, and their progenitors, the type II cells (AEC2) (65). AEC2 cells are important for generating pulmonary surfactant, a crucial mixture of lipids and proteins that is responsible for reducing surface tension in the alveoli and therefore preventing collapse at exhalation. Mucociliary clearance, which is the combined action of mucus secretion by goblet cells and the beating cilia of ciliated cells, actively transports particles, including pathogens/viruses, out of the upper airway (63). As a first line of defense, epithelial cells also initiate the innate immune response by production of cytokines and chemokines and subsequent recruitment of immune cells to the site of infection (64, 66).

In healthy individuals, the cellular composition of the epithelium differs throughout the airway, which causes a gradient of susceptibility to different respiratory viruses depending on their cell tropism (62). ACE2, the receptor that is utilized by SARS-CoV and SARS-CoV-2, as well as the protease TMPRSS2 are mostly expressed on ciliated cells and AEC2 (67-69), rendering them the primary target of initial infection. Also, MERS-CoV was found to infect AECs (70). Besides the infection of AECs in the lower respiratory tract by the highly pathogenic coronaviruses, SARS-CoV-2 and MERS-CoV were also reported to target non-ciliated cells in the upper respiratory regions (69, 71, 72). Studies have shown that in the

nasal epithelium SARS-CoV-2 displays a tropism for ciliated cells, while MERS-CoV preferentially targets non-ciliated cells, like goblet cells (73). HCoV-OC43 likewise infects primarily ciliated cells, while HCoV-229E targets non-ciliated cells, and both these common cold viruses primarily infect the upper respiratory tract (74). SARS-CoV-2 variants were first observed to evolve continuously with respect to their capacity to infect the respiratory epithelium, mainly through mutations in the Spike protein that led to enhanced binding to the ACE2 receptor and entry into the host cell (75, 76). Later, although the Omicron strains also displayed higher efficacy in binding to the ACE2 receptor (77), they were reported to be more dependent on the host cell protease cathepsin L and were less efficient in using TMPRSS2 (42). Earlier strains were more efficient at replicating in lung epithelium and infecting the lower airway, while subsequent Omicron variants have adapted to replicating in the upper airway, consequently yielding less severe respiratory symptoms, at least in healthy individuals (78, 79). Their adaptation to the upper airway, especially the nasal epithelium, was reported to be a possible reason for the observed increased transmission, alongside stronger affinity for the ACE2 receptor and increased immune evasion through changes in the antigenic structure of the spike (80, 81). Accordingly, studies that investigated the basic reproduction numbers for SARS-CoV-2 variants, showed that the Omicron variant is 3.8 times more transmissible than the delta variant (82) and infection rates in the population increased faster during the Omicron wave than with any other variants (83).

In patients with chronic lung diseases like asthma or chronic obstructive pulmonary disease (COPD), the epithelium changes structurally and functionally. The composition of airway epithelium cells in such chronic diseases can differ, and epithelial barrier function and immune responses were shown to be impaired (63). In the lungs of asthma patients, for example, more mucus-producing cells were observed than in healthy airways (84), and in asthma and COPD patients, there is an increased susceptibility to respiratory infections, as shown for rhinovirus, SARS-CoV-2, or MERS-CoV (85-87). Therefore, the presence of infection-promoting host factors, like receptors or proteases, on specific cells, as well as the proportion of those cells in specific anatomical locations, can determine susceptibility to and spread of infection. Understanding, which cells are infected, which host responses are elicited, and which factors influence infection kinetics, are important to develop treatment for patients with respiratory infections like COVID-19.

SARS-CoV-2 pathogenesis and immune responses

While common cold coronaviruses like HCoV-229E only cause mild symptoms in the upper respiratory tract of healthy individuals, infection with the potentially highly pathogenic SARS-CoV, SARS-CoV-2 and MERS-CoV can lead to severe symptoms also in the lower respiratory tract (88). Coronavirus disease 2019 (COVID-19), the disease associated with SARS-CoV-2 infection, can present as a variety of clinical symptoms, from asymptomatic infection to very severe disease, and the exact determinants for these differences are not known. In healthy young individuals, especially children, SARS-CoV-2 infection often is asymptomatic or causes only mild common cold symptoms (89, 90). However, in older individuals, people with underlying medical conditions, but frequently also in adolescents or young adults, COVID-19 can be life-threatening (91, 92). A study that analyzed all confirmed cases from the start of the pandemic in February 2020 in China, reported an overall case fatality rate of 2.3% (93), others reported that 3-20% of infected patients required hospital care (88, 94, 95). Over the course of the pandemic, following the implementation of vaccination and antiviral strategies, and the advent and predominance of the Omicron variants, the case fatality rate has decreased drastically, to below 0.3% in August 2022 (96). Although SARS-CoV-2 initially infects the respiratory epithelium, infection can lead to multi-systemic disease. Often an infection is accompanied by fever, cough, muscle aches, fatigue, and/or shortness of breath. In severe cases patients can suffer from acute respiratory distress syndrome (ARDS), which can greatly impact lung function and lead to tissue fibrosis, multi-organ failure, and death (88). Previously, such severe disease outcomes were also seen with SARS-CoV or MERS-CoV infection (97, 98). Over time it became clear that SARS-CoV-2 infection can also have long-term consequences and can cause quite unique post-infection symptoms. The loss of smell or taste, caused by olfactory dysfunction during the acute stage of the infection, can affect patients for a long time, and more seriously, “Post-COVID-19 condition” or “Long COVID” has developed in a few percent of infected people (99, 100). Long COVID is described as symptoms affecting the lung, heart, gastrointestinal tract, blood vessels, and nervous system, among others, which are a consequence of the infection, but remain present long after the acute infection has resolved. Possible underlying mechanisms include immune dysregulation, microbiota disruption, autoimmunity, blood clotting dysfunctionalities, endothelial cell abnormalities, and dysfunctional neurological signalling (100). This illustrates the wide impact that SARS-CoV-2 infection can have on the entire human body, with in some cases severe impact on the daily function and quality of life of patients.

During initial infection, the immune system plays a crucial role in combating respiratory viruses. As mentioned earlier, the epithelial cells are the first to initiate an innate immune

response to an invading pathogen (63). Intracellular sensing of viral RNA (dsRNA or RNA with a 5'-triphosphate group) by retinoic acid-inducible gene I-like receptors (RLRs) like MDA5 or RIG-I (101, 102) leads to interaction with MAVS, which induces phosphorylation of IRF3, ultimately resulting in transcriptional upregulation of the expression of type I and type III interferons (103, 104). Toll-like receptors on the cell or in endosomes, detect pathogen-associated molecular patterns (PAMPs) and likewise activate signalling kinase cascades that activate transcription of proinflammatory cytokines (105), type I interferons, and IFN-stimulated genes (ISGs) (104). Inflammasomes, like NLRP3, and cytosolic sensors other than RLRs were also described to trigger type I IFN and proinflammatory cytokine production upon sensing of SARS-CoV-2 (104, 106, 107). The binding of secreted IFNs to IFN receptors further stimulates the expression of interferon-stimulated genes (ISGs) whose products exert a range of antiviral effects (108). SARS-CoV-2 and other coronaviruses counter the innate immune response of host cells by several viral immune evasion mechanisms. They do so by expressing a number of proteins that (also) have immune evasion activities (104, 109, 110), and presumably also by preventing detection by hiding viral RNAs that can trigger intracellular sensing inside DMVs (53), and by modifying their RNAs to mimic the 5' cap structure of host mRNAs (103, 111). The interferon response was reported to be delayed following infection with highly pathogenic coronaviruses, which evade the innate immune response (112). When IFN response is initially blocked and delayed, unhindered virus replication can later lead to a strong and persistent IFN and proinflammatory cytokine response, which can cause hyperinflammation and long-term (immune) pathologies, as shown previously for SARS-CoV and SARS-CoV-2 (113, 114). Early on, studies have shown an association between high levels of IL-6, IL-1, IFNγ, TNFα, NF-Kb, and other chemokines, and high morbidity in patients infected with SARS-CoV-2 (104, 115-117). Systemic damage to tissue and severe consequences of a dysregulated immune response and hyperinflammation are well documented for COVID-19 patients (118), albeit not fully understood, also due to genetic and immunological differences between infected individuals. Age, immune status, and underlying medical conditions of patients are risk factors and determinants for disease outcome.

Human primary airway epithelial cell culture to study coronaviruses

To study coronavirus replication, host responses and pathogenesis, and to develop antiviral therapies, *in vitro* cell culture models are required. Most commonly, conventional monolayer cell cultures of immortalized or tumor cell lines are used, like Vero E6 (African green monkey cells) or lung epithelial cell lines like Calu-3 or A549 (119). Their use has

advantages, like low costs and minimal effort, as most laboratories have these cultures already in use. They are sufficient for initial drug screening purposes (120), where high-throughput screening is essential to reduce time and costs during drug discovery. However, for further drug evaluation, these simplified monocellular systems are often not sufficiently representing the infected host organism, which can affect infection characteristics and drug identification (121). Propagation of SARS-CoV-2 in Vero E6 cells for example, results in rapid virus adaptation and loss of the S protein's furin cleavage site (122), which can be prevented by using a lung epithelial cell line (123). There has been progress in the development of advanced *in vitro* models like organoids, organ-on-chip models, and air-liquid interface (ALI) airway epithelial cell culture (124), that better represent the tissue in question as it exists *in vivo*. Human primary airway epithelial cells that are cultured at ALI (HAE-ALI) have become a well-characterized model in the research of respiratory infections, for example for disease modelling or studying virus receptors, cell tropism, or immune responses (125). To develop ALI cultures, primary cells are isolated from donor lung tissue and grown on a membrane, where they are exposed to air on their apical side and cell culture medium on their basal side (126) (**Figure 3**). *In vivo*, the cellular composition can differ depending on the anatomical location in the respiratory tract or the age or disease of a given patient. To recapitulate different anatomical locations in the respiratory tract, cells from different locations can be cultured, like the nasal cavity, trachea, bronchi, or alveoli. Isolation of nasal epithelial cells is the least invasive procedure, performed by nasal brushing. The advantage of using primary cells instead of conventional immortalized or tumor cell lines is that the former differentiate into the different cell types and organization as present in the pseudostratified lung epithelium *in vivo*. Thus, differentiated HAE-ALI cultures contain basal cells, secretory cells, club cells, and ciliated cells (**Figure 3**). The secretory goblet cells also produce mucus, which is moved through the action of beating cilia (127, 128). It was shown that HAE-ALI cultures represent the *in vivo* epithelium transcriptome (129). In HAE-ALI cultures, the cellular composition of the modelled epithelium can differ depending on the individual donor involved (130), differentiation time (131, 132), as well as culture conditions (133). Furthermore, inflammatory disease states in the lung, which also affect the epithelial cells (134, 135), can be modelled and immune cells can be co-cultured with these cells (136). The epithelial cells of HAE-ALI cultures elicit immune responses that recapitulate those observed *in vivo*, as was shown in cultures of nasal, bronchial, or alveolar cells (137-139). During the SARS-CoV-2 pandemic, HAE-ALI cultures were extensively used to study infection (31, 71, 132, 140), host responses (139, 141), or the impact of antiviral drug treatment (142, 143). All human coronaviruses are able to infect HAE-ALI cultures, which renders them a good model for comparative studies between highly or low pathogenic coronaviruses. In

the search for antiviral drugs, a positive result in HAE-ALI cultures increases the likelihood that the *in vitro* efficacy of a drug will translate into animal models and the clinic.

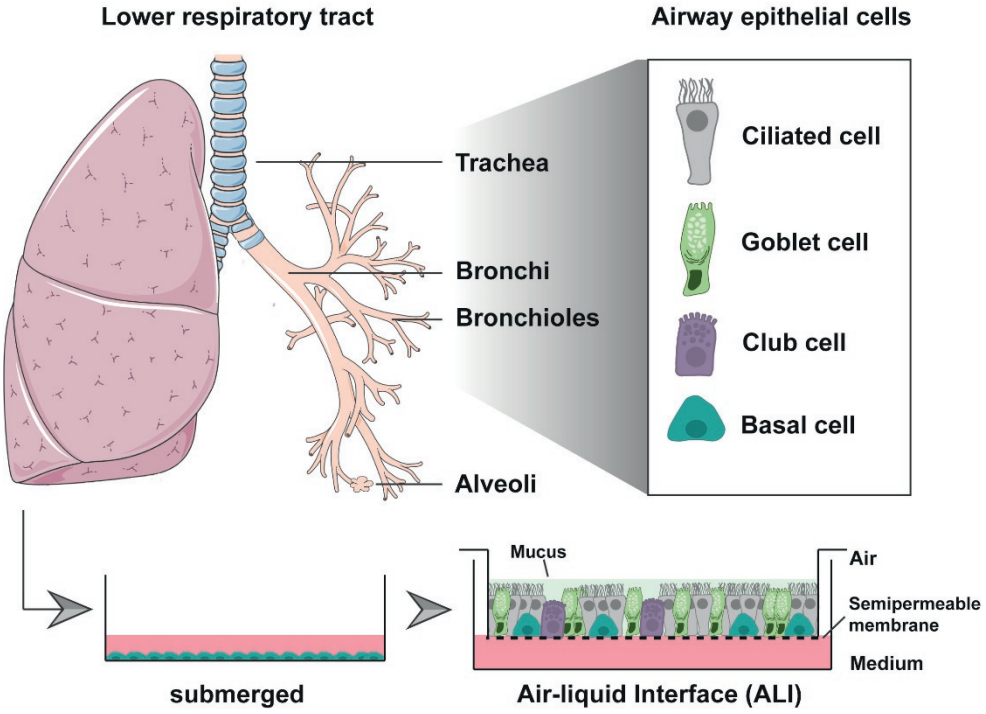

Figure 3: The lower respiratory tract contains trachea, bronchi, bronchioles, and alveoli, the latter being the region where gas exchange occurs. The epithelium of trachea and bronchi contains various cell types, primarily ciliated, goblet, club, and basal cells. Human lung tissue from these regions can be obtained to isolate primary epithelial cells, and culture them on transwell membranes at the air-liquid interface to obtain well-differentiated cultures. The figure was partly generated using Servier Medical Art, provided by Servier, licensed under a Creative Commons Attribution 3.0 Unported License.

Antiviral drug discovery

Antiviral drugs and vaccines are the two key approaches to prevent or fight infectious diseases. During the SARS-CoV-2 pandemic, the development of vaccines succeeded at unprecedented speed, but still took over a year and demanded large budgets and effort. During this time, we would have benefited from having broad-spectrum antivirals at hand, to use in the clinic shortly post exposure or prophylactically in (local) outbreak settings.

However, although SARS-CoV and MERS-CoV emerged many years prior to the SARS-CoV-2 pandemic, no registered antivirals had been developed for clinical use against highly pathogenic coronaviruses.

There are two general approaches to antiviral drug development: one can either target the virus directly (direct-acting antivirals, DAA) or target host factors or pathways that the virus requires to replicate (host-directed antivirals, HDA) (144) (**Figure 4**). Direct-acting antivirals in principle are more specific, having activity against a more narrow range of viruses, but have a lower chance of toxicity. Due to virus evolution, there is more potential for the development of resistance against direct-acting antiviral compounds (145). Essentially, many steps of the viral replication cycle can be targeted, like virus entry, virus-cell fusion, RNA synthesis or other viral enzyme functions, or virus assembly (144). Host-directed antivirals, on the other hand, may have activity against a broad spectrum of viruses, while lowering the likelihood of resistance development, but present a higher risk of unwanted side effects (145). Therefore, a drug that has maximum selectivity towards the target, either a viral or host target, and minimal side effects on the host would be an optimal candidate.

The number of available antiviral drug treatments has slowly increased since the first antiviral drug was approved in 1963 (146). A review from 2002 listed more than 30 approved antiviral drugs (144), and a review from 2016 reported 90 approved drugs (145). However, these 90 drugs target a total of only nine human viruses, mainly the retrovirus human immunodeficiency virus (HIV), and DNA viruses like herpes simplex or human papillomavirus, and the RNA viruses influenza virus, respiratory syncytial virus and hepatitis C virus (HCV) (145). Since 2016, multiple other drugs that inhibit virus replication have been developed, targeting influenza virus (147), HIV (148), HCV (149), and most recently SARS-CoV-2 (150), all of them being DAAs. Successful drug categories, in general, are nucleoside analogues, protease inhibitors, entry inhibitors, fusion inhibitors, IMP dehydrogenase inhibitors, and neuraminidase inhibitors, to name a few (144, 145). Currently, the majority of approved antiviral drugs are DAAs, with the exception of entry inhibitors, like antagonists of the HIV receptor or co-receptor (151, 152), or the IMP dehydrogenase inhibitor ribavirin (153), although additional modes of action have been postulated for ribavirin (154). However, many HDAs that are targeting kinases or other signalling pathways are in preclinical development (155, 156). Furthermore, RNA-based or peptide-based therapeutics are new promising fields within the antiviral drug development landscape (157-159). Other treatment options do not inhibit virus replication, but modulate or stimulate the host's immune responses, such as pegylated interferon treatment, targeting inflammatory responses, and administering convalescent plasma or monoclonal antibodies (145, 160).

There are different approaches to the identification or development of new therapeutics. Antiviral drug discovery can be target-based, e.g. based on the known structure of a viral protein. Another way of finding candidate drugs is repurposing of already registered drugs (161, 162) (**Figure 4**). To identify hits from a number of newly developed compounds or a list of repurposing candidates, high-throughput screening is done. This can be done *in vitro* through phenotypic screening, where cell lines are used to evaluate drugs, for example, for their protective effect from cell death upon infection.

Recent advances in bioinformatics and artificial intelligence (AI) have broadened the options to screen for antivirals *in silico* (163), by either identifying new drugs or screening for potential repurposing candidates. AI can also assist in analyzing new drug targets, optimizing the drug development process, and predicting the properties of new candidate drugs, therefore de-risking drug development through identifying problems early and reducing the risk of failure. Repurposing of drugs offers the advantages of accelerating drug development, especially in an outbreak situation. Already existing knowledge of pharmacokinetics, pharmacodynamics, drug formulation, and safety profiles can decrease the time from preclinical assessment to clinical use. With regard to antiviral drugs, only ribavirin, which was reported to have different mechanisms of action (164), or the DNA polymerase inhibitor tenofovir have been previously approved by the FDA to treat more diseases than originally intended (145, 160). The RNA polymerase inhibitors remdesivir and the nucleoside analogue molnupiravir, which were already known as a broad-spectrum antivirals, were repurposed in the search for drugs to treat SARS-CoV-2 infection (143, 165). Other antiviral therapies that were successfully repurposed are immunomodulators, like corticosteroids, cytokine antagonists, or interferon therapies, which are not used to treat acute infections as they do not inhibit virus replication, but modulate the immune response.

Drug discovery can be divided into several stages: the phase of early drug discovery, which encompasses target identification and initial compound development; pre-clinical development; clinical development, which includes human trials; and regulatory approval and post-market evaluation (159) (**Figure 4**). Pre-clinical development encompasses several steps from initial target or drug candidate identification to clinical trials in human, and essentially entails investigation of pharmacodynamics, e.g. mode of action, efficacy and safety, and pharmacokinetics/ADME (adsorption, distribution, metabolism, excretion) and formulation of a drug (166). These properties can be evaluated partially *in vitro*, and *in vivo* in cell culture and animal infection models. During early drug discovery, high-throughput assays are performed in conventional monocellular cell lines, by treating infected cells with potential antiviral compounds, and with a simple readout that either shows protection from infection or inhibition of virus replication (167). Thus, a large number of chemical compounds can be screened, minimizing costs, manpower, and time. During pre-clinical

testing, the efficacy of a drug candidate can be confirmed in more advanced models, like ALI cultures, and moved into the next phases of drug development.

Drugs against SARS-CoV-2

Before the start of the SARS-CoV-2 pandemic, only two antiviral compounds against SARS-CoV or MERS-CoV had been tested in clinical trials or reported in case studies, which were the HIV protease inhibitors lopinavir and ritonavir (168) and the nucleoside analogue ribavirin (169-171). Studies reported reduced mortality for MERS-CoV-infected patients treated with lopinavir/ritonavir and interferon-β, and inconclusive results were reported for ribavirin. Furthermore, *in vitro* studies have identified multiple drugs possibly inhibiting these two zoonotic coronaviruses (172, 173). In the search for effective antivirals against SARS-CoV-2, researchers quickly screened drugs that were previously studied for their ability to block SARS-CoV and MERS-CoV, or other viruses (174). These drug repurposing efforts identified many potential inhibitors of SARS-CoV-2 replication. *In vitro*, those drugs might have yielded good test results, as reported for example for the RNA synthesis inhibitor favipiravir, the protease inhibitor lopinavir, or the anti-parasitic drug chloroquine (175-177). However, studies showing good efficacy *in vitro* did not translate into successful clinical trials (178, 179). This discrepancy of drug efficacy between *in vitro* and *in vivo* studies can result from the use of cell lines that lack relevance. Although chloroquine initially displayed promising results in Vero E6 cells (180), it was later shown that it does not protect human lung cells from SARS-CoV-2 infection (181). Remdesivir, the first drug that was approved for emergency use authorization (EUA), later received full authorization, albeit there is inconsistent evidence up until today about its efficacy and safety (182-184). However, studies did not always take into account the reduced efficacy of remdesivir when treatment is given to hospitalized patients with progressed disease, at a point where inhibition of virus replication does not lead to improvement (185). Remdesivir acts as a nucleoside analogue and inhibits the viral RNA-dependent RNA polymerase by terminating viral RNA synthesis (186). While remdesivir is administered intravenously, a derivative of remdesivir, VV116, is an oral drug that was recently approved for marketing in China (187). Other drugs were EUA approved but never fully approved, like molnupiravir, which, as a nucleoside analogue, inhibits viral replication by reducing the fidelity of viral RNA synthesis (188). Clinical studies evaluating molnupiravir as modestly efficacious led this drug to be approved for EUA by the FDA, however it was never approved further. While it is approved by the FDA, in Europe the EUA was later withdrawn (189, 190). To date only one orally given DAA has been approved as a treatment against SARS-CoV-2, with high quality of evidence

and strong recommendations from health agencies, which is ritonavir-boosted nirmatrelvir (marketed as Paxlovid by Pfizer), a compound that inhibits the main viral protease nsp5 (150, 184). Another promising inhibitor, which also targets the main protease and was approved for emergency use in Japan, is ensitrelvir (marketed as Xocova) (191). Both of these drugs were developed using target-based drug design. Notably, Pfizer scientists already had a compound in hand, that was developed against the main protease of SARS-CoV, thus substantially shortening the time of initial drug discovery (192). The fact that the main viral protease is indispensable for virus replication and is highly conserved across coronaviruses, makes it a good target for antiviral drug development and yielded one of the first successful SARS-CoV-2 antiviral treatment (49, 184). Potential inhibitors of the nsp3 papainlike protease have also been described (193, 194). Other studies have identified additional drug targets within the SARS-CoV-2 replication cycle, such as the nsp13 helicase (195), which is important for viral RNA synthesis, the nsp14 and nsp16 methyltransferases (196) or the nsp15 endonuclease (197), which is necessary for evasion of the host immune response (162). The nsp12 RdRp, like the main protease, also shows a high degree of conservation across coronaviruses (198, 199) and has potential as drug target for broad-spectrum active compounds, such as remdesivir. Furthermore, the nidovirus RdRp-associated nucleotidyltransferase (NiRAN) domain and nsp9, both essential for the capping of the viral RNA (200), are potential targets, and also the binding with associated nsp8 can be targeted (201). Further approaches are inhibition of entry, through blocking the spike protein (202) or the ACE2 receptor (203), or assembly, through targeting of the N proteins (160). Furthermore, interferon has been explored as a treatment option in multiple clinical trials, however with variable outcomes (204) and not resulting in approved treatment options. Many studies that employed the gene-editing tool CRISPR/Cas9 or small interfering RNA (siRNA) have identified host factors that are important for virus replication and therefore possible targets for drug development (205, 206). However, up until now, there are no successfully developed host-directed drugs that inhibit SARS-CoV-2 replication. There are approved HDAs that target other viruses, like hepatitis C virus (HCV) or human immunodeficiency virus (HIV), which are the infectious agents that most antiviral drugs were developed for prior to the SARS-CoV-2 pandemic (155). The efforts to develop HDAs against SARS-CoV-2 are ongoing with many small-molecule drugs in clinical trials and the therapeutic landscape evolving rapidly. This is not only important to treat SARS-CoV-2 infections but, considering the potential broad-spectrum activity of these compounds, also to prepare us for the next coronavirus outbreak. During the pandemic, it was quickly realized that COVID-19 can present itself with severe symptoms even after SARS-CoV-2 replication in patients has waned. Damage can be inflicted by a deregulated and exacerbated inflammatory response, triggered by SARS-CoV-2, leading to acute respiratory

distress syndrome (ARDS), pulmonary fibrosis, and multiple organ failure (207). Drug treatments reducing these disease symptoms, rather than inhibiting viral replication, have become important for therapeutic use. Host-directed drugs that are approved for the treatment of COVID-19 are immunomodulatory, like tocilizumab (IL-6 receptor antagonist) or baricitinib (JAK kinase inhibitor), which both suppress the inflammatory response (184). Also corticosteroids, like dexamethasone, were used early on for their anti-inflammatory effect (208) and are recommended for the treatment of systemic inflammation (209). Multiple trials have investigated the application of combination therapy, by simultaneously treating COVID-19 patients with an antiviral drug and immunomodulatory drugs (210). Optimal strategies for combating SARS-CoV-2 and its associated disease COVID-19 would involve drugs that inhibit virus replication and also exhibit a beneficial therapeutic effect, to prevent exacerbation of disease. Furthermore, for the treatment of COVID-19 patients, it is crucial to take into account the stage of disease (early in infection or advanced inflammatory disease) and the health status of the patient.

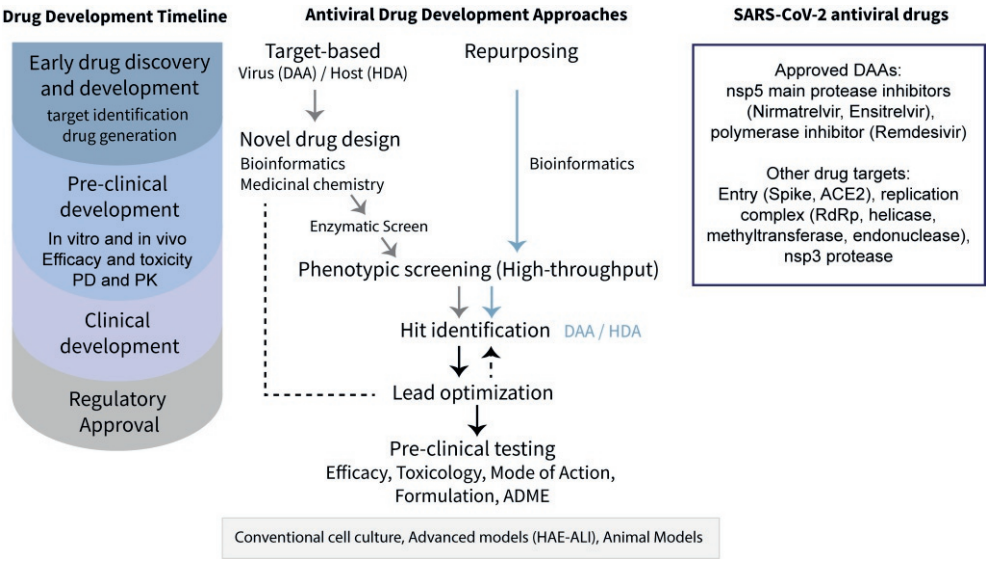

Figure 4: Antiviral drug development timeline and approaches. The currently approved antiviral therapies against SARS-CoV-2, and other main drug targets that are studied, are listed. Part of the figure is adapted from (160) and reproduced with permission from Springer Nature.

Outline of the thesis

The overall aims of this research project were to study coronavirus infection biology in lung epithelial cells and to contribute to the discovery of antiviral compounds. Therefore, primary human airway epithelial cells cultured at the air-liquid interface were used as an advanced model to recapitulate coronavirus infection of the human lung epithelium and host responses to SARS-CoV-2 and other coronaviruses. Host-directed antiviral approaches were evaluated by testing several groups of small-molecule compounds for their efficacy and broad-spectrum activity.

Understanding coronaviruses

In **Chapter 2**, HAE-ALI cultures were employed to set up and characterize an infection model with SARS-CoV-2. This cell culture model represents the respiratory epithelium very well and can reflect structural and functional changes as seen in individual donors or disease states. Therefore, it was used to study the impact of the presence of specific epithelial cells on SARS-CoV-2 infection. Differences in cellular composition based on anatomical origin, differentiation time or drug treatment and their effects on virus replication and viral cell-entry factors were investigated. In **Chapter 3**, the approach was broadened to compare infection with the potentially highly pathogenic SARS-CoV-2, SARS-CoV, and MERS-CoV and low pathogenic HCoV-229E and HCoV-OC43 viruses. RNA sequencing was used to identify differences in the host response to these viruses. The knowledge gained was used to identify possible antiviral compounds.

Targeting coronaviruses

Chapters 4 and 5 describe our efforts to repurpose and identify small-molecule drugs to combat SARS-CoV-2 and other coronaviruses. HAE-ALI cultures were utilized to detect antiviral activity in this advanced model. In **Chapter 4**, the compound R-Propranolol was studied for its anti-angiogenic and antiviral properties. By employing human lung endothelial cells, it was shown that propranolol blocks the upregulation of expression of angiogenic factors, which are induced by infection and potentially contribute to lung pathogenesis. R-propranolol also efficiently inhibited the replication of other highly pathogenic coronaviruses. In **Chapter 5**, several inhibitors of ER-resident α-glucosidase I and II were screened for antiviral activity against SARS-CoV-2. These comprised iminosugar compounds, which are studied as antivirals for decades, and cyclophellitols, a newer class of inhibitors. We identified 1,6-*epi*-cyclophellitol cyclosulphate as superior, as it most potently blocked ER α-glucosidase II activity and reduced virus infectivity. The broad-

spectrum activity of the antivirals identified in **Chapters 4** and **5** makes them interesting candidates to explore further for the treatment of coronavirus infections.

In **Chapter 6**, the research projects described in this thesis are discussed with regard to current literature. Additionally, new advances in SARS-CoV-2 drug development and the importance of the use of advanced cell culture models are discussed.

References

1. Lauring AS, Andino R. 2010. Quasispecies Theory and the Behavior of RNA Viruses. PLOS Pathogens 6:e1001005.
2. Reed KD. 2018. Viral Zoonoses, Reference Module in Biomedical Sciences. Elsevier.
3. Cavanagh D. 1997. Nidovirales: a new order comprising Coronaviridae and Arteriviridae. Arch Virol 142:629-33.
4. Woo PCY, de Groot RJ, Haagmans B, Lau SKP, Neuman BW, Perlman S, Sola I, van der Hoek L, Wong ACP, Yeh SH. 2023. ICTV Virus Taxonomy Profile: Coronaviridae 2023. J Gen Virol 104.
5. Woo PC, Lau SK, Lam CS, Lau CC, Tsang AK, Lau JH, Bai R, Teng JL, Tsang CC, Wang M, Zheng BJ, Chan KH, Yuen KY. 2012. Discovery of seven novel Mammalian and avian coronaviruses in the genus deltacoronavirus supports bat coronaviruses as the gene source of alphacoronavirus and betacoronavirus and avian coronaviruses as the gene source of gammacoronavirus and deltacoronavirus. J Virol 86:3995-4008.
6. Weiss SR, Navas-Martin S. 2005. Coronavirus pathogenesis and the emerging pathogen severe acute respiratory syndrome coronavirus. Microbiol Mol Biol Rev 69:635-64.
7. Tsang KW, Ho PL, Ooi GC, Yee WK, Wang T, Chan-Yeung M, Lam WK, Seto WH, Yam LY, Cheung TM, Wong PC, Lam B, Ip MS, Chan J, Yuen KY, Lai KN. 2003. A cluster of cases of severe acute respiratory syndrome in Hong Kong. N Engl J Med 348:1977-85.
8. Zaki AM, van Boheemen S, Bestebroer TM, Osterhaus ADME, Fouchier RAM. 2012. Isolation of a Novel Coronavirus from a Man with Pneumonia in Saudi Arabia. N Engl J Med. 367:1814-1820.
9. Ruiz-Aravena M, McKee C, Gamble A, Lunn T, Morris A, Snedden CE, Yinda CK, Port JR, Buchholz DW, Yeo YY, Faust C, Jax E, Dee L, Jones DN, Kessler MK, Falvo C, Crowley D, Bharti N, Brook CE, Aguilar HC, Peel AJ, Restif O, Schountz T, Parrish CR, Gurley ES, Lloyd-Smith JO, Hudson PJ, Munster VJ, Plowright RK. 2022. Ecology, evolution and spillover of coronaviruses from bats. Nature Reviews Microbiology 20:299-314.
10. Mok CKP, Zhu A, Zhao J, Lau EHY, Wang J, Chen Z, Zhuang Z, Wang Y, Alshukairi AN, Baharoon SA, Wang W, Tan W, Liang W, Oladipo JO, Perera R, Kuranga SA, Peiris M, Zhao J. 2021. T-cell responses to MERS coronavirus infection in people with occupational exposure to dromedary camels in Nigeria: an observational cohort study. Lancet Infect Dis 21:385-395.
11. Li W, Shi Z, Yu M, Ren W, Smith C, Epstein JH, Wang H, Crameri G, Hu Z, Zhang H, Zhang J, McEachern J, Field H, Daszak P, Eaton BT, Zhang S, Wang LF. 2005. Bats are natural reservoirs of SARS-like coronaviruses. Science 310:676-9.
12. Zhu N, Zhang D, Wang W, Li X, Yang B, Song J, Zhao X, Huang B, Shi W, Lu R, Niu P, Zhan F, Ma X, Wang D, Xu W, Wu G, Gao GF, Tan W. 2020. A Novel Coronavirus from Patients with Pneumonia in China, 2019. N Engl J Med 382:727-733.
13. Wacharapluesadee S, Tan CW, Maneeorn P, Duengkae P, Zhu F, Joyjinda Y, Kaewpom T, Chia WN, Ampoot W, Lim BL, Worachotsueptrakun K, Chen VC-W, Sirichan N, Ruchisrisarod C, Rodpan A, Noradechanon K, Phaichana T, Jantarat N, Thongnumchaima B, Tu C, Crameri G, Stokes MM, Hemachudha T, Wang L-F. 2021. Evidence for SARS-CoV-2 related coronaviruses circulating in bats and pangolins in Southeast Asia. Nature Communications 12:972.
14. Pagani I, Ghezzi S, Alberti S, Poli G, Vicenzi E. 2023. Origin and evolution of SARS-CoV-2. Eur Phys J Plus 138:157.
15. Zhou P, Yang X-L, Wang X-G, Hu B, Zhang L, Zhang W, Si H-R, Zhu Y, Li B, Huang C-L, Chen H-D, Chen J, Luo Y, Guo H, Jiang R-D, Liu M-Q, Chen Y, Shen X-R, Wang X, Zheng X-S, Zhao K, Chen Q-J, Deng F, Liu L-L, Yan B, Zhan F-X, Wang Y-Y, Xiao G-F, Shi Z-L. 2020. A pneumonia outbreak associated with a new coronavirus of probable bat origin. Nature 579:270-273.

16. World Health Organization (WHO). 2023. Statement on the fifteenth meeting of the IHR (2005) Emergency Committee on the COVID-19 pandemic. Geneva: WHO.
17. Looi M-K. 2023. Covid-19: WHO adds JN.1 as new variant of interest. BMJ 383:p2975.
18. Caldas LA, Carneiro FA, Higa LM, Monteiro FL, da Silva GP, da Costa LJ, Durigon EL, Tanuri A, de Souza W. 2020. Ultrastructural analysis of SARS-CoV-2 interactions with the host cell via high resolution scanning electron microscopy. Scientific Reports 10:16099.
19. Hartenian E, Nandakumar D, Lari A, Ly M, Tucker JM, Glaunsinger BA. 2020. The molecular virology of coronaviruses. Journal of Biological Chemistry 295:12910-12934.
20. Li Q, Wu J, Nie J, Zhang L, Hao H, Liu S, Zhao C, Zhang Q, Liu H, Nie L, Qin H, Wang M, Lu Q, Li X, Sun Q, Liu J, Zhang L, Li X, Huang W, Wang Y. 2020. The Impact of Mutations in SARS-CoV-2 Spike on Viral Infectivity and Antigenicity. Cell 182:1284-1294.e9.
21. Chakraborty C, Bhattacharya M, Sharma AR, Mallik B. 2022. Omicron (B.1.1.529) - A new heavily mutated variant: Mapped location and probable properties of its mutations with an emphasis on S-glycoprotein. Int J Biol Macromol 219:980-997.
22. Berry DM, Cruickshank JG, Chu HP, Wells RJH. 1964. The structure of infectious bronchitis virus. Virology 23:403-407.
23. Jackson CB, Farzan M, Chen B, Choe H. 2022. Mechanisms of SARS-CoV-2 entry into cells. Nature Reviews Molecular Cell Biology 23:3-20.
24. Greaney AJ, Loes AN, Crawford KHD, Starr TN, Malone KD, Chu HY, Bloom JD. 2021. Comprehensive mapping of mutations in the SARS-CoV-2 receptor-binding domain that affect recognition by polyclonal human plasma antibodies. Cell Host Microbe 29:463-476.e6.
25. Li W, Moore MJ, Vasilieva N, Sui J, Wong SK, Berne MA, Somasundaran M, Sullivan JL, Luzuriaga K, Greenough TC, Choe H, Farzan M. 2003. Angiotensin-converting enzyme 2 is a functional receptor for the SARS coronavirus. Nature 426:450-4.
26. Huang Y, Yang C, Xu X-f, Xu W, Liu S-w. 2020. Structural and functional properties of SARS-CoV-2 spike protein: potential antivirus drug development for COVID-19. Acta Pharmacologica Sinica 41:1141-1149.
27. Wang N, Shi X, Jiang L, Zhang S, Wang D, Tong P, Guo D, Fu L, Cui Y, Liu X, Arledge KC, Chen YH, Zhang L, Wang X. 2013. Structure of MERS-CoV spike receptor-binding domain complexed with human receptor DPP4. Cell Res 23:986-93.
28. Hofmann H, Pyrc K, van der Hoek L, Geier M, Berkhout B, Pöhlmann S. 2005. Human coronavirus NL63 employs the severe acute respiratory syndrome coronavirus receptor for cellular entry. Proc Natl Acad Sci U S A 102:7988-93.
29. Li Z, Tomlinson ACA, Wong AHM, Zhou D, Desforges M, Talbot PJ, Benlekbir S, Rubinstein JL, Rini JM. 2019. The human coronavirus HCoV-229E S-protein structure and receptor binding. eLife 8:e51230.
30. Hulswit RJG, Lang Y, Bakkers MJG, Li W, Li Z, Schouten A, Ophorst B, van Kuppeveld FJM, Boons G-J, Bosch B-J, Huizinga EG, de Groot RJ. 2019. Human coronaviruses OC43 and HKU1 bind to 9-O-acetylated sialic acids via a conserved receptor-binding site in spike protein domain A. Proc Natl Acad Sci USA, 116:2681-2690.
31. Zhou B, Thao TTN, Hoffmann D, Taddeo A, Ebert N, Labroussaa F, Pohlmann A, King J, Steiner S, Kelly JN, Portmann J, Halwe NJ, Ulrich L, Trüeb BS, Fan X, Hoffmann B, Wang L, Thomann L, Lin X, Stalder H, Pozzi B, de Brot S, Jiang N, Cui D, Hossain J, Wilson MM, Keller MW, Stark TJ, Barnes JR, Dijkman R, Jores J, Benarafa C, Wentworth DE, Thiel V, Beer M. 2021. SARS-CoV-2 spike D614G change enhances replication and transmission. Nature 592:122-127.
32. Mykytyn AZ, Breugem TI, Riesebosch S, Schipper D, van den Doel PB, Rottier RJ, Lamers MM, Haagmans BL. 2021. SARS-CoV-2 entry into human airway organoids is serine protease-mediated and facilitated by the multibasic cleavage site. eLife 10:e64508.

33. Johnson BA, Xie X, Bailey AL, Kalveram B, Lokugamage KG, Muruato A, Zou J, Zhang X, Juelich T, Smith JK, Zhang L, Bopp N, Schindewolf C, Vu M, Vanderheiden A, Winkler ES, Swetnam D, Plante JA, Aguilar P, Plante KS, Popov V, Lee B, Weaver SC, Suthar MS, Routh AL, Ren P, Ku Z, An Z, Debbink K, Diamond MS, Shi P-Y, Freiberg AN, Menachery VD. 2021. Loss of furin cleavage site attenuates SARS-CoV-2 pathogenesis. Nature 591:293-299.
34. Hoffmann M, Kleine-Weber H, Schroeder S, Krüger N, Herrler T, Erichsen S, Schiergens TS, Herrler G, Wu N-H, Nitsche A, Müller MA, Drosten C, Pöhlmann S. 2020. SARS-CoV-2 Cell Entry Depends on ACE2 and TMPRSS2 and Is Blocked by a Clinically Proven Protease Inhibitor. Cell 181:271-280.e8.
35. Fan X, Cao D, Kong L, Zhang X. 2020. Cryo-EM analysis of the post-fusion structure of the SARS-CoV spike glycoprotein. Nat Commun 11:3618.
36. Coutard B, Valle C, de Lamballerie X, Canard B, Seidah NG, Decroly E. 2020. The spike glycoprotein of the new coronavirus 2019-nCoV contains a furin-like cleavage site absent in CoV of the same clade. Antiviral Res 176:104742.
37. Bosch BJ, Bartelink W, Rottier PJ. 2008. Cathepsin L functionally cleaves the severe acute respiratory syndrome coronavirus class I fusion protein upstream of rather than adjacent to the fusion peptide. J Virol 82:8887-90.
38. Burkard C, Verheije MH, Wicht O, van Kasteren SI, van Kuppeveld FJ, Haagmans BL, Pelkmans L, Rottier PJM, Bosch BJ, de Haan CAM. 2014. Coronavirus Cell Entry Occurs through the Endo-/Lysosomal Pathway in a Proteolysis-Dependent Manner. PLOS Pathogens 10:e1004502.
39. Matsuyama S, Ujike M, Morikawa S, Tashiro M, Taguchi F. 2005. Protease-mediated enhancement of severe acute respiratory syndrome coronavirus infection. Proc Natl Acad Sci U S A 102:12543-7.
40. Huang IC, Bosch BJ, Li F, Li W, Lee KH, Ghiran S, Vasilieva N, Dermody TS, Harrison SC, Dormitzer PR, Farzan M, Rottier PJ, Choe H. 2006. SARS coronavirus, but not human coronavirus NL63, utilizes cathepsin L to infect ACE2-expressing cells. J Biol Chem 281:3198-203.
41. Bayati A, Kumar R, Francis V, McPherson PS. 2021. SARS-CoV-2 infects cells after viral entry via clathrin-mediated endocytosis. J Biol Chem 296:100306.
42. Shuai H, Chan JF, Hu B, Chai Y, Yuen TT, Yin F, Huang X, Yoon C, Hu JC, Liu H, Shi J, Liu Y, Zhu T, Zhang J, Hou Y, Wang Y, Lu L, Cai JP, Zhang AJ, Zhou J, Yuan S, Brindley MA, Zhang BZ, Huang JD, To KK, Yuen KY, Chu H. 2022. Attenuated replication and pathogenicity of SARS-CoV-2 B.1.1.529 Omicron. Nature 603:693-699.
43. Lempp FA, Soriaga LB, Montiel-Ruiz M, Benigni F, Noack J, Park YJ, Bianchi S, Walls AC, Bowen JE, Zhou J, Kaiser H, Joshi A, Agostini M, Meury M, Dellota E, Jr., Jaconi S, Cameroni E, Martinez-Picado J, Vergara-Alert J, Izquierdo-Useros N, Virgin HW, Lanzavecchia A, Veesler D, Purcell LA, Telenti A, Corti D. 2021. Lectins enhance SARS-CoV-2 infection and influence neutralizing antibodies. Nature 598:342-347.
44. Cantuti-Castelvetri L, Ojha R, Pedro LD, Djannatian M, Franz J, Kuivanen S, van der Meer F, Kallio K, Kaya T, Anastasina M, Smura T, Levanov L, Szirovicza L, Tobi A, Kallio-Kokko H, Österlund P, Joensuu M, Meunier FA, Butcher SJ, Winkler MS, Mollenhauer B, Helenius A, Gokce O, Teesalu T, Hepojoki J, Vapalahti O, Stadelmann C, Balistreri G, Simons M. 2020. Neuropilin-1 facilitates SARS-CoV-2 cell entry and infectivity. Science 370:856-860.
45. Wang S, Qiu Z, Hou Y, Deng X, Xu W, Zheng T, Wu P, Xie S, Bian W, Zhang C, Sun Z, Liu K, Shan C, Lin A, Jiang S, Xie Y, Zhou Q, Lu L, Huang J, Li X. 2021. AXL is a candidate receptor for SARS-CoV-2 that promotes infection of pulmonary and bronchial epithelial cells. Cell Research.
46. Wang K, Chen W, Zhang Z, Deng Y, Lian JQ, Du P, Wei D, Zhang Y, Sun XX, Gong L, Yang X, He L, Zhang L, Yang Z, Geng JJ, Chen R, Zhang H, Wang B, Zhu YM, Nan G, Jiang JL, Li L, Wu J, Lin

P, Huang W, Xie L, Zheng ZH, Zhang K, Miao JL, Cui HY, Huang M, Zhang J, Fu L, Yang XM, Zhao Z, Sun S, Gu H, Wang Z, Wang CF, Lu Y, Liu YY, Wang QY, Bian H, Zhu P, Chen ZN. 2020. CD147-spike protein is a novel route for SARS-CoV-2 infection to host cells. Signal Transduct Target Ther 5:283.

47. Malone B, Urakova N, Snijder EJ, Campbell EA. 2022. Structures and functions of coronavirus replication–transcription complexes and their relevance for SARS-CoV-2 drug design. Nature Reviews Molecular Cell Biology 23:21-39.
48. Lee HJ, Shieh CK, Gorbalenya AE, Koonin EV, La Monica N, Tuler J, Bagdzhadzhyan A, Lai MM. 1991. The complete sequence (22 kilobases) of murine coronavirus gene 1 encoding the putative proteases and RNA polymerase. Virology 180:567-82.
49. Anand K, Ziebuhr J, Wadhwani P, Mesters JR, Hilgenfeld R. 2003. Coronavirus main proteinase (3CLpro) structure: basis for design of anti-SARS drugs. Science 300:1763-7.
50. Park GJ, Osinski A, Hernandez G, Eitson JL, Majumdar A, Tonelli M, Henzler-Wildman K, Pawłowski K, Chen Z, Li Y, Schoggins JW, Tagliabracci VS. 2022. The mechanism of RNA capping by SARS-CoV-2. Nature 609:793-800.
51. Knoops K, Kikkert M, Worm SH, Zevenhoven-Dobbe JC, van der Meer Y, Koster AJ, Mommaas AM, Snijder EJ. 2008. SARS-coronavirus replication is supported by a reticulovesicular network of modified endoplasmic reticulum. PLoS Biol 6:e226.
52. Cortese M, Lee JY, Cerikan B, Neufeldt CJ, Oorschot VMJ, Köhrer S, Hennies J, Schieber NL, Ronchi P, Mizzon G, Romero-Brey I, Santarella-Mellwig R, Schorb M, Boermel M, Mocaer K, Beckwith MS, Templin RM, Gross V, Pape C, Tischer C, Frankish J, Horvat NK, Laketa V, Stanifer M, Boulant S, Ruggieri A, Chatel-Chaix L, Schwab Y, Bartenschlager R. 2020. Integrative Imaging Reveals SARS-CoV-2-Induced Reshaping of Subcellular Morphologies. Cell Host Microbe 28:853-866.e5.
53. Snijder EJ, Limpens R, de Wilde AH, de Jong AWM, Zevenhoven-Dobbe JC, Maier HJ, Faas F, Koster AJ, Bárcena M. 2020. A unifying structural and functional model of the coronavirus replication organelle: Tracking down RNA synthesis. PLoS Biol 18:e3000715.
54. Angelini MM, Akhlaghpour M, Neuman BW, Buchmeier MJ. 2013. Severe acute respiratory syndrome coronavirus nonstructural proteins 3, 4, and 6 induce double-membrane vesicles. mBio 4.
55. Wolff G, Limpens R, Zevenhoven-Dobbe JC, Laugks U, Zheng S, de Jong AWM, Koning RI, Agard DA, Grünewald K, Koster AJ, Snijder EJ, Bárcena M. 2020. A molecular pore spans the double membrane of the coronavirus replication organelle. Science 369:1395-1398.
56. V'kovski P, Kratzel A, Steiner S, Stalder H, Thiel V. 2021. Coronavirus biology and replication: implications for SARS-CoV-2. Nature Reviews Microbiology 19:155-170.
57. Gorbalenya AE, Enjuanes L, Ziebuhr J, Snijder EJ. 2006. Nidovirales: evolving the largest RNA virus genome. Virus Res 117:17-37.
58. Gong Y, Qin S, Dai L, Tian Z. 2021. The glycosylation in SARS-CoV-2 and its receptor ACE2. Signal Transduction and Targeted Therapy 6:396.
59. Bouwman KM, Tomris I, Turner HL, van der Woude R, Shamorkina TM, Bosman GP, Rockx B, Herfst S, Snijder J, Haagmans BL, Ward AB, Boons G-J, de Vries RP. 2021. Multimerization- and glycosylation-dependent receptor binding of SARS-CoV-2 spike proteins. PLOS Pathogens 17:e1009282.
60. Casas-Sanchez A, Romero-Ramirez A, Hargreaves E, Ellis CC, Grajeda BI, Estevao IL, Patterson EI, Hughes GL, Almeida IC, Zech T, Acosta-Serrano Á. 2022. Inhibition of Protein N-Glycosylation Blocks SARS-CoV-2 Infection. mBio 13:e03718-21.
61. Ghosh S, Dellibovi-Ragheb TA, Kerviel A, Pak E, Qiu Q, Fisher M, Takvorian PM, Bleck C, Hsu VW, Fehr AR, Perlman S, Achar SR, Straus MR, Whittaker GR, de Haan CAM, Kehrl J, Altan-Bonnet G, Altan-Bonnet N. 2020. β-Coronaviruses Use Lysosomes for Egress Instead of the Biosynthetic Secretory Pathway. Cell 183:1520-1535.e14.

62. Iwasaki A, Foxman EF, Molony RD. 2017. Early local immune defences in the respiratory tract. Nature reviews Immunology 17:7-20.
63. Hiemstra PS, McCray PB, Jr., Bals R. 2015. The innate immune function of airway epithelial cells in inflammatory lung disease. The European respiratory journal 45:1150-1162.
64. Hewitt RJ, Lloyd CM. 2021. Regulation of immune responses by the airway epithelial cell landscape. Nature Reviews Immunology 21:347-362.
65. Guillot L, Nathan N, Tabary O, Thouvenin G, Le Rouzic P, Corvol H, Amselem S, Clement A. 2013. Alveolar epithelial cells: Master regulators of lung homeostasis. The International Journal of Biochemistry & Cell Biology 45:2568-2573.
66. Parker D, Prince A. 2011. Innate immunity in the respiratory epithelium. American journal of respiratory cell and molecular biology 45:189-201.
67. Ahn JH, Kim J, Hong SP, Choi SY, Yang MJ, Ju YS, Kim YT, Kim HM, Rahman MDT, Chung MK, Hong SD, Bae H, Lee CS, Koh GY. 2021. Nasal ciliated cells are primary targets for SARS-CoV-2 replication in the early stage of COVID-19. J Clin Invest 131.
68. Ziegler CGK, Allon SJ, Nyquist SK, Mbano IM, Miao VN, Tzouanas CN, Cao Y, Yousif AS, Bals J, Hauser BM, Feldman J, Muus C, Wadsworth MH, II, Kazer SW, Hughes TK, Doran B, Gatter GJ, Vukovic M, Taliaferro F, Mead BE, Guo Z, Wang JP, Gras D, Plaisant M, Ansari M, Angelidis I, Adler H, Sucre JMS, Taylor CJ, Lin B, Waghray A, Mitsialis V, Dwyer DF, Buchheit KM, Boyce JA, Barrett NA, Laidlaw TM, Carroll SL, Colonna L, Tkachev V, Peterson CW, Yu A, Zheng HB, Gideon HP, Winchell CG, Lin PL, Bingle CD, Snapper SB, Kropski JA, Theis FJ, et al. 2020. SARS-CoV-2 Receptor ACE2 Is an Interferon-Stimulated Gene in Human Airway Epithelial Cells and Is Detected in Specific Cell Subsets across Tissues. Cell 181:1016-1035.e19.
69. Zhu N, Wang W, Liu Z, Liang C, Wang W, Ye F, Huang B, Zhao L, Wang H, Zhou W, Deng Y, Mao L, Su C, Qiang G, Jiang T, Zhao J, Wu G, Song J, Tan W. 2020. Morphogenesis and cytopathic effect of SARS-CoV-2 infection in human airway epithelial cells. Nature Communications 11:3910.
70. de Wit E, Rasmussen AL, Falzarano D, Bushmaker T, Feldmann F, Brining DL, Fischer ER, Martellaro C, Okumura A, Chang J, Scott D, Benecke AG, Katze MG, Feldmann H, Munster VJ. 2013. Middle East respiratory syndrome coronavirus (MERS-CoV) causes transient lower respiratory tract infection in rhesus macaques. Proc Natl Acad Sci U S A 110:16598-603.
71. Hao S, Ning K, Kuz CA, Vorhies K, Yan Z, Qiu J. 2020. Long-Term Modeling of SARS-CoV-2 Infection of In Vitro Cultured Polarized Human Airway Epithelium. mBio 11.
72. Kindler E, Jónsdóttir HR, Muth D, Hamming OJ, Hartmann R, Rodriguez R, Geffers R, Fouchier RAM, Drosten C, Müller MA, Dijkman R, Thiel V, Buchmeier MJ. 2013. Efficient Replication of the Novel Human Betacoronavirus EMC on Primary Human Epithelium Highlights Its Zoonotic Potential. mBio 4:e00611-12.
73. Otter Clayton J, Fausto A, Tan Li H, Khosla Alisha S, Cohen Noam A, Weiss Susan R. 2023. Infection of primary nasal epithelial cells differentiates among lethal and seasonal human coronaviruses. Proc Natl Acad Sci U S A 120:e2218083120.
74. Dijkman R, Jebbink MF, Koekkoek SM, Deijs M, Jónsdóttir HR, Molenkamp R, Ieven M, Goossens H, Thiel V, van der Hoek L. 2013. Isolation and characterization of current human coronavirus strains in primary human epithelial cell cultures reveal differences in target cell tropism. Journal of virology 87:6081-6090.
75. Liu Y, Liu J, Johnson BA, Xia H, Ku Z, Schindewolf C, Widen SG, An Z, Weaver SC, Menachery VD, Xie X, Shi P-Y. 2022. Delta spike P681R mutation enhances SARS-CoV-2 fitness over Alpha variant. Cell Reports 39:110829.
76. Hou YJ, Chiba S, Halfmann P, Ehre C, Kuroda M, Dinnon KH, Leist SR, Schäfer A, Nakajima N, Takahashi K, Lee RE, Mascenik TM, Graham R, Edwards CE, Tse LV, Okuda K, Markmann AJ, Bartelt L, de Silva A, Margolis DM, Boucher RC, Randell SH, Suzuki T, Gralinski LE, Kawaoka

Y, Baric RS. 2020. SARS-CoV-2 D614G variant exhibits efficient replication ex vivo and transmission in vivo. Science 370:1464-1468.
77. Mannar D, Saville JW, Zhu X, Srivastava SS, Berezuk AM, Tuttle KS, Marquez AC, Sekirov I, Subramaniam S. 2022. SARS-CoV-2 Omicron variant: Antibody evasion and cryo-EM structure of spike protein-ACE2 complex. Science 375:760-764.
78. Hui KPY, Ho JCW, Cheung M-c, Ng K-c, Ching RHH, Lai K-l, Kam TT, Gu H, Sit K-Y, Hsin MKY, Au TWK, Poon LLM, Peiris M, Nicholls JM, Chan MCW. 2022. SARS-CoV-2 Omicron variant replication in human bronchus and lung ex vivo. Nature 603:715-720.
79. Lamers MM, Mykytyn AZ, Breugem TI, Groen N, Knoops K, Schipper D, van Acker R, van den Doel PB, Bestebroer T, Koopman CD, Reusken C, Muraro MJ, GeurtsvanKessel CH, van Royen ME, Peters PJ, Zhang J, Haagmans BL. 2022. SARS-CoV-2 Omicron efficiently infects human airway, but not alveolar epithelium. Preprint bioRxiv 2022.01.19.476898.
80. Willett BJ, Grove J, MacLean OA, Wilkie C, De Lorenzo G, Furnon W, Cantoni D, Scott S, Logan N, Ashraf S, Manali M, Szemiel A, Cowton V, Vink E, Harvey WT, Davis C, Asamaphan P, Smollett K, Tong L, Orton R, Hughes J, Holland P, Silva V, Pascall DJ, Puxty K, da Silva Filipe A, Yebra G, Shaaban S, Holden MTG, Pinto RM, Gunson R, Templeton K, Murcia PR, Patel AH, Klenerman P, Dunachie S, Dunachie S, Klenerman P, Barnes E, Brown A, Adele S, Kronsteiner B, Murray SM, Abraham P, Deeks A, Ansari MA, de Silva T, Turtle L, Moore S, Austin J, et al. 2022. SARS-CoV-2 Omicron is an immune escape variant with an altered cell entry pathway. Nature Microbiology 7:1161-1179.
81. Cui Z, Liu P, Wang N, Wang L, Fan K, Zhu Q, Wang K, Chen R, Feng R, Jia Z, Yang M, Xu G, Zhu B, Fu W, Chu T, Feng L, Wang Y, Pei X, Yang P, Xie XS, Cao L, Cao Y, Wang X. 2022. Structural and functional characterizations of infectivity and immune evasion of SARS-CoV-2 Omicron. Cell 185:860-871.e13.
82. Liu Y, Rocklöv J. 2022. The effective reproductive number of the Omicron variant of SARS-CoV-2 is several times relative to Delta. J Travel Med 29.
83. Araf Y, Akter F, Tang YD, Fatemi R, Parvez MSA, Zheng C, Hossain MG. 2022. Omicron variant of SARS-CoV-2: Genomics, transmissibility, and responses to current COVID-19 vaccines. J Med Virol 94:1825-1832.
84. Grainge CL, Davies DE. 2013. Epithelial Injury and Repair in Airways Diseases. Chest 144:1906-1912.
85. Wark PA, Johnston SL, Bucchieri F, Powell R, Puddicombe S, Laza-Stanca V, Holgate ST, Davies DE. 2005. Asthmatic bronchial epithelial cells have a deficient innate immune response to infection with rhinovirus. J Exp Med 201:937-47.
86. Osan J, Talukdar SN, Feldmann F, DeMontigny BA, Jerome K, Bailey KL, Feldmann H, Mehedi M. 2022. Goblet Cell Hyperplasia Increases SARS-CoV-2 Infection in Chronic Obstructive Pulmonary Disease. Microbiol Spectr 10:e0045922.
87. Seys LJM, Widagdo W, Verhamme FM, Kleinjan A, Janssens W, Joos GF, Bracke KR, Haagmans BL, Brusselle GG. 2017. DPP4, the Middle East Respiratory Syndrome Coronavirus Receptor, is Upregulated in Lungs of Smokers and Chronic Obstructive Pulmonary Disease Patients. Clinical Infectious Diseases 66:45-53.
88. Lamers MM, Haagmans BL. 2022. SARS-CoV-2 pathogenesis. Nature Reviews Microbiology 20:270-284.
89. Guan WJ, Ni ZY, Hu Y, Liang WH, Ou CQ, He JX, Liu L, Shan H, Lei CL, Hui DSC, Du B, Li LJ, Zeng G, Yuen KY, Chen RC, Tang CL, Wang T, Chen PY, Xiang J, Li SY, Wang JL, Liang ZJ, Peng YX, Wei L, Liu Y, Hu YH, Peng P, Wang JM, Liu JY, Chen Z, Li G, Zheng ZJ, Qiu SQ, Luo J, Ye CJ, Zhu SY, Zhong NS. 2020. Clinical Characteristics of Coronavirus Disease 2019 in China. N Engl J Med 382:1708-1720.
90. Dong Y, Mo X, Hu Y, Qi X, Jiang F, Jiang Z, Tong S. 2020. Epidemiology of COVID-19 Among Children in China. Pediatrics 145.

91. Chen N, Zhou M, Dong X, Qu J, Gong F, Han Y, Qiu Y, Wang J, Liu Y, Wei Y, Xia J, Yu T, Zhang X, Zhang L. 2020. Epidemiological and clinical characteristics of 99 cases of 2019 novel coronavirus pneumonia in Wuhan, China: a descriptive study. Lancet 395:507-513.
92. Huang C, Wang Y, Li X, Ren L, Zhao J, Hu Y, Zhang L, Fan G, Xu J, Gu X, Cheng Z, Yu T, Xia J, Wei Y, Wu W, Xie X, Yin W, Li H, Liu M, Xiao Y, Gao H, Guo L, Xie J, Wang G, Jiang R, Gao Z, Jin Q, Wang J, Cao B. 2020. Clinical features of patients infected with 2019 novel coronavirus in Wuhan, China. Lancet 395:497-506.
93. Epidemiology Working Group for NCIP Epidemic Response, Zhonghua Liu Xing Bing Xue Za Z. 2020. The epidemiological characteristics of an outbreak of 2019 novel coronavirus diseases (COVID-19) in China. Chinese Center for Disease Control and Prevention 41:145-151.
94. Petersen E, Koopmans M, Go U, Hamer DH, Petrosillo N, Castelli F, Storgaard M, Al Khalili S, Simonsen L. 2020. Comparing SARS-CoV-2 with SARS-CoV and influenza pandemics. Lancet Infect Dis 20:e238-e244.
95. Mahajan S, Caraballo C, Li SX, Dong Y, Chen L, Huston SK, Srinivasan R, Redlich CA, Ko AI, Faust JS, Forman HP, Krumholz HM. 2021. SARS-CoV-2 Infection Hospitalization Rate and Infection Fatality Rate Among the Non-Congregate Population in Connecticut. Am J Med 134:812-816.e2.
96. Horita N, Fukumoto T. 2023. Global case fatality rate from COVID-19 has decreased by 96.8% during 2.5 years of the pandemic. J Med Virol 95:e28231.
97. Lew TWK, Kwek T-K, Tai D, Earnest A, Loo S, Singh K, Kwan KM, Chan Y, Yim CF, Bek SL, Kor AC, Yap WS, Chelliah YR, Lai YC, Goh S-K. 2003. Acute Respiratory Distress Syndrome in Critically Ill Patients With Severe Acute Respiratory Syndrome. JAMA 290:374-380.
98. van den Brand JM, Smits SL, Haagmans BL. 2015. Pathogenesis of Middle East respiratory syndrome coronavirus. J Pathol 235:175-84.
99. Butowt R, Bilinska K, von Bartheld CS. 2023. Olfactory dysfunction in COVID-19: new insights into the underlying mechanisms. Trends Neurosci 46:75-90.
100. Davis HE, McCorkell L, Vogel JM, Topol EJ. 2023. Long COVID: major findings, mechanisms and recommendations. Nat Rev Microbiol 21:133-146.
101. Yin X, Riva L, Pu Y, Martin-Sancho L, Kanamune J, Yamamoto Y, Sakai K, Gotoh S, Miorin L, De Jesus PD, Yang CC, Herbert KM, Yoh S, Hultquist JF, García-Sastre A, Chanda SK. 2021. MDA5 Governs the Innate Immune Response to SARS-CoV-2 in Lung Epithelial Cells. Cell Rep 34:108628.
102. Thorne LG, Reuschl AK, Zuliani-Alvarez L, Whelan MVX, Turner J, Noursadeghi M, Jolly C, Towers GJ. 2021. SARS-CoV-2 sensing by RIG-I and MDA5 links epithelial infection to macrophage inflammation. Embo j 40:e107826.
103. Kim Y-M, Shin E-C. 2021. Type I and III interferon responses in SARS-CoV-2 infection. Experimental & Molecular Medicine 53:750-760.
104. Diamond MS, Kanneganti T-D. 2022. Innate immunity: the first line of defense against SARS-CoV-2. Nature Immunology 23:165-176.
105. Zheng M, Karki R, Williams EP, Yang D, Fitzpatrick E, Vogel P, Jonsson CB, Kanneganti T-D. 2021. TLR2 senses the SARS-CoV-2 envelope protein to produce inflammatory cytokines. Nature Immunology 22:829-838.
106. Zheng M, Williams EP, Malireddi RKS, Karki R, Banoth B, Burton A, Webby R, Channappanavar R, Jonsson CB, Kanneganti TD. 2020. Impaired NLRP3 inflammasome activation/pyroptosis leads to robust inflammatory cell death via caspase-8/RIPK3 during coronavirus infection. J Biol Chem 295:14040-14052.
107. Rui Y, Su J, Shen S, Hu Y, Huang D, Zheng W, Lou M, Shi Y, Wang M, Chen S, Zhao N, Dong Q, Cai Y, Xu R, Zheng S, Yu X-F. 2021. Unique and complementary suppression of cGAS-STING

and RNA sensing- triggered innate immune responses by SARS-CoV-2 proteins. Signal Transduction and Targeted Therapy 6:123.
108. Schneider WM, Chevillotte MD, Rice CM. 2014. Interferon-stimulated genes: a complex web of host defenses. Annu Rev Immunol 32:513-45.
109. Totura AL, Baric RS. 2012. SARS coronavirus pathogenesis: host innate immune responses and viral antagonism of interferon. Curr Opin Virol 2:264-75.
110. Clementz MA, Chen Z, Banach BS, Wang Y, Sun L, Ratia K, Baez-Santos YM, Wang J, Takayama J, Ghosh AK, Li K, Mesecar AD, Baker SC. 2010. Deubiquitinating and Interferon Antagonism Activities of Coronavirus Papain-Like Proteases. J.Virol. 84:4619-4629.
111. Minkoff JM, tenOever B. 2023. Innate immune evasion strategies of SARS-CoV-2. Nature Reviews Microbiology 21:178-194.
112. Kindler E, Thiel V, Weber F. 2016. Interaction of SARS and MERS Coronaviruses with the Antiviral Interferon Response. Adv Virus Res 96:219-243.
113. Frere JJ, Serafini RA, Pryce KD, Zazhytska M, Oishi K, Golynker I, Panis M, Zimering J, Horiuchi S, Hoagland DA, Møller R, Ruiz A, Kodra A, Overdevest JB, Canoll PD, Borczuk AC, Chandar V, Bram Y, Schwartz R, Lomvardas S, Zachariou V, tenOever BR. 2022. SARS-CoV-2 infection in hamsters and humans results in lasting and unique systemic perturbations after recovery. Sci Transl. Med. 14:eabq3059.
114. Channappanavar R, Fehr AR, Vijay R, Mack M, Zhao J, Meyerholz DK, Perlman S. 2016. Dysregulated Type I Interferon and Inflammatory Monocyte-Macrophage Responses Cause Lethal Pneumonia in SARS-CoV-Infected Mice. Cell Host Microbe 19:181-93.
115. Leisman DE, Ronner L, Pinotti R, Taylor MD, Sinha P, Calfee CS, Hirayama AV, Mastroiani F, Turtle CJ, Harhay MO, Legrand M, Deutschman CS. 2020. Cytokine elevation in severe and critical COVID-19: a rapid systematic review, meta-analysis, and comparison with other inflammatory syndromes. Lancet Respir Med 8:1233-1244.
116. Blanco-Melo D, Nilsson-Payant BE, Liu W-C, Uhl S, Hoagland D, Møller R, Jordan TX, Oishi K, Panis M, Sachs D, Wang TT, Schwartz RE, Lim JK, Albrecht RA, tenOever BR. 2020. Imbalanced Host Response to SARS-CoV-2 Drives Development of COVID-19. Cell 181:1036-1045.e9.
117. Nilsson-Payant BE, Uhl S, Grimont A, Doane AS, Cohen P, Patel RS, Higgins CA, Acklin JA, Bram Y, Chandar V, Blanco-Melo D, Panis M, Lim JK, Elemento O, Schwartz RE, Rosenberg BR, Chandwani R, tenOever BR. 2021. The NF-κB Transcriptional Footprint Is Essential for SARS-CoV-2 Replication. J Virol 95:e0125721.
118. Paludan SR, Mogensen TH. 2022. Innate immunological pathways in COVID-19 pathogenesis. Sci Immunol. 7:eabm5505.
119. Heinen N, Klöhn M, Steinmann E, Pfaender S. 2021. In Vitro Lung Models and Their Application to Study SARS-CoV-2 Pathogenesis and Disease. Viruses 13.
120. Zaliani A, Vangeel L, Reinshagen J, Iaconis D, Kuzikov M, Keminer O, Wolf M, Ellinger B, Esposito F, Corona A, Tramontano E, Manelfi C, Herzog K, Jochmans D, De Jonghe S, Chiu W, Francken T, Schepers J, Collard C, Abbasi K, Claussen C, Summa V, Beccari AR, Neyts J, Gribbon P, Leyssen P. 2022. Cytopathic SARS-CoV-2 screening on VERO-E6 cells in a large-scale repurposing effort. Scientific Data 9:405.
121. Bestion E, Halfon P, Mezouar S, Mège JL. 2022. Cell and Animal Models for SARS-CoV-2 Research. Viruses 14.
122. Ogando NS, Dalebout TJ, Zevenhoven-Dobbe JC, Limpens R, van der Meer Y, Caly L, Druce J, de Vries JJC, Kikkert M, Bárcena M, Sidorov I, Snijder EJ. 2020. SARS-coronavirus-2 replication in Vero E6 cells: replication kinetics, rapid adaptation and cytopathology. J Gen Virol 101:925-940.

123. Lamers MM, Mykytyn AZ, Breugem TI, Wang Y, Wu DC, Riesebosch S, van den Doel PB, Schipper D, Bestebroer T, Wu NC, Haagmans BL. 2021. Human airway cells prevent SARS-CoV-2 multibasic cleavage site cell culture adaptation. Elife 10.
124. Wang Y, Wang P, Qin J. 2022. Human Organoids and Organs-on-Chips for Addressing COVID-19 Challenges. Adv Sci (Weinh) 9:e2105187.
125. Rijsbergen LC, van Dijk LLA, Engel MFM, de Vries RD, de Swart RL. 2021. In Vitro Modelling of Respiratory Virus Infections in Human Airway Epithelial Cells – A Systematic Review. Front. Immunol.
126. Hiemstra PS, Tetley TD, Janes SM. 2019. Airway and alveolar epithelial cells in culture. European Respiratory Journal 54:1900742.
127. Lodes N. SK, Perniss A., Nietzer S., Oberwinkler H., May T., Walles T., Hebestreit H., Hackenberg S., Steinke M. 2020. Investigation on Ciliary Functionality of Different Airway Epithelial Cell Lines in Three-Dimensional Cell Culture. Tissue Eng Part A 26:432-440.
128. Ross AJ, Dailey LA, Brighton LE, Devlin RB. 2007. Transcriptional Profiling of Mucociliary Differentiation in Human Airway Epithelial Cells. Am J Respir Cell Mol Biol. 37:169-185.
129. Dvorak A, Tilley AE, Shaykhiev R, Wang R, Crystal RG. 2011. Do airway epithelium air-liquid cultures represent the in vivo airway epithelium transcriptome? Am J Respir Cell Mol Biol 44:465-73.
130. Bovard D, Giralt A, Trivedi K, Neau L, Kanellos P, Iskandar A, Kondylis A, Luettich K, Frentzel S, Hoeng J, Peitsch MC. 2020. Comparison of the basic morphology and function of 3D lung epithelial cultures derived from several donors. Current Research in Toxicology 1:56-69.
131. Belgacemi R, Luczka E, Ancel J, Diabasana Z, Perotin JM, Germain A, Lalun N, Birembaut P, Dubernard X, Mérol JC, Delepine G, Polette M, Deslée G, Dormoy V. 2020. Airway epithelial cell differentiation relies on deficient Hedgehog signalling in COPD. EBioMedicine 51:102572.
132. Thaler M, Wang Y, van der Does AM, Faiz A, Ninaber DK, Ogando NS, Beckert H, Taube C, Salgado-Benvindo C, Snijder EJ, Bredenbeek PJ, Hiemstra PS, van Hemert MJ. 2023. Impact of Changes in Human Airway Epithelial Cellular Composition and Differentiation on SARS-CoV-2 Infection Biology. Journal of Innate Immunity 15:562-580.
133. Leung C, Wadsworth SJ, Yang SJ, Dorscheid DR. 2020. Structural and functional variations in human bronchial epithelial cells cultured in air-liquid interface using different growth media. Am J Physiol Lung Cell Mol Physiol 318:L1063-l1073.
134. Mertens TCJ, Karmouty-Quintana H, Taube C, Hiemstra PS. 2017. Use of airway epithelial cell culture to unravel the pathogenesis and study treatment in obstructive airway diseases. Pulmonary Pharmacology & Therapeutics 45:101-113.
135. Goldmann T, Zissel G, Watz H, Drömann D, Reck M, Kugler C, Rabe KF, Marwitz S. 2018. Human alveolar epithelial cells type II are capable of TGFβ-dependent epithelial-mesenchymal-transition and collagen-synthesis. Respiratory Research 19:138.
136. Barreto-Duran E, Szczepański A, Gałuszka-Bulaga A, Surmiak M, Siedlar M, Sanak M, Rajfur Z, Milewska A, Lenart M, Pyrć K. 2022. The interplay between the airway epithelium and tissue macrophages during the SARS-CoV-2 infection. Front Immunol
137. Vanderheiden A, Ralfs P, Chirkova T, Upadhyay AA, Zimmerman MG, Bedoya S, Aoued H, Tharp GM, Pellegrini KL, Manfredi C, Sorscher E, Mainou B, Lobby JL, Kohlmeier JE, Lowen AC, Shi P-Y, Menachery VD, Anderson LJ, Grakoui A, Bosinger SE, Suthar MS. 2020. Type I and Type III Interferons Restrict SARS-CoV-2 Infection of Human Airway Epithelial Cultures. J Virol. 94:e00985-20.
138. Huang J, Hume AJ, Abo KM, Werder RB, Villacorta-Martin C, Alysandratos KD, Beermann ML, Simone-Roach C, Lindstrom-Vautrin J, Olejnik J, Suder EL, Bullitt E, Hinds A, Sharma A, Bosmann M, Wang R, Hawkins F, Burks EJ, Saeed M, Wilson AA, Mühlberger E, Kotton DN.

2020. SARS-CoV-2 Infection of Pluripotent Stem Cell-Derived Human Lung Alveolar Type 2 Cells Elicits a Rapid Epithelial-Intrinsic Inflammatory Response. Cell Stem Cell 27:962-973.e7.
139. Pizzorno A, Padey B, Julien T, Trouillet-Assant S, Traversier A, Errazuriz-Cerda E, Fouret J, Dubois J, Gaymard A, Lescure FX, Dulière V, Brun P, Constant S, Poissy J, Lina B, Yazdanpanah Y, Terrier O, Rosa-Calatrava M. 2020. Characterization and Treatment of SARS-CoV-2 in Nasal and Bronchial Human Airway Epithelia. Cell Rep Med 1:100059.
140. Mache C, Schulze J, Holland G, Bourquain D, Gensch J-M, Oh D-Y, Nitsche A, Dürrwald R, Laue M, Wolff T. 2022. SARS-CoV-2 Omicron variant is attenuated for replication in a polarized human lung epithelial cell model. Communications Biology 5:1138.
141. Mulay A, Konda B, Garcia G, Yao C, Beil S, Villalba JM, Koziol C, Sen C, Purkayastha A, Kolls JK, Pociask DA, Pessina P, de Aja JS, Garcia-de-Alba C, Kim CF, Gomperts B, Arumugaswami V, Stripp BR. 2021. SARS-CoV-2 infection of primary human lung epithelium for COVID-19 modeling and drug discovery. Cell Reports 35:109055.
142. Do TND, Chatterjee AK, Gallay PA, Bobardt MD, Vangeel L, De Jonghe S, Neyts J, Jochmans D. 2021. A robust SARS-CoV-2 replication model in primary human epithelial cells at the air liquid interface to assess antiviral agents. Antiviral Research 2021.03.25.436907.
143. Sheahan TP, Sims AC, Zhou S, Graham RL, Pruijssers AJ, Agostini ML, Leist SR, Schäfer A, Dinnon KH, Stevens LJ, Chappell JD, Lu X, Hughes TM, George AS, Hill CS, Montgomery SA, Brown AJ, Bluemling GR, Natchus MG, Saindane M, Kolykhalov AA, Painter G, Harcourt J, Tamin A, Thornburg NJ, Swanstrom R, Denison MR, Baric RS. 2020. An orally bioavailable broad-spectrum antiviral inhibits SARS-CoV-2 in human airway epithelial cell cultures and multiple coronaviruses in mice. Science Transl. Med.
144. De Clercq E. 2002. Strategies in the design of antiviral drugs. Nature Reviews Drug Discovery 1:13-25.
145. De Clercq E, Li G. 2016. Approved Antiviral Drugs over the Past 50 Years. Clin Microbiol Rev 29:695-747.
146. De Clercq E. 1997. In search of a selective antiviral chemotherapy. Clin Microbiol Rev 10:674-693.
147. Ng KE. 2019. Xofluza (Baloxavir Marboxil) for the Treatment Of Acute Uncomplicated Influenza. Pharmacy & Therapeutics 44:9-11.
148. Gilead Sciences Canada I. 2018. CADTH Common Drug Reviews, Clinical Review Report: Bictegravir/Emtricitabine/Tenofovir Alafenamide (B/FTC/TAF) (Biktarvy): A complete regimen for the treatment of HIV-1 infection in adults with no known substitution associated with resistance to the individual components of Biktarvy. Canadian Agency for Drugs and Technologies in Health. Copyright © 2018 Canadian Agency for Drugs and Technologies in Health., Ottawa (ON).
149. Gilead Sciences Canada I. 2018. CADTH Common Drug Reviews, Pharmacoeconomic Review Report: Sofosbuvir/Velpatasvir/Voxilaprevir (Vosevi): Hepatitis C infection genotype 1 to 6. Canadian Agency for Drugs and Technologies in Health. Copyright © 2018 Canadian Agency for Drugs and Technologies in Health., Ottawa (ON).
150. Harris E. 2023. FDA Grants Full Approval to Paxlovid, COVID-19 Antiviral Treatment. Jama 329:2118.
151. Bredeek UF, Harbour MJ. 2007. CCR5 antagonists in the treatment of treatment-naive patients infected with CCR5 tropic HIV-1. Eur J Med Res 12:427-34.
152. Chahine EB. 2021. Fostemsavir: The first oral attachment inhibitor for treatment of HIV-1 infection. Am J Health Syst Pharm 78:376-388.
153. Keppeke GD, Calise SJ, Chan EKL, Andrade LEC. 2019. Ribavirin induces widespread accumulation of IMP dehydrogenase into rods/rings structures in multiple major mouse organs. Antiviral Res 162:130-135.

154. Thomas E, Ghany MG, Liang TJ. 2012. The application and mechanism of action of ribavirin in therapy of hepatitis C. Antivir Chem Chemother 23:1-12.
155. Chaudhuri S, Symons JA, Deval J. 2018. Innovation and trends in the development and approval of antiviral medicines: 1987–2017 and beyond. Antiviral Research 155:76-88.
156. Kumar N, Sharma S, Kumar R, Tripathi BN, Barua S, Ly H, Rouse BT. 2020. Host-Directed Antiviral Therapy. Clin Microbiol. Rev 33:10.1128/cmr.00168-19.
157. Mousavi Maleki MS, Sardari S, Ghandehari Alavijeh A, Madanchi H. 2022. Recent Patents and FDA-Approved Drugs Based on Antiviral Peptides and Other Peptide-Related Antivirals. International Journal of Peptide Research and Therapeutics 29:5.
158. Zhu Y, Zhu L, Wang X, Jin H. 2022. RNA-based therapeutics: an overview and prospectus. Cell Death & Disease 13:644.
159. Meganck RM, Baric RS. 2021. Developing therapeutic approaches for twenty-first-century emerging infectious viral diseases. Nature Medicine 27:401-410.
160. Li G, Hilgenfeld R, Whitley R, De Clercq E. 2023. Therapeutic strategies for COVID-19: progress and lessons learned. Nature Reviews Drug Discovery 22:449-475.
161. Riva L, Yuan S, Yin X, Martin-Sancho L, Matsunaga N, Pache L, Burgstaller-Muehlbacher S, De Jesus PD, Teriete P, Hull MV, Chang MW, Chan JF-W, Cao J, Poon VK-M, Herbert KM, Cheng K, Nguyen T-TH, Rubanov A, Pu Y, Nguyen C, Choi A, Rathnasinghe R, Schotsaert M, Miorin L, Dejosez M, Zwaka TP, Sit K-Y, Martinez-Sobrido L, Liu W-C, White KM, Chapman ME, Lendy EK, Glynne RJ, Albrecht R, Ruppin E, Mesecar AD, Johnson JR, Benner C, Sun R, Schultz PG, Su AI, García-Sastre A, Chatterjee AK, Yuen K-Y, Chanda SK. 2020. Discovery of SARS-CoV-2 antiviral drugs through large-scale compound repurposing. Nature 586:113-119.
162. von Delft A, Hall MD, Kwong AD, Purcell LA, Saikatendu KS, Schmitz U, Tallarico JA, Lee AA. 2023. Accelerating antiviral drug discovery: lessons from COVID-19. Nature Reviews Drug Discovery 22:585-603.
163. Tiwari PC, Pal R, Chaudhary MJ, Nath R. 2023. Artificial intelligence revolutionizing drug development: Exploring opportunities and challenges. Drug Dev Res 84(8):1652-1663.
164. Parker WB. 2005. Metabolism and antiviral activity of ribavirin. Virus Research 107:165-171.
165. Cihlar T, Mackman RL. 2022. Journey of remdesivir from the inhibition of hepatitis C virus to the treatment of COVID-19. Antiviral Therapy 27:13596535221082773.
166. Steinmetz KL, Spack EG. 2009. The basics of preclinical drug development for neurodegenerative disease indications. BMC Neurology 9:S2.
167. de Wilde AH, Raj VS, Oudshoorn D, Bestebroer TM, van Nieuwkoop S, Limpens R, Posthuma CC, van der Meer Y, Bárcena M, Haagmans BL, Snijder EJ, van den Hoogen BG. 2013. MERS-coronavirus replication induces severe in vitro cytopathology and is strongly inhibited by cyclosporin A or interferon-α treatment. J Gen Virol 94:1749-1760.
168. Arabi YM, Alothman A, Balkhy HH, Al-Dawood A, AlJohani S, Al Harbi S, Kojan S, Al Jeraisy M, Deeb AM, Assiri AM, Al-Hameed F, AlSaedi A, Mandourah Y, Almekhlafi GA, Sherbeeni NM, Elzein FE, Memon J, Taha Y, Almotairi A, Maghrabi KA, Qushmaq I, Al Bshabshe A, Kharaba A, Shalhoub S, Jose J, Fowler RA, Hayden FG, Hussein MA, Arabi YM, Alothman A, Balkhy HH, Al-Dawood A, AlJohani S, Al Harbi S, Kojan S, Al Jeraisy M, Deeb AM, Jose J, Hussein MA, Al Muhaidib M, Sadat M, Al Anizi H, Dael R, Assiri AM, AlMazroa M, Asiri A, Memish ZA, Ghazal SS, Alfaraj SH, Bafaqeeh F, et al. 2018. Treatment of Middle East Respiratory Syndrome with a combination of lopinavir-ritonavir and interferon-β1b (MIRACLE trial): study protocol for a randomized controlled trial. Trials 19:81.
169. Al Ghamdi M, Alghamdi KM, Ghandoora Y, Alzahrani A, Salah F, Alsulami A, Bawayan MF, Vaidya D, Perl TM, Sood G. 2016. Treatment outcomes for patients with Middle Eastern Respiratory Syndrome Coronavirus (MERS CoV) infection at a coronavirus referral center in the Kingdom of Saudi Arabia. BMC Infect Dis 16:174.

170. Momattin H, Al-Ali AY, Al-Tawfiq JA. 2019. A Systematic Review of therapeutic agents for the treatment of the Middle East Respiratory Syndrome Coronavirus (MERS-CoV). Travel Medicine and Infectious Disease 30:9-18.
171. Stockman LJ, Bellamy R, Garner P. 2006. SARS: Systematic Review of Treatment Effects. PLOS Medicine 3:e343.
172. Totura AL, Bavari S. 2019. Broad-spectrum coronavirus antiviral drug discovery. Expert Opin Drug Discov 14:397-412.
173. Wilde AHd, Jochmans D, Posthuma CC, Zevenhoven-Dobbe JC, Nieuwkoop Sv, Bestebroer TM, Hoogen BGvd, Neyts J, Snijder EJ. 2014. Screening of an FDA-Approved Compound Library Identifies Four Small-Molecule Inhibitors of Middle East Respiratory Syndrome Coronavirus Replication in Cell Culture. Antimicrobial agents and chemotherapy 58:4875-4884.
174. Santos IA, Grosche VR, Bergamini FRG, Sabino-Silva R, Jardim ACG. 2020. Antivirals Against Coronaviruses: Candidate Drugs for SARS-CoV-2 Treatment? Front Microbiol 11:1818.
175. Pruijssers AJ, George AS, Schäfer A, Leist SR, Gralinksi LE, Dinnon KH, Yount BL, Agostini ML, Stevens LJ, Chappell JD, Lu X, Hughes TM, Gully K, Martinez DR, Brown AJ, Graham RL, Perry JK, Du Pont V, Pitts J, Ma B, Babusis D, Murakami E, Feng JY, Bilello JP, Porter DP, Cihlar T, Baric RS, Denison MR, Sheahan TP. 2020. Remdesivir Inhibits SARS-CoV-2 in Human Lung Cells and Chimeric SARS-CoV Expressing the SARS-CoV-2 RNA Polymerase in Mice. Cell Reports 32:107940.
176. Simonis A, Theobald SJ, Fätkenheuer G, Rybniker J, Malin JJ. 2021. A comparative analysis of remdesivir and other repurposed antivirals against SARS-CoV-2. EMBO Mol Med 13:e13105.
177. Vincent MJ, Bergeron E, Benjannet S, Erickson BR, Rollin PE, Ksiazek TG, Seidah NG, Nichol ST. 2005. Chloroquine is a potent inhibitor of SARS coronavirus infection and spread. Virol J 2:69.
178. Cao B, Wang Y, Wen D, Liu W, Wang J, Fan G, Ruan L, Song B, Cai Y, Wei M, Li X, Xia J, Chen N, Xiang J, Yu T, Bai T, Xie X, Zhang L, Li C, Yuan Y, Chen H, Li H, Huang H, Tu S, Gong F, Liu Y, Wei Y, Dong C, Zhou F, Gu X, Xu J, Liu Z, Zhang Y, Li H, Shang L, Wang K, Li K, Zhou X, Dong X, Qu Z, Lu S, Hu X, Ruan S, Luo S, Wu J, Peng L, Cheng F, Pan L, Zou J, Jia C, et al. 2020. A Trial of Lopinavir–Ritonavir in Adults Hospitalized with Severe Covid-19. N Engl J Med 382:1787-1799.
179. Avezum Á, Oliveira GBF, Oliveira H, Lucchetta RC, Pereira VFA, Dabarian AL, D´O Vieira R, Silva DV, Kormann APM, Tognon AP, De Gasperi R, Hernandes ME, Feitosa ADM, Piscopo A, Souza AS, Miguel CH, Nogueira VO, Minelli C, Magalhães CC, Morejon KML, Bicudo LS, Souza GEC, Gomes MAM, Fo JJFR, Schwarzbold AV, Zilli A, Amazonas RB, Moreira FR, Alves LBO, Assis SRL, Neves PDMM, Matuoka JY, Boszczowski I, Catarino DGM, Veiga VC, Azevedo LCP, Rosa RG, Lopes RD, Cavalcanti AB, Berwanger O. 2022. Hydroxychloroquine versus placebo in the treatment of non-hospitalised patients with COVID-19 (COPE – Coalition V): A double-blind, multicentre, randomised, controlled trial. The Lancet Regional Health – Americas 11.
180. Wang M, Cao R, Zhang L, Yang X, Liu J, Xu M, Shi Z, Hu Z, Zhong W, Xiao G. 2020. Remdesivir and chloroquine effectively inhibit the recently emerged novel coronavirus (2019-nCoV) in vitro. Cell Research 30:269-271.
181. Hoffmann M, Mösbauer K, Hofmann-Winkler H, Kaul A, Kleine-Weber H, Krüger N, Gassen NC, Müller MA, Drosten C, Pöhlmann S. 2020. Chloroquine does not inhibit infection of human lung cells with SARS-CoV-2. Nature 585:588-590.
182. Grundeis F, Ansems K, Dahms K, Thieme V, Metzendorf MI, Skoetz N, Benstoem C, Mikolajewska A, Griesel M, Fichtner F, Stegemann M. 2023. Remdesivir for the treatment of COVID-19. Cochrane Database Syst Rev 1:Cd014962.

183. Beigel JH, Tomashek KM, Dodd LE, Mehta AK, Zingman BS, Kalil AC, Hohmann E, Chu HY, Luetkemeyer A, Kline S, Lopez de Castilla D, Finberg RW, Dierberg K, Tapson V, Hsieh L, Patterson TF, Paredes R, Sweeney DA, Short WR, Touloumi G, Lye DC, Ohmagari N, Oh M-d, Ruiz-Palacios GM, Benfield T, Fätkenheuer G, Kortepeter MG, Atmar RL, Creech CB, Lundgren J, Babiker AG, Pett S, Neaton JD, Burgess TH, Bonnett T, Green M, Makowski M, Osinusi A, Nayak S, Lane HC. 2020. Remdesivir for the Treatment of Covid-19 — Final Report. N Engl J Med 383:1813-1826.
184. Toussi SS, Hammond JL, Gerstenberger BS, Anderson AS. 2023. Therapeutics for COVID-19. Nature Microbiology 8:771-786.
185. Mehta RM, Bansal S, Bysani S, Kalpakam H. 2021. A shorter symptom onset to remdesivir treatment (SORT) interval is associated with a lower mortality in moderate-to-severe COVID-19: A real-world analysis. Int J Infect Dis 106:71-77.
186. Kokic G, Hillen HS, Tegunov D, Dienemann C, Seitz F, Schmitzova J, Farnung L, Siewert A, Höbartner C, Cramer P. 2021. Mechanism of SARS-CoV-2 polymerase stalling by remdesivir. Nature Communications 12:279.
187. Cao Z, Gao W, Bao H, Feng H, Mei S, Chen P, Gao Y, Cui Z, Zhang Q, Meng X, Gui H, Wang W, Jiang Y, Song Z, Shi Y, Sun J, Zhang Y, Xie Q, Xu Y, Ning G, Gao Y, Zhao R. 2023. VV116 versus Nirmatrelvir-Ritonavir for Oral Treatment of Covid-19. N Engl J Med 388:406-417.
188. Kabinger F, Stiller C, Schmitzová J, Dienemann C, Kokic G, Hillen HS, Höbartner C, Cramer P. 2021. Mechanism of molnupiravir-induced SARS-CoV-2 mutagenesis. Nature Structural & Molecular Biology 28:740-746.
189. Syed YY. 2022. Molnupiravir: First Approval. Drugs 82:455-460.
190. European Medicines Agency (EMA) CfMPfHUC. 2023. Withdrawal assessment report Lagevrio, EMA/116128/2023. https://wwwemaeuropaeu/en/documents/withdrawal-report/withdrawal-assessment-report-lagevrio_enpdf.
191. Mukae H, Yotsuyanagi H, Ohmagari N, Doi Y, Sakaguchi H, Sonoyama T, Ichihashi G, Sanaki T, Baba K, Tsuge Y, Uehara T. 2023. Efficacy and Safety of Ensitrelvir in Patients With Mild-to-Moderate Coronavirus Disease 2019: The Phase 2b Part of a Randomized, Placebo-Controlled, Phase 2/3 Study. Clin Infect Dis 76:1403-1411.
192. Hoffman RL, Kania RS, Brothers MA, Davies JF, Ferre RA, Gajiwala KS, He M, Hogan RJ, Kozminski K, Li LY, Lockner JW, Lou J, Marra MT, Mitchell LJ, Jr., Murray BW, Nieman JA, Noell S, Planken SP, Rowe T, Ryan K, Smith GJ, 3rd, Solowiej JE, Steppan CM, Taggart B. 2020. Discovery of Ketone-Based Covalent Inhibitors of Coronavirus 3CL Proteases for the Potential Therapeutic Treatment of COVID-19. J Med Chem 63:12725-12747.
193. Shan H, Liu J, Shen J, Dai J, Xu G, Lu K, Han C, Wang Y, Xu X, Tong Y, Xiang H, Ai Z, Zhuang G, Hu J, Zhang Z, Li Y, Pan L, Tan L. 2021. Development of potent and selective inhibitors targeting the papain-like protease of SARS-CoV-2. Cell Chem Biol 28:855-865.e9.
194. Yuan S, Gao X, Tang K, Cai JP, Hu M, Luo P, Wen L, Ye ZW, Luo C, Tsang JO, Chan CC, Huang Y, Cao J, Liang R, Qin Z, Qin B, Yin F, Chu H, Jin DY, Sun R, Chan JF, Cui S, Yuen KY. 2022. Targeting papain-like protease for broad-spectrum coronavirus inhibition. Protein Cell 13:940-953.
195. Newman JA, Douangamath A, Yadzani S, Yosaatmadja Y, Aimon A, Brandão-Neto J, Dunnett L, Gorrie-stone T, Skyner R, Fearon D, Schapira M, von Delft F, Gileadi O. 2021. Structure, mechanism and crystallographic fragment screening of the SARS-CoV-2 NSP13 helicase. Nature Communications 12:4848.
196. Kottur J, White KM, Rodriguez ML, Rechkoblit O, Quintana-Feliciano R, Nayar A, García-Sastre A, Aggarwal AK. 2023. Structures of SARS-CoV-2 N7-methyltransferase with DOT1L and PRMT7 inhibitors provide a platform for new antivirals. PLoS Pathog 19:e1011546.

197. Saramago M, Costa VG, Souza CS, Bárria C, Domingues S, Viegas SC, Lousa D, Soares CM, Arraiano CM, Matos RG. 2022. The nsp15 Nuclease as a Good Target to Combat SARS-CoV-2: Mechanism of Action and Its Inactivation with FDA-Approved Drugs. Microorganisms 10.
198. Snijder EJ, Bredenbeek PJ, Dobbe JC, Thiel V, Ziebuhr J, Poon LL, Guan Y, Rozanov M, Spaan WJ, Gorbalenya AE. 2003. Unique and conserved features of genome and proteome of SARS-coronavirus, an early split-off from the coronavirus group 2 lineage. J Mol Biol 331:991-1004.
199. Martin R, Li J, Parvangada A, Perry J, Cihlar T, Mo H, Porter D, Svarovskaia E. 2021. Genetic conservation of SARS-CoV-2 RNA replication complex in globally circulating isolates and recently emerged variants from humans and minks suggests minimal pre-existing resistance to remdesivir. Antiviral Res 188:105033.
200. Yan L, Huang Y, Ge J, Liu Z, Lu P, Huang B, Gao S, Wang J, Tan L, Ye S, Yu F, Lan W, Xu S, Zhou F, Shi L, Guddat LW, Gao Y, Rao Z, Lou Z. 2022. A mechanism for SARS-CoV-2 RNA capping and its inhibition by nucleotide analog inhibitors. Cell 185:4347-4360.e17.
201. Mutlu O, Ugurel OM, Sariyer E, Ata O, Inci TG, Ugurel E, Kocer S, Turgut-Balik D. 2022. Targeting SARS-CoV-2 Nsp12/Nsp8 interaction interface with approved and investigational drugs: an in silico structure-based approach. J Biomol Struct Dyn 40:918-930.
202. Loo YM, McTamney PM, Arends RH, Abram ME, Aksyuk AA, Diallo S, Flores DJ, Kelly EJ, Ren K, Roque R, Rosenthal K, Streicher K, Tuffy KM, Bond NJ, Cornwell O, Bouquet J, Cheng LI, Dunyak J, Huang Y, Rosenbaum AI, Pilla Reddy V, Andersen H, Carnahan RH, Crowe JE, Jr., Kuehne AI, Herbert AS, Dye JM, Bright H, Kallewaard NL, Pangalos MN, Esser MT. 2022. The SARS-CoV-2 monoclonal antibody combination, AZD7442, is protective in nonhuman primates and has an extended half-life in humans. Sci Transl Med 14:eabl8124.
203. Du W, Hurdiss DL, Drabek D, Mykytyn AZ, Kaiser FK, González-Hernández M, Muñoz-Santos D, Lamers MM, van Haperen R, Li W, Drulyte I, Wang C, Sola I, Armando F, Beythien G, Ciurkiewicz M, Baumgärtner W, Guilfoyle K, Smits T, van der Lee J, van Kuppeveld FJM, van Amerongen G, Haagmans BL, Enjuanes L, Osterhaus A, Grosveld F, Bosch BJ. 2022. An ACE2-blocking antibody confers broad neutralization and protection against Omicron and other SARS-CoV-2 variants of concern. Sci Immunol 7:eabp9312.
204. Jhuti D, Rawat A, Guo CM, Wilson LA, Mills EJ, Forrest JI. 2022. Interferon Treatments for SARS-CoV-2: Challenges and Opportunities. Infect Dis Ther 11:953-972.
205. Daniloski Z, Jordan TX, Wessels H-H, Hoagland DA, Kasela S, Legut M, Maniatis S, Mimitou EP, Lu L, Geller E, Danziger O, Rosenberg BR, Phatnani H, Smibert P, Lappalainen T, tenOever BR, Sanjana NE. 2021. Identification of Required Host Factors for SARS-CoV-2 Infection in Human Cells. Cell 184:92-105.e16.
206. Rebendenne A, Roy P, Bonaventure B, Chaves Valadão AL, Desmarets L, Rouillé Y, Tauziet M, Arnaud-Arnould M, Giovanni D, Lee Y, DeWeirdt P, Hegde M, Garcia de Gracia F, McKellar J, Wencker M, Dubuisson J, Belouzard S, Moncorgé O, Doench JG, Goujon C. 2021. Bidirectional genome-wide CRISPR screens reveal host factors regulating SARS-CoV-2, MERS-CoV and seasonal coronaviruses. Preprint BioRxiv:2021.05.19.444823.
207. Silva MJA, Ribeiro LR, Gouveia MIM, Marcelino BDR, Santos CSD, Lima KVB, Lima L. 2023. Hyperinflammatory Response in COVID-19: A Systematic Review. Viruses 15.
208. Ferreto LED, Bortoloti DS, Fortes PCN, Follador F, Arruda G, Ximenez JP, Wendt GW. 2021. Dexamethasone for treating SARS-CoV-2 infection: a systematic review and meta-analysis. Sao Paulo Med J 139:657-661.
209. The WHO Rapid Evidence Appraisal for COVID-19 Therapies Working Group. 2020. Association Between Administration of Systemic Corticosteroids and Mortality Among Critically Ill Patients With COVID-19: A Meta-analysis. JAMA 324:1330-1341.

210. Akinbolade S, Coughlan D, Fairbairn R, McConkey G, Powell H, Ogunbayo D, Craig D. 2022. Combination therapies for COVID-19: An overview of the clinical trials landscape. Br J Clin Pharmacol 88:1590-1597.

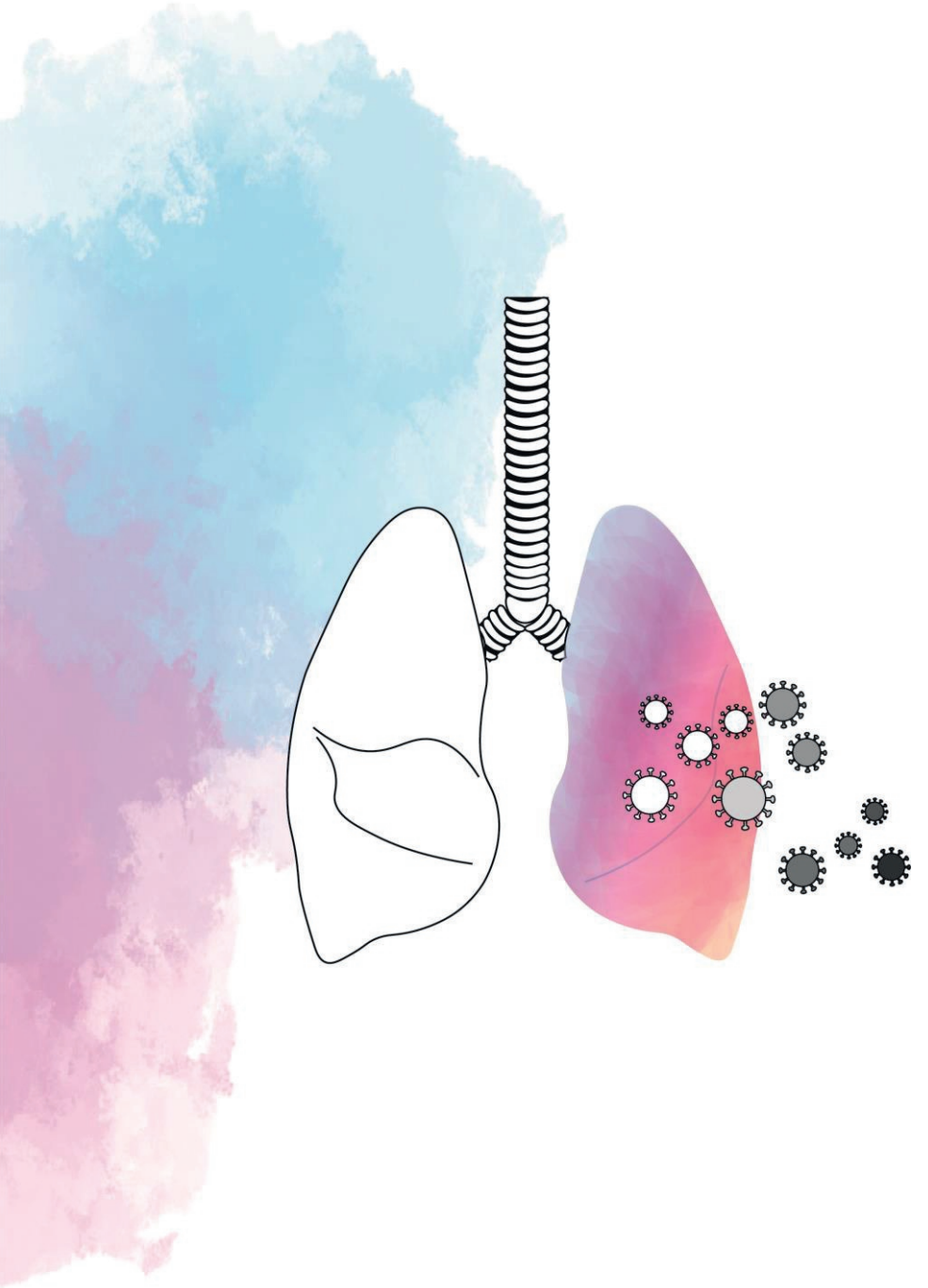

Chapter 2

Impact of Changes in human airway epithelial cellular composition and differentiation on SARS-CoV-2 infection biology

Melissa Thaler[1]*, Ying Wang[2]*, Anne M. van der Does[2], Alen Faiz[3], Dennis K. Ninaber[2], Natacha S. Ogando[1], Hendrik Beckert[4], Christian Taube[4], Clarisse Salgado-Benvindo[1], Eric J. Snijder[1], Peter J. Bredenbeek[1], Pieter S. Hiemstra[2#], Martijn J. van Hemert[1#]

[1] Department of Medical Microbiology, Leiden University Medical Center, Leiden, The Netherlands
[2] Department of Pulmonology, Leiden University Medical Center, Leiden, The Netherlands
[3] University of Technology Sydney, Respiratory Bioinformatics and Molecular Biology (RBMB), School of Life Sciences, Sydney, Australia
[4] Department of Pulmonary Medicine, University Medical Center Essen – Ruhrlandklinik, Essen, Germany

* These authors share first authorship
# These authors share senior authorship

Journal of Innate Immunity (2023) 15 (1): 562–580

Abstract

The consequences of infection with severe acute respiratory syndrome coronavirus 2 (SARS-CoV-2) can range from asymptomatic to fatal disease. Variations in epithelial susceptibility to SARS-CoV-2 infection depend on the anatomical location from the proximal to distal respiratory tract. However, the cellular biology underlying these variations is not completely understood. Thus, air-liquid interface (ALI) cultures of well-differentiated primary human tracheal and bronchial epithelial cells were employed to study the impact of epithelial cellular composition and differentiation on SARS-CoV-2 infection by transcriptional (RNA sequencing) and immunofluorescent analyses. Changes of cellular composition were investigated by varying time of differentiation or by using specific compounds. We found that SARS-CoV-2 primarily infected ciliated cells but also goblet cells and transient secretory cells. Viral replication was impacted by differences in cellular composition, which depended on culturing time and anatomical origin. A higher percentage of ciliated cells correlated with a higher viral load. However, DAPT-treatment, which increased number of ciliated cells and reduced goblet cells, decreased viral load, indicating the contribution of goblet cells to infection. Cell-entry factors, especially cathepsin L and transmembrane protease serine 2, were also affected by differentiation time. In conclusion, our study demonstrates that viral replication is affected by changes in cellular composition, especially in cells related to the mucociliary system. This could explain in part the variable susceptibility to SARS-CoV-2 infection between individuals and between anatomical locations in the respiratory tract.

Introduction

Since December 2019, severe acute respiratory syndrome coronavirus 2 (SARS-CoV-2) has rapidly spread worldwide. The burden of the associated coronavirus disease 2019 (COVID-19) has an enormous medical, social and economic impact (211). Furthermore, the continuing emergence of virus variants, such as the delta and omicron variants, are associated with additional waves of COVID-19 cases (212, 213). This illustrates the threat of these viruses to prolong the current pandemic or lead to new large outbreaks in the future. Besides different clinical outcomes due to SARS-CoV-2 variants, even people infected with the same virus variant present with varying clinical signs and symptoms depending on age (214), sex (215), weight (216), environment (217), other medical conditions (216, 218), immune status (219), and possibly other yet to be identified factors.

SARS-CoV-2 was first isolated from the lower respiratory tract of COVID-19 patients (15, 220). The epithelium serves as the first barrier to SARS-CoV-2 infection in the respiratory tract and therefore the subsequent epithelial response to infection (antiviral and

inflammatory responses) plays an important role in the outcome of infection. The respiratory tract spans from the nasal cavity to the terminal bronchioles, ending in the alveoli where gas exchange occurs. The airways are lined by the airway epithelium, which includes various cell types, of which ciliated, secretory goblet and club cells, and basal cells are present in the highest numbers (221, 222). These cell types have their own distinct functions. For instance, goblet cells secrete mucus, which captures inhaled particles like respiratory viruses, while the continuous beating cilia from ciliated cells help to transport this mucus with entrapped particles towards the pharynx, collectively called mucociliary clearance (MCC). Although the airway epithelium shares similar cell types throughout the respiratory tract, the proportion of each cell type is dependent on the anatomical location (223). In addition, in many patients with lung diseases such as asthma or chronic obstructive pulmonary disease (COPD), epithelial cellular composition is altered (222). In primary airway epithelial cell cultures, which are differentiated at the air-liquid interface (ALI), cellular composition of the airway epithelium depends on the individual donor (224), differentiation time (131), and culture conditions (133). So far, the impact of epithelial cellular composition on SARS-CoV-2 infection biology has not been completely elucidated. Previous studies have demonstrated a difference in host susceptibility to SARS-CoV-2 infection depending on the location of virus-host interaction in the respiratory tract (225). However, it is unclear to what extent the differences in viral replication link to variation in epithelial cellular composition. SARS-CoV-2 targets ciliated and secretory cells (71, 226), possibly via strands of mucus attached to cilia tips (227). Therefore, changes in the proportion of these target cells might affect viral replication. SARS-CoV-2 cellular tropism furthermore depends on host proteins that are involved in virus entry, including angiotensin converting enzyme 2 (ACE2) and proteases like transmembrane protease serine 2 (TMPRSS2) and cathepsin L (CTSL), as well as alternative receptors (e.g. cluster of differentiation 147 [CD147], 78-kDa glucose-regulated protein [GRP78], tyrosine-protein kinase receptor UFO [AXL]), which all have been demonstrated to be expressed in variable levels on human airway epithelial cells (45, 228-230). Recent research demonstrated that SARS-CoV-2 cell-entry factors are primarily expressed in bronchial transient secretory cells (231), indicating these transiently differentiating cells might contribute to a great extent to initial infection.

While research on the susceptibility of respiratory epithelial cells to SARS-CoV-2 infection often focuses on a specific cell-type, function or protein of interest (232), we aimed to investigate how various changes in cellular differentiation and composition affect SARS-CoV-2 infection biology. This knowledge can support our understanding of how these factors could contribute to local, and - more importantly - airway disease-associated differences in susceptibility. To this end, we used primary human bronchial (PBEC) and tracheal epithelial cells (PTEC) and differentiated them at the air-liquid interface (ALI) for up

to 5 weeks. We characterized virus replication, spread, localization, immune responses, and expression of SARS-CoV-2-entry factors, as well as compared cellular composition between both types of cultures. Furthermore, we investigated how infection characteristics were influenced by modulation of the cellular composition and by the duration of culture.

Results

Susceptibility of airway epithelial cultures to SARS-CoV-2 differs between individual donors

To investigate the effect of differentiation status and cellular composition of the airway epithelium on SARS-CoV-2 infection biology, we first aimed to establish a reliable infection model. We investigated donor-dependent variability in infection by comparing SARS-CoV-2 replication kinetics in cultures of 4 individual donors and a mix of those donors. Between the single donor cultures, we observed some variation in viral load (**Figure 1a**). Cultures derived from mixes of primary cells from these donors (donor mix) showed comparable infection kinetics with regard to this variation, and immunofluorescence staining confirmed similar numbers of infected cells at 72 hours post infection (hpi) for single donors and donor mix (**Figure 1b**). Thus ALI-PBEC cultures of mixed donor cells proved to be a representative model to investigate characteristics of airway epithelial cell cultures and to test many variables, while keeping sample size relatively limited.

We performed infections at a relatively low multiplicity of infection (MOI) to model the initial stage of infection by initially only infecting a fraction of susceptible cells and observe the virus spread across the epithelium over time. Four independent experiments were performed using ALI-PBEC derived from the same donor mix. After infection with SARS-CoV-2 (estimated 30,000 PFU per insert), we observed an increase in viral load (extracellular copies of viral RNA) over time, to approximately 10^{11} copies/ml at 72 hpi (**Figure 1c**). Immunofluorescence staining of the epithelial cultures for viral nucleocapsid protein also showed a gradual increase in the number of infected cells over time (**Figure 1d**). The number of infected cells was low and generally detected at the edge of the insert (**Figure S1a**) as also previously reported (233).

To validate the relevance of our cell culture model for studying epithelial defence against SARS-CoV-2 infection, we measured antiviral responses (IFN-β1 and IFN-λ1) and inflammatory cytokines (IL-6 and IL-8 [CXCL8]) (**Figure S1**). We observed that SARS-CoV-2 infection did not affect mRNA levels of *IFNB1* and *IFNL1* at 24 and 48 h, but strongly increased their expression at 72 hpi (**Figure S1b**). At 72 hpi, mRNA levels of both *IL6* and *CXCL8* displayed a modest but significant increase in SARS-CoV-2-infected cultures (**Figure**

S1c). We established reproducible and robust infection kinetics in this model, accompanied by a significant but late epithelial antiviral and inflammatory response that is characteristic for SARS-CoV-2 infection (234).

SARS-CoV-2 primarily infects epithelial cells involved in mucociliary clearance

Previous studies have indicated that within the human respiratory tract, predominantly ciliated cells, but also goblet cells of the airway epithelium can be infected with SARS-CoV-2 (226), as well as alveolar epithelial cells (138, 235). To assess if ciliated and goblet cells were also the target cells in our cultures, we investigated the colocalization of SARS-CoV-2 nucleocapsid protein with either acetylated α-tubulin and FOXJ1 as markers for ciliated cells, or MUC5AC as a marker for goblet cells. Recently, a new transient secretory cell subtype which is positive for markers of ciliated and goblet cells, was suggested to be particularly susceptible to SARS-CoV-2 based on ACE2 and TMPRSS2 expression (236). We observed presence of most of the viral nucleocapsid protein in acetylated α-tubulin-positive ciliated cells in ALI-PBEC cultures, with less presence in $MUC5AC^+$ goblet cells (**Figure 1e**), showing that both cell types can indeed be infected by SARS-CoV-2. Additionally, immunofluorescence staining showed that few transient secretory cells - defined as FOXJ1 and MUC5AC double-positive cells - were present and infected by SARS-CoV-2 (**Figure 1f**).
We next investigated if the number of SARS-CoV-2 target cells in the single donor cultures depicted in **Figure 1a**, correlated with the level of infection. Interestingly, quantification by immunofluorescence staining showed that cultures from donor 3, which had the higher initial viral load (at 24 hpi) compared to cells from donor 1 with the lowest initial viral load, constituted a higher proportion of $FOXJ1^+$ ciliated cells, as well as transient secretory cells (**Figure 1g**). This result suggests that the differences in susceptibility of cultures from different donors to viral infection might be associated with variation in the percentages of the different SARS-CoV-2 target cells.

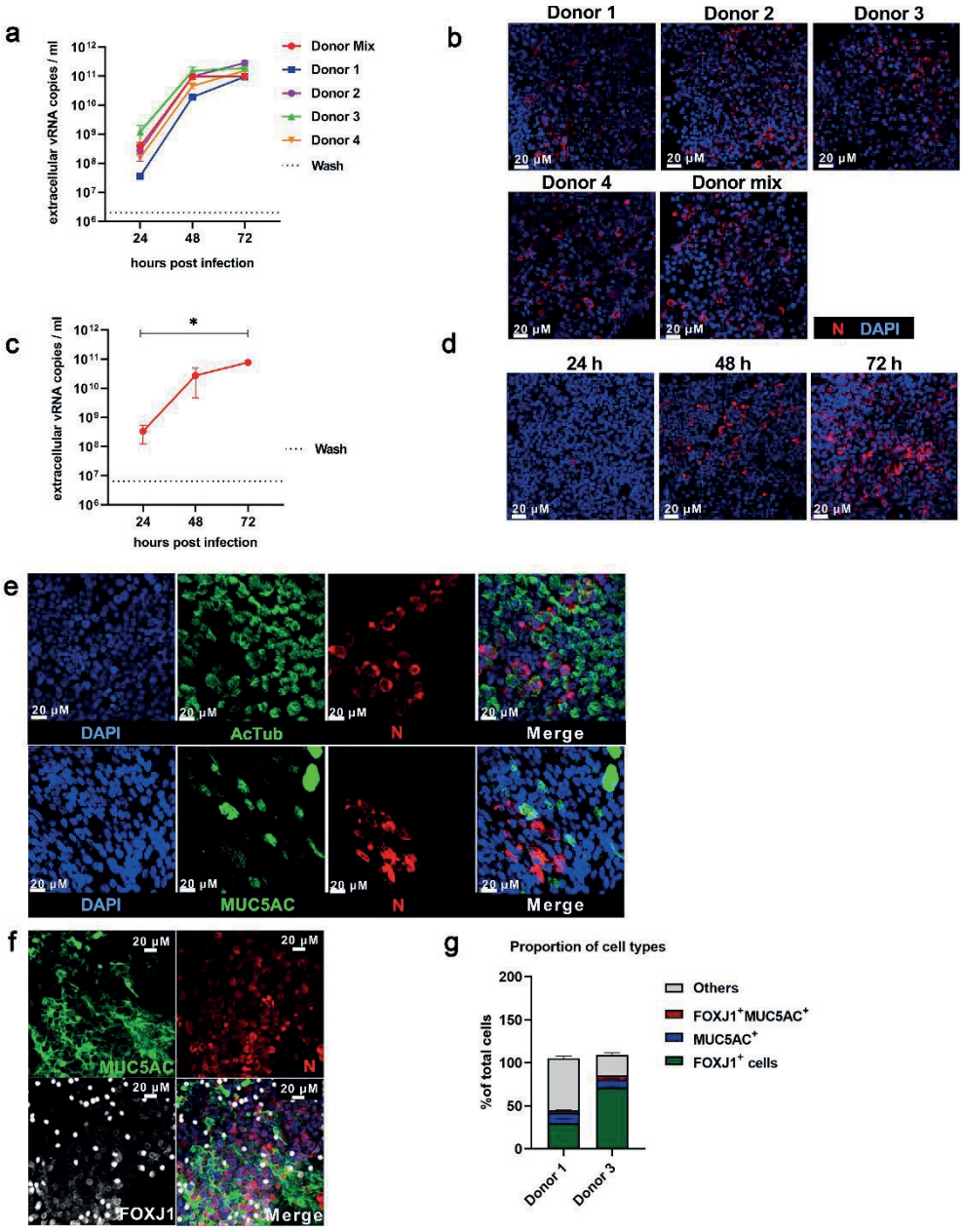

Figure 1: Characterization of a SARS-CoV-2 infection model using air-liquid interface cultures of primary bronchial epithelial cells. Mixes of PBEC derived from 4-5 individual donors were cultured for 5 weeks at ALI before they were infected with SARS-CoV-2 (30,000 PFU per insert). (a) The viral load in cultures derived from single donors or a mix of these donors (in red) was determined by quantifying the level of extracellular viral RNA copies by RT-qPCR. The dashed line represents the amount of (input) viral RNA that remained in the last wash after washing the inserts at 2 hpi (mean of all donors). (b) The infected cells were stained with rabbit polyclonal anti-

SARS-CoV-2 N protein antibody (JUC3) and with 4',6-diamidino-2-phenylindole (DAPI), and visualized by immunofluorescence microscopy at 72 hpi. Images shown at 400 x original magnification are representative merged z-stack images for results obtained with cells from random areas of the inserts. (c) The viral load at 24, 48 and 72 hpi in cultures was determined by quantifying the number of extracellular viral RNA copies by RT-qPCR. Data are mean ± SEM. n=4 independent experiments with the same donor mix. (d) For immunofluorescence microscopy, cells were fixed at 72 hpi and (double) labelled with rabbit polyclonal anti-SARS-CoV-2 N protein antibody (JUC3) and with DAPI for nuclear staining. Images shown at 400 x original magnification are representative merged z-stack images for results obtained with cells from 3 independent experiments. (e) Immunofluorescence staining at 72 hpi, with antibodies against acetylated α-tubulin (ciliated cell marker) or MUC5AC (goblet cell marker) in combination with anti-SARS-CoV-2 N protein antibody (JUC3) and DAPI for nuclear staining. Immunofluorescence images shown are representative merged z-stack images for results of 3 independent experiments with 630 x original magnification. (f) Immunofluorescence staining with antibodies against MUC5AC and FOXJ1 (ciliated cell marker) with anti-SARS-CoV-2 N protein antibody and DAPI for nuclear staining. Immunofluorescence images shown are representative merged z-stack images for results of 3 independent experiments with 400 x original magnification. (g) Quantification of immunostaining of $FOXJ1^+$, $MUC5AC^+$ and $FOXJ1^+MUC5AC^+$ or other cells in cultures of two single donors was performed with Image J software.

Modulating epithelial cellular composition has moderate effects on SARS-CoV-2 infection

To further explore the association between epithelial cellular composition and viral infection, we skewed cellular differentiation of ALI-PBEC during the last 2 weeks of differentiation to either an enrichment in ciliated cells at the cost of goblet cells, or towards an enrichment in goblet cells at the expense of ciliated cells using DAPT or interleukin 13 (IL-13), respectively (237-239). We infected these cultures with SARS-CoV-2 to analyse if enrichment in one of these cell types impacted infection kinetics. We could verify that DAPT treatment caused a marked increase in the number of ciliated cells ($FOXJ1^+$ and acetylated α-$tubulin^+$), while the number of goblet cells ($MUC5AC^+$) was decreased (**Figure 2a** and **S2a**). Conversely, IL-13 treatment increased the fraction of goblet cells and decreased the number of ciliated cells (**Figure 2A** and **S2A**), also confirmed at gene expression level (**Figure S2b**). Additionally, a small percentage of FOXJ1 and MUC5AC double-positive transient secretory cells was detected in all cultures, which was not significantly affected by IL-13 or DAPT treatment (**Figure S2a**).

We infected these DAPT- or IL-13-treated cultures with SARS-CoV-2 and in line with the data shown in **Figure 1**, detected by immunofluorescence staining that only a few cells were infected at 24 hpi in untreated and treated cultures (**Figure 2b**). At 48 and 72 hpi, all cultures showed an increase in viral load compared to 24 hpi (**Figure 2b**), demonstrating that viral infection and replication was feasible in all cultures despite the significant change in cellular composition between these conditions. In IL-13-treated cell cultures, intracellular viral RNA levels were highest at 48 hpi, while being similar to control again at 72 hpi (**Figure 2c**). To

our surprise the level of intracellular SARS-CoV-2 RNA was lower in DAPT-treated cells at all time points compared to the controls (**Figure 2c**). Similar trends were found for the release of infectious particles, as shown in **Figure 2d**. When we checked for cell types infected with SARS-CoV-2 in DAPT-treated cultures, due to the lack of goblet cells, ciliated cells were the only identified cells. In IL-13-treated cultures we observed infection of ciliated and goblet cells, similar to control cultures. (**Figure 2e**).

To exclude the possibility that the effects observed in DAPT-treated cultures were a direct consequence of inhibition of Notch signalling rather than epithelial remodelling, we treated cells with DAPT either starting 24 h before (and during) infection (a time period considered insufficient to cause a shift in epithelial differentiation) or directly after infection. These short-term treatments with DAPT did not result in significant changes in the intracellular viral RNA copies or production of infectious progeny, suggesting that inhibition of Notch signalling itself has no direct effect on SARS-CoV-2 replication (**Figure S2c**). These data suggest that rather than one cell-type alone, possibly the interplay between goblet and ciliated cells is important for susceptibility of ALI-PBEC to SARS-CoV-2 infection.

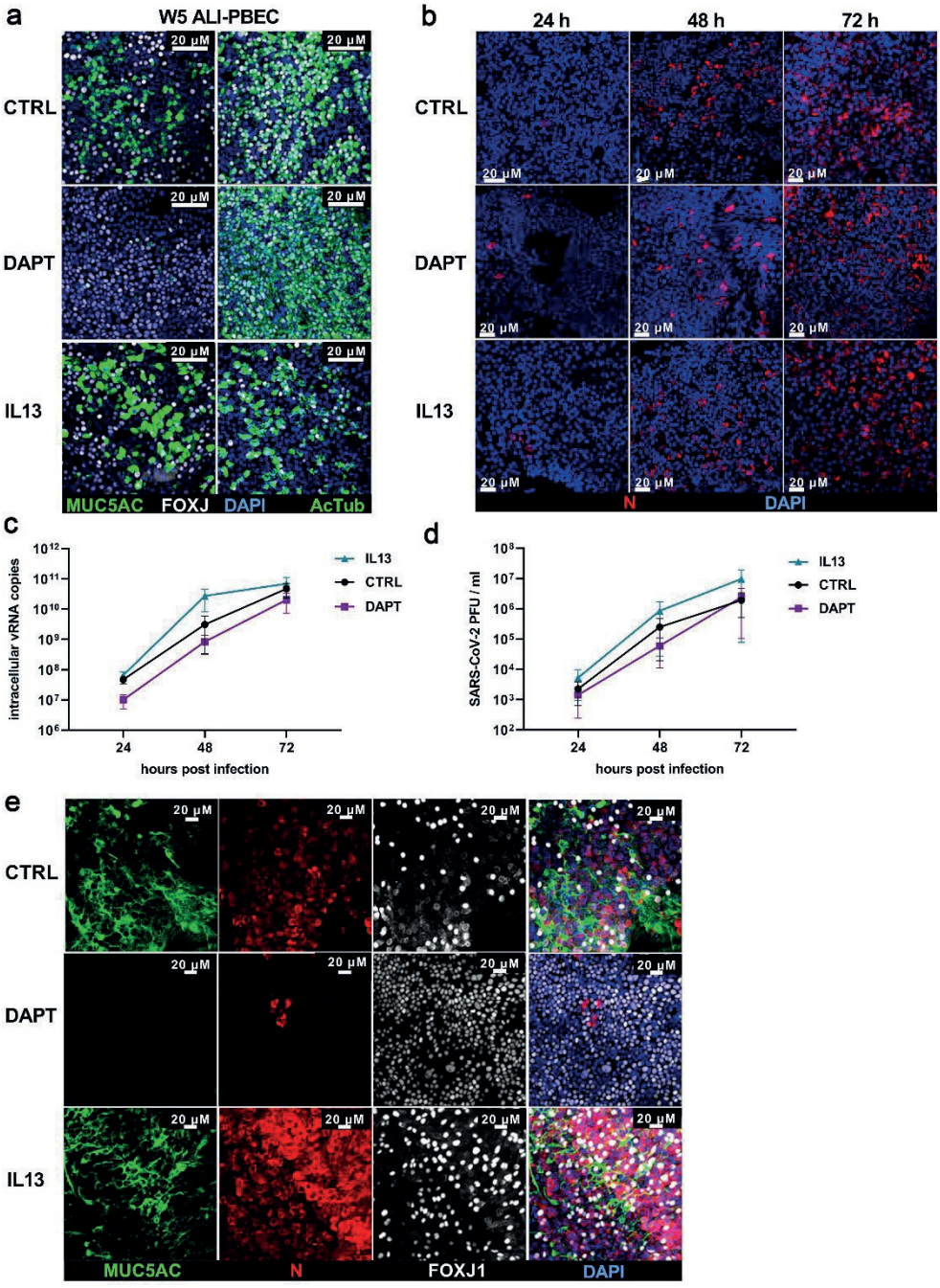

Figure 2: Effect of IL-13 treatment, and DAPT-mediated inhibition of Notch signaling on epithelial susceptibility to SARS-CoV-2 infection. ALI-PBEC (mix of 4-5 donors) were differentiated for 3 weeks, before addition of DAPT (5 µM) or IL-13 (1 ng/ml) and differentiation for an additional 2 weeks. (a) After in total 5 weeks of differentiation,

ALI-PBEC were fixed, stained using primary antibodies against MUC5AC and FOXJ1 (goblet cell marker, ciliated cell marker) or acetylated α-tubulin together with FOXJ1 (ciliated cell markers) in combination with DAPI for nuclear staining, analyzed by immunofluorescence microscopy and quantified by ImageJ. Immunofluorescence images shown are representative merged z-stack images for results of 3 independent experiments with 400 x original magnification. (b) SARS-CoV-2 infected cells were stained with primary antibodies against SARS-CoV-2 N protein (JUC3) in combination with DAPI for nuclear staining. Immunofluorescence images shown are representative merged z-stack images for results of 3 independent experiments with 400 x original magnification. (c) Intracellular viral RNA copies were measured by RT-qPCR. (d) Plaque assay was performed to titrate viral progeny in the apical washes. n=3 independent experiments derived from 3 different donor mixes. Data are mean ± SEM. Analysis of differences was conducted using two-way ANOVA with a Tukey/Bonferroni post-hoc test. Significant differences are indicated by *P<0.05 compared with untreated samples. (e) Immunostaining of control, DAPT- or IL-13-treated cultures at 72 hpi with antibodies against MUC5AC (goblet cell marker), FOXJ1 (ciliated cell marker) and SARS-CoV-2 N protein in combination with DAPI for nuclear staining. Immunofluorescence images shown are representative merged z-stack images for results of 3 independent experiments with 400 x original magnification.

Origin and culture duration of human airway epithelial cells affect SARS-CoV-2 infection

Next, we wanted to investigate how differentiation time and anatomical origin of the epithelial cultures affected SARS-CoV-2 infection biology. To this end, we employed cells isolated from bronchial or tracheal tissue and allowed ALI-PBEC and ALI-PTEC to differentiate for 3, 4 or 5 weeks, after which they were infected with 30,000 PFU of SARS-CoV-2. Viral load was analysed at 72 hpi. In both ALI-PBEC and ALI-PTEC, an increase in intra- and extracellular viral RNA as well as infectious virus particles was observed with longer differentiation time, with the highest viral load observed in cultures differentiated for 5 weeks after start of ALI (**Figure 3a-3c**). A gradual 1-2 log increase in SARS-CoV-2 progeny production was observed when cultures had been differentiated up to 5 weeks when compared to 3 weeks of differentiation (**Figure S3a**). Immunofluorescence staining of these cultures for the viral nucleocapsid protein also demonstrated an increase in the number of infected cells with increasing culture duration (**Figure 3c**). Significantly higher viral load was observed in ALI-PBEC compared to ALI-PTEC, with an average 10-fold difference in extracellular SARS-CoV-2 RNA copies (**Figure 3a-3b**) and infectious progeny (**Figure 3c**), in particular in 5-week differentiated cultures. In conclusion, our results show that both the anatomical origin of the epithelial cells and the culture duration had a profound effect on the susceptibility of airway epithelial cells to SARS-CoV-2 infection.

Time of culturing affects the proportion of cell types related to mucociliary clearance

Since we found increased viral infection upon prolonged differentiation time and additionally we observed that SARS-CoV-2 infection targets mostly ciliated cells, goblet cells and transient secretory cells (which we also confirmed for ALI-PTEC (**Figure S3c**)), we hypothesized that the numbers of these target cells changed over time of differentiation. We compared cellular composition between 3, 4 and 5 week-differentiated cultures and found that these cultures at all time points expressed markers related to all dominant epithelial cell types (ciliated, goblet, club and basal cells) in ALI-PBEC and PTEC (**Figure S3b**). However, there were clear differences in the proportions of goblet and ciliated cells over time of differentiation (**Figure 3d**). Using FOXJ1 and acetylated α-tubulin as markers for ciliated cells, we observed that the percentage of $FOXJ1^+$ cells was significantly higher in ALI-PBEC after 5-week culture compared to 3-week cultures. Also the percentage of ciliated cells was significantly higher in ALI-PBEC than in ALI-PTEC at all culture durations (**Figure 3e**). The change in the percentage of $MUC5AC^+$ goblet cells was not significant over time in ALI-PBEC and ALI-PTEC (**Figure 3e**). Additionally, the number of transient secretory cells was higher in ALI-PBEC than in ALI-PTEC (**Figure 3e**). Furthermore, mRNA levels of *FOXJ1* were significantly increased in 4 week ALI-PBEC compared to 3 week cultures, however they did not further increase in 5 week cultures (**Figure S3d**). In addition, *FOXJ1* mRNA was higher in 4/5-week ALI-PBEC cultures compared to 4/5-week PTEC cultures (**Figure S3d**). *MUC5AC* mRNA levels were higher at week 5 in ALI-PTEC cultures compared to week 3, and also higher than in week 5 ALI-PBEC (**Figure S3d**). In contrast, there was no significant difference in the expression of *SCGB1A1* (club cell marker) and *TP63* (basal cell marker) (**Figure S3d**). These results suggest that despite the early presence of transcripts which are specific for certain cell types, differentiation of certain cell types (which also requires expression at the protein level) continues for several weeks in cultures at ALI. Altogether, we found differences in the percentage of ciliated cells between PTEC and PBEC and between cultures that differed in their incubation time at ALI, which was in line with differences in viral load.

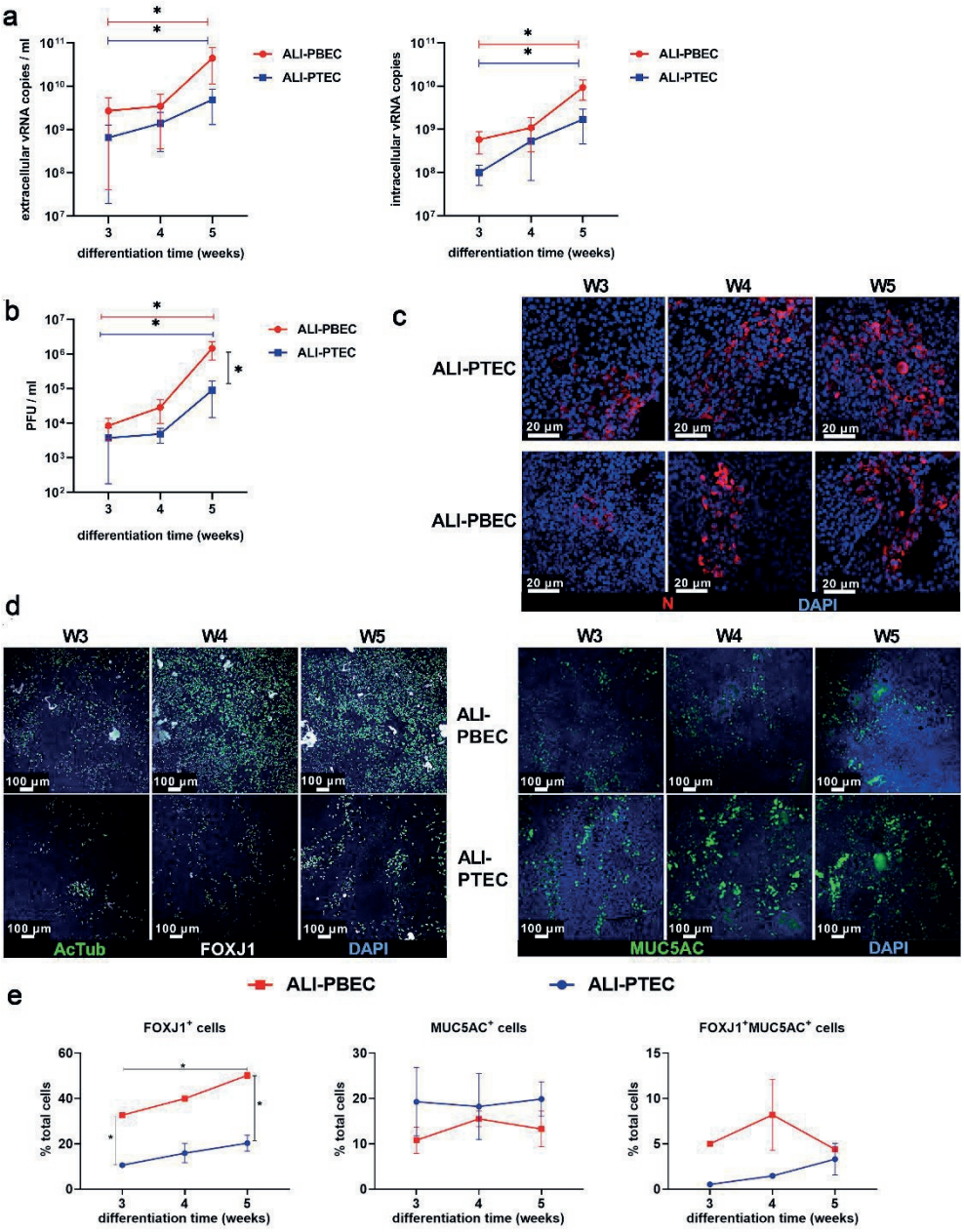

Figure 3: Effect of culture duration on SARS-CoV-2 infection in PTEC and PBEC. ALI-PBEC/ALI-PTEC (mix of 5 donors) cultured for 3-5 weeks were infected with SARS-CoV-2 (30,000 PFU per insert). (a) Extracellular viral RNA copies in the apical wash or intracellular copies were measured by RT-qPCR. (b) Viral infectious progeny was quantified by plaque assay in Vero E6 cells. Mean values ± SEM from 3 independent experiments using 3 different donor mixes are shown. Statistical analysis was conducted using two-way ANOVA with a Tukey/Bonferroni post-

hoc test. Significant differences are indicated by *P<0.05. (c) Cells were stained for immunofluorescence microscopy with rabbit polyclonal anti-SARS-CoV-2 N protein antibody (JUC3) and DAPI for nuclear staining. Images shown are representative merged z-stack images for results obtained with ALI-PBEC and ALI-PTEC from the same 3 independent experiments shown in A-B at 400 x original magnification. (d) Immunofluorescence staining of 3, 4, 5 week cultures using antibodies against acetylated α-tubulin and FOXJ1 (ciliated cell markers) or MUC5AC (goblet cell marker) in combination with DAPI for nuclear staining. Images shown are representative merged z-stack images for results of 3 independent experiments with 100x original magnification. (e) Quantification of $FOXJ^+$, $MUC5AC^+$ cells and $FOXJ1^+MUC5AC^+$ cells was done by Image J software.

Changes in gene expression associated with SARS-CoV-2 target cells

To further explore the gradual increase in susceptibility to SARS-CoV-2 infection with longer culture time, we compared the expression profiles of 3-week and 5-week uninfected differentiated cultures by bulk RNA-Seq and applied cellular deconvolution. We identified 169 differentially expressed genes, of which expression of 49 genes was upregulated while expression of 120 genes was downregulated in ALI-PBEC at 5 vs 3 weeks (Figure 4a and **Table S1**). In ALI-PTEC, the expression of 32 genes increased, and 26 genes showed decreased expression in 5-week cultures compared to 3-week cultures (**Figure 4b** and **Table S1**). Gene set enrichment analysis was conducted to identify the top differentially upregulated and downregulated gene sets in ALI-PBEC between week 5 and week 3 (**Table 1**). A striking difference in ALI-PBEC between week 5 and week 3 was observed for the gene sets related to markers of ciliated and basal cells. Cellular deconvolution analysis further showed that the relative proportion of ciliated cells was increased in 5-week ALI-PBEC cultures and the same trend was also found for ALI-PTEC (**Figure 4c** and **4d**). Altogether, RNA-Seq analysis did not reveal additional changes in cell types between the 3 and 5 week culture duration.

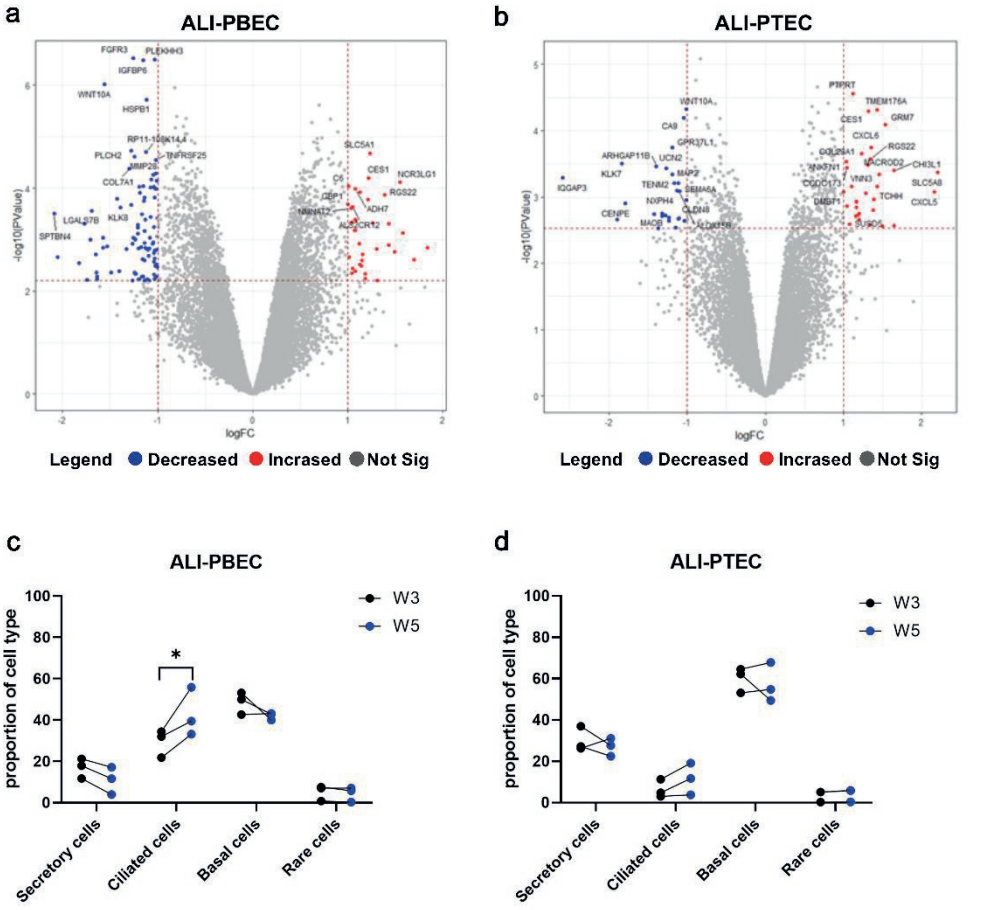

Figure 4: Transcriptional responses comparing 3 and 5 weeks-differentiated primary bronchial and tracheal cells using RNA-Seq analysis. PBEC and PTEC were cultured at ALI for 3 weeks or 5 weeks. RNA was isolated from these samples and used for RNA-Seq analysis. (a-b) Volcano plots depicting changes in the gene expression profiles of 5-week cultures compared to 3-week cultures from ALI-PBEC or ALI-PTEC. The DEGs were considered significant when they had a Benjamini Hochberg p value<0.1 and a fold change>|2. Genes depicted in red are significantly upregulated while genes depicted in blue are significantly downregulated in 5-week cultures compared to 3-week cultures in ALI-PBEC (a) or ALI-PTEC (b). (c-d) The relative proportion of different cell types for each donor mix in ALI-PBEC (c) cultures and ALI-PTEC (d) cultures as determined by cellular deconvolution of the transcriptomic datasets.

Table 1: Top 10 gene sets of the differentially expressed genes analyzed using gene set enrichment analysis (GSEA). P value was calculated from the hypergeometric distribution for (k-1, K, N - K, n) where k is the number of genes in the intersection of the query set with a set from MSigDB; K is the number of genes in the set from MSigDB; N is the total number of gene universe (all known human gene symbols); n is the number of genes in the query set. FDR q-value means the false discovery rate analog of hypergeometric p-value after correction for multiple hypothesis testing according to Benjamini and Hochberg. The gene sets related to cellular composition of lung are highlighted in bold.

Direction	Gene Set Name	# Genes in Gene Set (K)	Description	# Genes in Overlap (k)	k/K	p-value	FDR q-value
Upregulated	MURARO_PANCREAS_DUCTAL_CELL	1276		12	0.0094	9.25E-9	1.79E-4
Upregulated	GOBP_DEFENSE_RESPONSE	1739	Reactions, triggered in response to the presence of a foreign body or the occurrence of an injury, which result in restriction of damage to the organism attacked or prevention/recovery from the infection caused by the attack. [GOC:go_curators]	12	0.0069	2.7E-7	2.3E-3
Upregulated	WP_PROXIMAL_TUBULE_TRANSPORT	58	Proximal tubule transport	4	0.0690	5.25E-7	2.3E-3
Upregulated	WP_NRF2_PATHWAY	145	NRF2 pathway	5	0.0345	5.77E-7	2.3E-3
Upregulated	DESCARTES_FETAL_INTESTINE_INTESTINAL_EPITHELIAL_CELLS	276	descartes DE_gene_by_organ.csv, fold.change>5, qval<0.05, pval<0.05	6	0.0217	5.94E-7	2.3E-3
Upregulated	REACTOME_G_ALPHA_I_SIGNALLING_EVENTS	314	G alpha (i) signalling events	6	0.0191	1.26E-6	3.46E-3
Upregulated	GOMF_SOLUTE_SODIUM_SYMPORTER_ACTIVITY	72	Enables the transfer of a solute or solutes from one side of a membrane to the other according to the reaction: solute(out) + Na+(out) = solute(in) + Na+(in). [GOC:ai]	4	0.0556	1.26E-6	3.46E-3
Upregulated	WP_NUCLEAR_RECEPTORS_METAPATHWAY	321	Nuclear receptors meta-pathway	6	0.0187	1.43E-6	3.46E-3
Upregulated	**TRAVAGLINI_LUNG_CILIATED_CELL**	**1094**		**9**	**0.0082**	**2.59E-6**	**5.57E-3**
Upregulated	TRAVAGLINI_LUNG_MACROPHAGE_CELL	201		5	0.0249	2.88E-6	5.58E-3
Downregulated	GOCC_SUPRAMOLECULAR_COMPLEX	1329	A cellular component that consists of an indeterminate number of proteins or macromolecular complexes, organized into a regular, higher-order structure such as a polymer, sheet, network or a fiber. [GOC:dos]	18	0.0135	9.81E-9	8.53E-5
Downregulated	**TRAVAGLINI_LUNG_PROLIFERATING_BASAL_CELL**	**891**		**15**	**0.0168**	**1.12E-8**	**8.53E-5**
Downregulated	HAY_BONE_MARROW_STROMAL	767		14	0.0183	1.32E-8	8.53E-5

Downregulated	TRAVAGLINI_ LUNG_BASAL_CELL	188		8	0.0426	3.6E-8	1.61E-4
Downregulated	GOCC_SUPRAMOLECULAR_POLYMER	996	A polymeric supramolecular structure. [GOC:dos]	15	0.0151	4.84E-8	1.61E-4
Downregulated	ZHONG_PFC_C2_ UNKNOWN_NPC	76		6	0.0789	5.04E-8	1.61E-4
Downregulated	HALLMARK_KRAS_ SIGNALING_DN	200	Genes down-regulated by KRAS activation.	8	0.0400	5.81E-8	1.61E-4
Downregulated	NABA_ MATRISOME	1026	Ensemble of genes encoding extracellular matrix and extracellular matrix-associated proteins	15	0.0146	7.1E-8	1.72E-4
Downregulated	MANNO_MIDBRAIN_NEUROTYPES_ HNPROG	229	Cell types are named using anatomical and functional mnemonics prefixed by 'm' or'h' to indicate mouse and human respectively: OMTN, oculomotor and trochlear nucleus; Sert, serotonergic; NbM, medial neuroblast; NbDA, neuroblast dopaminergic; DA0-2, dopaminergic neurons; RN, red nucleus; Gaba1-2, GABAergic neurons; mNbL1-2, lateral neuroblasts; NbML1-5, mediolateral neuroblasts; NProg, neuronal progenitor; Prog, progenitor medial floorplate (FPM), lateral floorplate (FPL), midline (M), basal plate (BP); Rgl1-3, radial glia-like cells; Mgl, microglia; Endo, endothelial cells; Peric, pericytes; Epend, ependymal; OPC, oligodendrocyte precursor cells.	8	0.0349	1.64E-7	3.45E-4
Downregulated	FAN_EMBRYONIC_ CTX_MICROGLIA_1	155		7	0.0452	1.78E-7	3.45E-4

Cell culture duration alters expression of SARS-CoV-2 entry factors

The expression of host proteins that have been linked to entry of SARS-CoV-2 varies between the different airway epithelial cell types (229). Therefore, we investigated whether the observed increase in susceptibility to SARS-CoV-2 with increased differentiation time and the effect of the anatomical origin, was related to the expression of the main receptor ACE2, or other factors involved in entry. We compared the mRNA levels of different viral entry factors between the single-donor cultures that displayed the highest and lowest viral load (**Figure 1a, Figure 5a**). Interestingly, the culture with the highest viral load expressed higher mRNA levels of *CTSL* and *TMPRSS2* at baseline, while other factors did not differ.

Furthermore, we assessed the expression of cell-entry factors in cultures of varying differentiation time using our RNA-Seq dataset (**Figure 5b**). In both ALI-PBEC and ALI-PTEC cultures, there was a significant increase in expression of *TMPRSS2* in 5-week cultures compared to 3-week cultures. In addition, expression of *CTSL* was significantly increased while expression of *CD147* was decreased at 5 weeks compared to 3 weeks in ALI-PBEC. However, expression of *NRP1* was reduced at 5 weeks compared to 3 weeks in ALI-PTEC, and expression of *ACE2*, *FURIN* and *NRP1* was lower in 3-week ALI-PBEC compared to 3-week ALI-PTEC (**Figure 5b**). We compared the expression of these genes by RT-qPCR in 3- and 5-week cultures, and also included 4-week cultures (**Figure S4a**). With longer culture duration, in both ALI-PBEC and ALI-PTEC, gene expression of *CTSL* and *TMPRSS2* indeed increased over time and a significant increase was found in expression of *TMPRSS2* in 4-week ALI-PBEC compared to 3-week cultures. Gene expression of *ACE2* and *GRP78* did not change with culture duration. A significant increase in expression of *CD147* was observed in 4-week ALI-PBEC compared to 3-week cultures (**Figure S4a**). Treatment with DAPT or IL-13 did not affect expression of SARS-CoV-2 entry factors (**Figure S4b**). These findings indicated that changes in expression of *CTSL* and *TMPRSS2* could (in part) be responsible for the observed differences in susceptibility to SARS-CoV-2 infection between 3-, 4- and 5-week differentiated cultures.

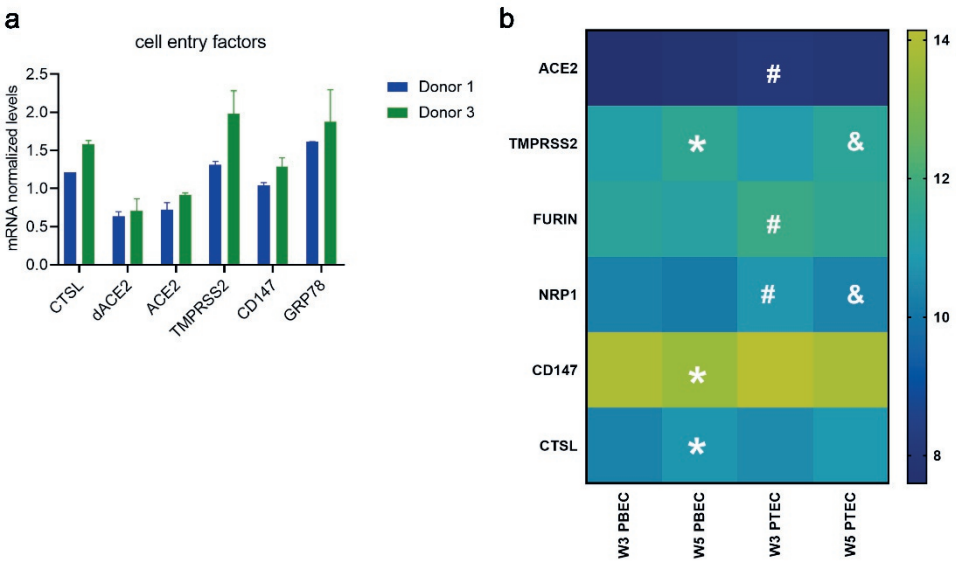

Figure 5: Effect of donor variation and culture duration on expression of SARS-CoV-2 cell-entry factors. (a) RT-qPCR analysis of gene expression of viral cell-entry factors in two single donor cultures at 5 weeks. Data are mean values ± SEM. n=2 duplicated wells per donor. (b) Heatmap of transcriptional changes (RNA-Seq data) of SARS-CoV-2 cell-entry factors in 3-week and 5-week PBEC and PTEC. Differences were assessed by a two-way ANOVA

with Tukey's test and the significant difference were considered at $P < 0.05$. *= 5-week ALI-PBEC vs 3-week ALI-PBEC; &=5-week ALI-PTEC vs 3-week ALI-PTEC; #=3-week ALI-PTEC vs 3-week ALI-PBEC.

Cell culture duration does not affect SARS-CoV-2-induced antiviral responses

Antiviral responses in the epithelium are critical for protection against viral infections. Therefore, we investigated whether antiviral responses changed depending on the ALI culture duration, and whether this could provide an additional explanation of the observed increased susceptibility to infection with longer culture times. In ALI-PTEC, SARS-CoV-2-induced mRNA levels of both *IFNB1* and *IFNL1* increased significantly with culture duration. When cultures were infected at week 3 or 4 there was little *IFNB1* or *IFNL1* mRNA produced, while expression of these genes was strongly upregulated by SARS-CoV-2 infection in 5 week old cultures (**Figure S5a** and **S5b**). Gene expression analysis of *IFNB1* and *IFNL1* showed a similar increasing trend in ALI-PBEC upon infection (**Figure S5c** and **S5d**). When 5-week PBEC were (long-term) treated with DAPT, we observed lower SARS-CoV-2-induced antiviral responses than in untreated and IL-13-treated cultures (**Figure S5e** and **5f**). All these findings correlate with the observed differences in the number of infected cells and viral load resulting from culture duration and DAPT and IL-13 treatment (**Figure 2**). This suggests that antiviral responses were not affected by differentiation time or long-term DAPT/IL-13 treatment, but rather differed as a direct consequence of differences in the level of infection.

Discussion

Here we investigated the influence of cellular composition and differentiation of human primary airway epithelial cell cultures on SARS-CoV-2 infection biology. Our key finding is that changes in cell types related to mucociliary clearance, i.e. ciliated and goblet cells, influence SARS-CoV-2 infection of human primary airway epithelial cells. Specifically, a higher percentage of ciliated cells appears to be the main contributing factor to a higher level of infection. This is likely a consequence of their higher susceptibility to infection in comparison to the other cell-types, and possibly their contribution to spreading of virus across the epithelial surface of the culture. Nevertheless, our data also suggest that the presence of mucus and/or goblet cells is important, since a reduction in goblet cells reduced viral load, even in cultures with a higher percentage of ciliated cells. Finally, we provide experimental evidence for infection of transient secretory cells by SARS-CoV-2.

With regard to differentiation time, there is no golden standard protocol for ALI-primary airway epithelial cell cultures to obtain cultures that best resemble the human epithelial

cellular composition. Literature reports that differentiation times anywhere between 2 and 6 weeks after start of air-liquid interface culture are needed to have all key cell-types present in culture (71, 226, 240).

In line with a recent study investigating SARS-CoV-2 infection using primary airway epithelial cells(226), and based on our own study comparing 3-5 week old cultures, we decided to use 5 weeks differentiated ALI-PBEC cultures. We found a reproducible increase in viral titers over time post infection. In addition, cultures of well-differentiated airway epithelial cells adequately model *in vivo* host antiviral responses (137, 241), which we could confirm also for SARS-CoV-2 infection by detecting increased mRNA levels of *IL-6* and *CXCL8*. In contrast, downregulated expression of *IL-6* and *CXCL8* was reported in the human bronchial epithelial cell line 16HBE (242).

We confirmed that both ciliated and goblet cells were infected by SARS-CoV-2 in our ALI-cultures, whereas no infected club and basal cells were detected (data not shown). This is consistent with results from recent studies looking into the cellular tropism of SARS-CoV-2 showing infection of multiple epithelial cell types, among them ciliated cells, goblet cells and club cells of the airway epithelium, and type 2 alveolar epithelial cells (68, 71, 226, 243). Additionally, we also observed cells co-expressing markers of ciliated cells (FOXJ1) and goblet cells (MUC5AC) in our cultures. This specific cell population, which was recently reported by e.g. Garcia *et al.* (244) and by Vieira Braga et al (245), is suggested to represent a transitional state between goblet and ciliated cells, and was recently labelled as transient secretory cells (231). Based on their relatively high co-expression of ACE2 and TMPRSS2, Lukassen et al. (231) suggested that these transient secretory cells may be particularly vulnerable to SARS-CoV-2 infection. Whereas we showed for the first time that SARS-CoV-2 was also able to infect these cells, it remains unknown if the low percentage of these cells in our culture model significantly contributed to the overall level of infection. Considering the role in mucociliary clearance of ciliated, goblet and potentially transient secretory cells, we conclude that cells involved in mucociliary clearance are predominantly infected by SARS-CoV-2.

To investigate the role of cellular composition in susceptibility to viral infection, we skewed cell differentiation with the Notch signalling inhibitor DAPT (238), which resulted in cultures that constituted a high number of ciliated cells but lacked goblet cells and transient secretory cells. Surprisingly the viral load in these cultures was reduced compared to untreated cultures. A possible explanation would be that ciliated cells become infected by the virus, and mucus produced by goblet cells helps spread the infection after release, which would be consistent with previous findings that SARS-CoV-2 infects ciliated cells with attached mucus (246). Conversely, the modulation with IL-13, (slightly) increased viral loads compared to control and DAPT-treated cultures, which is in line with the suggestion from

other studies that patients with allergic asthma, a disease associated with IL-13-induced changes in epithelial cell composition, may be somewhat more susceptible to SARS-CoV-2 infection (247). Others have observed that treatment with IL-13 reduced viral RNA copies in ALI-cultured airway epithelial cells (248, 249). There is no clear explanation for this discrepancy, although the reduced levels of *ACE2* after IL-13 treatment that were found in these studies might have been responsible for the reduced infection levels. However, in our studies ACE2 expression was not affected by IL-13 treatment. Furthermore, we used a much lower MOI (0.03 versus 0.5), and therefore even if IL-13 reduces the number of the main target cells (e.g. ciliated cells) this is not expected to have much effect in our setup, because the amount of susceptible cells will likely not be limiting due to the low MOI. Collectively, our observations indicate that DAPT- and IL-13-mediated modulation of epithelial cell differentiation does not provide a simple link between differences in epithelial cell composition and susceptibility to SARS-CoV-2 infection. A combination of factors appears to play a role. For example, mucus secretion by goblet cells (250), when excessive, could hinder clearance of the virus in the epithelium. We therefore used additional approaches to study the contributing effect of cellular composition to SARS-CoV-2 infection. We could demonstrate that changes in cellular composition either linked to anatomical origin, donor or culture time, influenced SARS-CoV-2 infection. The shared outcome was that for each variable the number of target cells correlated to the viral load, suggesting that the percentage of ciliated cells is a strong contributing factor to the SARS-CoV-2 infection rate. Considering that expression of viral entry factors varies between different cell types, we furthermore investigated their expression in cells from different donors, the effect of culture duration, and the impact of treatment with DAPT and IL-13. According to literature, all main cell types express *TMPRSS2,* and highest expression is found in transient secretory cells (231). *CTSL* gene expression was reported to be higher in ciliated cells compared to other epithelial cell types (251). When we compared two single donors, cell cultures isolated from one donor expressed more *CTSL* and *TMPRSS2,* which was in line with the observed higher viral replication and higher abundance of ciliated cells in this donor. In our study, an increased expression of *CTSL* as well as *TMPRSS2* was also found with prolonged culture duration. Thus, the difference in *CTSL* expression could link to changes in the ciliated cell number, which supports the role of ciliated cells in viral replication. Furthermore in line with this, CTSL levels were recently found to be positively correlated with severity of disease in COVID-19 patients, pointing to its role in enhancement of infection (252). Other studies evaluated the role of CTSL and TMPRSS2 in SARS-CoV-2 infection by using E64d (an inhibitor of cysteine proteases, including CTSL) and camostat mesylate (an inhibitor of serine proteases, including TMPRSS2) (228, 253). It was shown that both E64d and camostat

mesylate inhibited infection by Wuhan, Delta and Omicron isolates, confirming the role of CTSL and TMPRSS2 in viral entry.

We excluded possible effects of changes in antiviral responses on the gradual increase in viral infection with the prolonged culture duration, since we did not observe lower expression of type I and III IFNs over culture time at ALI, but rather found a correlation with the level of viral replication.

Our study demonstrates that the use of mixed donor cultures is an efficient way to recapitulate natural variability between donors while saving on resources (cells, culture plastics and media) that can be in high demand/short supply during pandemics. The level of donor-to-donor variation was also represented in inter-experimental variation when using the same donor mix. Inevitably, our study has some limitations. First, it needs to be noted that the comparison between PBEC and PTEC in this study should be interpreted with caution, because PBEC were derived from tumor-free resected bronchial tissue from (ex-) smoking patients with lung cancer, and PTEC were from donor lungs without lung disease. Second, the fact that we used an early pandemic SARS-CoV-2 strain in our studies could be considered a limitation, but this variant is still widely used as model in (fundamental) studies on virus replication and antivirals. Studying this virus is still important to increase our preparedness for future outbreaks of highly pathogenic zoonotic coronaviruses. Several other studies have already compared the replication of different viruses, including recent omicron variants in human airway epithelial cell cultures (75, 140, 253). It would be interesting to investigate if variants like alpha or delta, which have been reported to have a replicative advantage in human airway epithelial cell cultures, are likewise impacted by the changes in differentiated cultures that we observed in this study. Finally, we used cultures containing only epithelial cells. Adding immune cells to the culture system could offer interesting possibilities for future studies to investigate their impact on host responses during infection.

Overall, in this study we have established that epithelial cell types related to mucociliary clearance (i.e. ciliated, goblet cells and transient secretory cells) seem pivotal for SARS-CoV-2 infection and spread of the infection over the epithelial tissue. This study underlines the importance of assessing these cell types and the role of mucus when studying how SARS-CoV-2 infection biology is affected in patients with chronic lung disease, such as those with chronic type 2 inflammation in asthma or in COPD, where epithelial remodelling likely has shifted these cell-type ratios.

Materials and Methods

Cell culture

PBEC were isolated from tumor-free resected bronchial tissue that was obtained from patients undergoing resection surgery for lung cancer at the Leiden University Medical Center (Leiden, the Netherlands). Patients from which this PBEC were derived were enrolled in the biobank via a no-objection system for coded anonymous further use of such tissue (www.coreon.org). However, since 1-9-2022, patients have been enrolled in the biobank using active informed consent in accordance with local regulations from the LUMC biobank with approval by the institutional medical ethical committee (B20.042/Ab/ab and B20.042/Kb/kb). PTEC were isolated from residual tracheal and main stem bronchial tissue from lung transplant donors post-mortem at the University Medical Center Essen (Essen, Germany). Use of such donor tissue for research was approved by the ethical committee of the Medical faculty of the University Duisburg-Essen (ID: 19-8717-BO). (254).

To achieve mucociliary differentiation, PBEC and PTEC were cultured at the ALI as previously described (237). Briefly, epithelial cell cultures from individual donors or mixed donors were seeded onto 12-insert Transwell membranes (Corning Costar, Cambridge, MA, USA), which were coated with PBS supplemented with 5 µg/ml human fibronectin (Promocell, Heidelberg, Germany), 30 µg/ml PureCol (Advanced BioMatrix, CA, USA) and 10 µg/ml bovine serum albumin (Fraction V; Thermo Fisher Scientific, Carlsbad, CA, USA), in a 1:1 mixture of Bronchial Epithelial Cell Medium-basal (BEpiCM-b; ScienCell, Sanbio) and Dulbecco's modified Eagle's medium (DMEM) (Stemcell Technologies, Köln, Germany), further referred to as B/D medium. This B/D medium contains 12.5 mM HEPES, bronchial epithelial cell growth supplement, 100 U/ml penicillin, 100 ug/ml streptomycin (all from ScienCell), 2 mM glutaMAX (Thermo Fisher Scientific). B/D medium was supplemented during submerged culture with 1 nM EC23 (light-stable retinoic acid receptor agonist; Tocris, Abingdon, UK). For individual donors, the seeding intensity was 40,000 cells/12-insert and for mixed donors approximately 150,000 cells (30,000 cells/donor when mixing cells from 5 donors and 40,000 cells/donor when using 4 donors). For the donor mixes, the higher seeding density compared to individual cultures resulted in near-confluency to avoid selective advantage of possible faster-proliferating cells of specific donors.After confluency was reached, the apical medium was removed and cells were cultured at the ALI in B/D medium with 50 nM EC23 for 3-5 weeks; during this period, medium was refreshed and the apical side was washed three times a week with warm PBS to remove excess mucus.

To shift cell differentiation towards an increased number of goblet or ciliated cells, ALI- PBEC were incubated in BD medium supplemented with 50 nM EC23, and either 1 ng/ml IL-13 (Peprotech) or 5 µM DAPT (γ-secretase inhibitor, TOCRIS) from day 22 to day 35 culture

time. To assess the direct effect of DAPT, we treated cells with DAPT either starting 24 h before (and during) infection (a time period considered insufficient to cause a shift in epithelial differentiation) or directly after infection.
Vero E6 cells (master stock MM-3 from dept. of Medical Microbiology collection, characterized by full genome sequencing) were maintained in Dulbecco's modified Eagle's medium with 4.5 g/l glucose with L-glutamine (DMEM; Lonza), supplemented with 8% foetal calf serum (FBS; CapriCorn Scientific) and 100 U/ml of penicillin/streptomycin (Sigma-Aldrich). All cell cultures were maintained at 37°C. Infections for plaque assays in Vero E6 cells were performed in Eagle's minimal essential medium with 25 mM HEPES (EMEM; Lonza) supplemented with 2% FCS, 2 mM L-glutamine (Sigma-Aldrich), and 100 U/ml of penicillin/streptomycin (Sigma-Aldrich) .

SARS-CoV-2 virus

The clinical isolate SARS-CoV-2/Leiden-0002 was isolated from a nasopharyngeal sample collected at the LUMC (GenBank accession nr. MT510999). The virus was passaged twice in Vero E6 cells to obtain the virus stock used for infection. Virus titers were determined by plaque assay as described before (255). All experiments with infectious SARS-CoV-2 were performed at the Leiden University Medical Center biosafety level 3 facilities.

SARS-CoV-2 infection of ALI-PBEC

Prior to infection, the mucus was removed by washing the apical surface of the ALI cultures with 200 µl PBS and aspirating it after a 10-min incubation at 37°C. Basal medium was changed every two days. Cells were infected with 200 µl of inoculum prepared in PBS, containing 30,000 PFU of SARS-CoV-2, per insert for 2 h at 37°C on a rocking platform (estimated MOI of 0.03). PBS was used as solvent control and in mock-infected cells as inoculum. After removal of the inoculum, the apical side was washed three times with PBS and cells were incubated at 37°C. Viral progeny was harvested from the apical side at 24, 48 and 72 hpi as described in the next section.
Cells were infected after 3 to 5 weeks of differentiation as indicated. For cells under DAPT or IL-13 treatment, the medium was supplemented with 1 ng/ml IL-13 or 5 µM DAPT after 3 weeks of differentiation, and after 5-week culture time in total (2 weeks of treatment), PBEC were infected. After infection, the basal medium was replaced by fresh B/D medium also supplemented with IL-13 or DAPT.

RNA isolation, quantitative RT-PCR/real-time PCR (RT-qPCR) and plaque assay analysis

Apical washes were harvested following a 10-min incubation at 37°C with 200 µl PBS. RNA was isolated from half the volume of apical washes (100 µl) after addition of 800 ul of TriPure Isolation Reagent (Sigma-Aldrich). Tripure reagent was spiked with Equine arteritis virus (EAV) to control for variation in RNA extraction efficiency and possible inhibitors of RT-qPCR. Intracellular RNA was isolated by adding 500 ul of TriPure reagent directly to cells on the insert. Samples were stored at -20°C until RNA was isolated using the Direct-zol™ -96 RNA plate isolation (Zymo), 5PRIME Phase Lock Gel extraction (Quantabio) or Maxwell® 16 simply RNA tissue kit (Promega, the Netherlands). The Phosphoglycerate kinase 1 (*PGK-1*) was used as a reference gene for normalization when intracellular RNA was analysed. Primers and probes for EAV and *PGK-1* (Sigma-Aldrich) and the normalization procedure were performed as described before(255). Viral RNA was quantified by internally controlled multiplex RT-qPCR using the TaqMan™ Fast Virus 1-Step Master Mix (Thermo Fisher Scientific) as described previously (256), but with modifications as listed in **Table 2**. A standard curve generated by RT-qPCR on 10-fold serial dilutions of a T7 RNA polymerase-generated *in vitro* transcript containing the target sequences was used for absolute quantification of RNA copy numbers.

For analysis of the transcriptional response of epithelial cells to infection, RNA was reverse-transcribed and cDNA was amplified by real-time qPCR (Bio-Rad, Veenendaal, the Netherlands) using specific primers. Relative normalized gene expression compared to reference genes Ribosomal Protein L13a (RPL13A) and ATP synthase, H^+ transporting, mitochondrial F1 complex, beta polypeptide (ATP5B) were calculated according to the standard curve method. Reference genes were selected out of 8 candidate reference genes using the "Genorm" software (Genorm; Primer Design, Southampton, UK). RT-qPCR was performed on a CFX384 Touch™ Real-Time PCR Detection System (Bio-Rad) using a program consisting of 5 min at 50°C and 20 s at 95°C (or 3 min at 95°C when cDNA was used), followed by 45 cycles of 5 s at 95°C and 30 s at 60°C or 63°C (depending on primers). Primer pairs are listed in **Table 2**.

For quantification of the number of infectious virus particles, the apical wash was serially diluted and infectious titers were determined by plaque assay on Vero E6 as described previously (255).

Table 2: Primer sequences

Gene	Forward primer (5'-3')	Reverse primer (5'-3')
E	ACAGGTACGTTAATAGTTAATAGCGT	ATATTGCAGCAGTACGCACACA
E probe	TexRed-ACACTAGCCATCCTTACTGCGCTTCG-BHQ1	
RdRp	GTGARATGGTCATGTGTGGCGG	CARATGTTAAASACACTATTAGCATA

RdRp probe	FAM-CAGGTGGAACCTCATCAGGAGATGC-BHQ1	
MUC5AC	CCTTCGACGGACAGAGCTAC	TCTCGGTGACAACACGAAAG
FOXJ1	GGAGGGGACGTAAATCCCTA	TTGGTCCCAGTAGTTCCAGC
SCGB1A1	ACATGAGGGAGGCAGGGGCTC	ACTCAAAGCATGGCAGCGGCA
TP63	CCACCTGGACGTATTCCACTG	TCGAATCAAATGACTAGGAGGGG
IFNL1	GGACGCCTTGGAAGAGTCACT	AGAAGCCTCAGGTCCCAATTC
IFNB1	ATGACCAACAAGTGTCTCCTCC	GGAATCCAAGCAAGTTGTAGCTC
CXCL8	CTGGACCCCAAGGAAAAC	TGGCAACCCTACAACAGAC
IL6	CAGAGCTGTGCAGATGAGTAC A	GATGAGTTGTCATGTCCTGCA
ACE2	CGTCTGAATGACAACAGCCTAGA	AATGCCAACCACTATCACTCCC
TMPRSS2	AATCGGTGTGTTCGCCTCTAC	CGTAGTTCTCGTTCCAGTCGT
CD147	CAGAGTGAAGGCTGTGAAGTCG	TGCGAGGAACTCACGAAGAAC
GRP78	GGAAAGAAGGTTACCCATGC	AGAAGAGACACATCGAAGGT
ATP5B	TCACCCAGGCTGGTTCAGA	AGTGGCCAGGGTAGGCTGAT
RPL13A	AAGGTGGTGGTCGTACGCTGTG	CGGGAAGGGTTGGTGTTCATCC

Immunofluorescence staining

For analysis by immunofluorescence, ALI cultures were rinsed using PBS and cells were fixed by adding 3% (w/v) paraformaldehyde diluted in PBS into the basal and apical compartments followed by incubation at room temperature for at least 35 min. Next, inserts were washed two times with PBS and stored in PBS with 10 mM glycine at 4°C until further use. Ice-cold methanol was added for 10 min at 4°C, and PBS containing 1% (w/v) BSA, 0.3% (w/v) Triton-X-100 (PBT) was used to block non-specific binding sites and permeabilize cells for 30 min at 4°C. Membranes were excised from the insert and cut into 4 pieces that were incubated overnight at 4°C with specific antibodies at the following dilutions: rabbit anti-SARS-CoV-2 N antibody (JUC3,1:500 (167)), human anti-SARS-CoV-2 Spike antibody (P008_076 (257)), mouse anti-MUC5AC antibody (1:200; Thermo Fisher Scientific), mouse anti-acetylated α-tubulin (1/100; Sigma Aldrich) or goat anti-FOXJ1 antibody (1:200; R&D, Minneapolis, MN, USA). After washing, membranes were incubated with corresponding secondary antibodies: donkey anti-rabbit, donkey anti-mouse or donkey anti-goat Alexa-fluor antibodies (all diluted 1:200, Thermo Fisher Scientific) and 4',6-diamidino-2-phenylindole (DAPI, 1:200, Sigma-Aldrich) in the dark for 30 min at room temperature. Next, membranes were transferred to glass slides and covered with prolong gold anti-fading reagent (Thermo Fisher Scientific) and a coverslip (VWR, Amsterdam, the Netherlands). Slides were viewed using a Leica TCS SP8 confocal microscope (Leica Microsystems, Wetzlar, Germany), the Andor Dragonfly 500 spinning disk confocal (Andor Technology, Belfast, UK), or the ZEISS Axio Scan.Z1 Slide Scanner (ZEISS, Oberkochen,

Germany) at 100 x /400 x / 630 x original magnification according to experimental requirements. Positive-stained cells from three random areas of each insert membrane of each independent experiment were quantified by ImageJ.

RNA sequencing and analysis

The samples harvested from 3-week and 5-week differentiated ALI-PBEC and ALI-PTEC were used to perform RNA sequencing (RNA-Seq) at GenomeScan (Leiden, the Netherlands). Total RNA was extracted using TriPure Isolation Reagent and Maxwell® 16 simply RNA tissue kit and passed the quality control (QC) measured by the Fragment Analyzer. Then mRNA was isolated based on poly-A selection and RNA fragmentation was performed. After that, cDNA was synthesized for adapter ligation and PCR amplification. A data set of 12 samples was generated using an Illumina NovaSeq6000 sequencer and the quality for the raw data was determined with third-party (FastQC v0.11.9) and in-house (FastQA v3.1.25) QC tools. The paired-end reads were trimmed to remove possible adapter sequences using cutadapt v2.10 and mapped to the human GRCh37.75 (Homo_sapiens.GRCh37.75.dna.primary assembly.fa). Based on the mapped locations in the alignment file the frequency of how often a read was mapped on a transcript was determined with HTSeq v0.11.0. RNA-Seq analysis was performed using the R package DeSeq2 with the read counts≥10 read counts. Differential expression was conducted comparing virus infection at each time point to time matched no virus control/mock. Gene signatures were made using the Gene Set Variation Analysis (GSVA) package. The differentially expressed genes (DEGs) were generated by comparing data in 5-week cultures compared to 3-week cultures and the significant differences were considered when they had a Benjamini Hochberg p value<0.1 and a fold change>|2|. The gene sets of differentially expressed genes were further analysed by gene set enrichment analysis (GSEA) using the website www.gsea-msigdb.org as previously reported (258, 259).

Cellular deconvolution

The relative proportion of each cell type (ciliated, secretory, basal and rare cells) was predicted using cellular deconvolution analysis of bulk RNA-Seq data as previously described (260). To this end, genes were selected using AutoGeneS software on the Human Lung Cell Atlas v1.0 dataset (261) based on minimized correlation and maximized distance between clusters. After that, genes with the most stable results across cohorts were selected and used to deduce major cell type proportions. The RNA-Seq data was subsequently normalized to counts per million (CPM), and highly variable (HV) genes (N=5,000) were selected. Next, on all samples bulk deconvolution was performed using the

CIBERSORT support vector regression (SVR) method (262). The relative proportion of cell types was compared between 3-week cultures and 5-week cultures from ALI-PBEC or ALI-PTEC using paired two-way ANOVA with Tukey's test.

Statistical analysis

Statistical analysis was performed in GraphPad PRISM 9.0 (GraphPad Software Inc., La Jolla, CA). Differences were assessed by a paired one-way with Tukey's test, paired two-way ANOVA with Tukey's test or paired, two-tailed t test. Data are shown as mean values ± SEM and differences were considered significant at $P < 0.05$.

Statement of Ethics

Patients from which this PBEC were derived were enrolled in the biobank via a no-objection system for coded anonymous further use of such tissue (www.coreon.org). However, since 1-9-2022, patients have been enrolled in the biobank using active informed consent in accordance with local regulations from the LUMC biobank with approval by the institutional medical ethical committee (B20.042/Ab/ab and B20.042/Kb/kb). For the present study, cells from patients were used that were collected before 1-9-2022, and based on the regulations of the no-objection system, individual informed consent was not needed. PTEC were isolated from residual tracheal and main stem bronchial tissue from lung transplant donors post-mortem at the University Medical Center Essen (Essen, Germany). Use of such donor tissue for research was approved by the ethical committee of the Medical faculty of the University Duisburg-Essen (ID: 19-8717-BO). Written informed consent for the use of PTEC was provided by the transplant recipients of the respective lungs.

Conflict of Interest Statement

The authors have no conflicts of interest to declare.

Funding Sources

This study was supported by a COVID-19 MKMD grant from the Netherlands Organization for Health Research and Development (ZonMw) and the Dutch Society for the Replacement of Animal Testing (Stichting Proefdiervrij) (grant #114025007). C.S.-B. was supported by the Coordination for the Improvement of Higher Education Personnel (CAPES) (process no.

88881.171440/2018-01), Ministry of Education, Brazil. Part of this research was supported by the Leiden University Fund (LUF), the Bontius Foundation, and donations from the crowdfunding initiative “wake up to corona”. This study has also received funding from the European Union's Horizon 2020 research and Innovation program under grant No 10100362 (the SCORE project). Part of RNA-Seq and analysis was supported by a RSEOH-CAG Rapid Response Research Initiative and a RSEOH-CAG 2021 Extension Grant. Collection of primary human tracheal epithelial cells was supported by grants from the Deutsche Forschungsgemeinschaft (DFG) (Ta 275/7-1 and Ta 275/8-1) to C.T.

Author Contributions

Melissa Thaler, Ying Wang, Anne M. van der Does, Peter J. Bredenbeek, Pieter S. Hiemstra and Martijn J. van Hemert were involved in study design and conceptualization. Melissa Thaler, Ying Wang, Dennis K. Ninaber, Natacha S. Ogando, Clarisse Salgado-Benvindo performed experiments. Alen Faiz performed RNA-Seq analysis and cellular deconvolution. Hendrik Beckert, Christian Taube collected and isolated human tracheal epithelial cells. Melissa Thaler and Ying Wang wrote the manuscript. Anne M. van der Does, Pieter S. Hiemstra, Martijn J. van Hemert, Eric J. Snijder and Peter J. Bredenbeek revised the manuscript. The final version was critically reviewed and approved by all authors.

Data Availability Statement

The RNA-Seq data that support the findings of this study will be openly available in the repository European Genome-Phenome Archive (EGA). Until then all data are available upon reasonable request by contacting the corresponding author. All other data generated or analysed during this study are included in this article.

Supplementary Material

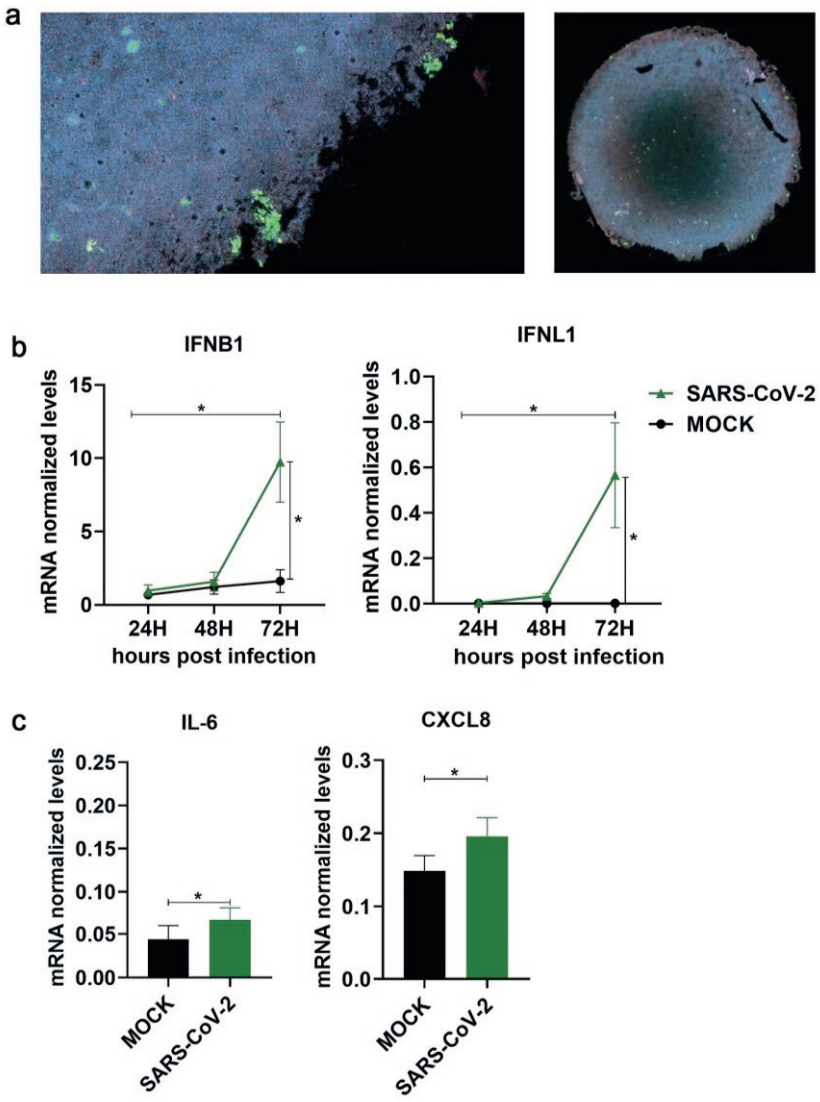

Figure S1: Infection and immune responses of a primary airway epithelial cell culture model. ALI-PBEC (mix of 5 donors) cultured for 5 weeks at ALI were infected with SARS-CoV-2 (30,000 PFU per insert) (a) Representative image of immunostaining with anti-SARS-CoV-2 spike protein antibody (green), anti-N protein antibody (JUC3; red) and DAPI (blue) for nuclear staining was captured by ZEISS slide scanner (b) Analysis of gene expression of *IFNB1*, *IFNL1* and (c) *IL6* and *CXCL8* (IL-8) normalized to two reference genes (*RPL13A/ATP5B*) in mixes of 5 donors by RT-qPCR. The graphs represent the mRNA levels at 72 hpi. Data are mean values ± SEM. n=3 independent experiments derived from the same donor mix cultured for at least 4 weeks. Statistical analysis was conducted using two-way ANOVA with a Tukey/Bonferroni post-hoc test. Significant differences are indicated by *P<0.05.

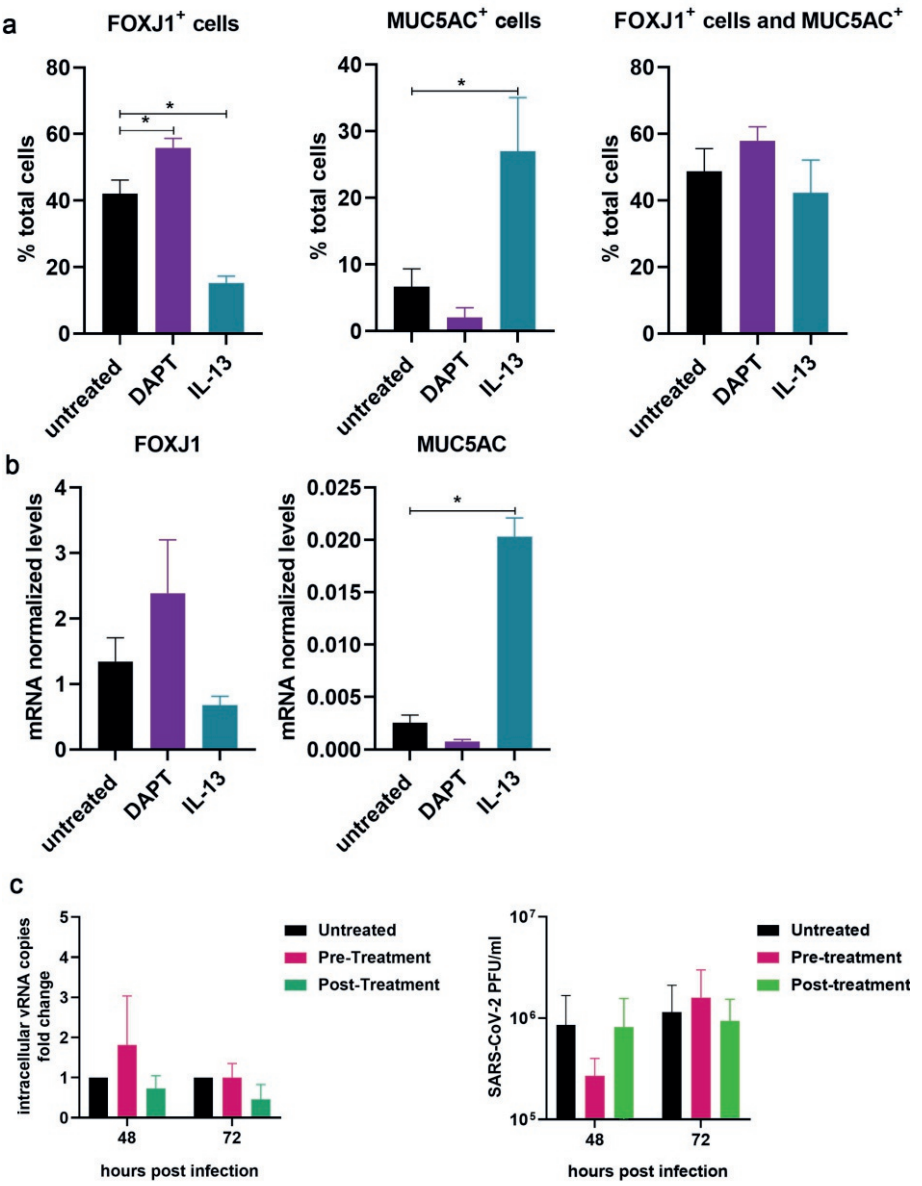

Figure S2: Effect of long-term DAPT/IL-13 exposure on epithelial cell composition and effect of acute DAPT/IL-13 exposure on susceptibility to SARS-CoV-2 infection. ALI-PBEC (mix of 4-5 donors) were differentiated for 3 weeks, before addition of DAPT (5 µM) or IL-13 (1 ng/ml), followed by differentiation for an additional 2 weeks. (a) After 5 weeks of differentiation, ALI-PBEC were fixed, stained and analyzed by immunofluorescence using primary antibodies against MUC5AC and FOXJ1 (goblet cell marker, ciliated cell marker) in combination with DAPI for nuclear staining. The quantification of FOXJ1-positive cells and MUC5AC-positive cells was done by ImageJ software. Data are mean ± SEM. (b) mRNA levels of *FOXJ1* and *MUC5AC* were measured by RT-qPCR. Data are mean ± SEM. Analysis of differences was conducted using paired t test. (c) Short-term treatment with DAPT was

performed in cells after 5 weeks of differentiation. Cells were either pre-treated with DAPT for 24 h (pre-treatment) or post-treated directly after infection (post-treatment). Intracellular SARS-CoV-2 RNA copies were measured by RT-qPCR and plaque assay was performed with apical washes to quantify infectious virus titers. n=3 independent experiments. Data are mean ± SEM. Fold change in intracellular RNA copies was compared to untreated controls. Statistical analysis was performed using a paired t test. Significant differences are indicated by *P<0.05.

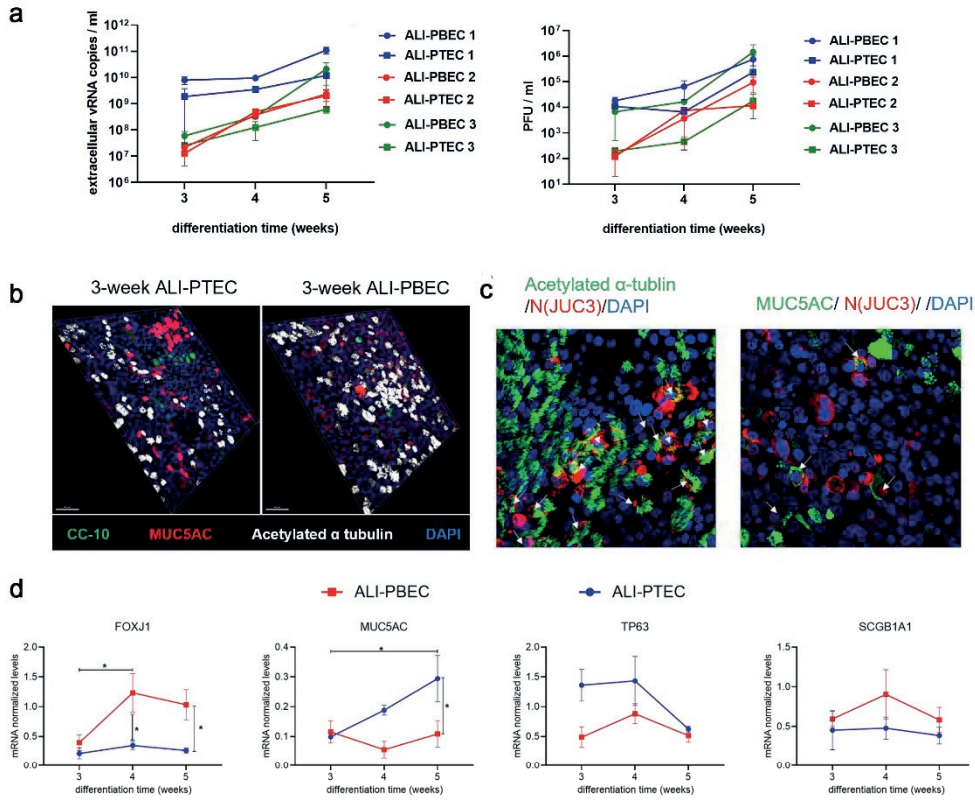

Figure S3: Effect of culture duration on infection and epithelial cell-specific genes in PTEC and PBEC. (a) Extracellular viral RNA copies in the apical wash were measured by RT-qPCR and viral infectious progeny was determined by plaque assay in Vero E6 cells. Mean values ± SEM is presented from 3 independent experiments using 3 different donor mixes. (b) Immunofluorescence staining of PTEC and PBEC with antibodies against CC-10 (Club cell marker), MUC5AC (goblet cell marker), acetylated α-tubulin (ciliated cell marker) in combination with DAPI for nuclear staining. (c) Immunofluorescence staining of PTEC with antibodies against acetylated α-tubulin and SARS-CoV-2 N protein in combination with DAPI. Immunofluorescence images shown are representative merged z-stack images for results of 3 independent experiments with 630 x original magnification. (d) ALI-PTEC/PBEC (mix of 5 donors) were differentiated at ALI for 3, 4 or 5 weeks, and analyzed by RT-qPCR to measure gene expression of FOXJ1 (ciliated cell marker), MUC5AC (goblet cell marker), SCGB1A1 (club cell marker) and TP63 (basal cell marker). n=3 independent experiments at 3-5 weeks derived from three donor mixes the same as used in Fig.3. Data are mean ± SEM. Analysis of differences was conducted using two-way ANOVA with a Tukey/Bonferroni post-hoc test. Significant differences are indicated by *P<0.05.

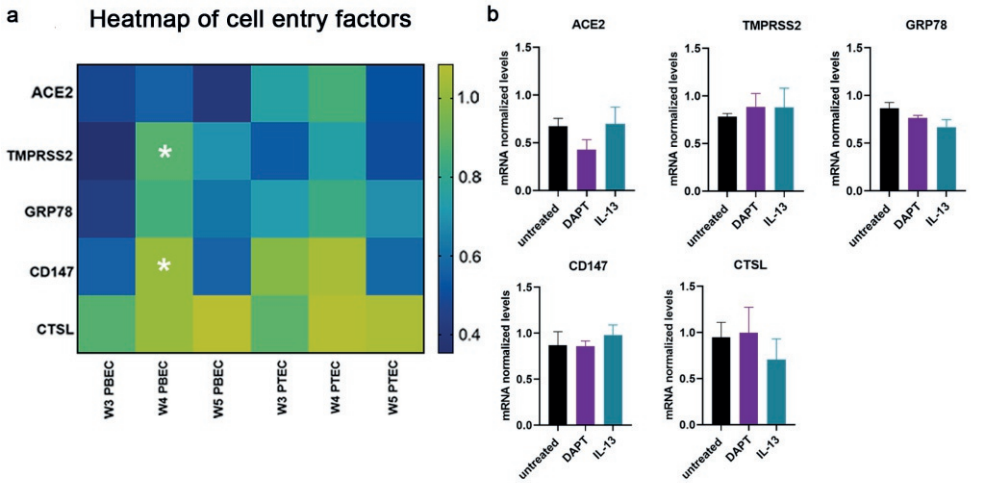

Figure S4: Effect of culture duration and DAPT/IL13 treatment on expression of SARS-CoV-2 cell-entry factors. (a) Analysis of gene expression of viral cell-entry factors by RT-qPCR in 3, 4 and 5 week uninfected cultures of PTEC and PBEC and (b) in DAPT or IL-13 treated 5 week-differentiated cultures. Data are mean values ± SEM. n=3 independent experiments derived from three donor mixes. Statistical analysis was conducted using two-way ANOVA with a Tukey post-hoc test or one-way ANOVA with Dunnett test. Significant differences are indicated by $P<0.05$. *= 5-week ALI-PBEC vs 3-week ALI-PBEC.

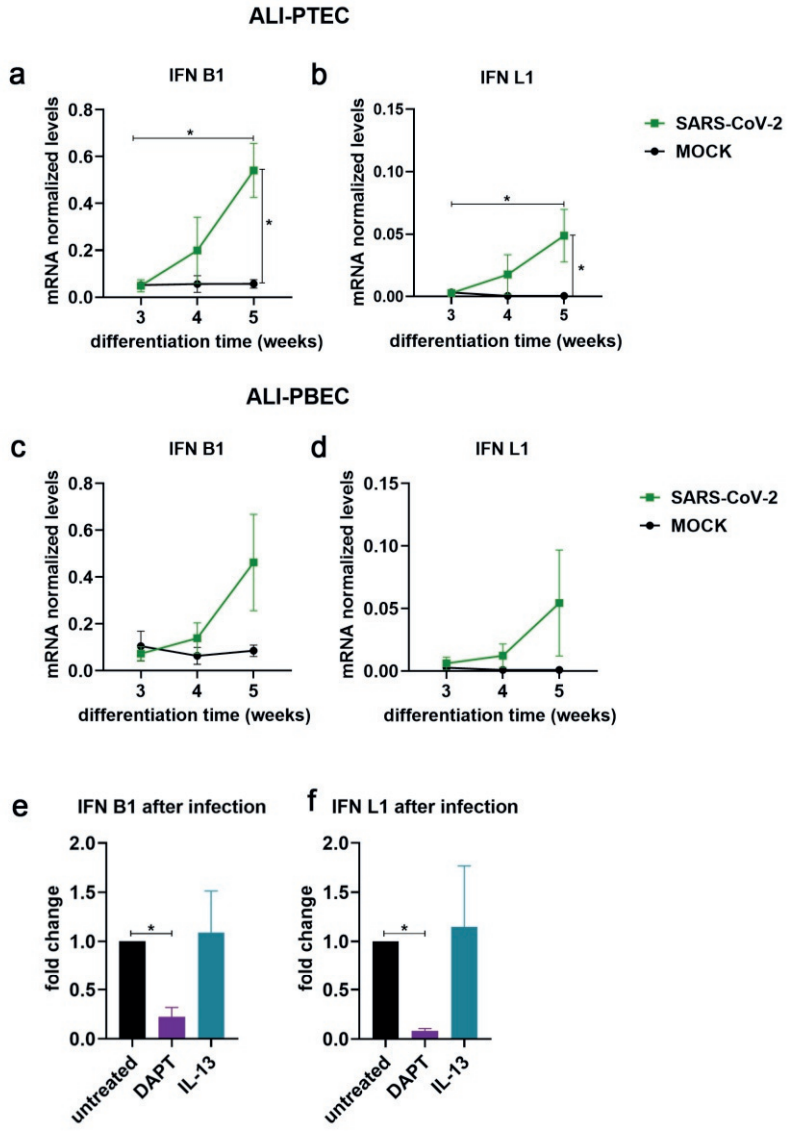

Figure S5: Antiviral responses after SARS-CoV-2 infection. ALI-PTEC and PBEC cultured for 3-5 weeks (A-D), and 5-week ALI-PBEC (E, F) cultured at ALI in presence or absence of DAPT or IL-13 (during the last 2 weeks), were infected by SARS-CoV-2 (30,000 PFU per insert). Cells were lysed at 72 hpi to quantify mRNA levels of *IFNB1* (a/c/e) and *IFNL1* (b/d/f) by RT-qPCR. n=3 independent experiments using 3 different donor mixes. Data are mean ± SEM. Fold change in E and F was compared to untreated controls. Analysis of differences was conducted using two-way ANOVA with a Tukey/Bonferroni post-hoc test. Significant differences are indicated by *P<0.05.

Table S1: The differentially expressed genes in ALI-PBEC and ALI-PTEC between 3-week and 5-week cultures

Gene symbol	logFC	logCPM	F	P value	FDR
ALI-PBEC					
GBP1	1,002649	5,59286	28,42654	0,000205	0,011999
C6	1,008593	4,598683	34,17632	9,24E-05	0,011252
FAM13C	1,01462	1,686769	15,42701	0,002161	0,028787
NMNAT2	1,040247	2,463503	27,22633	0,000245	0,012624
VEPH1	1,040893	1,215865	12,34508	0,004528	0,04146
KIF26B	1,047462	2,465433	23,28812	0,000464	0,01499
SUSD5	1,048884	0,593884	13,23716	0,003618	0,037666
ALS2CR12	1,052709	3,056197	27,67302	0,000229	0,012344
TEKT3	1,073256	0,717851	21,28602	0,000662	0,017229
ADH7	1,076298	6,748417	33,31955	0,000103	0,011252
SLC1A1	1,077068	5,080468	21,27037	0,000663	0,017229
GCNT4	1,079011	1,61263	23,97091	0,000414	0,014456
GNA14	1,082498	2,955824	12,76014	0,004075	0,039248
SERPING1	1,083826	3,388572	23,87261	0,000421	0,014456
CXCL3	1,087681	3,835865	9,254044	0,010664	0,06513
LINC00689	1,101837	1,213377	7,917803	0,016176	0,081168
RP11-356I2.4	1,122523	0,167388	18,21206	0,001194	0,022104
CCL20	1,124136	4,278383	10,84357	0,006751	0,051083
CCDC173	1,129108	4,661543	32,15727	0,000121	0,011477
SFRP2	1,130373	1,308617	10,19488	0,008098	0,056111
ARG2	1,131078	2,939088	13,98017	0,003021	0,034592
GLYATL2	1,139479	0,778915	13,64786	0,003273	0,036107
ZNF853	1,145346	0,872255	7,059498	0,021529	0,095652
ACTBL2	1,146252	1,202529	14,67346	0,002567	0,031485
OXGR1	1,154019	0,362324	8,221797	0,01467	0,077218
TM6SF1	1,157709	0,157218	15,9499	0,001924	0,026801
ZSCAN12P1	1,177114	0,305378	10,76975	0,00689	0,051681
AFAP1L2	1,184962	2,2387	12,23583	0,004657	0,042023
UCHL1	1,187467	1,02622	11,45645	0,005715	0,046538
UCA1	1,203382	2,242207	8,053701	0,015481	0,079529
DMBT1	1,214279	5,708363	29,85375	0,000166	0,011477

CES1	1,220755	5,121919	37,27795	6,28E-05	0,010533
SLC5A1	1,231942	3,193087	47,33052	2,09E-05	0,007842
RP11-642P15.1	1,25914	0,94976	23,23305	0,000469	0,015018
EEF1A2	1,292066	1,559594	6,937111	0,022454	0,098292
RP1-27K12.2	1,303139	2,755264	16,99273	0,001536	0,024375
IL22RA1	1,313443	0,205781	11,12312	0,006253	0,048826
HLA-DQA1	1,318172	3,113733	9,05018	0,01134	0,067178
CYP24A1	1,330907	3,752493	8,916734	0,011811	0,068671
RGS22	1,388349	3,30457	31,34144	0,000135	0,011477
SLC6A20	1,427783	2,039617	23,02251	0,000486	0,015242
MAP1B	1,430696	3,968576	17,9179	0,001267	0,022561
CTSV	1,492403	3,621686	16,42133	0,001736	0,025711
NCR3LG1	1,550185	1,734731	35,59817	7,72E-05	0,011007
CXCL5	1,557573	3,176724	9,935025	0,008726	0,058225
CHI3L1	1,576727	1,837262	20,73273	0,000732	0,017984
GPNMB	1,699773	6,046425	14,86666	0,002455	0,030665
AL121901.1	1,810156	1,657353	10,00457	0,008553	0,05784
SLC5A8	1,836587	1,7187	17,35876	0,001422	0,023594
SPTBN4	-2,09053	2,377134	25,71497	0,000311	0,013732
AC022596.6	-2,0531	2,060019	15,32716	0,00221	0,029127
EXOC3L1	-1,82355	1,023619	14,22714	0,002849	0,033538
PLCD4	-1,76792	1,754185	22,92399	0,000494	0,015302
IQGAP3	-1,7452	0,909495	11,2558	0,006032	0,047916
LGALS7	-1,70892	4,387691	19,0473	0,00101	0,020535
LGALS7B	-1,69201	3,76449	26,46105	0,000276	0,013273
CYP26C1	-1,64831	1,05923	15,95419	0,001922	0,026801
CYP4F23P	-1,6461	2,028523	12,52156	0,004328	0,040383
ASPM	-1,63808	1,457722	11,77712	0,005249	0,044623
PLA2G4F	-1,63644	2,389311	11,3363	0,005903	0,047229
PDE11A	-1,60907	3,468886	10,12901	0,008252	0,056692
MAOB	-1,57209	1,719884	19,53167	0,000919	0,020088
KRT13	-1,5713	8,159369	17,33201	0,00143	0,023671
WNT10A	-1,55668	5,014215	88,11726	9,64E-07	0,00322
KLK7	-1,52867	4,871598	17,55299	0,001366	0,023371
MYOT	-1,49218	1,383578	12,49269	0,00436	0,040602

ALOX15B	-1,42438	4,068088	30,08054	0,000161	0,011477
CKAP2L	-1,42374	0,387569	7,749934	0,017085	0,083565
KCNE4	-1,40436	1,775868	12,70016	0,004137	0,039553
KLK8	-1,38961	1,394874	27,35364	0,000241	0,012533
EFS	-1,32513	1,430937	16,95673	0,001548	0,024423
COL7A1	-1,29595	7,750315	40,8237	4,15E-05	0,009439
MEGF6	-1,28014	4,888583	28,19833	0,000212	0,012091
CYP26B1	-1,27924	7,61654	9,465685	0,010011	0,063124
PLCH2	-1,27526	6,836023	48,42031	1,87E-05	0,007842
RP5-1085F17.3	-1,26647	0,327113	18,20274	0,001196	0,022104
TNNI2	-1,26069	4,253661	11,14312	0,006219	0,048644
RP11-235E17.6	-1,26026	2,578247	19,50609	0,000924	0,020119
FGFR3	-1,25858	7,297273	110,6972	2,94E-07	0,001553
EGFL6	-1,24513	3,665653	12,44813	0,00441	0,040906
HMHA1	-1,24382	3,55872	7,978989	0,015858	0,080375
MMP28	-1,24275	5,290207	45,78856	2,44E-05	0,008486
GPT	-1,23928	0,373352	12,28928	0,004593	0,041765
CLEC2D	-1,23812	1,918601	19,119	0,000996	0,020423
RHBDL1	-1,23676	2,113606	19,16153	0,000988	0,020339
ECM1	-1,22886	4,151404	12,24362	0,004648	0,042017
MEX3B	-1,22089	1,358241	8,708329	0,012593	0,071092
RP11-268J15.5	-1,20935	2,56421	22,61057	0,000522	0,01548
CYP2T2P	-1,20801	6,446988	21,97836	0,000584	0,016352
FAM229A	-1,20618	2,868697	20,50802	0,000764	0,018271
CSRNP3	-1,20084	1,439979	11,40015	0,005802	0,046872
PCP2	-1,20062	0,595494	7,173733	0,020707	0,093452
PLK1	-1,19771	1,865708	17,22768	0,001462	0,023788
CAPNS2	-1,19411	1,982033	11,36996	0,00585	0,046994
ADIRF	-1,19009	3,253925	34,07615	9,36E-05	0,011252
PTTG1	-1,18856	3,121655	32,07054	0,000122	0,011477
BDKRB1	-1,17456	0,394196	17,47789	0,001387	0,023391
GHR	-1,17168	0,534359	9,381281	0,010266	0,063814
ANKRD9	-1,16422	4,305996	25,46552	0,000324	0,01378
FOXN4	-1,16263	3,312565	11,79335	0,005226	0,044623
HSD11B2	-1,15791	4,53207	14,92014	0,002425	0,030371

IGFBP6	-1,15351	7,240489	108,5039	3,27E-07	0,001553
KRT14	-1,14903	4,978784	10,55921	0,007306	0,05301
RP11-44N21.1	-1,14886	0,745321	11,82374	0,005185	0,044414
VMO1	-1,14822	7,730684	34,33033	9,06E-05	0,011252
NAPSA	-1,14532	0,73691	9,183362	0,010893	0,065801
KCP	-1,14261	2,294007	29,44502	0,000176	0,011598
WFDC3	-1,14259	2,556692	10,05651	0,008426	0,057345
CENPE	-1,14219	1,280905	7,721378	0,017246	0,084056
CFD	-1,13951	3,218426	14,73457	0,002531	0,031258
TMEM160	-1,13884	3,549933	30,43181	0,000153	0,011477
SNCG	-1,13843	2,811491	21,10013	0,000684	0,017421
AIFM3	-1,13564	2,050572	11,13285	0,006237	0,048753
RBBP8NL	-1,1341	3,470603	18,30167	0,001172	0,021877
CTU1	-1,12955	2,727798	17,31734	0,001435	0,023671
ABCC9	-1,12894	4,376523	24,04358	0,000409	0,014456
KLK6	-1,12721	3,030986	9,409648	0,01018	0,063582
RP11-108K14.4	-1,12421	3,403741	47,91893	1,97E-05	0,007842
FES	-1,12125	2,078394	17,20445	0,001469	0,023788
HSPB1	-1,11756	8,551601	77,27061	1,89E-06	0,004484
PRSS3	-1,11568	1,316268	9,743191	0,009226	0,060129
CHRM3	-1,11185	2,125622	11,38383	0,005828	0,046894
POU5F1	-1,11076	3,685524	8,312625	0,014253	0,076077
CDCA3	-1,10493	0,745953	9,322954	0,010446	0,064373
LIME1	-1,10456	2,077558	16,8718	0,001576	0,024625
UNC5CL	-1,10099	1,164797	9,878959	0,008869	0,058684
RP11-538D16.2	-1,10034	1,293376	10,81006	0,006814	0,051351
AC009061.1	-1,0961	2,198033	15,63168	0,002064	0,027967
NDUFA13	-1,08936	1,374798	11,11447	0,006268	0,048826
UCN2	-1,08535	1,380242	17,16759	0,00148	0,023892
GPS2	-1,08416	1,109488	8,343	0,014117	0,075712
ANKRD2	-1,08102	0,646797	7,804956	0,016781	0,082601
CYP2E1	-1,07754	2,401679	19,55921	0,000915	0,020032
HES6	-1,07393	4,396359	24,81671	0,00036	0,014136
RP5-1074L1.4	-1,07384	1,133285	8,676116	0,012719	0,071522
HCN3	-1,07207	2,945652	33,76532	9,75E-05	0,011252

NYAP1	-1,06774	-0,30713	8,367067	0,01401	0,075365
ADAMTSL4	-1,06769	4,669001	8,592351	0,013055	0,072607
C19orf40	-1,06529	0,537614	9,758387	0,009185	0,059996
LTBP4	-1,06463	6,480215	36,66196	6,76E-05	0,010608
KIFC1	-1,06155	0,992713	7,844801	0,016564	0,082067
ADAMTSL5	-1,05223	3,977505	18,22178	0,001191	0,022104
FAM173A	-1,04914	3,761411	38,47602	5,44E-05	0,01008
C12orf54	-1,0457	0,473343	8,517447	0,013363	0,07355
AP001053.11	-1,045	1,784287	18,49842	0,001127	0,021576
WNT2B	-1,04208	1,98975	16,13253	0,001848	0,02628
KDR	-1,03952	3,400876	12,14524	0,004767	0,042533
IQCJ-SCHIP1	-1,03685	0,963322	14,41452	0,002726	0,03274
NFATC4	-1,03594	5,418897	22,16864	0,000564	0,016106
PRKCDBP	-1,03538	4,92231	34,12324	9,31E-05	0,011252
PRICKLE4	-1,03464	6,185696	30,46854	0,000152	0,011477
SPINK5	-1,0342	4,561195	11,50763	0,005638	0,046276
DLK2	-1,03399	3,666093	33,64215	9,91E-05	0,011252
PLEKHH3	-1,03309	6,09077	109,4289	3,12E-07	0,001553
PPP1R35	-1,03304	3,717862	16,69999	0,001635	0,024991
FLG-AS1	-1,02837	3,84126	15,16394	0,002294	0,029745
BRICD5	-1,02297	2,700028	13,73493	0,003204	0,035576
TNFRSF25	-1,02002	4,588371	44,42559	2,81E-05	0,008905
TRIM7	-1,01838	3,731958	39,00875	5,11E-05	0,009989
PTMS	-1,01763	6,404615	33,33356	0,000103	0,011252
RP11-783K16.13	-1,01354	1,096157	13,9964	0,00301	0,034487
CTD-3214H19.6	-1,01297	0,204872	7,51536	0,018461	0,087378
PCDHB15	-1,01281	1,23667	16,91976	0,00156	0,024465
RP11-258C19.7	-1,01247	1,280704	11,74446	0,005294	0,044769
PHYHIP	-1,01103	4,106824	36,22729	7,14E-05	0,010778
AC005262.2	-1,00651	1,244988	8,153251	0,014995	0,078099
ZNF648	-1,00603	3,002909	13,40844	0,003469	0,036849
DBP	-1,00518	4,433981	24,40215	0,000385	0,014257
GDPD3	-1,00033	2,191338	19,86287	0,000863	0,019631

Gene symbol	logFC	logCPM	F	P value	FDR
ALI-PTEC					
DMBT1	1,003702	5,708363	20,07165	0,000829	0,076555
ANKFN1	1,03626	3,177326	26,0421	0,000295	0,067598
RP11-247L20.4	1,03854	0,903807	17,57343	0,00136	0,084818
CCDC173	1,040203	4,661543	24,83022	0,000359	0,067598
NCR3LG1	1,075958	1,734731	14,66594	0,002571	0,091098
VNN3	1,102569	2,739779	20,95719	0,000703	0,075288
PTPRT	1,121797	3,408321	44,66975	2,74E-05	0,0534
AC005281.1	1,152108	1,904765	15,93077	0,001932	0,089116
FAM167A	1,160504	1,696483	18,33648	0,001164	0,081002
DSCAML1	1,161098	1,538778	18,19868	0,001197	0,082086
PLA1A	1,165826	1,232803	17,35953	0,001422	0,085482
RND2	1,188845	2,016029	16,12771	0,00185	0,088906
SUSD5	1,195827	0,593884	16,28759	0,001787	0,088694
DAAM2	1,200075	1,531415	15,37768	0,002185	0,090206
COL28A1	1,231637	3,080218	27,89596	0,000222	0,062312
USH1C	1,28638	1,140772	19,77719	0,000877	0,076555
TMEM176B	1,310352	2,70275	25,33272	0,000331	0,067598
CES1	1,319449	5,121919	39,111	5,05E-05	0,0534
VEPH1	1,330778	1,215865	14,55405	0,002639	0,091701
RGS22	1,340184	3,30457	26,62032	0,00027	0,06463
CXCL6	1,348396	4,33736	29,33268	0,000179	0,062312
CCL20	1,381199	4,278383	16,82882	0,00159	0,087603
RP11-642P15.1	1,387534	0,94976	18,68823	0,001085	0,080108
TMEM176A	1,425233	2,424882	39,54631	4,80E-05	0,0534
TCHH	1,429566	2,34236	21,01183	0,000696	0,075219
MACROD2	1,458391	1,356867	23,45164	0,000452	0,067598
BDNF	1,499378	0,727706	14,38546	0,002745	0,092443
GRM7	1,534808	2,010926	35,11407	8,20E-05	0,0534
CYP2A13	1,6437	4,77677	14,5103	0,002666	0,092091
CHI3L1	1,645907	1,837262	24,19878	0,000398	0,067598
CXCL5	2,16049	3,176724	19,96095	0,000847	0,076555
SLC5A8	2,198774	1,7187	23,7566	0,000429	0,067598
IQGAP3	-2,59342	0,909495	22,71009	0,000513	0,068158

ASPM	-1,89113	1,457722	15,38539	0,002181	0,090206
KLK7	-1,83656	4,871598	25,61704	0,000316	0,067598
CENPE	-1,78737	1,280905	17,97174	0,001253	0,082286
FBXO24	-1,41878	0,139514	16,18092	0,001829	0,088694
ARHGAP11B	-1,39201	1,100907	25,09047	0,000344	0,067598
PLCD4	-1,36981	1,754185	14,04437	0,002975	0,096749
MAOB	-1,32147	1,719884	16,32054	0,001774	0,088694
ECM1	-1,31965	4,151404	15,93715	0,001929	0,089116
LGALS7B	-1,2755	3,76449	16,05833	0,001878	0,089116
UCN2	-1,26972	1,380242	24,58247	0,000374	0,067598
LMNB1	-1,23352	2,202663	15,1922	0,002279	0,090908
KRT14	-1,23213	4,978784	15,69549	0,002035	0,090206
GPR37L1	-1,19404	2,34757	29,30917	0,00018	0,062312
MAP2	-1,18982	2,346671	23,38027	0,000457	0,067598
TENM2	-1,1629	2,100679	21,7164	0,000612	0,070391
RP4-758J18.10	-1,14543	0,954296	14,1606	0,002894	0,094976
NXPH4	-1,12633	2,059991	20,22591	0,000805	0,076555
RHBDL1	-1,11214	2,113606	15,52982	0,002112	0,090206
SEMA6A	-1,1117	2,970364	21,65018	0,000619	0,070391
ALDOC	-1,10159	4,805836	15,56031	0,002097	0,090206
ALOX15B	-1,09932	4,068088	20,08179	0,000828	0,076555
CA9	-1,04728	3,850175	37,16396	6,36E-05	0,0534
FIBIN	-1,03703	1,317875	15,218	0,002266	0,090908
CLDN8	-1,01129	4,270443	18,61824	0,0011	0,080108
WNT10A	-1,01129	5,014215	39,60865	4,77E-05	0,0534

References

1. Chakraborty I, Maity P. COVID-19 outbreak: Migration, effects on society, global environment and prevention. Sci Total Environ. 2020 Aug 1;728:138882.
2. Toyoshima Y, Nemoto K, Matsumoto S, Nakamura Y, Kiyotani K. SARS-CoV-2 genomic variations associated with mortality rate of COVID-19. J Hum Genet. 2020 Dec;65(12):1075-82.
3. Yurkovetskiy L, Wang X, Pascal KE, Tomkins-Tinch C, Nyalile TP, Wang Y, et al. Structural and Functional Analysis of the D614G SARS-CoV-2 Spike Protein Variant. Cell. 2020 Oct 29;183(3):739-51.e8.
4. Trevisan C, Noale M, Prinelli F, Maggi S, Sojic A, Di Bari M, et al. Age-Related Changes in Clinical Presentation of Covid-19: the EPICOVID19 Web-Based Survey. Eur J Intern Med. 2021;86:41-47.
5. Alwani M, Yassin A, Al-Zoubi RM, Aboumarzouk OM, Nettleship J, Kelly D, et al. Sex-based differences in severity and mortality in COVID-19. Rev Med Virol. 2021 Nov;31(6):e2223.
6. Yu W, Rohli KE, Yang S, Jia P. Impact of obesity on COVID-19 patients. J Diabetes Complications. 2021 Mar;35(3):107817.
7. Carraturo F, Del Giudice C, Morelli M, Cerullo V, Libralato G, Galdiero E, et al. Persistence of SARS-CoV-2 in the environment and COVID-19 transmission risk from environmental matrices and surfaces. Environ Pollut. 2020 Oct;265(Pt B):115010.
8. Bansal M. Cardiovascular disease and COVID-19. Diabetes Metab Syndr. 2020 May-Jun;14(3):247-50.
9. Ovsyannikova IG, Haralambieva IH, Crooke SN, Poland GA, Kennedy RB. The role of host genetics in the immune response to SARS-CoV-2 and COVID-19 susceptibility and severity. Immunol Rev. 2020;296(1):205-19.
10. Park SE. Epidemiology, virology, and clinical features of severe acute respiratory syndrome -coronavirus-2 (SARS-CoV-2; Coronavirus Disease-19). Clin Exp Pediatr. 2020 4;63(4):119-24.
11. Zhou P, Yang X-L, Wang X-G, Hu B, Zhang L, Zhang W, et al. A pneumonia outbreak associated with a new coronavirus of probable bat origin. Nature. 2020 2020/03/01;579(7798):270-73.
12. Hiemstra PS, McCray PB, Jr., Bals R. The innate immune function of airway epithelial cells in inflammatory lung disease. Eur Respir J. 2015 Apr;45(4):1150-62.
13. Iwasaki A, Foxman EF, Molony RD. Early local immune defences in the respiratory tract. Nat Rev Immunol. 2017 Jan;17(1):7-20.
14. Iwasaki A, Foxman EF, Molony RD. Early local immune defences in the respiratory tract. Nature Reviews Immunology. 2017 2017/01/01;17(1):7-20.
15. Bovard D, Giralt A, Trivedi K, Neau L, Kanellos P, Iskandar A, et al. Comparison of the basic morphology and function of 3D lung epithelial cultures derived from several donors. Curr Res Toxicol. 2020 Jun 10;1:56-69.
16. Belgacemi R, Luczka E, Ancel J, Diabasana Z, Perotin JM, Germain A, et al. Airway epithelial cell differentiation relies on deficient Hedgehog signalling in COPD. EBioMedicine. 2020 Jan;51:102572.
17. Leung C, Wadsworth SJ, Yang SJ, Dorscheid DR. Structural and functional variations in human bronchial epithelial cells cultured in air-liquid interface using different growth media. American journal of physiology Lung cellular and molecular physiology. 2020 May 1;318(5):L1063-l73.
18. Hou YJ, Okuda K, Edwards CE, Martinez DR, Asakura T, Dinnon KH, 3rd, et al. SARS-CoV-2 Reverse Genetics Reveals a Variable Infection Gradient in the Respiratory Tract. Cell. 2020 Jul 23;182(2):429-46.e14.
19. Hao S, Ning K, Kuz CA, Vorhies K, Yan Z, Qiu J. Long-Term Modeling of SARS-CoV-2 Infection of In Vitro Cultured Polarized Human Airway Epithelium. mBio. 2020 Nov 6;11(6).

20. Zhu N, Wang W, Liu Z, Liang C, Wang W, Ye F, et al. Morphogenesis and cytopathic effect of SARS-CoV-2 infection in human airway epithelial cells. Nat Commun. 2020 Aug 6;11(1):3910.
21. Ehre C. SARS-CoV-2 Infection of Airway Cells. N Engl J Med. 2020 Sep 3;383(10):969.
22. Aguiar JA, Tremblay BJ, Mansfield MJ, Woody O, Lobb B, Banerjee A, et al. Gene expression and in situ protein profiling of candidate SARS-CoV-2 receptors in human airway epithelial cells and lung tissue. Eur Respir J. 2020 Sep;56(3).
23. Hoffmann M, Kleine-Weber H, Schroeder S, Krüger N, Herrler T, Erichsen S, et al. SARS-CoV-2 Cell Entry Depends on ACE2 and TMPRSS2 and Is Blocked by a Clinically Proven Protease Inhibitor. Cell. 2020 Apr 16;181(2):271-80.e8.
24. Sungnak W, Huang N, Bécavin C, Berg M, Queen R, Litvinukova M, et al. SARS-CoV-2 entry factors are highly expressed in nasal epithelial cells together with innate immune genes. Nat Med. 2020 May;26(5):681-87.
25. Wang S, Qiu Z, Hou Y, Deng X, Xu W, Zheng T, et al. AXL is a candidate receptor for SARS-CoV-2 that promotes infection of pulmonary and bronchial epithelial cells. Cell Research. 2021 2021/01/08.
26. Lukassen S, Chua RL, Trefzer T, Kahn NC, Schneider MA, Muley T, et al. SARS-CoV-2 receptor ACE2 and TMPRSS2 are primarily expressed in bronchial transient secretory cells. Embo j. 2020 May 18;39(10):e105114.
27. Bridges JP, Vladar EK, Huang H, Mason RJ. Respiratory epithelial cell responses to SARS-CoV-2 in COVID-19. 2022;Thorax 77(2):203-09.
28. Mulay A, Konda B, Garcia G, Jr., Yao C, Beil S, Villalba JM, et al. SARS-CoV-2 infection of primary human lung epithelium for COVID-19 modeling and drug discovery. Cell reports. 2021;35(5):109055-55.
29. Salgado-Benvindo C, Thaler M, Tas A, Ogando NS, Bredenbeek PJ, Ninaber DK, et al. Suramin Inhibits SARS-CoV-2 Infection in Cell Culture by Interfering with Early Steps of the Replication Cycle. Antimicrob Agents Chemother. 2020 Jul 22;64(8).
30. Huang J, Hume AJ, Abo KM, Werder RB, Villacorta-Martin C, Alysandratos KD, et al. SARS-CoV-2 Infection of Pluripotent Stem Cell-Derived Human Lung Alveolar Type 2 Cells Elicits a Rapid Epithelial-Intrinsic Inflammatory Response. Cell Stem Cell. 2020 Dec 3;27(6):962-73.e7.
31. Katsura H, Sontake V, Tata A, Kobayashi Y, Edwards CE, Heaton BE, et al. Human Lung Stem Cell-Based Alveolospheres Provide Insights into SARS-CoV-2-Mediated Interferon Responses and Pneumocyte Dysfunction. Cell Stem Cell. 2020 Dec 3;27(6):890-904.e8.
32. Lukassen S, Chua RL, Trefzer T, Kahn NC, Schneider MA, Muley T, et al. SARS-CoV-2 receptor ACE2 and TMPRSS2 are primarily expressed in bronchial transient secretory cells. EMBO J. 2020;39(10):e105114-e14.
33. Mertens TCJ, van der Does AM, Kistemaker LE, Ninaber DK, Taube C, Hiemstra PS. Cigarette smoke differentially affects IL-13-induced gene expression in human airway epithelial cells. Physiological reports. 2017 Jul;5(13).
34. Amatngalim GD, Schrumpf JA, Dishchekenian F, Mertens TCJ, Ninaber DK, van der Linden AC, et al. Aberrant epithelial differentiation by cigarette smoke dysregulates respiratory host defence. Eur Respir J. 2018 Apr;51(4).
35. Wang Y, Ninaber DK, van Schadewijk A, Hiemstra PS. Tiotropium and Fluticasone Inhibit Rhinovirus-Induced Mucin Production via Multiple Mechanisms in Differentiated Airway Epithelial Cells. Front Cell Infect Microbiol. 2020;10:278.
36. Zhang H, Rostami MR, Leopold PL, Mezey JG, O'Beirne SL, Strulovici-Barel Y, et al. Expression of the SARS-CoV-2 ACE2 Receptor in the Human Airway Epithelium. American journal of respiratory and critical care medicine. 2020 Jul 15;202(2):219-29.

37. Lieberman NAP, Peddu V, Xie H, Shrestha L, Huang M-L, Mears MC, et al. In vivo antiviral host transcriptional response to SARS-CoV-2 by viral load, sex, and age. PLOS Biology. 2020;18(9):e3000849.
38. Vanderheiden A, Ralfs P, Chirkova T, Upadhyay AA, Zimmerman MG, Bedoya S, et al. Type I and Type III Interferons Restrict SARS-CoV-2 Infection of Human Airway Epithelial Cultures. 2020;94(19):e00985-20.
39. Liao Y, Li X, Mou T, Zhou X, Li D, Wang L, et al. Distinct infection process of SARS-CoV-2 in human bronchial epithelial cell lines. J Med Virol. 2020 Nov;92(11):2830-38.
40. Bost P, Giladi A, Liu Y, Bendjelal Y, Xu G, David E, et al. Host-Viral Infection Maps Reveal Signatures of Severe COVID-19 Patients. Cell. 2020 2020/06/25/;181(7):1475-88.e12.
41. Ziegler CGK, Allon SJ, Nyquist SK, Mbano IM, Miao VN, Tzouanas CN, et al. SARS-CoV-2 Receptor ACE2 Is an Interferon-Stimulated Gene in Human Airway Epithelial Cells and Is Detected in Specific Cell Subsets across Tissues. Cell. 2020;181(5):1016-35.e19.
42. Ruiz García S, Deprez M, Lebrigand K, Cavard A, Paquet A, Arguel MJ, et al. Novel dynamics of human mucociliary differentiation revealed by single-cell RNA sequencing of nasal epithelial cultures. Development. 2019 Oct 23;146(20).
43. Vieira Braga FA, Kar G, Berg M, Carpaij OA, Polanski K, Simon LM, et al. A cellular census of human lungs identifies novel cell states in health and in asthma. Nature Medicine. 2019 2019/07/01;25(7):1153-63.
44. Kimura H, Francisco D, Conway M, Martinez FD, Vercelli D, Polverino F, et al. Type 2 inflammation modulates ACE2 and TMPRSS2 in airway epithelial cells. J Allergy Clin Immunol. 2020 Jul;146(1):80-88.e8.
45. Eger K, Bel EH. Asthma and COVID-19: do we finally have answers? Eur Respir J. 2021 Mar;57(3).
46. Bonser LR, Eckalbar WL, Rodriguez L, Shen J, Koh KD, Ghias K, et al. The Type 2 Asthma Mediator IL-13 Inhibits Severe Acute Respiratory Syndrome Coronavirus 2 Infection of Bronchial Epithelium. 2022; AM J Respir Cell Mol Biol. 66(4):391-401.
47. Morrison CB, Edwards CE, Shaffer KM, Araba KC, Wykoff JA, Williams DR, et al. SARS-CoV-2 infection of airway cells causes intense viral and cell shedding, two spreading mechanisms affected by IL-13. Proceedings of the National Academy of Sciences of the United States of America. 2022 Apr 19;119(16):e2119680119.
48. Liu Y, Lv J, Liu J, Li M, Xie J, Lv Q, et al. Mucus production stimulated by IFN-AhR signaling triggers hypoxia of COVID-19. Cell Res. 2020 Dec;30(12):1078-87.
49. Ravindra NG, Alfajaro MM, Gasque V, Huston NC, Wan H, Szigeti-Buck K, et al. Single-cell longitudinal analysis of SARS-CoV-2 infection in human airway epithelium identifies target cells, alterations in gene expression, and cell state changes. PLoS Biol. 2021 Mar;19(3):e3001143.
50. Zhao M-M, Yang W-L, Yang F-Y, Zhang L, Huang W-J, Hou W, et al. Cathepsin L plays a key role in SARS-CoV-2 infection in humans and humanized mice and is a promising target for new drug development. Signal Transduction and Targeted Therapy. 2021 2021/03/27;6(1):134.
51. Hui KPY, Ho JCW, Cheung MC, Ng KC, Ching RHH, Lai KL, et al. SARS-CoV-2 Omicron variant replication in human bronchus and lung ex vivo. Nature. 2022 Mar;603(7902):715-20.
52. Liu Y, Liu J, Johnson BA, Xia H, Ku Z, Schindewolf C, et al. Delta spike P681R mutation enhances SARS-CoV-2 fitness over Alpha variant. Cell Reports. 2022 2022/05/17/;39(7):110829.
53. Mache C, Schulze J, Holland G, Bourquain D, Gensch J-M, Oh D-Y, et al. SARS-CoV-2 Omicron variant is attenuated for replication in a polarized human lung epithelial cell model. Communications Biology. 2022 2022/10/27;5(1):1138.

54. Schrumpf JA, Ninaber DK, van der Does AM, Hiemstra PS. TGF-β1 Impairs Vitamin D-Induced and Constitutive Airway Epithelial Host Defense Mechanisms. Journal of innate immunity. 2020;12(1):74-89.
55. Kovacikova K, Morren BM, Tas A, Albulescu IC, van Rijswijk R, Jarhad DB, et al. 6'-β-Fluoro-Homoaristeromycin and 6'-Fluoro-Homoneplanocin A Are Potent Inhibitors of Chikungunya Virus Replication through Their Direct Effect on Viral Nonstructural Protein 1. Antimicrob Agents Chemother. 2020 Mar 24;64(4).
56. Corman VM, Landt O, Kaiser M, Molenkamp R, Meijer A, Chu DK, et al. Detection of 2019 novel coronavirus (2019-nCoV) by real-time RT-PCR. Euro Surveill. 2020 Jan;25(3).
57. de Wilde AH, Raj VS, Oudshoorn D, Bestebroer TM, van Nieuwkoop S, Limpens R, et al. MERS-coronavirus replication induces severe in vitro cytopathology and is strongly inhibited by cyclosporin A or interferon-α treatment. The Journal of general virology. 2013 Aug;94(Pt 8):1749-60.
58. Graham C, Seow J, Huettner I, Khan H, Kouphou N, Acors S, et al. Neutralization potency of monoclonal antibodies recognizing dominant and subdominant epitopes on SARS-CoV-2 Spike is impacted by the B.1.1.7 variant. Immunity. 2021 2021/06/08/;54(6):1276-89.e6.
59. Mootha VK, Lindgren CM, Eriksson K-F, Subramanian A, Sihag S, Lehar J, et al. PGC-1α-responsive genes involved in oxidative phosphorylation are coordinately downregulated in human diabetes. Nature Genetics. 2003 2003/07/01;34(3):267-73.
60. Subramanian A, Tamayo P, Mootha VK, Mukherjee S, Ebert BL, Gillette MA, et al. Gene set enrichment analysis: A knowledge-based approach for interpreting genome-wide expression profiles. Proceedings of the National Academy of Sciences. 2005;102(43):15545-50.
61. Aliee H, Massip F, Qi C, Stella de Biase M, van Nijnatten JL, Kersten ETG, et al. Determinants of SARS-CoV-2 receptor gene expression in upper and lower airways. medRxiv. 2020 Sep 2.
62. Sikkema L, Strobl D, Zappia L, Madissoon E, Markov N, Zaragosi L, et al. An integrated cell atlas of the human lung in health and disease. Preprint bioRxiv. 2022:2022.03.10.483747.
63. Newman AM, Liu CL, Green MR, Gentles AJ, Feng W, Xu Y, et al. Robust enumeration of cell subsets from tissue expression profiles. Nat Methods. 2015 May;12(5):453-7.

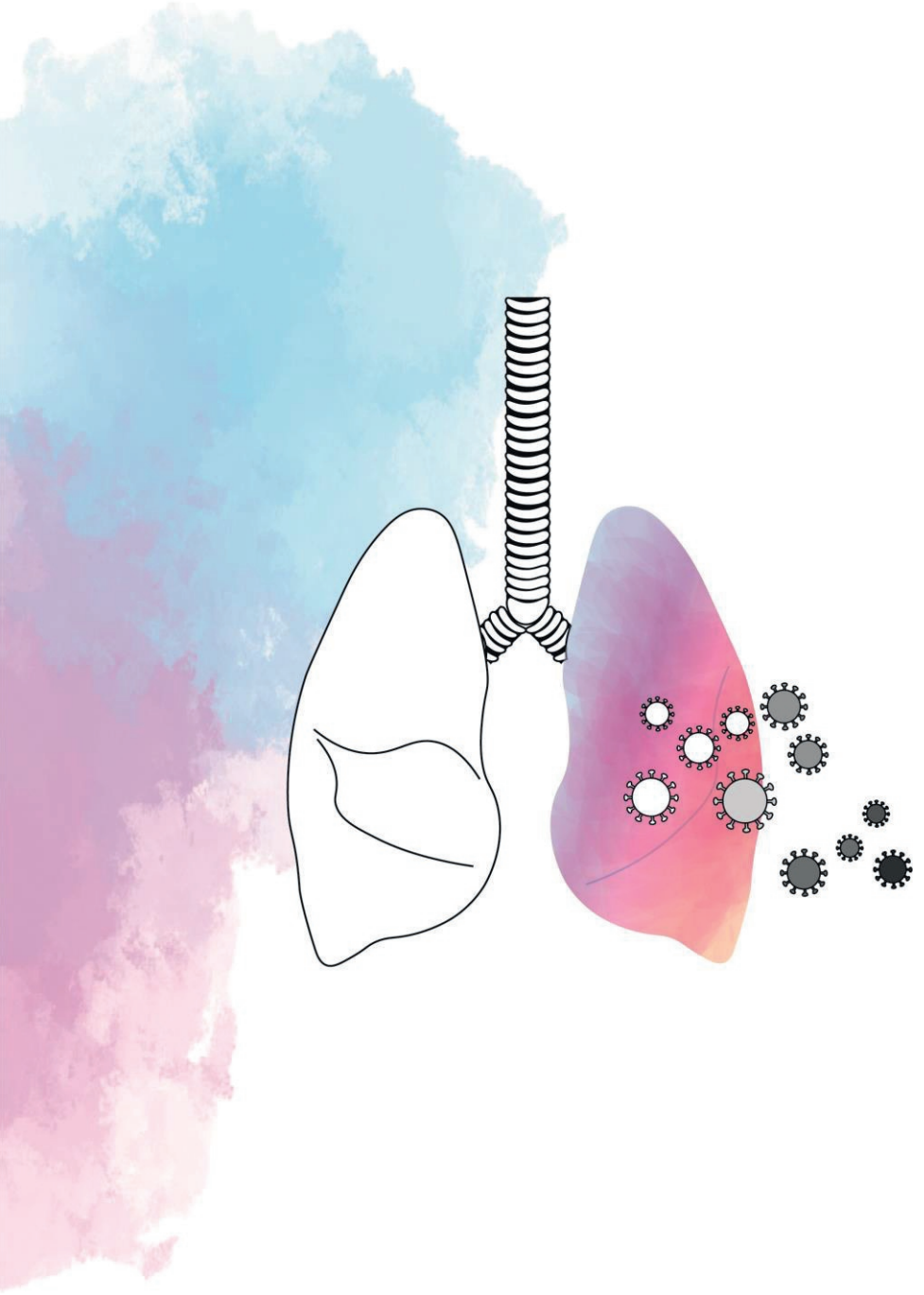

Chapter 3

SARS-CoV-2-infected human airway epithelial cell cultures uniquely lack interferon and immediate early gene responses caused by other coronaviruses

Melissa Thaler[1]*, Ying Wang[2]*, Clarisse Salgado-Benvindo[1], Nathan Ly[3], Anouk A Leijs[1], Dennis K Ninaber[2], Philip Hansbro[4], Fia Boedijono[4], Martijn J van Hemert[1], Pieter S Hiemstra[2], Anne M van der Does[2#], Alen Faiz[3#]

[1] Department of Medical Microbiology, Leiden University Medical Center, Leiden, the Netherlands

[2] PulmoScience Lab, Department of Pulmonology, Leiden University Medical Center, Leiden, the Netherlands

[3] University of Technology Sydney, Respiratory Bioinformatics and Molecular Biology (RBMB), School of Life Sciences, Sydney, Australia

[4] Centre for Inflammation, Centenary Institute and University of Technology Sydney, Faculty of Science, Sydney, Australia

* These authors contributed equally

# These authors share senior authorship

Running title: Unique transcriptional profile by SARS-CoV-2

Journal of Clinical & Translational Immunology, 13: e1503

Abstract

Severe acute respiratory syndrome coronavirus 2 (SARS-CoV-2) is a member of a class of highly pathogenic coronaviruses. The large family of coronaviruses; however; also includes members that cause only mild symptoms, like human coronavirus-229E (HCoV-229E) or OC43 (HCoV-OC43). Unravelling how molecular (and cellular) pathophysiology differs between highly and low pathogenic coronaviruses is important for the development of therapeutic strategies. Here, we analyzed the transcriptome of primary human bronchial epithelial cells (PBEC), differentiated at the air-liquid interface (ALI) after infection with SARS-CoV-2, SARS-CoV, Middle East Respiratory Syndrome (MERS)-CoV and HCoV-229E using bulk RNA sequencing. ALI-PBEC were efficiently infected by all viruses, and SARS-CoV, MERS-CoV and HCoV-229E infection resulted in a largely similar transcriptional response. The response to SARS-CoV-2 infection differed markedly as it uniquely lacked the increase in expression of immediate early genes, including *FOS*, *FOSB* and *NR4A1* that was observed with all other coronaviruses. This finding was further confirmed in publicly available experimental and clinical datasets. Interfering with NR4A1 signaling in Calu-3 lung epithelial cells resulted in a 100-fold reduction in extracellular RNA copies of SARS-CoV-2 and MERS-CoV, suggesting an involvement in virus replication. Furthermore, a lack in induction of interferon-related gene expression characterized the main difference between the highly pathogenic coronaviruses and low pathogenic viruses HCoV-229E and HCoV-OC43. Our results demonstrate a previously unknown suppression of a host response gene set by SARS-CoV-2 and confirms a difference in interferon-related gene expression between highly pathogenic and low pathogenic coronaviruses.

Keywords: primary airway epithelial cells; coronavirus; SARS-CoV-2; RNA sequencing; immediate early genes

Introduction

The outbreak of severe acute respiratory syndrome coronavirus 2 (SARS-CoV-2) that started late 2019 constituted an enormous threat to human health worldwide. Together with other highly pathogenic coronaviruses such as SARS-CoV and Middle East respiratory syndrome coronavirus (MERS-CoV), SARS-CoV-2 belongs to the genus *betacoronavirus* (β-CoV), of the *coronaviridae* family. These coronaviruses share many similarities but also exhibit evident differences. For human coronaviruses, the primary site of infection is the respiratory tract. However, there are marked differences in their host entry requirements, pathogenicity and

transmissibility (263). For example, the use of different host receptors for viral entry helps to explain differences in tissue tropism. SARS-CoV-2 furthermore demonstrates higher transmissibility, a wider range of clinical symptoms and lower mortality rates compared to SARS-CoV and MERS-CoV (263, 264). Not all human coronaviruses cause severe clinical symptoms. In fact, many of them only cause mild symptoms in healthy individuals. Human coronavirus 229E (HCoV-229E) (265), a member of the *alphacoronavirus* (α-CoV) genus, or human coronavirus OC43 (HCoV-OC43) (266), a member of the *betacoronavirus* genus, are two of the causative agents of the common cold. While HCoV-229E and HCoV-OC43 cause only mild symptoms in the upper respiratory tract of healthy people, SARS-CoV, SARS-CoV-2 and MERS-CoV may also infect the lower respiratory tract, resulting in a much wider range of respiratory illnesses and other non-pulmonary clinical manifestations that can be life threatening. It is important for the development of therapeutic strategies against infection with SARS-CoV-2, but also other (future) pathogenic coronaviruses, to understand the differences in their unique pathological characteristics.

RNA sequencing studies have shed light on many aspects of SARS-CoV-2 pathobiology. For example, bulk and single cell-RNA sequencing revealed the spatial distribution of cell entry factor expression and cell tropism (infection biology) within the respiratory epithelium (236, 267-269). Transcriptional analysis also showed differences between mild and severe COVID-19 cases and the diversity in immune responses (243, 270). Furthermore, infection of ciliated cells, the main cell type targeted by SARS-CoV-2, was demonstrated to lead to a significant downregulation of cilium assembly and motility pathways (267).

Despite our increasing knowledge on SARS-CoV-2 infection biology there are still important gaps in our understanding of what distinguishes SARS-CoV-2 from other coronaviruses in terms of pathogenesis and transmission. Comparing host responses during the initial phase of the infection of the respiratory epithelium between SARS-CoV-2 and other (highly pathogenic and low pathogenic) coronaviruses may provide important clues on how SARS-CoV-2 establishes its distinct effects.

Recent research has compared infectivity of various coronavirus strains in human nasal epithelial cultures (73), but this study did not provide insight into host transcriptional responses and was limited to the nasal region. Others have compared transcriptional responses to coronavirus infection by combining several independent datasets (271), or with only a limited number of different coronaviruses (272). Here we sought to determine the differences in the transcriptional response of well-differentiated primary bronchial epithelial cell cultures to infection with highly pathogenic SARS-CoV, SARS-CoV-2, MERS-CoV and low pathogenic HCoV-229E and in specific experiments also HCoV-OC43. Paired comparative analysis revealed differences between the host responses to these viruses and uncovered modulations of signaling pathways that were unique to SARS-CoV-2 infection.

Results

Successful infections of primary airway epithelial cells with SARS-CoV, SARS-CoV-2, MERS-CoV or HCoV-229E

To compare the transcriptional response of airway epithelial cells to various coronaviruses, we infected 6 week-differentiated ALI-PBEC (273) from 4 donors with an equal amount (~30,000 PFU) of either highly pathogenic SARS-CoV, SARS-CoV-2 or MERS-CoV, or low pathogenic HCoV-H229E. The relatively low amount of PFU was chosen to be representative for an initial infection (and subsequent spread over the tissue). Cultures were harvested at 6, 12, 24, 48 and 72 hpi followed by RNA isolation. RNA collected at 24, 48 and 72 hpi was subsequently used to perform bulk RNA-seq analysis (workflow is depicted in Figure **1a**). Viral replication was assessed by analysis of the RNA-seq datasets at 24, 48 and 72 hpi and additionally for each harvested time point (6, 12, 24, 48 and 72 hpi) by RT-qPCR analysis. The normalized viral genome counts (measured by RNA-Seq) of all coronaviruses showed a significant increase over the 72 h incubation period, with MERS-CoV having the highest observed increase (**Figure 1b**). These results were confirmed by quantification of intracellular viral RNA copies by RT-qPCR (**Figure 1c**). Furthermore, expression of genes encoding structural and non-structural proteins were increasing during infection time (**Figure 1d**) confirming active replication. A strong increase in subgenomic RNA encoding the most abundant viral protein N was observed for infections with all coronaviruses (**Figure 1d**).

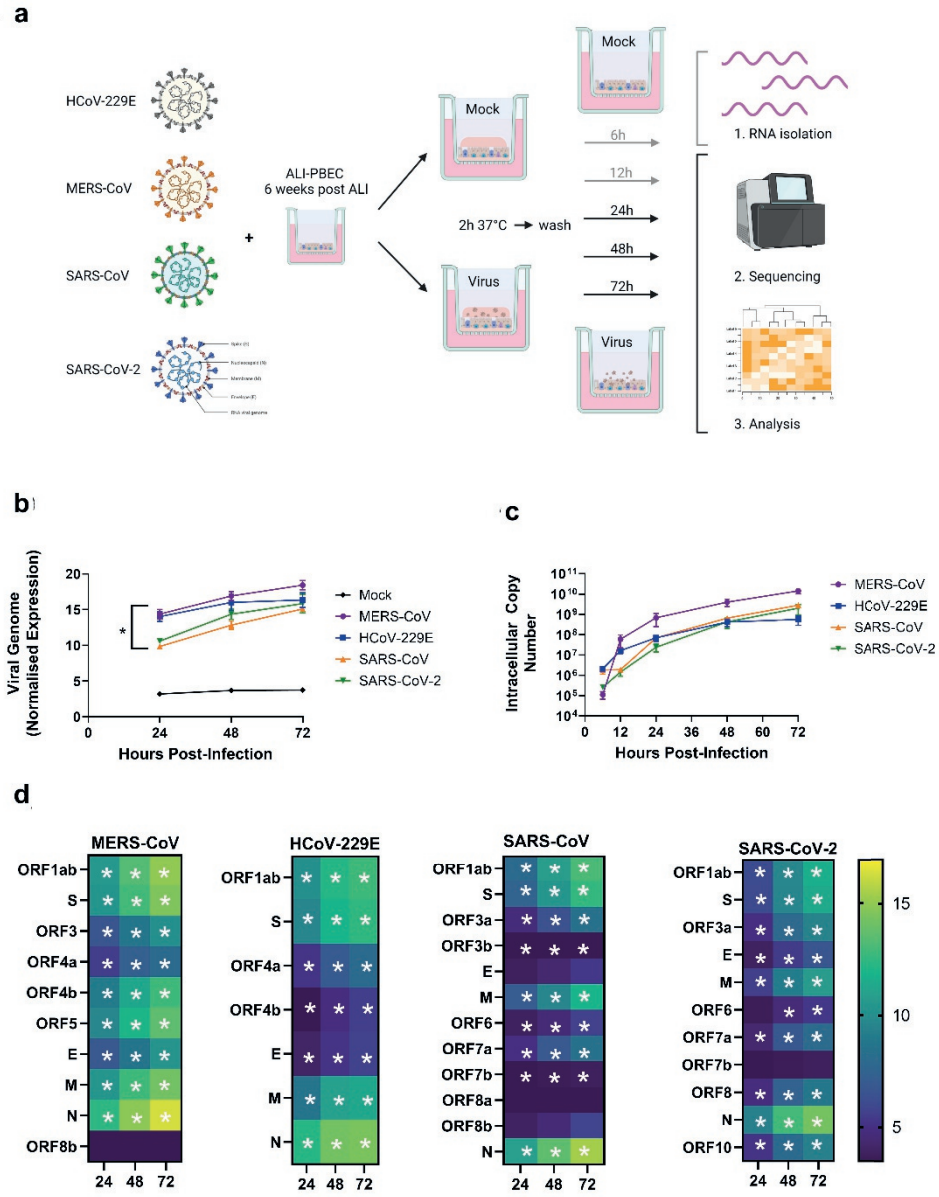

Figure 1: Experimental design and replication kinetics of several coronaviruses in ALI-PBEC. (a) Schematic diagram of experimental design and infection protocol. ALI-PBEC that were differentiated for 6 weeks were infected in parallel with four different coronaviruses. At several time-points after infection RNA was harvested from these cultures and RNA from the 24, 48 and 72h time points was analyzed by bulk RNA-seq. (b) Replication of coronaviruses in ALI-PBEC over the 72h period was assessed by mapping the viral sequences in the bulk RNA-seq dataset. Significant differences between virus and mock for all time-points was assessed using a two-way ANOVA followed by an unprotected Fisher's least significance difference test and (c) intracellular viral RNA copies

at each time-point were measured by RT-qPCR. (d) Viral reads were mapped against the respective genome sequence and changes in the abundance of sequences mapping to the various viral open reading frames during infection are summarized. Statistics were conducted using a paired edgeR differential expression analysis comparing all viruses to mock. Data are shown as mean ± SEM of cultures derived from $n = 4$ different donors and differences were considered significant at $P < 0.05$. Figure 1a was created with BioRender.com.

Gene expression of entry-related factors is changed during coronavirus infection of airway epithelial cells

A principal component analysis (PCA) of the complete RNA-seq dataset demonstrated that samples clustered based on donor ID (**Figure 2a**). This finding is not unexpected and could be explained by differences in cell composition of the cultured airway epithelium between donors. Cellular deconvolution of these samples showed that each donor had a distinct profile of ciliated, mucosecretory and basal cells (**Figure 2b**), which was not altered by the different coronavirus infections (Supplementary **Figure 1**). Next, we focused on the expression of known coronavirus entry-related factors and determined whether changes occurred during infection (**Figure 2c**). Overall, we mostly observed a decrease in expression of these genes during infection, except for SARS-CoV-2. Angiotensin converting enzyme 2 (*ACE2*) and transmembrane serine protease 2 (*TMPRSS2*), the genes encoding for the main viral entry receptor and protease that cleaves the SARS-CoV-2 S-protein for subsequent cell entry, respectively, were not significantly altered in most of our samples. Significant changes were only found for *TMPRSS2* at later time-points in SARS-CoV (48 hpi) and MERS-CoV (72 hpi) infection, compared to mock-infected controls. Cathepsin L (*CTSL)* expression declined significantly over time in MERS-CoV and HCoV-229E-infected cultures, while *Furin* expression increased. Neuropilin-1 (*NRP1*), which was described as a co-receptor for SARS-CoV-2 cell entry (274) showed an increase in expression at 24 h and 48 h after SARS-CoV-2 infection, but then declined at 72 hpi (**Figure 2c**). Together these data indicate that infection results in shifts in expression of various factors involved in coronavirus entry, which may mediate further spread upon initial infection in the epithelial cultures.

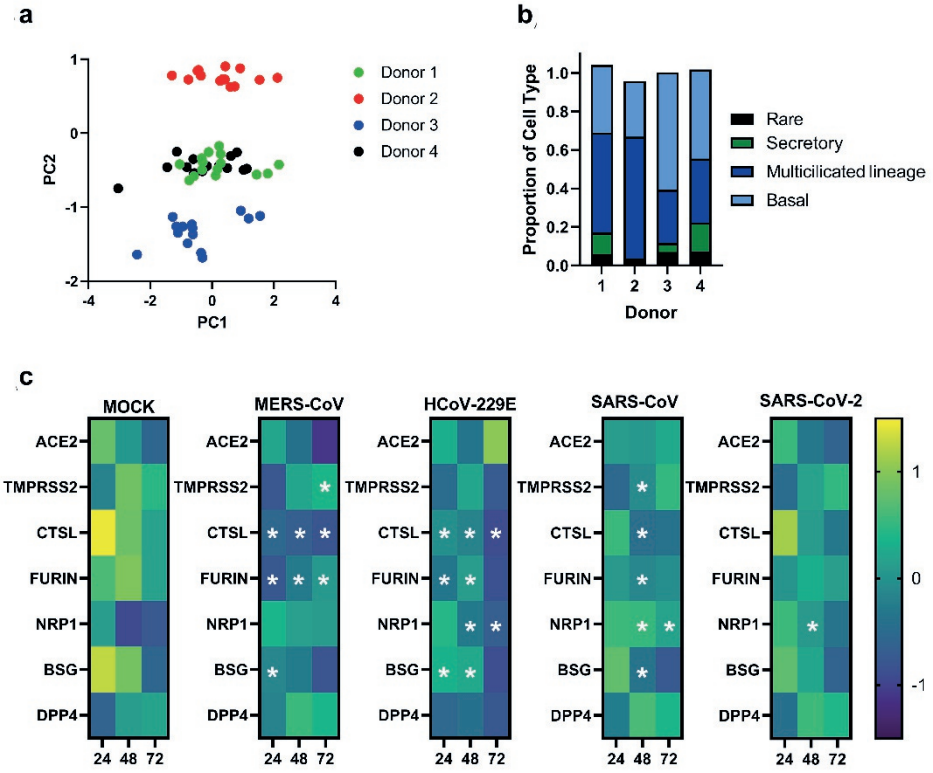

Figure 2: Donor-dependent clustering of samples, cellular composition and expression of viral entry-related genes in well-differentiated ALI-PBEC. PBEC that were differentiated for 6 weeks at ALI were infected in parallel with four different coronaviruses. (a) PCA of transcriptional profiles of all cell culture samples over time of infection. (b) Relative proportion of different cell types for each donor determined by cellular deconvolution of the transcriptomic dataset. (c) Changes in expression of common viral entry-related genes over time of infection (n = 4). Statistics were conducted using a paired edgeR differential expression analysis comparing all viruses to mock where a *P-value < 0.05 was considered significant.

Increased immediate early gene expression by airway epithelial cells infected with SARS-CoV, MERS-CoV and HCoV-229E

Before addressing the SARS-CoV-2 transcriptional profiles, we first compared the expression profiles of ALI-PBEC in response to SARS-CoV, MERS-CoV and HCoV-229E at 24, 48 and 72 hpi. ALI-PBEC infected with SARS-CoV showed significant different expression of 80 genes at 24 hpi, compared to the control, of which 69 were increased in expression and 11 decreased in expression. In MERS-CoV-infected cells, we identified 934 differentially

expressed genes, of which 580 were increased and 354 decreased in expression at 24 hpi. Cells infected with HCoV-229E displayed an increased expression of 433 genes and reduced expression of 162 genes at 24 hpi (FDR<0.05, FC>1.5). The significantly changed genes at 24 hpi are depicted in volcano plots in **Figure 3a-c** and **Table S3** (results of the other time-points (48 h and 72 h) are included in Supplementary **Figure 2**) and the total expression profiles over time in **Figure 3d**. A specific set of genes (see methods section) was significantly increased at all time-points after start of infection with SARS-CoV, MERS-CoV and HCoV-229E. Many of these belong to a group of well-known genes, called immediate early genes (IEGs), which play an important role in the cell's rapid response to its external environment (275). The remarkable overlap in these genes between ALI-PBEC infected with SARS-CoV, MERS-CoV or HCoV-229E (**Figure 3e** and Supplementary **Figure 2**) was dominated by *FOS*, *NR4A1* and *FOSB* gene expression and their increased expression was extracted from the RNA-seq dataset (**Figure 3e**) and supported by RT-qPCR analysis of these genes (**Figure 3f**). To confirm our findings, we investigated *FOS*, *NR4A1* and *FOSB* gene expression also in two publicly available datasets of primary airway epithelial cells and Calu-3 cells infected with MERS-CoV and SARS-CoV, respectively (**Figure 3g-h**). These datasets supported our results showing upregulation of *FOS*, *NR4A1* and *FOSB* gene expression following MERS-CoV and SARS-CoV infection (**Figure 3g-h**). Together these results indicate an activation of the expression of specific IEGS by these coronaviruses and their sustained high level of expression for at least 72 hpi.

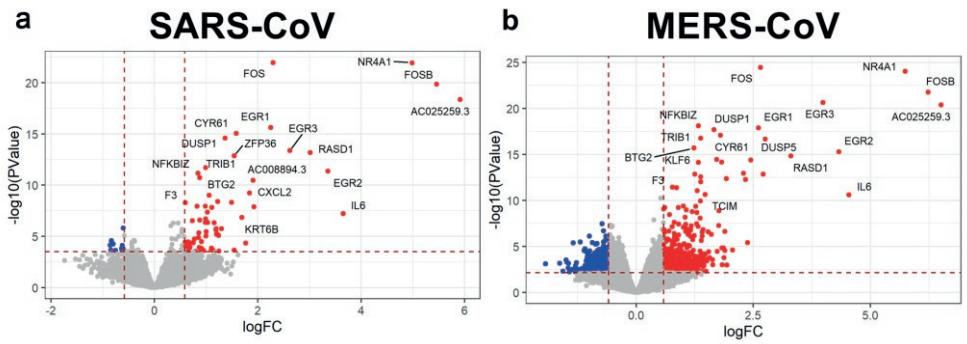

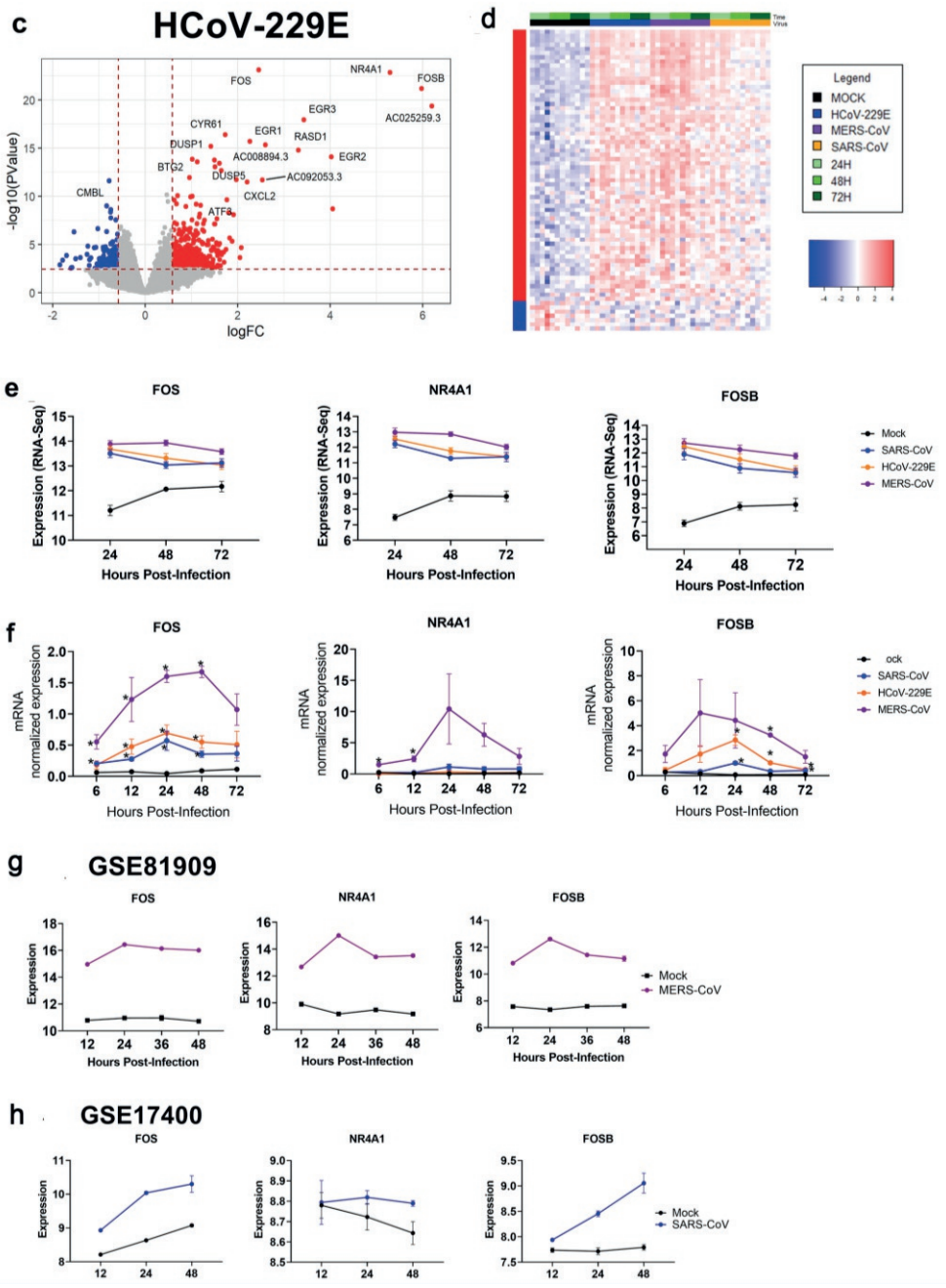

Figure 3: Gene expression profiles of well-differentiated primary bronchial epithelial cell cultures infected with three different coronaviruses. (a) Volcano plots depicting gene expression profiles of bronchial epithelial cell cultures infected with (a) SARS-CoV (b) MERS-CoV or (c) HCoV-229E at 24 hpi in comparison to the uninfected

controls. Red dots indicate significantly upregulated genes and blue dots indicate significantly downregulated genes. (d) Heatmap of significantly changed genes during infection with SARS-CoV, MERS-CoV or HCoV-229E and mock as uninfected control (log2fold change> |1.5| and FDR<0.05). (e) Changes in gene expression of FOS, NR4A1 and FOSB during infection with three different coronaviruses using data from the RNA-seq analysis. (f) The same genes as in Figure 3E were analyzed for all harvested time-points using traditional qPCR. Data are expressed as normalized values for *ATP5B* and *OAZ1*. (g) A publicly available microarray dataset (GSE81909) was used to analyze the impact of MERS-CoV infection on these three IEGs in primary airway epithelial cells. (h) A publicly available dataset (GSE17400) was assessed to analyze the effect of SARS-CoV infection on these IEGs in Calu-3 cells during 48 h with an MOI of 0.1. Data from a-f were from $n = 4$ different donors. Significant differences between virus infection and mock for all time-points was assessed using a two-way ANOVA followed by an unprotected Fisher's least significance difference test, $*P < 0.05$ was considered significant, data from e-h are depicted as mean ± SEM.

Airway epithelial cells infected with SARS-CoV-2 display a distinct transcriptional response that lacks induction of immediate early genes

Next, we addressed the specific transcriptional responses of ALI-PBEC cultures following SARS-CoV-2 infection. Strikingly, gene expression analysis identified that despite a viral load that was comparable to the other viruses, no genes were significantly changed at 24 and 48 hpi (data not shown). At 72 hpi, there were no significantly increased genes while a decrease in 3 genes was observed (*FOS*, *NR4A1* and *FOSB)* (**Figure 4a**, **Table S4**). These results show that SARS-CoV-2-infected ALI-PBEC lack the increased IEG expression that was observed for the other coronaviruses, while even a decrease in the gene expression of *FOS*, *NR4A1* and *FOSB* in SARS-CoV-2-infected ALI-PBEC was observed (**Figure 4b**). Using RT-qPCR, we confirmed that over the time course of 6-72 hpi there was no increase in expression of these genes (**Figure 4c**). Only *FOS* mRNA expression was increased at 48 hpi compared to mock infection. However, compared to the other three coronaviruses, the upregulation of *FOS* expression by SARS-CoV-2 was minimal, and not supported by the results of the RNA-seq data. Furthermore, we conducted an analysis of signature genes increased by SARS-CoV, MERS-CoV and HCoV-229E at all time points (included genes are listed in the methods section). It was evident from this analysis that SARS-CoV-2 did not increase these genes to the same extent as the other coronaviruses did and even appeared to actively suppress them compared to the control group (**Figure 4d**). This signature gene set was furthermore validated to be changed in MERS-CoV and SARS-CoV infections reported in publicly available datasets (**Figure 4e-f**).

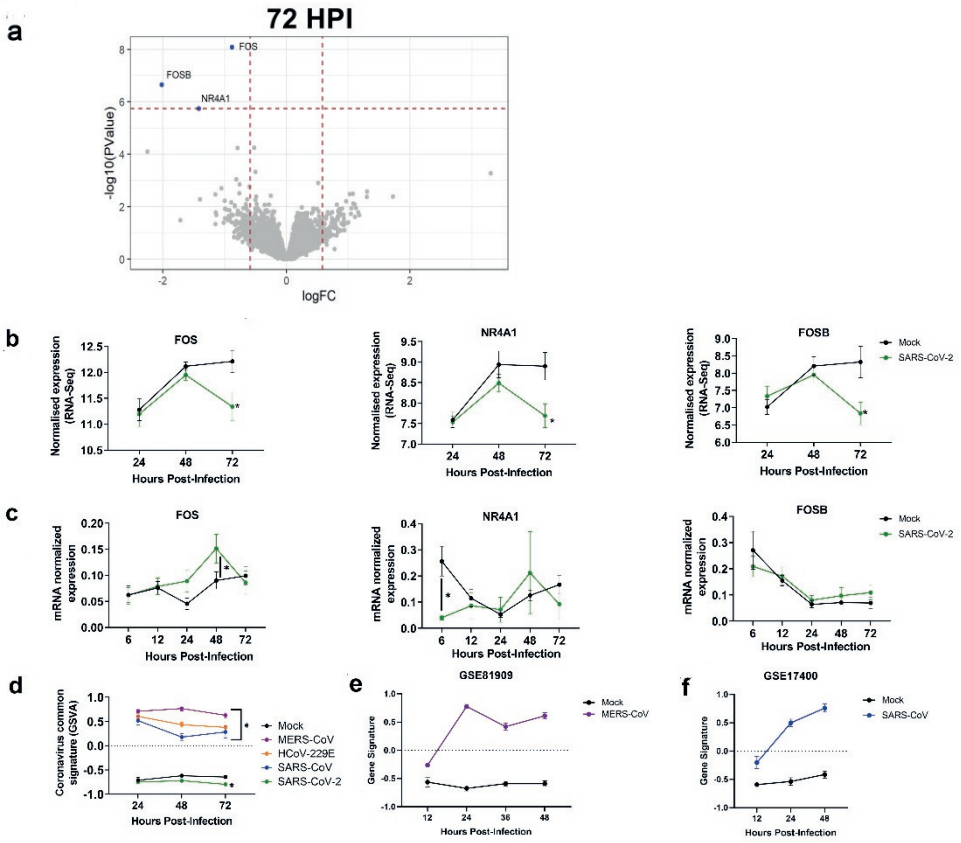

Figure 4: Gene expression profiles of well-differentiated primary bronchial epithelial cells during SARS-CoV-2 infection. (a) Volcano plot depicting gene expression profiles of bronchial epithelial cell cultures infected with SARS-CoV-2 at 72 hpi (*n* = 4). (b) The expression of FOS, *NR4A1* and *FOSB* over a 72h infection period with SARS-CoV-2 using data from the RNA-seq analysis (*n* = 4). (c) The same genes as in figure b were analyzed for all time-points using traditional qPCR. (d) Comparison of a MERS-CoV, SARS-CoV, HCoV-229E signature gene set between all coronavirus infected cultures at 24, 48 and 72 hpi (*n* = 4). (e) A publicly available microarray dataset (GSE81909) was assessed to analyze the impact of MERS-CoV infection on the MERS-CoV, SARS-CoV, HCoV-229E signature gene set. (f) A publicly available dataset (GSE17400) was assessed to analyze the effect of SARS-CoV infection on the MERS-CoV, SARS-CoV, HCoV-229E signature gene set. Significant differences between virus infection and mock for all time-points was assessed using a two-way ANOVA followed by an unprotected Fisher's least significance difference test, $*P < 0.05$ was considered significant, data from b-f are depicted as mean ± SEM.

Validation of the effects of SARS-CoV-2 on immediate early gene expression by lung epithelial cells

To better understand and confirm our findings, we further investigated publicly available datasets. First, we analyzed the total IEG gene set in three publicly available RNA-seq datasets, derived from bronchial or alveolar epithelial cells infected with SARS-CoV-2 for various time-points, of which none showed a significant change in gene expression (**Figure S4**) compared to the uninfected control. Next, we analyzed these datasets to specifically assess the expression of the most prominently changed genes in our dataset, including *FOS*, *FOSB* and *NR4A1*. In the first dataset: GSE153970, collected from primary human airway epithelial cells cultured at ALI, (infected with SARS-CoV-2 at an MOI of 0.25 and analyzed at 48 hpi) a significant decrease in *FOS* gene expression was found in SARS-CoV-2-infected cultures, accompanied by a lack in upregulation of *FOSB* and *NR4A1* (**Figure 5a**), mirroring our results. Similar results for *FOS* (**Figure 5b**) expression were found at 48 hpi in primary lung alveolar type-2 epithelial cells in a 3D organoid culture infected with SARS-CoV-2 (GSE155518; **Figure 5b**). Finally, we validated our findings using a dataset that originated from a study on SARS-CoV-2 infection of ALI-PBEC, that included samples harvested at 6-96 hpi (GSE175779; **Figure 5c**). This dataset displayed no significant increase in *FOS*, *NR4A1* and *FOSB* gene expression (only a decrease at 48 hpi for *FOSB*) over the 96 h course of infection (**Figure 5c**), like all other SARS-CoV-2 datasets.

To understand if the observed differences in the changes of these specific genes between SARS-CoV-2 and the other coronavirus-infected cultures were a consequence of a difference in viral load or kinetics, we also analyzed cultures that were infected with a higher dose, 10^6 PFU, of SARS-CoV-2 (estimated MOI of 1). We followed gene expression levels in this culture for a longer period, up to 7 days post infection. We assessed viral replication and changes over time using plaque assay and RT-qPCR. Analysis of infectious virus produced over seven days showed a peak in the accumulation of infectious progeny at 4-5 days post infection with more than 10^6 PFU/ml, and a corresponding strong increase in intracellular viral RNA up to 3 days p.i. (**Figure 5d**). We furthermore detected a significant increase in *NR4A1* expression from 3-5 days post infection (**Figure 5e**) and a slight increase in *FOSB* expression at day 4 after SARS-CoV-2 infection while no effects on *FOS* expression was observed (**Figure 5e**), suggesting a delayed response to SARS-CoV-2. Nevertheless, despite these changes, the increased expression of these genes observed at later time points with a higher MOI was still substantially lower than upon infection with SARS-CoV, MERS-CoV or HCoV-229E in the original experiments where a lower MOI was used. To obtain further insight, we also assessed IEG expression in publicly available datasets of infected cultures and individuals analyzed with single-cell RNA sequencing. In well-differentiated human PBEC cultures

infected with SARS-CoV-2 and analyzed at 7 days post-infection, single-cell RNA sequencing results showed that resting basal and multiciliated cells had a significantly lower enrichment score for the IEG gene set in infected cells compared to non-infected cells (**Figure 5f**). Finally, we assessed IEG expression in a clinical dataset that was generated by nucleo-seq analysis of cells derived from deceased uninfected or SARS-CoV-2-infected individuals. Confirming our findings, no increase in IEG gene expression was observed. In alveolar type-2 epithelial cells, differentiating and mature lymphatic endothelial cells, and monocytes showed a significantly lower enrichment score in infected compared to non-infected individuals, while secretory epithelial cells showed a strong trend (**Figure 5g**). Together these results demonstrate that, unlike all other coronaviruses tested, SARS-CoV-2 does not induce and might even actively suppress IEG expression in epithelial cells and potentially other cell-types.

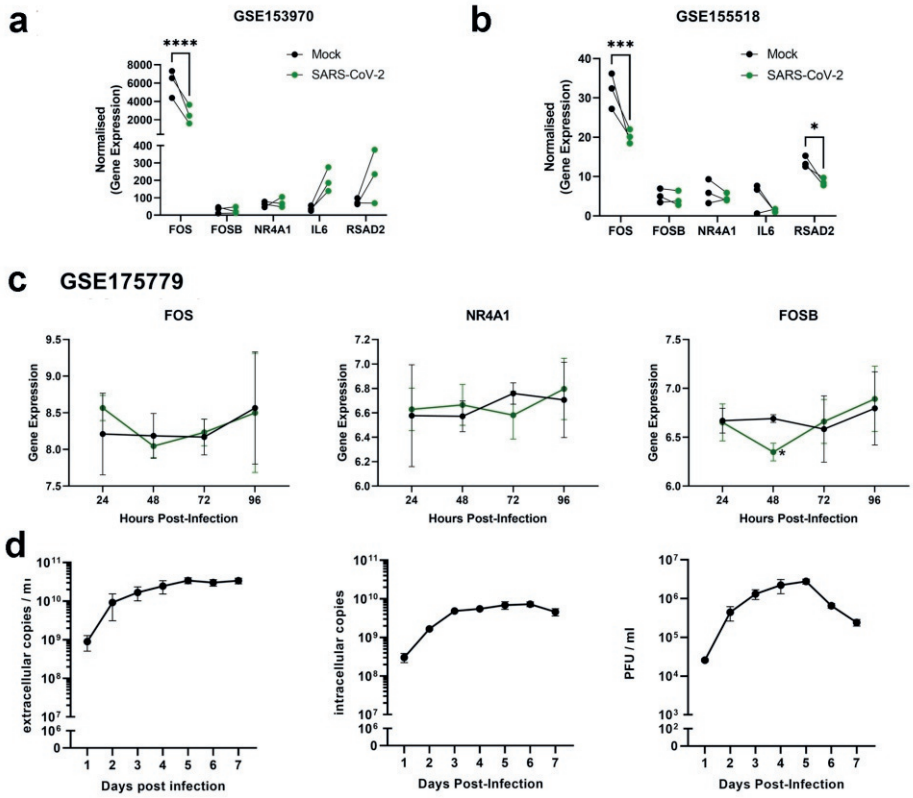

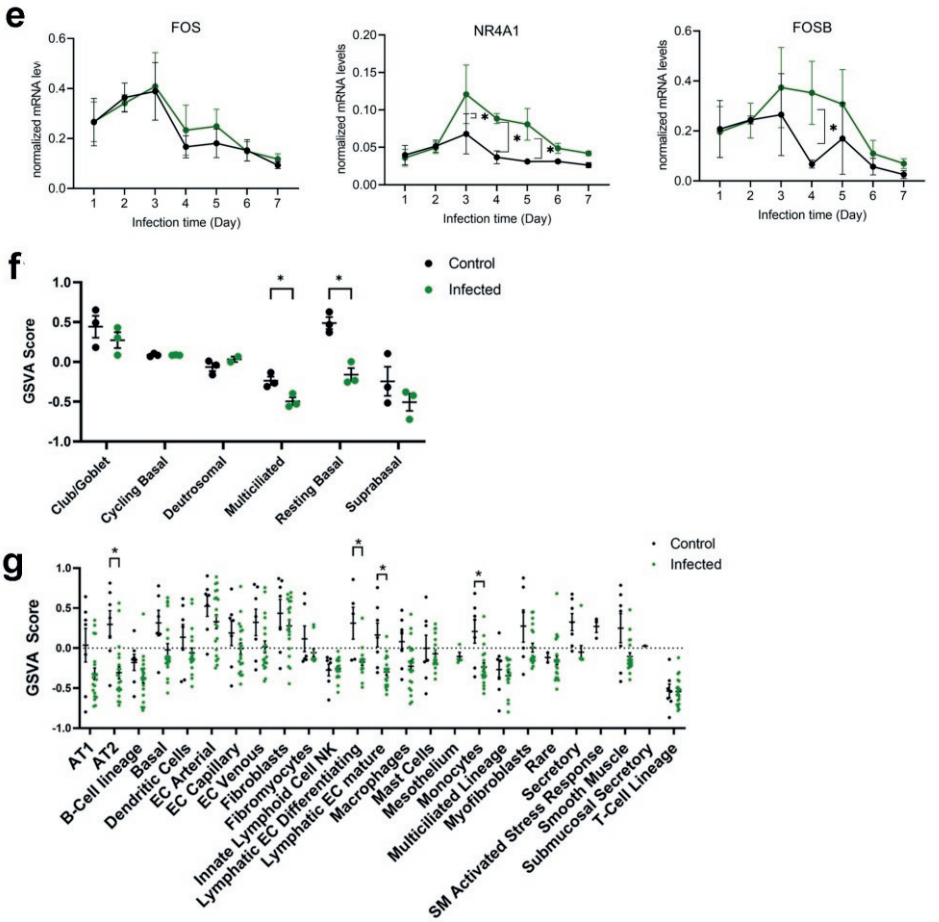

Figure 5: Analysis of IEG expression upon SARS-CoV-2 infection of epithelial cells in public datasets and in long-term infection. (a) A publicly available dataset (GSE153970) with RNA-seq analysis on primary epithelial cell cultures mock-infected or infected with SARS-CoV-2 at a MOI=0.25 at 48 hpi was analyzed for *FOS, NR4A1* and *FOSB* expression. (b) A publicly available dataset (GSE155518) derived from primary human lung alveolar epithelial organoid cultures infected with SARS-CoV-2 was analyzed for *FOS, NR4A1* and *FOSB* expression. (c) A publicly available dataset (GSE175779) from primary human bronchial epithelial cells infected with SARS-CoV-2 over a 96 h infection period was analyzed for *FOS, NR4A1* and *FOSB* expression. (d) RT-qPCR measurement of extracellular (left graph) and intracellular viral RNA (middle graph), and plaque assay measurement of infectious virus particles (right graph) in the apical wash of SARS-CoV-2 infected ALI-PBEC over 7 days; $n = 3$ independent donors. (e) The expression of IEGs was measured by qPCR in ALI-PBEC infected with SARS-CoV-2 for 7 days. Data are shown as mean ± SEM; $n = 3$ independent donors. Significant differences between virus infection and mock for all time-points was assessed using a two-way ANOVA followed by an unprotected Fisher's least significance difference test, $*P < 0.05$ was considered significant, data are depicted as mean ± SEM. (f) GSVA analysis of the IEG gene set on a publicly available single-cell RNA-Seq dataset (269) from well-differentiated human bronchial epithelial cell cultures infected with SARS-CoV-2 and analyzed 7 days post infection. Significant differences between infected and uninfected cultures was tested using a two-way ANOVA with Bonferroni correction$*P < 0.05$ was considered

significant (g) GSVA analysis of the IEG gene set on a publicly available Nucleo-Seq dataset (276) from cells derived from tissue from deceased COVID-19 patients and deceased uninfected individuals. Significant differences between infected and uninfected individuals per cell-type was tested using an unpaired T-test with Bonferroni correction. *P <0.05 was considered significant.

NR4A1 antagonist suppresses coronavirus replication

Since *FOS*, *FOSB* and *NR4A1* gene expression was consistently lacking in epithelial transcriptional responses to SARS-CoV-2, we next investigated their contribution to viral infection by modulation of their activity, or modulation of related signaling pathways, using small molecules. FOS and FOSB are associated with the JNK/AP1 pathway, therefore based on literature, we selected the compounds Sp600125 (JNK inhibitor) and T-5224 (AP-1 transcription factor inhibitor) to modulate this pathway. We furthermore selected DIM-C-pPhOH (NR4A1 antagonist) and Cytosporone B (NR4A1 agonist) for modulation of the NR4A1 pathway. We compared the effects of these compounds in SARS-CoV-2 and MERS-CoV infected Calu-3 cells, since the increase in expression of the associated IEG genes was most pronounced after MERS-CoV infection while it was absent after SARS-CoV-2 infection. Sp600125, T-5224 and Cytosporone B had no effect on viral replication in viral load reduction assays with Calu-3 lung epithelial cells (**Figure 6**). Interestingly, DIM-C-pPhOH, which inhibits the activity of nuclear receptor 4A1 (NR4A1), resulted in a two-log reduction of extracellular viral RNA copies for SARS-CoV-2 as well as MERS-CoV infected cells (**Figure 6**). When we treated uninfected cells in parallel, we observed no cytotoxicity with 10 µM of DIM-C-pPhOH (Supplementary **figure 3**). The inhibitory effect of the modulation of NR4A1 activity on virus replication suggests its possible involvement in infection biology.

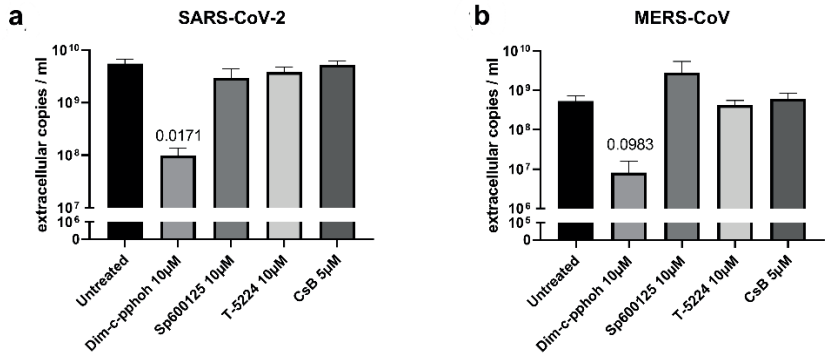

Figure 6: Effect of compounds that modulate pathways related to IEGs on SARS-CoV-2 and MERS-CoV infection. (a) Effect of compounds that modulate pathways related to JNK/AP-1 pathway and NR4A1 on SARS-CoV-2 and (b)

MERS-CoV infection in Calu-3 cells. DIM-C-pPhOH (NR4A1 antagonist), Sp600125 (JNK inhibitor), T-5224 (AP-1 transcription factor inhibitor) and Cytosporone B (CsB; NR4A1 agonist). Calu-3 cells were preincubated for 1 h with these compounds and subsequently infected with SARS-CoV-2 or MERS-CoV (MOI of 1) in 150 µl infection medium for 1 h. After 24 h of incubation with compounds supernatants were harvested. Extracellular copies were measured by RT-qPCR. Data are shown as mean ± SEM. *n* = 4 independent experiments for SARS-CoV-2 and *n* = 3 independent experiments for MERS-CoV, except for Sp600125 *n* = 2 independent experiments were performed for both viruses. Statistical significance was tested between a compound and the untreated control using a two-tailed paired *t*-test. The *P*--value is indicated in the graph and is considered significant <0.05.

Difference in transcriptional responses between primary bronchial epithelial cultures infected with highly pathogenic and low pathogenic coronaviruses

To improve our understanding on why some coronaviruses are highly pathogenic while others are low pathogenic, we next compared transcriptional responses of epithelial cultures infected with highly pathogenic coronavirus strains (i.e., SARS-CoV; SARS-CoV-2 and MERS-CoV) with those infected with low pathogenic HCoV-229E and HCoV-OC43. We originally only included HCoV-229E in the comparison, since HCoV-OC43 does not infect bronchial epithelial cells at 37°C. However, to increase the power of our observations with low pathogenic coronaviruses, we next performed independent additional experiments at 33°C using the same donors but infected them with HCoV-OC43 (see Methods section). At 24 hpi we detected 5 significantly changed genes with 4 genes decreased in expression and one gene increased. The four decreased genes included (AL022323.4 (KIAA1671)), a protein with -to our knowledge- no known function in the context of highly pathogenic coronaviruses and *CARNS1*, *EPX* and *MIR210HG*. The one gene that was increased in expression was *CLDN8*. At 48 and 72 hpi, we identified 397 and 744 genes significantly different, respectively (**Figure 7a-d**, **Table S5**). We observed that both HCoV-229E and HCoV-OC43 induced a stronger interferon response than coronaviruses that are highly pathogenic (**Figure 7e**). Notably, the experiments in which infection with HCoV-OC43 was performed at 33°C also included SARS-CoV-2 as a control, to account for the possibility that the temperature affects the host immune response. When we investigated the expression of each interferon individually, IFN-β1 was undetectable and no significant differences were observed in IFN-α1; however; IFN-λ1 was found to be expressed higher in HCoV-229E and HCoV-OC43 at 72 h than coronaviruses that are highly pathogenic (**Figure 7f-g**). This evasion of IFN responses has been described for highly pathogenic coronaviruses (109, 277) and may explain why the host is more readily able to fight off an infection with HCoV-229E or HCoV-OC43. To support that this difference in gene expression profiles related to interferon has functional consequences for infection, we infected ALI-PBEC with SARS-CoV-2 and treated these cultures with IFN-λ1 right at the start of infection. We found that this indeed

lowered the level of SARS-CoV-2 in the cultures as the IFN-λ1 treatment led to >1 log reduction in viral load in all four tested donors compared to the untreated infected cultures (**Figure 7h**). Together these data demonstrate that the suppression of IFNs by SARS-CoV-2 favors its replication, which is also likely for the other high-pathogenic viruses.

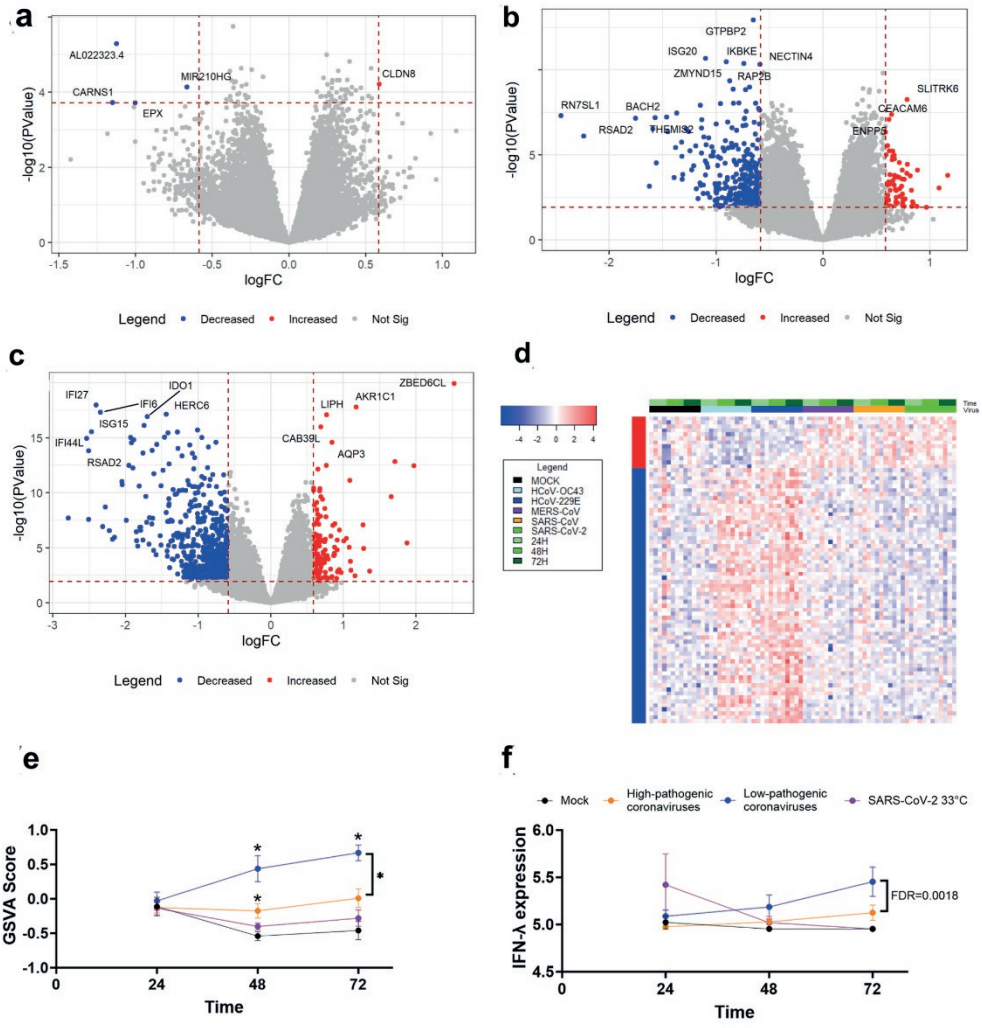

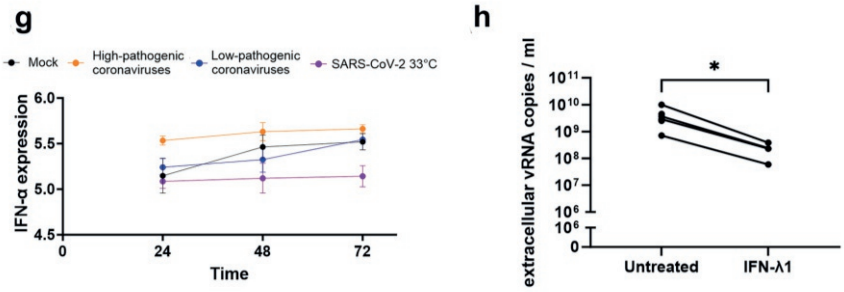

Figure 7: Analysis of interferon (-response) genes upon coronavirus infection and effects of IFN-λ1 supplementation on viral load. (a) Volcano plots depicting shared gene expression profiles of bronchial epithelial cell cultures infected with SARS-CoV, SARS-CoV-2 or MERS-CoV for (a) 24, (b) 48 hpi or (c) 72 hpi in comparison to HCoV-229E and HCoV-OC43; *n* = 4. Red dots indicate significantly upregulated genes and blue dots indicate significantly downregulated genes. (d) Heatmap of the overlap of significantly changed genes during 24, 48 and 72 hpi infection with SARS-CoV-2, SARS-CoV, MERS-CoV or HCoV-229E or HCoV-OC43 and mock as uninfected control. (e) Gene set variation analysis (GSVA) was performed on interferon response genes after 24, 48 and 72 hpi (*n* = 4) in highly pathogenic (orange) and low pathogenic (blue) coronavirus-infected cultures. As HCoV-OC43 infection was conducted at 33°C, SARS-CoV-2 infection at 33°C was included as control (pink). (f) IFN-λ1 and (g) IFN-α1 gene expression after 24, 48 and 72 hpi (*n* = 4) in highly pathogenic (orange) and low pathogenic (blue) coronavirus-infected cultures. The error bar indicates the standard deviation. Significant difference in increased gene expression over time of infection ($P < 0.05$) are shown by the * symbol. Two-way ANOVA followed by an unprotected Fisher's least significance difference test was conducted to test for significance. (h) ALI-PBEC cultures were pre-treated with 5 ng mL^{-1} interferon-lambda (IFN-λ1) for 60 min and subsequently infected with SARS-CoV-2 for 3 days with IFN-λ1 present in the basal medium. Extracellular viral RNA copies are depicted in log scale. Data in Fig. 7h are tested with a paired *t*-test and are depicted as mean ± SEM. *n* = 4 independent donors.

Discussion

Here we report marked differences in the transcriptional response of primary human bronchial epithelial cells to infection with SARS-CoV-2 when compared to infection with other highly pathogenic and low pathogenic coronaviruses. Infection with SARS-CoV, MERS-CoV and low pathogenic HCoV-229E evoked a partially overlapping transcriptional response, characterized by a significant and sustained increase in expression of IEGs such as *FOS*, *NR4A1* and *FOSB.* In contrast, the response to SARS-CoV-2 infection was characterized by the absence of such an increase and the only DEGs in the SARS-CoV-2 dataset that were significantly downregulated at 72 hpi were *FOS*, *NR4A1* and *FOSB*. Infection with SARS-CoV-2 at a higher MOI and prolonged incubation, i.e. for 7 days, did also not lead to an increase in the expression of the genes that were upregulated during SARS-CoV, MERS-CoV or HCoV-229E infection. We furthermore confirmed the increased

expression of these IEGs by MERS-CoV and SARS-CoV and the lack thereof by SARS-CoV-2 infection in publicly available data sets, including a clinical dataset. Treatment of infected cells with an NR4A1 antagonist decreased viral load, suggesting that the differential IEG gene expression may contribute to the kinetics of infection and potentially the pathogenicity of coronaviruses. Furthermore, we observed that activation of genes involved in interferon signaling was readily induced upon infection with the low pathogenic HCoV-229E and HCoV-OC43, whereas no such induction was observed with the three highly pathogenic coronaviruses, including SARS-CoV-2.

Where others have focused on the pathways that are activated by SARS-CoV-2 infection (278), the comparison between SARS-CoV-2 and other coronaviruses performed here highlight that SARS-CoV-2 may suppress or not induce expression in pathways that are activated by other coronaviruses. Many of the genes that were upregulated in cells infected with SARS-CoV, MERS-CoV and HCoV-229E, but not SARS-CoV-2, were IEGs. It still remains a question whether SARS-CoV-2 actively suppresses expression of these genes or lacks the ability to induce their expression. IEGs are a group of genes with various functional activities that are coordinately and rapidly upregulated in response to a diverse set of stress or proliferation-inducing stimuli. Their expression does not require *de novo* synthesis of proteins encoded by other genes, explaining their rapid induction. Besides being an IEG itself, recently it was established that *NR4A1* also regulates expression of IEGs (279), in particular, NR4A1 suppresses expression of IEGs including *FOS* and *FOSB*. This demonstrates the complexity of the signaling regarding these IEGs. In our study, we treated Calu-3 cells with the NR4A1 inhibitor DIM-C-pPhOH, thereby mimicking the putative SARS-CoV-2-mediated suppression of NR4A1 activation and found reduced replication of both SARS-CoV-2 and MERS-CoV. Nevertheless, it should be noted that despite the differences in IEG expression levels, the extent of infection was similar in all coronavirus-infected cultures. Therefore, it is more likely that the suppression of IEGs is affecting the inflammatory/immune response following epithelial infection rather than the viral levels. Furthermore, several of these IEGs such as *FOS* and *FOSB* are related to the JNK/AP-1 pathway, which has an essential role in cell death of infected cells via apoptosis and necrosis, and is important for the cellular response to pro-inflammatory stimuli, and thus could limit progression of infection (280). It is additionally involved in innate and adaptive immunity through for example, its relation to NF-κB (281). The lack of the pro-apoptotic function and regulatory role of the inflammation response of JNK/AP-1 related pathways could lead to prolongation of SARS-CoV-2 infection and/or delayed symptom development, especially early in infection. It may also contribute to the dysregulation of cytokine and chemokine responses. How SARS-CoV-2 exactly inhibits expression of IEGs will be of interest for further studies as the complexity of regulation of these IEGs requires in-depth analysis.

Activation of the JNK/AP-1 signaling pathway also occurs in response to other respiratory viruses like influenza or RSV (282, 283), and small-molecule inhibitors of this pathway were even shown to act as antivirals against influenza infection (284). Also treatment with the NR4A1 agonist cytosporone B controlled Influenza A replication via regulation of anti-viral responses in mice (285). Studying the role of IEGs in virus replication and infection biology is therefore interesting beyond coronaviruses.

Further research is needed to evaluate donor differences in the observed changes in gene expression in response to the variable coronaviruses. Our dataset only included a limited number of donors, with variable cellular composition. Unfortunately, we had to eliminate one donor from our dataset as it did not display transcriptional responses to infection with any of the viruses. We have repeated the SARS-CoV-2 infection with cells from the same donor and then comparable responses were found between donors using targeted PCR reactions, suggesting that a technical issue in the RNA sequencing explained these findings with this donor. To overcome the limitation of having included only 4 donors, we validated the outcomes in several publicly available datasets, we assessed expression of both the whole IEG gene set and several individual DEGs, in these datasets, which supported our findings. Importantly, the single cell RNA sequencing dataset confirmed that the absence of IEG expression that we detected in our SARS-CoV-2-infected cultures was also present in samples from infected humans. We furthermore confirmed the lack in IEGs expression by SARS-CoV-2 in the additional donors (not included in the RNA sequencing data set) that were tested in the prolonged infection experiment, in which also more virus was used to infect the cells. We can, however, not exclude that -in addition to the observations reported in this study- additional differences may have been missed as a result of the relatively low number of replicates. We can also formally not exclude that the presence of a tumor in the lung tissue has affected the surrounding tumor-free tissue from which the bronchial epithelial cells were isolated; however; obtaining lung tissue from healthy donors is a challenge for obvious reasons. We have validated our findings in datasets of others and could confirm our findings, and therefore we think that the use of this type of tissue has not affected our conclusions. The fact that we used a SARS-CoV-2 isolate from the first wave of the pandemic, and not the less pathogenic Omicron variant of SARS-CoV-2, can be viewed as a limitation. However, we specifically aimed to understand how highly pathogenic SARS-CoV-2 variants that cause severe disease redirect epithelial responses, also in view of preparedness for future pandemics.

We also aimed for functional translation of the effects found on interferon genes. However, to translate what we observed especially regarding the effect of modulation of NR4A1 and the JNK/AP-1 pathway on coronavirus replication and pathogenesis, studies will need to be performed on primary cell cultures of more donors. To this end, future experiments should

also include a larger range of viral doses to study the impact of initial infection severity on our findings. Finally, we largely focused on gene expression and our findings would likely benefit from larger scale proteomics approaches to gain further insights in the exact modulation of the signaling pathways by SARS-CoV-2 for example.

Our results also demonstrated an important difference in epithelial transcriptional responses after infection with pathogenic and low pathogenic coronaviruses. Induction of interferon-related genes was less strong by the pathogenic coronavirus strains when compared to low pathogenic HCoV-229E and HCoV-OC43. While an efficient interferon and interferon-stimulated genes response was reported for HCoV-229E and HCoV-OC43 (286), a lower response has been reported previously for pathogenic coronaviruses (287-289) and is also less strong than pathogenic influenza A H1N1 (290). This effect perhaps points to mechanisms of immune evasion through multiple possible mechanisms (291). When our cultures were supplemented with IFN-λ1 during infection, reduced SARS-CoV-2 levels were observed, supporting a role for suppression of interferon-mediated antiviral defenses in the pathogenicity of coronaviruses such as SARS-CoV-2. Recently, Banday and colleagues (292) showed similar results for SARS-CoV-2 using IFN-β and IFN -λ in a colon epithelial cell line (Caco-2), while Feld and colleagues (293) showed in outpatient COVID-19 patients that treatment with pegylated interferon lambda resulted in a more rapid clearance for SARS-CoV-2 compared to the placebo group. Finally, also in bronchial epithelial cell cultures this effect was confirmed using IFN-β1 and IFN-λ2 (294).

If we take all our results together, an interesting difference can be observed between low pathogenic coronaviruses, highly pathogenic coronaviruses with high mortality such as MERS-CoV and SARS-CoV, and with SARS-CoV-2 that is somewhere in between those two severity levels. Low pathogenic coronaviruses show a quick induction of both interferon-related genes and IEGs. Highly pathogenic MERS-CoV and SARS-CoV, that have an increased mortality compared to SARS-CoV-2 (295), show a lack of interferon gene induction but a strong induction of IEGs, whereas SARS-CoV-2 lacks both induction of interferon-related genes and IEGs. These changes could explain how low pathogenic strains are quickly cleared by a strong antiviral response, which combined with rapid induction of IEGs likely results in local inflammation-related symptoms. On the other hand, MERS-CoV and SARS-CoV impair/delay anti-viral defenses, thereby extending infection time, which combined with a quick induction of IEGs, likely results in strong inflammation and related symptoms correlated to the high level of infection. Uniquely, SARS-CoV-2 also impairs anti-viral responses; however; combined with a lack in IEG induction, inflammation is likely only local until the viral titers become so high that the resulting tissue damage promotes inflammation that leads to typical COVID-19 symptoms. This is clearly speculation but in line with the severity of the viruses and translation of these findings into those in human subjects would

be an exciting next step. Additionally, since SARS-CoV-2 is associated with higher levels of asymptomatic infections (295), it would be interesting to investigate if in these patients the interferon response may be present while the induction of IEGs is still absent (296).
The findings from our study highlight differences in transcriptional responses of airway epithelial cells to SARS-CoV-2 infection compared to other coronaviruses. The lack of induction or even suppression of IEGs expression by SARS-CoV-2 was striking and uncharacteristic of previously known coronaviruses and may contribute to its pathogenicity in multiple ways. In addition, lack of transcriptional activation of the interferon pathway is a unique feature that may distinguish highly pathogenic from low pathogenic coronavirus infections. This knowledge can aid in the understanding of SARS-CoV-2 pathogenesis and support development of therapeutic (host-directed) strategies against coronaviruses in general.

Methods

Cell culture

Primary human bronchial epithelial cells (PBEC) were isolated from tumor-free resected bronchus rings obtained from lung cancer patients undergoing a resection surgery at the Leiden University Medical Center (LUMC, Leiden, the Netherlands). Patients from which this lung tissue was derived were enrolled in the biobank via a no-objection system for coded anonymous further use of such tissue (www.coreon.org). Within this framework, individual written informed consent is not needed. Since 01-09-2022, patients are enrolled in the biobank using written informed consent in accordance with local regulations from the LUMC biobank with approval by the institutional medical ethical committee (B20.042/Ab/ab and B20.042/Kb/kb). Donor baseline characteristics are provided in **Table S1**.
PBEC were biobanked as described (297). In short, after 2h of incubation of the bronchial ring in PBS supplemented with protease XIV, cells were scraped off and seeded in Keratinocyte-Serum Free Medium (KSFM, Life-technologies Europe B.V., the Netherlands) containing 0.2 ng/ml Epidermal Growth Factor (hEGF, Gibco, USA), 25 µg/ml Bovine Pituitary Extract (BPE, Life-technologies Europe B.V.), 1 µM isoproterenol (Sigma-Aldrich, USA) and 100 µg/ml primocin (Invivogen, the Netherlands) in 6-well plates (Corning Costar, USA) coated with 30 µg/ml PureCol (Advanced BioMatrix, USA), 5 µg/ml human fibronectin (Promocell, Germany), and 10 µg/ml bovine serum albumin (Fraction V; Thermo Fisher Scientific, USA). After cell cultures had reached 80-90% confluence, cells were harvested

using soft trypsin (Life-technologies Europe B.V.) and soybean trypsin inhibitor (SBTI, Sigma-Aldrich) and stored in liquid nitrogen until further use. Cryopreserved PBEC were thawed and expanded in a coated T75 flask (Greiner Bio- One, the Netherlands) until 80-90% confluency was reached after which cells were seeded in a 12-well cell culture insert (40,000 cells per insert; Transwell®, Corning Costar), coated as described above. Apical and basal sides of inserts were filled with a B/D medium supplemented with 1 nM EC23 (Tocris, UK). B/D medium is a mix of 50% Bronchial Epithelial Cell Medium-basal (BEpiCM-b; ScienCell, Sanbio) and 50% Dulbecco's modified Eagle's medium (DMEM; Stemcell Technologies, Germany) supplemented with 12.5 mM HEPES, bronchial epithelial cell growth supplements, 100 U/ml penicillin, 100 µg/ml streptomycin (all from ScienCell) and 1 mM glutaMAX (Thermo Fisher Scientific). After confluency was reached, the apical medium was removed and cells were cultured at the air-liquid interface (ALI) in B/D medium with 50 nM EC-23 for up to 5 to 6 weeks; medium was refreshed three times a week, each time the apical side was washed with pre-warmed PBS.

Calu-3 cells (ATCC, HTB-55TM) were cultured in Eagle's minimum essential medium (EMEM, Lonza), supplemented with 9% fetal calf serum (FCS; CapriCorn Scientific, USA), 1% non-essential amino acids (NEAA, Sigma-Aldrich), 2 mM L-glutamine (Sigma-Aldrich), 1 mM sodium pyruvate (Sigma-Aldrich) and 100 U/ml of penicillin/ streptomycin (P/S; Sigma-Aldrich). Infections were performed with the same medium, except that 2% FCS was used.
Vero E6 cells (Collection Medical Microbiology, LUMC) were cultured in DMEM with 4.5 g/l glucose with L-glutamin (DMEM; Lonza, Switzerland), supplemented with 8% FCS and 100 U/ml of P/S (Sigma-Aldrich). Infections in Vero E6 cells were performed in EMEM with 25 mM HEPES supplemented with 2% FCS (PAA), 2mM L-glutamine (Sigma-Aldrich), and 100 U/ml of P/S (Sigma-Aldrich).
HUH-7 cells (Collection Medical Microbiology, LUMC) were cultured in DMEM with 4.5 g/l glucose with L-glutamin (DMEM; Lonza, Switzerland), supplemented with 8% FCS, 1% non-essential amino acids (NEAA, Sigma-Aldrich), 2 mM L-glutamine (Sigma-Aldrich) and 100 U/ml of P/S (Sigma-Aldrich). Infections in HUH-7 cells were performed in EMEM with 25 mM HEPES supplemented with 2% FCS (PAA), 2mM L-glutamine (Sigma-Aldrich), and 100 U/ml of P/S (Sigma-Aldrich).
All cell cultures were maintained at 37°C in an atmosphere of 5% CO_2.

Virus stocks

All experiments with SARS-CoV, SARS-CoV-2 or MERS-CoV were performed at the LUMC biosafety level 3 facilities. The clinical isolate SARS-CoV-2/Leiden-0008 was isolated from a

nasopharyngeal sample collected at the LUMC during the first wave of the coronavirus pandemic in March 2020 (GenBank: MT705206.1). SARS-CoV-2/Leiden-0008 (Passage 2) and SARS-CoV isolate Frankfurt 1 (298) (Passage 4) were grown in Vero E6 cells. The SARS-CoV-2 stock was sequenced to exclude Vero cell adaptation in the spike S1/S2 cleavage site. MERS-CoV (N3/Jordan, GenBank: KJ614529.1) (Passage 3) and HCoV-229E (Passage 2, GenBank: NC_002645.1) were grown on HUH-7 cells. HCoV-OC43 was isolated from a bronchioalveolar lavage sample collected between 2018 and 2020 at the LUMC, and grown on primary bronchial epithelial cell cultures at the air-liquid interface. Next-generation sequencing was done and the isolate was mapped to the HCoV-OC43 strain ATCC VR-759 (GenBank: AY585228.1). Virus titers were determined by plaque assay on Vero E6 cells, and for MERS-CoV and HCoV-229E on HUH7 cells, as described before(299). Virus titer of HCoV-OC43 was determined by RT-qPCR, due to the lack of susceptible cells for plaque assay.

Viral infection of ALI-PBEC

The apical side of inserts was washed with 200 µl PBS for 10 min at 37°C to remove excess mucus and basal medium was refreshed prior to infection. Cells were infected with 30,000 plaque-forming units (PFU) of SARS-CoV-2, MERS-CoV, SARS-CoV and HCoV-229E in 200 µl PBS per insert for 2h at 37 °C on a rocking platform (estimated multiplicity of infection [MOI] of 0.03) (300, 301). For HCoV-OC43, the experiments were performed in an independent experiment, however using cultures from the same donors. Infections with HCoV-OC43 were performed at 33 °C and SARS-CoV-2 was taken along as a control at this temperature. The same multiplicity of infection for HCoV-OC43 was used as for the other coronavirus infections, but the titer was based on RT-qPCR measurement of the virus stock, in lack of a good cell culture model to perform a plaque assay experiment. For noninfected (mock) controls the same procedure was performed with PBS only. After removal of the inoculum, the apical side was washed three times with PBS and cells were incubated at 33 °C or 37 °C until sampling at several time points post infection (p.i.). At each sampling time-point, 200 µl of PBS was added to the apical side of the cells, and after incubation for 10 min at 37°C supernatant was harvested for quantification of infectious viral particles by plaque assay and RNA copies by RT-qPCR. Cells were then lysed using 200 µl of RNA lysis buffer (Promega, the Netherlands) or 250 µl Guanidine thiocyanate (GITC) reagent (3 M GITC (Fluka), 2% sarkosyl (Sigma-Aldrich), 50 mM Tris (Affymetrix), 20 mM EDTA (Sigma-Aldrich)) per insert. For long-term SARS-CoV-2 infection, cells were infected with 10^6 PFU of SARS-CoV-2 (estimated MOI of 1) in the same way as described above but the inserts were incubated for 1-7 days.

RNA isolation and quantitative real-time PCR (RT- qPCR)

Total intracellular RNA was robotically extracted using the Maxwell® 16 simply RNA tissue kit (Promega) and quantified using a NanoDrop™ One UV-Vis Spectrophotometer (Thermo Fisher Scientific) and stored at -80 ^{o}C until further use. Extracellular RNA was extracted by magnetic bead isolation. The full procedure for this isolation methods is described in the supplementary materials section.
For viral RNA measurement, the cellular reference gene *PGK1* served as control for intracellular RNA. Primers and Taqman probes for *PGK1* were obtained from a published source (299). Viral RNA was quantified by RT-qPCR using the TaqMan™ Fast Virus 1-Step Master Mix (Thermo Fisher Scientific), with primer concentrations for SARS-CoV-2 and SARS-CoV as described previously (256), for MERS-CoV and HCoV-229E with final primer concentrations of 450 nM each and probe concentrations of 200 nM, and for HCoV-OC43 with final primer concentrations of 1000 nM each and probe concentration of 166 nM. Further details on the qPCR methods related to virus and human genes are described in the supplementary materials section. Primer sequences are summarized in **Table S2**.

RNA sequencing

The quality of total RNA was determined by bioanalyser and sequenced by GenomeScan (Leiden, the Netherlands) using an Illumina NovaSeq6000 sequencer with 20 million paired-end reads per sample. The sequences were then trimmed using the Trimmomatic tool, version 0.33. Two consecutive computational strategies were applied for transcriptome reconstruction. First, the Spliced Transcripts Alignment to a Reference (STAR) version 2.5.3a was used to align and identify all reads that belong to the human genome (GRCh38). Samples were then mapped against respective virus genomes SARS-CoV-2 (NC_045512.2), MERS-CoV (NC_019843.3), SARS-CoV (AY291315.1), HCoV-229E (NC_002645.1) and HCoV-OC43 (NC_006213.1). Originally cultures derived from 5 donors were sequenced; however; one donor did not show transcriptional responses to any of the viruses and was therefore excluded from the dataset. RNA-Seq analysis and cellular deconvolution is outline in the supplementary materials.

Differential expression analysis

RNA-seq analysis was conducted using the R package EdgeR. Differential expression analysis was conducted comparing virus infection at each time point to time-matched no virus

control/mock using the following model (gene expression~ patient ID + cell treatment). For high pathogenic virus analysis, SARS-CoV, MERS-CoV and SARS-CoV-2 were merged together as one group and compared to HCoV-229E. Gene signatures were made using the Gene Set Variation Analysis (GSVA) package (version 1.44.5). Genes that were significantly increased in SARS-CoV, MERS-CoV and HCoV-229E-infected cultures across all time points FOS; NR4A1; FOSB; AC025259.3; EGR3; CYR61; EGR1; AC008894.3; RASD1; EGR2; ZFP36; CTGF; IL6 were used to make a general coronavirus signature. Additionally a general IFN response signature (IFIT1; ISG15; IFI6; OAS1; OASL; IFI44; HERC5; MX2; HERC6; OAS3; DDX58; IRF7; SAMD9; HELZ2; USP18; DDX60; LAMP3; EPSTI1; PLSCR1; EIF2AK2; PARP12; PARP9; PARP14; BST2; TRIM22; IFITM3; IRF9) was used to investigate the overall IFN response of each coronavirus. We compared transcriptional responses of epithelial cultures infected with highly pathogenic coronavirus strains (i.e., SARS-CoV; SARS-CoV-2 and MERS-CoV) with those infected with low pathogenic HCoV-229E and HCoV-OC43 at 24, 48 and 72 hours. Infection with HCoV-OC43 was conducted at 33^{o}C, hence for signature analysis, SARS-CoV-2 infection at 33^{o}C was used as a comparison. For all analyses, expression of a gene was considered significantly different with a Benjamini Hochberg corrected P value <0.05 and a Fold change>|1.5|. For the heatmaps, data was normalized using the function vst DeSeq2 package R.

Statistics

Statistical analysis was performed in GraphPad PRISM 9.0.1 (GraphPad Software Inc., CA). Performed statistical tests are indicated in the Figure legends. Data are shown as mean ± SEM of cultures derived from several donors and differences were considered significant at $p<0.05$.

Acknowledgements

This work was supported by a COVID-19 MKMD grant from the Netherlands Organization for Health Research and Development (ZonMw) and the Dutch Society for the Replacement of Animal Testing (Stichting Proefdiervrij) (grant #114025007), a RSEOH-CAG COVID-19 Rapid Response Research Initiative and a RSEOH-CAG 2021 Extension Grant. C.S-B. is supported by the Coordination for the Improvement of Higher Education Personnel (CAPES) (process no. 88881.171440/2018-01), Ministry of Education, Brazil. Part of this research was supported by the Leiden University Fund (LUF), the Bontius Foundation, and donations from the crowdfunding initiative “wake up to corona”.

Data availability statement

The datasets generated and/or analyzed during the current study will be made available upon publication via the European Genome-phenome Archive (EGA) but are currently available from the corresponding author on reasonable request.

Conflict of interest

All authors declare no competing interest in relation to this manuscript

Authors' contributions

YW, MT, MH, PSH, AD and AF were involved in study design and conceptualization. YW, MT, CS-B, AL DN PH and FB performed experiments. NL FB and AF performed RNA-seq analysis and cellular deconvolution. YW, MT, and AD wrote the manuscript. MH, PSH and AF revised the manuscript.

Corresponding author information:
Dr. Alen Faiz, Respiratory Bioinformatics and Molecular Biology (RBMB), School of Life Sciences, Building 4, Room 04.07.418, Thomas St, Ultimo NSW 2007
University of Technology Sydney, Sydney, Australia
E-mail: alen.faiz@uts.edu.au;
Phone: +61 (0) 420239776

Supplementary Material

Table S1: Donor characteristics

	Donor characteristics	Donor characteristics
	RNA-Seq	**Long-term**
Number of donors	4	3
Male/Female	2/2	2/1
Age (years) mean [SEM]	63.0 [1.1]	66.33 [7.1]
BMI mean [SEM]	31.2 [5.0]	31.1 [2.8]
Smoking status (non-/ex-/smokers)	0/3/1	02-01-2000
FEV1 % pred [SEM]	109.5 [6.1]	75.27 [4.0]

Abbreviations: SEM (standard error of mean); BMI (body mass index); FEV1 (forced expired volume in 1 sec) ; pred (predicted).

Table S2: Primer sequences

Gene	Encoding protein	Sequence forward primer	Sequence reverse primer	Probe
SARS-CoV-2 E	Envelope protein	ACAGGTACGTTAATAGTTAATAGCGT	ATATTGCAGCAGTACGCACACA	TexRed-ACACTAGCCATCCTTACTGCGCTTCG-BHQ1
SARS-CoV-2 RdRp	RNA-dependent RNA polymerase	GTGARATGGTCATGTGTGGCGG	CARATGTTAAASACACTATTAGCATA	FAM-CAGGTGGAACCTCATCAGGAGATGC-BHQ1
MERS-CoV N	Nucleocapsid protein	GTACCTCTTAATGCCAATTC	GAGCCAGTTGCxTTAATTC	TexRed-TCTGTCCTGTCTCCGCCAATAC-BHQ2

HCoV-229E M	Membrane protein	CATACTATCAACCCATTCAACAAG	CACGGCAACTGTCATGTATT	FAM-ATGAACCTGAACACCTGAAGCCAATCTATG-BHQ1
FOSB	FOSB	GCTGCAAGATCCCCTACGAAG	ACGAAGAAGTGTACGAAGGGTT	-
NR4A1	Nuclear receptor 4A1	ATGCCCTGTATCCAAGCCC	GTGTAGCCGTCCATGAAGGT	-
FOS	C-Fos	GGGGCAAGGTGGAACAGTTAT	CCGCTTGGAGTGTATCAGTCA	-
ATP5B	ATP synthase subunit beta	TCACCCAGGCTGGTTCAGA	AGTGGCCAGGGTAGGCTGAT	-
OAZ1	Ornithine decarboxylase antizyme 1	GGATCCTCAATAGCCACTGC	TACAGCAGTGGAGGGAGACC	-

Supplementary tables S3 – S5

The data of Table S3, table S4 and table S5 are shown in an online repository (figshare). Please find the (private) link to access the table below:

https://figshare.com/s/7eea9ca4e79760c369a5

Supplementary Figures

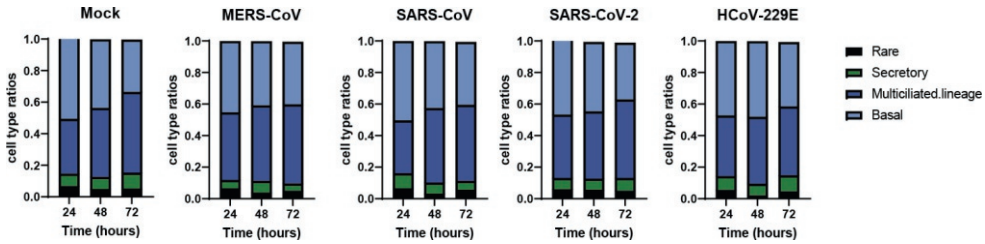

Figure S1: Cellular deconvolution during coronavirus infection of well-differentiated air-liquid interface (ALI) cultures of primary bronchial epithelial cells (PBEC). PBEC that were differentiated for 6 weeks at ALI were infected in parallel with four different coronaviruses. Relative proportion of different cell types of infected cultures over 72h determined by cellular deconvolution of the transcriptomic datasets. N=4 independent donors.

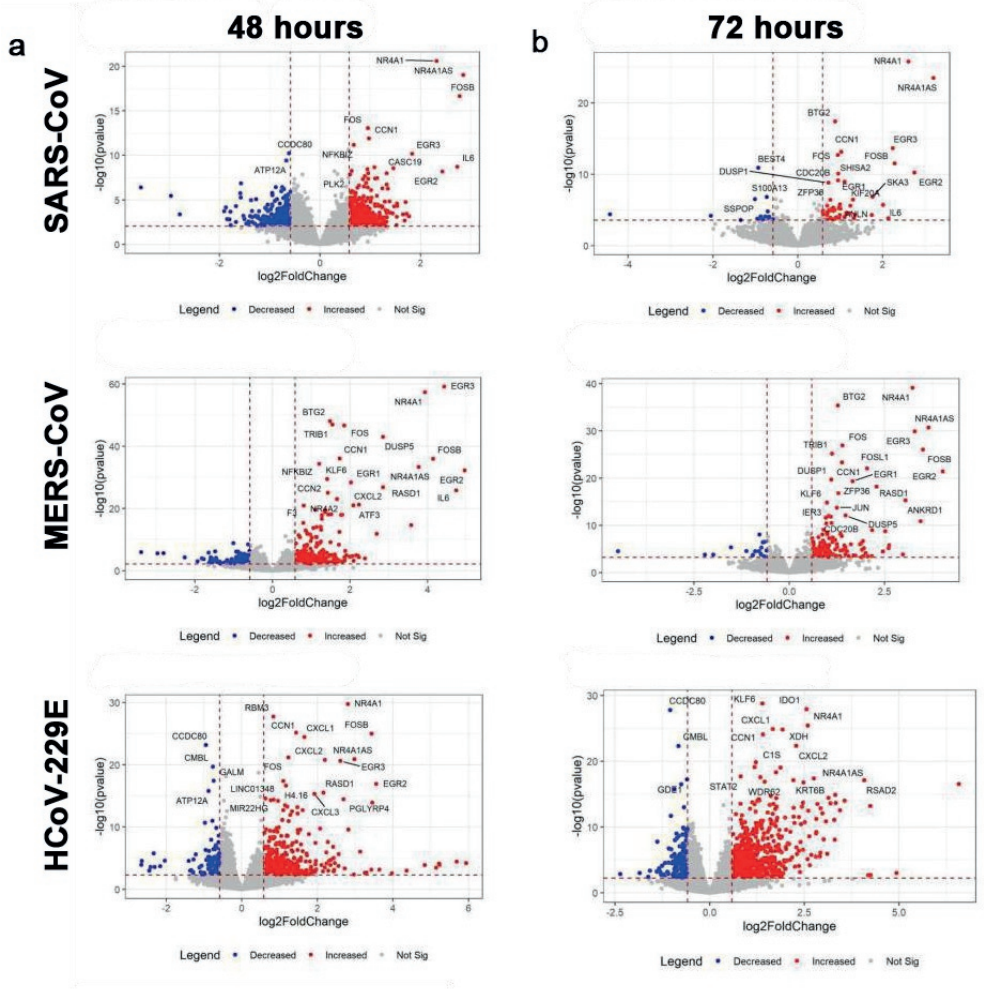

Figure S2: Gene expression profiles of well-differentiated primary bronchial epithelial cell cultures infected with three different coronaviruses. (a) Volcano plots depicting gene expression profiles of bronchial epithelial cell cultures infected with SARS-CoV, MERS-CoV or HCoV-299E after 48 h or (b) 72 h post infection in comparison to the uninfected controls. Red dots indicate significantly upregulated genes and blue dots indicate signficantly downregulated genes. N=4.

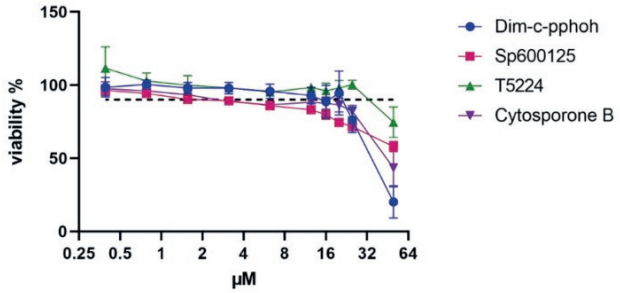

Figure S3: Cytotoxicity of tested JNK/AP-1 signaling modulating compounds on Calu-3 cells. Cell viability was measured by MTS assay after 24 h of treatment. The black dotted line indicates 90% viability. Mean values ± SD are shown, n=4.

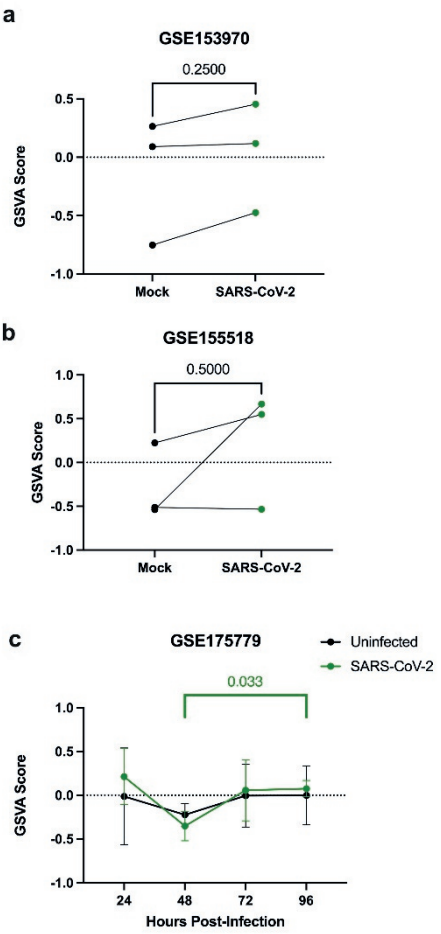

Figure S4: GSVA of IEG gene set on (a) A publicly available dataset (GSE153970) with RNA-seq analysis on primary epithelial cell cultures mock-infected or infected with SARS-CoV-2 at a MOI=0.25 at 48 hpi. (b) A publicly available dataset (GSE155518) derived from primary human lung alveolar epithelial organoid cultures infected with SARS-CoV-2 and assessed at 48 hpi. (c) A publicly available dataset (GSE175779) from primary human bronchial epithelial cells infected with SARS- CoV-2 over a 96 h infection period. Wilcoxon paired nonparametric statistical analysis was conducted on GSE153970 and GSE155518, while two-way ANOVA with Bonferroni correction was performed on GSE175779.

References

1. Zhu Z, Lian X, Su X, Wu W, Marraro GA, Zeng Y. 2020. From SARS and MERS to COVID-19: a brief summary and comparison of severe acute respiratory infections caused by three highly pathogenic human coronaviruses. Respiratory Research 21:224.
2. Abdelghany TM, Ganash M, Bakri MM, Qanash H, Al-Rajhi AMH, Elhussieny NI. 2021. SARS-CoV-2, the other face to SARS-CoV and MERS-CoV: Future predictions. Biomedical Journal 44:86-93.
3. Hamre D, Procknow JJ. 1966. A new virus isolated from the human respiratory tract. Proc Soc Exp Biol Med 121:190-3.
4. McIntosh K, Becker WB, Chanock RM. 1967. Growth in suckling-mouse brain of "IBV-like" viruses from patients with upper respiratory tract disease. Proc Natl Acad Sci U S A 58:2268-73.
5. Lukassen S, Chua RL, Trefzer T, Kahn NC, Schneider MA, Muley T, Winter H, Meister M, Veith C, Boots AW, Hennig BP, Kreuter M, Conrad C, Eils R. 2020. SARS-CoV-2 receptor ACE2 and TMPRSS2 are primarily expressed in bronchial transient secretory cells. The EMBO journal 39:e105114-e105114.
6. Ravindra NG, Alfajaro MM, Gasque V, Habet V, Wei J, Filler RB, Huston NC, Wan H, Szigeti-Buck K, Wang B, Wang G, Montgomery RR, Eisenbarth SC, Williams A, Pyle AM, Iwasaki A, Horvath TL, Foxman EF, Pierce RW, van Dijk D, Wilen CB. 2020. Single-cell longitudinal analysis of SARS-CoV-2 infection in human airway epithelium. PLOS Biol.
7. Aliee H, Massip F, Qi C, Stella de Biase M, van Nijnatten J, Kersten ET, Kermani NZ, Khuder B, Vonk JM, Vermeulen RC. 2022. Determinants of expression of SARS-CoV-2 entry-related genes in upper and lower airways. Allergy 77:690-694.
8. Johansen MD, Mahbub RM, Idrees S, Nguyen DH, Miemczyk S, Pathinayake P, Nichol K, Hansbro NG, Gearing LJ, Hertzog PJ, Gallego-Ortega D, Britton WJ, Saunders BM, Wark PA, Faiz A, Hansbro PM. 2022. Increased SARS-CoV-2 Infection, Protease, and Inflammatory Responses in Chronic Obstructive Pulmonary Disease Primary Bronchial Epithelial Cells Defined with Single-Cell RNA Sequencing. Am J Respir Crit Care Med 206:712-729.
9. Bost P, Giladi A, Liu Y, Bendjelal Y, Xu G, David E, Blecher-Gonen R, Cohen M, Medaglia C, Li H, Deczkowska A, Zhang S, Schwikowski B, Zhang Z, Amit I. 2020. Host-Viral Infection Maps Reveal Signatures of Severe COVID-19 Patients. Cell 181:1475-1488.e12.
10. Chua RL, Lukassen S, Trump S, Hennig BP, Wendisch D, Pott F, Debnath O, Thürmann L, Kurth F, Völker MT, Kazmierski J, Timmermann B, Twardziok S, Schneider S, Machleidt F, Müller-Redetzky H, Maier M, Krannich A, Schmidt S, Balzer F, Liebig J, Loske J, Suttorp N, Eils J, Ishaque N, Liebert UG, von Kalle C, Hocke A, Witzenrath M, Goffinet C, Drosten C, Laudi S, Lehmann I, Conrad C, Sander L-E, Eils R. 2020. COVID-19 severity correlates with airway epithelium–immune cell interactions identified by single-cell analysis. Nature Biotechnology 38:970-979.
11. Otter CJ, Fausto A, Tan LH, Khosla AS, Cohen NA, Weiss SR. 2023. Infection of primary nasal epithelial cells differentiates among lethal and seasonal human coronaviruses. Proc Natl Acad Sci U S A 120:e2218083120.
12. Jha PK, Vijay A, Halu A, Uchida S, Aikawa M. 2020. Gene Expression Profiling Reveals the Shared and Distinct Transcriptional Signatures in Human Lung Epithelial Cells Infected With SARS-CoV-2, MERS-CoV, or SARS-CoV: Potential Implications in Cardiovascular Complications of COVID-19. Front Cardiovasc Med 7:623012.
13. Jang Y, Seo SH. 2020. Gene expression pattern differences in primary human pulmonary epithelial cells infected with MERS-CoV or SARS-CoV-2. Arch Virol 165:2205-2211.
14. Thaler M, Wang Y, van der Does AM, Faiz A, Ninaber DK, Ogando NS, Beckert H, Taube C, Salgado-Benvindo C, Snijder EJ, Bredenbeek PJ, Hiemstra PS, van Hemert MJ. 2023. Impact

of changes in human airway epithelial cellular composition and differentiation on SARS-CoV-2 infection biology. J Innate Immun 15:562-80.
15. Cantuti-Castelvetri L, Ojha R, Pedro LD, Djannatian M, Franz J, Kuivanen S, van der Meer F, Kallio K, Kaya T, Anastasina M. 2020. Neuropilin-1 facilitates SARS-CoV-2 cell entry and infectivity. Science 370:856-860.
16. Bahrami S, Drablos F. 2016. Gene regulation in the immediate-early response process. Adv Biol Regul 62:37-49.
17. Melms JC, Biermann J, Huang H, Wang Y, Nair A, Tagore S, Katsyv I, Rendeiro AF, Amin AD, Schapiro D, Frangieh CJ, Luoma AM, Filliol A, Fang Y, Ravichandran H, Clausi MG, Alba GA, Rogava M, Chen SW, Ho P, Montoro DT, Kornberg AE, Han AS, Bakhoum MF, Anandasabapathy N, Suarez-Farinas M, Bakhoum SF, Bram Y, Borczuk A, Guo XV, Lefkowitch JH, Marboe C, Lagana SM, Del Portillo A, Tsai EJ, Zorn E, Markowitz GS, Schwabe RF, Schwartz RE, Elemento O, Saqi A, Hibshoosh H, Que J, Izar B. 2021. A molecular single-cell lung atlas of lethal COVID-19. Nature 595:114-119.
18. Totura AL, Baric RS. 2012. SARS coronavirus pathogenesis: host innate immune responses and viral antagonism of interferon. Curr Opin Virol 2:264-75.
19. Sa Ribero M, Jouvenet N, Dreux M, Nisole S. 2020. Interplay between SARS-CoV-2 and the type I interferon response. PLoS Pathog 16:e1008737.
20. Rex DAB, Dagamajalu S, Kandasamy RK, Raju R, Prasad TSK. 2021. SARS-CoV-2 signaling pathway map: A functional landscape of molecular mechanisms in COVID-19. J Cell Commun Signal 15:601-608.
21. Guo H, Golczer G, Wittner BS, Langenbucher A, Zachariah M, Dubash TD, Hong X, Comaills V, Burr R, Ebright RY, Horwitz E, Vuille JA, Hajizadeh S, Wiley DF, Reeves BA, Zhang JM, Niederhoffer KL, Lu C, Wesley B, Ho U, Nieman LT, Toner M, Vasudevan S, Zou L, Mostoslavsky R, Maheswaran S, Lawrence MS, Haber DA. 2021. NR4A1 regulates expression of immediate early genes, suppressing replication stress in cancer. Mol Cell 81:4041-4058.e15.
22. Weston CR, Davis RJ. 2007. The JNK signal transduction pathway. Curr Opin Cell Biol 19:142-9.
23. Huang G, Shi LZ, Chi H. 2009. Regulation of JNK and p38 MAPK in the immune system: signal integration, propagation and termination. Cytokine 48:161-9.
24. Ludwig S, Ehrhardt C, Neumeier ER, Kracht M, Rapp UR, Pleschka S. 2001. Influenza virus-induced AP-1-dependent gene expression requires activation of the JNK signaling pathway. J Biol Chem 276:10990-8.
25. Li XM, Sun SZ, Wu FL, Shi T, Fan HJ, Li DZ. 2016. Study on JNK/AP-1 signaling pathway of airway mucus hypersecretion of severe pneumonia under RSV infection. Eur Rev Med Pharmacol Sci 20:853-7.
26. Nacken W, Ehrhardt C, Ludwig S. 2012. Small molecule inhibitors of the c-Jun N-terminal kinase (JNK) possess antiviral activity against highly pathogenic avian and human pandemic influenza A viruses. Biol Chem 393:525-34.
27. Egarnes B, Blanchet MR, Gosselin J. 2017. Treatment with the NR4A1 agonist cytosporone B controls influenza virus infection and improves pulmonary function in infected mice. PLoS One 12:e0186639.
28. Duncan JKS, Xu D, Licursi M, Joyce MA, Saffran HA, Liu K, Gohda J, Tyrrell DL, Kawaguchi Y, Hirasawa K. 2023. Interferon regulatory factor 3 mediates effective antiviral responses to human coronavirus 229E and OC43 infection. Front Immunol 14:930086.
29. Lei X, Dong X, Ma R, Wang W, Xiao X, Tian Z, Wang C, Wang Y, Li L, Ren L, Guo F, Zhao Z, Zhou Z, Xiang Z, Wang J. 2020. Activation and evasion of type I interferon responses by SARS-CoV-2. Nat Commun 11:3810.

30. Siu KL, Yeung ML, Kok KH, Yuen KS, Kew C, Lui PY, Chan CP, Tse H, Woo PC, Yuen KY, Jin DY. 2014. Middle east respiratory syndrome coronavirus 4a protein is a double-stranded RNA-binding protein that suppresses PACT-induced activation of RIG-I and MDA5 in the innate antiviral response. J Virol 88:4866-76.
31. Frieman M, Ratia K, Johnston RE, Mesecar AD, Baric RS. 2009. Severe acute respiratory syndrome coronavirus papain-like protease ubiquitin-like domain and catalytic domain regulate antagonism of IRF3 and NF-kappaB signaling. J Virol 83:6689-705.
32. Stolting H, Baillon L, Frise R, Bonner K, Hewitt RJ, Molyneaux PL, Gore ML, Breathing Together C, Barclay WS, Saglani S, Lloyd CM. 2022. Distinct airway epithelial immune responses after infection with SARS-CoV-2 compared to H1N1. Mucosal Immunol 15:952-963.
33. Kim YM, Shin EC. 2021. Type I and III interferon responses in SARS-CoV-2 infection. Exp Mol Med 53:750-760.
34. Banday AR, Stanifer ML, Florez-Vargas O, Onabajo OO, Papenberg BW, Zahoor MA, Mirabello L, Ring TJ, Lee CH, Albert PS, Andreakos E, Arons E, Barsh G, Biesecker LG, Boyle DL, Brahier MS, Burnett-Hartman A, Carrington M, Chang E, Choe PG, Chisholm RL, Colli LM, Dalgard CL, Dude CM, Edberg J, Erdmann N, Feigelson HS, Fonseca BA, Firestein GS, Gehring AJ, Guo C, Ho M, Holland S, Hutchinson AA, Im H, Irby L, Ison MG, Joseph NT, Kim HB, Kreitman RJ, Korf BR, Lipkin SM, Mahgoub SM, Mohammed I, Paschoalini GL, Pacheco JA, Peluso MJ, Rader DJ, Redden DT, Ritchie MD, et al. 2022. Genetic regulation of OAS1 nonsense-mediated decay underlies association with COVID-19 hospitalization in patients of European and African ancestries. Nat Genet 54:1103-1116.
35. Feld JJ, Kandel C, Biondi MJ, Kozak RA, Zahoor MA, Lemieux C, Borgia SM, Boggild AK, Powis J, McCready J, Tan DHS, Chan T, Coburn B, Kumar D, Humar A, Chan A, O'Neil B, Noureldin S, Booth J, Hong R, Smookler D, Aleyadeh W, Patel A, Barber B, Casey J, Hiebert R, Mistry H, Choong I, Hislop C, Santer DM, Lorne Tyrrell D, Glenn JS, Gehring AJ, Janssen HLA, Hansen BE. 2021. Peginterferon lambda for the treatment of outpatients with COVID-19: a phase 2, placebo-controlled randomised trial. Lancet Respir Med 9:498-510.
36. Vanderwall ER, Barrow KA, Rich LM, Read DF, Trapnell C, Okoloko O, Ziegler SF, Hallstrand TS, White MP, Debley JS. 2022. Airway epithelial interferon response to SARS-CoV-2 is inferior to rhinovirus and heterologous rhinovirus infection suppresses SARS-CoV-2 replication. Sci Rep 12:6972.
37. Zhang C, Wang H, Wen Z, Gu M, Liu L, Li X. 2022. Asymptomatic Transmissibility Calls for Implementing a Zero-COVID Strategy to End the Current Global Crisis. Front Cell Infect Microbiol 12:836409.
38. Masood KI, Yameen M, Ashraf J, Shahid S, Mahmood SF, Nasir A, Nasir N, Jamil B, Ghanchi NK, Khanum I, Razzak SA, Kanji A, Hussain R, M ER, Hasan Z. 2021. Upregulated type I interferon responses in asymptomatic COVID-19 infection are associated with improved clinical outcome. Sci Rep 11:22958.
39. Amatngalim GD, Schrumpf JA, Dishchekenian F, Mertens TCJ, Ninaber DK, van der Linden AC, Pilette C, Taube C, Hiemstra PS, van der Does AM. 2018. Aberrant epithelial differentiation by cigarette smoke dysregulates respiratory host defence. Eur Respir J. 51:1701009.
40. Drosten C, Günther S, Preiser W, Van Der Werf S, Brodt H-R, Becker S, Rabenau H, Panning M, Kolesnikova L, Fouchier RA. 2003. Identification of a novel coronavirus in patients with severe acute respiratory syndrome. New England journal of medicine 348:1967-1976.
41. Kovacikova K, Morren BM, Tas A, Albulescu IC, van Rijswijk R, Jarhad DB, Shin YS, Jang MH, Kim G, Lee HW. 2020. 6′-β-Fluoro-homoaristeromycin and 6′-fluoro-homoneplanocin A are potent inhibitors of chikungunya virus replication through their direct effect on viral nonstructural protein 1. Antimicrobial Agents and Chemotherapy 64:e02532-19.

42. Mantlo E, Bukreyeva N, Maruyama J, Paessler S, Huang C. 2020. Antiviral activities of type I interferons to SARS-CoV-2 infection. Antiviral Res 179:104811.
43. Mache C, Schulze J, Holland G, Bourquain D, Gensch JM, Oh DY, Nitsche A, Durrwald R, Laue M, Wolff T. 2022. SARS-CoV-2 Omicron variant is attenuated for replication in a polarized human lung epithelial cell model. Commun Biol 5:1138.
44. Corman VM, Landt O, Kaiser M, Molenkamp R, Meijer A, Chu DK, Bleicker T, Brunink S, Schneider J, Schmidt ML, Mulders DG, Haagmans BL, van der Veer B, van den Brink S, Wijsman L, Goderski G, Romette JL, Ellis J, Zambon M, Peiris M, Goossens H, Reusken C, Koopmans MP, Drosten C. 2020. Detection of 2019 novel coronavirus (2019-nCoV) by real-time RT-PCR. Euro Surveill 25.

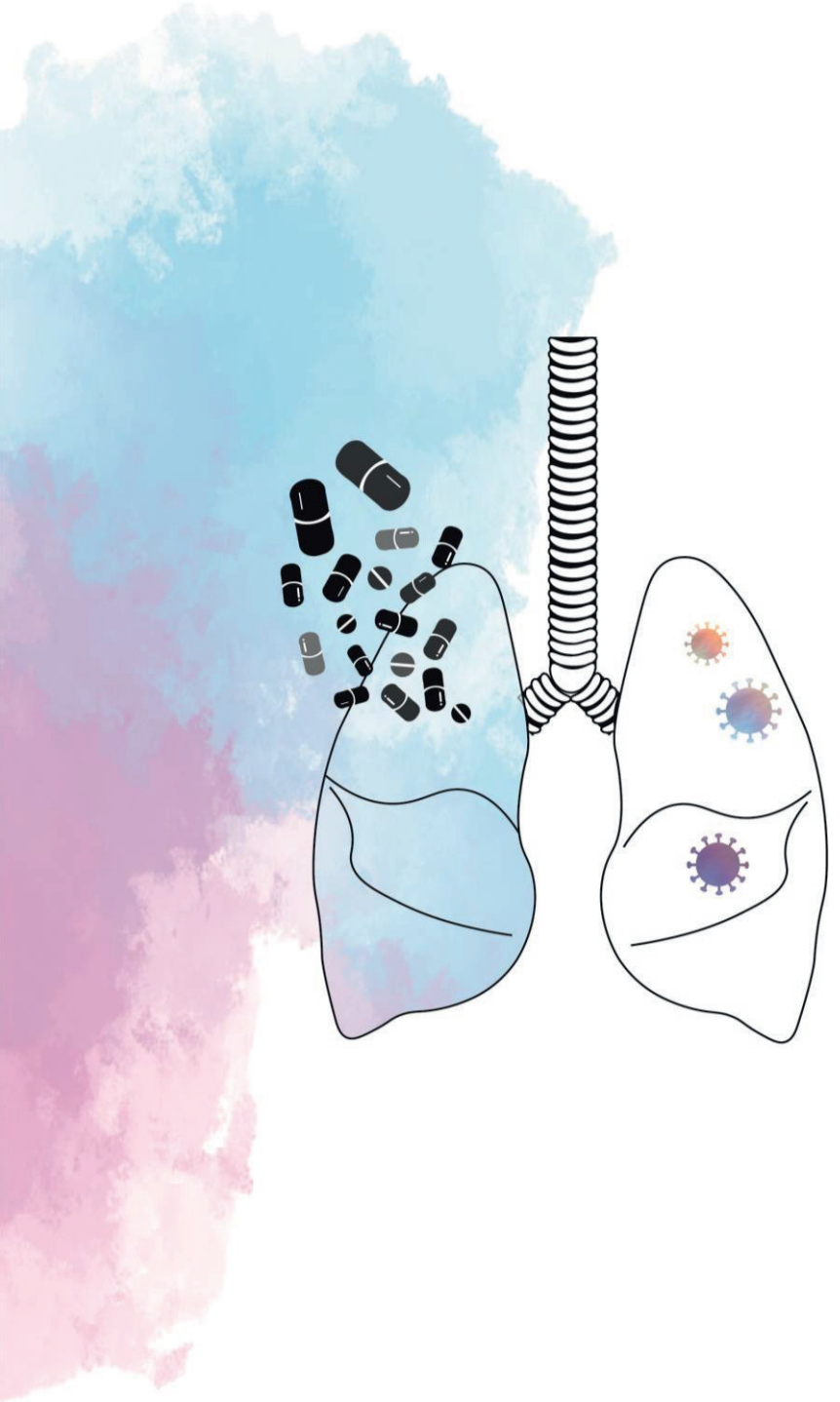

Chapter 4

R-propranolol has broad-spectrum anti-coronavirus activity and suppresses factors involved in pathogenic angiogenesis

Melissa Thaler[1], Clarisse Salgado-Benvindo[1], Anouk Leijs[1], Ali Tas[1], Dennis K. Ninaber[2], Jack L. Arbiser[3,4], Eric J. Snijder[1], Martijn J. van Hemert[1]

[1] Department of Medical Microbiology, Leiden University Medical Center, Leiden, The Netherlands
[2] Department of Pulmonology, Leiden University Medical Center, Leiden, The Netherlands
[3] Department of Dermatology, Emory University School of Medicine, Atlanta, GA, USA
[4] Division of Dermatology, Veterans Affairs Medical Center, Decatur, GA, USA

International Journal of Molecular Sciences, 2023, *24*(5), 4588

Abstract

The SARS-CoV-2 pandemic highlighted the need for broad-spectrum antivirals to increase our preparedness. Patients often require treatment by the time that blocking virus replication is less effective. Therefore, therapy should not only aim to inhibit the virus, but also to suppress pathogenic host responses, e.g. leading to microvascular changes and pulmonary damage. Clinical studies previously linked SARS-CoV-2 infection to pathogenic intussusceptive angiogenesis in the lungs, involving upregulation of angiogenic factors like ANGPTL4. The β-blocker propranolol is used to suppress aberrant ANGPTL4 expression in treatment of hemangiomas. We therefore, investigated the effect of propranolol on SARS-CoV-2 infection and expression of ANGPTL4. SARS-CoV-2 upregulated ANGPTL4 in endothelial and other cells, which could be suppressed with R-propranolol. The compound also inhibited replication of SARS-CoV-2 in Vero-E6 cells and reduced viral load by up to ~2 log in various cell lines and primary human airway epithelial cultures. R-propranolol is as effective as S-propranolol, but lacks the latter's undesired β-blocker activity. R-propranolol also inhibited SARS-CoV and MERS-CoV. It inhibited a post-entry step of the replication cycle, likely via host factors. The broad-spectrum antiviral effect and suppression of factors involved in pathogenic angiogenesis make R-propranolol an interesting molecule to explore further for treatment of coronavirus infections.

Introduction

Severe acute respiratory syndrome coronavirus 2 (SARS-CoV-2) emerged in 2019 and expanded the class of highly pathogenic human coronaviruses, also including SARS-CoV and Middle East respiratory syndrome-CoV (MERS-CoV). Although the lethality of SARS-CoV-2 infection is lower compared to SARS-CoV and MERS-CoV, its transmissibility is much higher, and its fast spread led to an unprecedented pandemic and an enormous burden on health care systems worldwide. The gravity of its associated disease, COVID-19, has called for the fast development of antiviral therapies or the repurposing of existing approved drugs. Although patients are often presenting only mild or even no symptoms, elderly people or those with underlying conditions can experience severe pulmonary damage and acute respiratory distress syndrome (ARDS) that can include endothelial and vascular damage, thromboinflammation, neutrophilic and macrophage dysfunction, immunopathology, and intussusceptive angiogenesis (302). The epithelium-endothelium environment during infection and pathological changes in the lung microvascular system have been investigated in several studies (303-305). Early in the pandemic, morphological changes like

intussusceptive angiogenesis in the lungs of deceased patients were described as distinct features of COVID-19, compared to influenza virus-infected or healthy lungs (306). While formation of new blood vessels is usually a well-regulated process in for example wound healing, unregulated angiogenesis can have negative implications leading to pathogenesis (305). Intussusceptive angiogenesis is a rapid process of blood vessel neoformation that happens due to splitting of an existing vessel into two, as opposed to sprouting angiogenesis. While the implications of vascular changes for response and repair to different lung pathologies are not well understood, it was reported that viral infections can dysregulate these processes by creating a pro-angiogenic environment of inflammation and hypoxia (307, 308). In line with these microvascular changes, transcriptional analysis identified upregulation of angiogenic factors, like *angptl4* and *VEGFA,* to a magnitude that appears unique for COVID-19 (306, 309). Angiogenic dysregulation and therapeutic interventions to control this process have been widely studied in the field of cancer research. One common type of tumor involving dysregulated blood vessel formation is infantile hemangioma. Propranolol, an approved and widely used non-selective β-blocker, is used to treat this condition, as this compound has also been shown to inhibit pro-angiogenic (transcription) factors (310, 311). Propranolol is a mixture of two enantiomers, R- and S-propranolol. Opposed to its S- counterpart, R-propranolol does not exert beta-blocker activity, but was shown to reduce the angiogenic factor ANGPTL4 (more efficiently) in hemangioma stem cells (310). Anti-angiogenic drugs are also used as safe treatment for idiopathic pulmonary fibrosis (312). Bevacizumab, a monoclonal antibody with anti-angiogenic property, is also evaluated in a clinical trial for its efficacy to reduce angiogenesis and vascular damage in COVID-19 patients (313). Therefore, in this study we aimed to investigate the effect of R-propranolol on the expression of angiogenesis factors that are induced by SARS-CoV-2 infection and to study its effect on virus replication. Besides an effect on ANGPTL4 expression, we - surprisingly - also uncovered a potent antiviral effect of Propranolol against a broad spectrum of highly pathogenic coronaviruses.

The emergence of SARS-CoV-2 as the third highly pathogenic coronavirus within 2 decades, shows the importance of developing broad-spectrum antivirals to prepare us for future outbreaks. The repurposing of already approved and safe drugs can present a faster and more efficient way into the clinic when an outbreak calls for a swift response. Our study suggests that the approved drug R-propranolol could function as a 'double-edged sword', inhibiting both virus replication and pathogenic host responses to infection. It might therefore be an interesting drug to explore further in clinical trials.

Results

SARS-CoV-2 infection upregulates angiogenic factor angptl4 in endothelial cells

To investigate whether the lung pathology-associated upregulation of angiogenic factors that was reported in COVID-19 patients, could also be observed in cell culture, we used Hulec-5a human lung endothelial cells as a relevant model for microvascular changes. We monitored expression of *angptl4*, which encodes for the Angiopoietin-like 4 protein and was reported to be upregulated in the lungs of COVID-19 patients (306). Hulec-5a cells could not be infected by SARS-CoV-2, which was also previously reported (303). These cells were also not susceptible to SARS-CoV, but could be infected with MERS-CoV, as indicated by the positive immunofluorescence staining for the viral membrane protein (M) and dsRNA (**Figure 1a**). Since Hulec-5a cells could not be infected with SARS-CoV-2, we used conditioned medium from SARS-CoV-2 infected Calu-3 lung epithelial cells, to mimic the epithelium-endothelium environment during infection. When Hulec-5a cells were incubated with conditioned medium we measured an increase in *angptl4* expression by RT-qPCR, in line with the reported effect of infection on the transcriptional changes in endothelial cells of patients (**Figure 1b**).

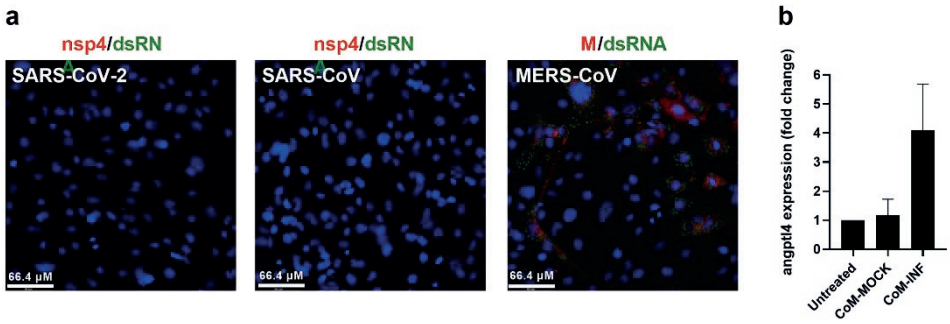

Figure 1: Infection of Hulec-5a lung endothelial cells with various coronaviruses and expression of angiogenic factor angptl4. (a) Hulec-5a cells were infected with SARS-CoV-2, SARS-CoV and MERS-CoV (Multiplicity of infection (MOI) 5) and after 48 h cells were fixed and stained with rabbit polyclonal anti-SARS-CoV nsp4 protein antibody for SARS-CoV-2 and SARS-CoV, rabbit polyclonal anti-MERS-CoV M protein antibody for MERS-CoV, mouse monoclonal anti-dsRNA antibody (J2) and with Hoechst, and visualized by immunofluorescence microscopy. Images are representative for results from 3 independent experiments. (b) Hulec-5a cells were incubated with conditioned medium from infected Calu-3 lung epithelial infected cells (CoM) for 24 h (diluted 1:1 with fresh medium). Intracellular RNA was isolated to quantify *angptl4* expression by RT-qPCR, using PGK1 as reference gene. n=3 independent experiments

R-Propranolol downregulates expression of the angiogenic factor angptl4

Angiogenic factors like ANGPTL4 are also upregulated in infantile hemangiomas and their expression can be suppressed with the drug Propranolol, or more specifically, the stereoisomer R-propranolol. R-propranolol exerts its inhibitory effect on angiogenic factors without having beta-blocker activity (310) and therefore, we aimed to investigate the effect of R-propranolol on the expression of SARS-CoV-2 induced angiogenesis factors. Since Hulec-5a cells were not susceptible to SARS-CoV-2 (**Figure 1**), we tested if *angptl4* expression was also upregulated during infection of Vero E6 cells and whether treatment with R-propranolol would suppress it. Vero E6 cells were treated with 50 µM of R-propranolol and were infected with SARS-CoV-2 at a MOI of 1. Analysis of total intracellular RNA isolated from infected cells at 16 hpi showed a strong increase in *angptl4* expression (**Figure 2a**). When infected cells were treated with R-propranolol, there was a significant reduction in *angptl4* expression, compared to untreated infected cells. Interestingly, when we measured intracellular viral RNA copies in those samples, we observed a 100-fold reduction in viral load in R-propranolol-treated cells compared to the infected untreated cells (**Figure 2b**). To uncouple the direct effect of R-propranolol on *angptl4* expression from its effect on virus replication, we used the chemical inducer phorbol-12-myristate-13-acetate (PMA) to increase *angptl4* expression. In Hulec-5a cells we observed that R-propranolol caused a moderate but significant downregulation of the PMA-induced increase in *angptl4* expression (**Figure 2c**). This suggested that at least part of the effect of R-propranolol on this angiogenic factor is independent from its effect on virus replication.

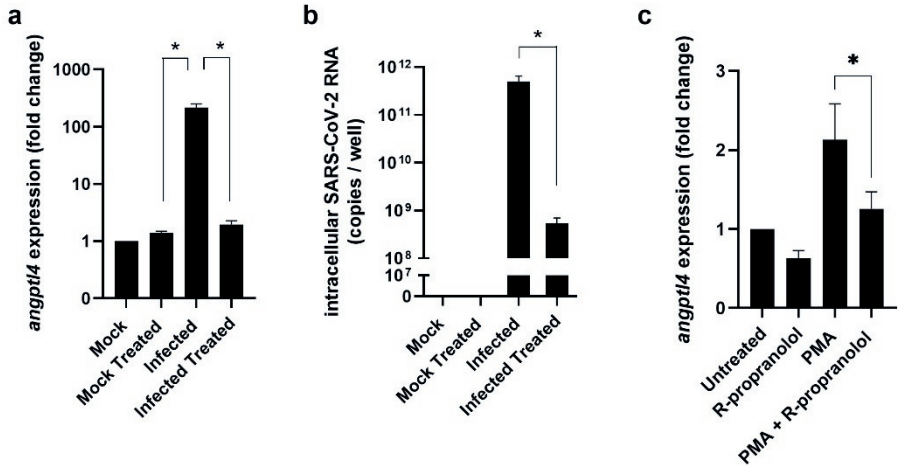

Figure 2: Effect of R-propranolol on the upregulation of *angptl4* by infection or PMA treatment. Vero E6 cells were infected with SARS-CoV-2 (MOI 1) in the absence or presence of 50 µM R-propranolol. (a) the fold increase

in *angptl4* RNA levels compared to untreated uninfected cells (Mock) and (b) intracellular viral RNA copies were quantified by RT-qPCR at 16 hpi. n=2 independent experiments (c) Hulec-5a cells were treated with 0.1 µM PMA and 6 h later 50 µM R-Propranolol was added. 12 h later the increase in *anptl4* expression was quantified by RT-qPCR. n=2 independent experiments. For normalization the levels of reference gene PGK1 were measured by RT-qPCR for all experiments. Data are mean ± SEM. Statistical analysis was conducted using ratio paired t-test and significant differences are indicated by *P<0.05.

R- and S-propranolol inhibit SARS-CoV-2 replication in cell culture

Quantification of intracellular viral RNA in the experiments to study *angptl4* expression suggested that R-propranolol inhibited virus replication. We therefore, assessed the effect of the compound in more detail in various antiviral assays. The marketed drug Propranolol contains a mixture of the stereoisomers S- and R-propranolol. We therefore assessed the effect of both S- and R-propranolol in cytopathic effect (CPE) reduction assays with SARS-CoV-2. Vero E6 cells were infected at a low MOI in the presence of compound, and after 72 h cell viability was measured by MTS assay. R-propranolol protected cells from infection with an IC50 of 12 µM (**Figure 3a**). S-propranolol inhibited SARS-CoV-2 replication with an IC50 of 15 µM (**Figure 3b**). We observed no cytotoxicity in uninfected cells that were treated in parallel with the same increasing concentrations of compounds. Since R-propranolol was slightly more effective than S-propranolol, and is devoid of the undesired beta-blocker activity, we decided to perform all further experiments with R-propranolol.

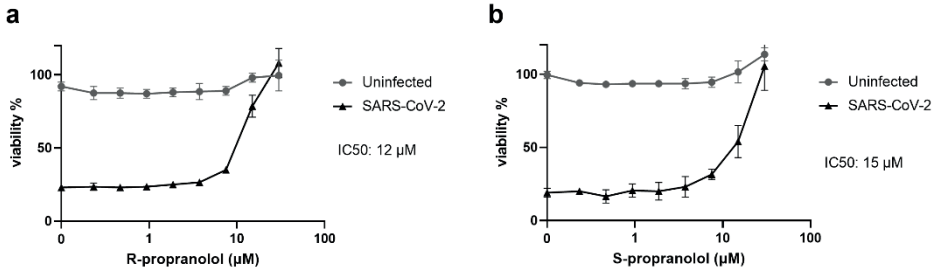

Figure 3: Effect of R-propranolol and S-propranolol on SARS-CoV-2-induced cytopathic effect in Vero E6 cells. CPE reduction assays were done on Vero E6 cells infected with SARS-CoV-2 (MOI of 0.015). Cells were pre-treated with and infected in the presence of (a) R-Propranolol, or (b) S-Propranolol. At 72 hpi cell viability was determined by MTS assay. n=2 independent experiments. Cell viability of uninfected compound-treated cells was measured in parallel to assess cytotoxicity of the compound. Mean ± SEM are shown. The 50% inhibitory concentration (IC50) was determined by non-linear regression with GraphPad Prism 6.

R-propranolol inhibits SARS-CoV-2 replication in various cell lines and air–liquid interface cultured primary human airway epithelial cells

To validate the antiviral effect of R-propranolol that was observed in CPE reduction assays (Fig. 3), we performed viral load reduction assays. Vero E6 cells were pre-treated with compound, infected at a MOI of 1 and at 16 hpi the viral load was determined by quantifying the number of extracellular viral RNA copies by RT-qPCR. In this single replication cycle experiment R-propranolol caused a significant and up to 100-fold reduction in extracellular viral RNA copies (**Figure 4a**), with a 90% effective concentration (EC90) of 20 µM. To assess whether the compound was also able to prevent spread of infection in human lung cells, we infected the human lung epithelial cell line H1299-hACE2 at an MOI of 0.001, treated it with compound and measured viral load after multiple rounds of replication at 48 hpi (**Figure 4b**). In this infection model we also observed a 100-fold reduction in viral load and an EC90 of 26 µM. Measurement of cell viability by MTS assay showed that the compound caused no cytotoxicity at the concentrations used in both cell lines.

To analyze the efficacy of R-propranolol in a more advanced infection model, we used primary bronchial epithelial cells that were cultured at the air-liquid interface (ALI-PBEC). This infection model efficiently recapitulates the pseudostratified epithelium of the lung and its infection by coronaviruses (Thaler et al., manuscript under revision). ALI-PBEC were infected with SARS-CoV-2 (MOI of ~0.1) and treated with 100 µM of R-propranolol on the apical side of the cells during the 2 h inoculation with virus. Infected control cells were treated with PBS instead of compound ("untreated" control). The compound was also added to the medium on the basal side of the cells and remained present until 48 hpi, when samples were harvested. We observed a significant reduction in viral load for R-propranolol treated cells compared to untreated controls (**Figure 4c**). Measurement of cell death (by LDH release) in untreated and treated ALI-PBEC indicated that R-propranolol caused no significant cytotoxicity under these conditions (**Figure 4d**).

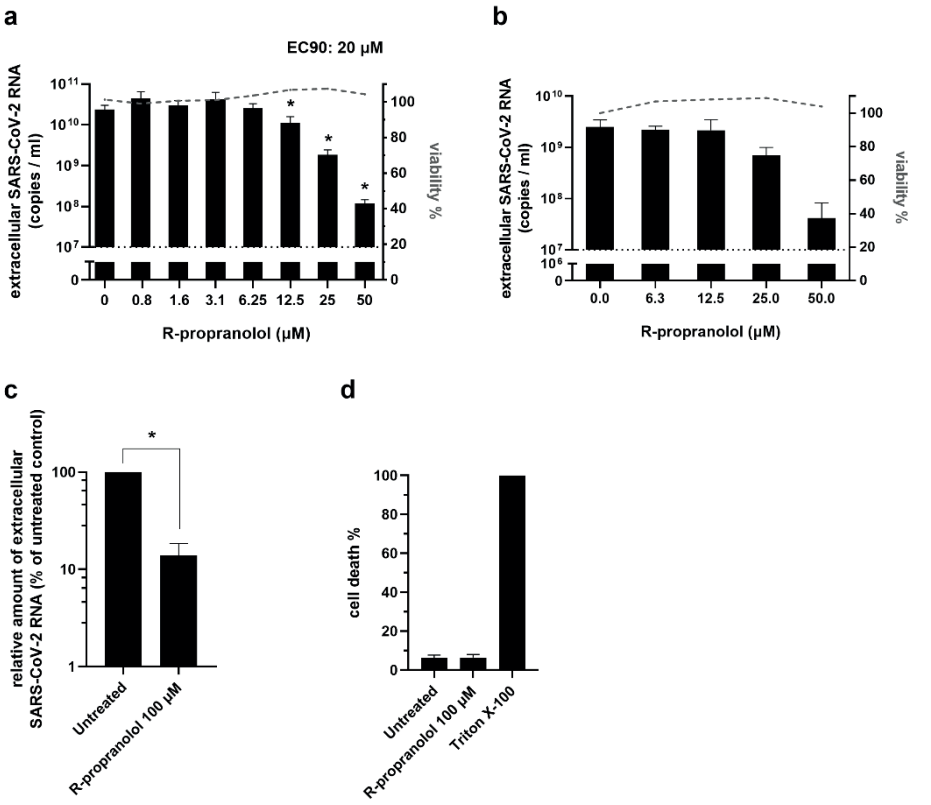

Figure 4: Effect of R-propranolol on replication of SARS-CoV-2 in Vero E6 and H1299-hACE2 cells and primary human bronchial epithelial cell cultures grown at the air-liquid interface (ALI-PBEC). (a) Viral load reduction assay on Vero E6 cells. Cells were infected with a MOI of 1 and at 16 hpi extracellular viral RNA copy numbers were determined by RT-qPCR. n=3 independent experiments. (b) H1299-hACE2 cells were infected at MOI 0.001 and the viral load in the medium at 48 hpi was determined by RT-qPCR. n=2 independent experiments. In parallel, cell viability of uninfected Vero E6 and H1299-hACE2 cells treated with R-propranolol was measured by MTS assay and data were normalized to untreated uninfected cells (% viability). (c) ALI-PBEC were treated with 100 µM R-propranolol and inoculated with SARS-coV-2 for 2 h (MOI ~0.1) in the presence of compound. After removal of the inoculum, the viral load in the apical wash was determined at 48 hpi. R-propranolol remained present in the basal medium until 48 hpi. n=3 independent experiments. Mean ± SEM are shown for all experiments. (d) In ALI-PBEC cytotoxicity was monitored by quantifying the release of LDH and data were normalized to ALI-PBEC treated with Triton X-100 (100 % cell death). n=2 independent experiments. Statistical analysis was conducted using two-way ANOVA with a Tukey/Bonferroni post-hoc test or in (c) with a t-test. Significant differences are indicated by *P<0.05.

R-propranolol inhibits SARS-CoV-2 at a post-entry step of the replication cycle

To elucidate the mode of action of R-propranolol, we first evaluated whether the compound affects the infectivity of viral particles, i.e. has virucidal activity. We therefore incubated SARS-CoV-2 with 50 or 150 µM of the compound for 1 h at 37 °C, before assessing the (remaining) number of infectious particles by plaque assay. Control treatment with 70% ethanol led to complete inactivation of the virus, but R-propranolol had no effect on the infectious titer compared to the untreated virus stock (**Figure 5a**).

To elucidate which step of the viral life cycle is affected by R-propranolol we performed a time-of-addition assay (**Figure 5b**). The strongest reduction in viral load was observed when cells were pretreated and the compound remained present during infection until the time of harvesting. Although less effective, treatment initiated at 2 hpi still reduced viral load, suggesting that the compound does not target attachment/entry of the virus. This was further supported by the observation that pretreatment alone (2 or 4 hours prior to infection) or presence of the compound in the inoculum only during infection (0-1 hpi) did not reduce the viral load. Together these results suggested that R-propranolol inhibited a post entry step of the replication cycle, possibly via its effect on a host factor(s).

To obtain more insight into the mode of action we compared the specific infectivity of treated and untreated samples (**Figure 5c**). Infectious progeny and extracellular genome copies were reduced to the same extent by R-propranolol treatment, suggesting the compound does not affect infectivity of viral genomes (e.g. does not compromise genome integrity) and does not affect the infectivity of released particles. It leads to an overall reduction in the release of infectious particles.

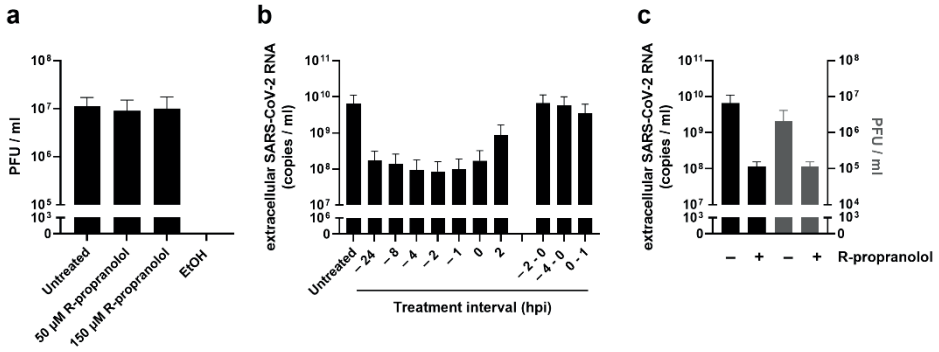

Figure 5: R-propranolol inhibits replication of SARS-CoV-2 at a post-entry step. (a) Effect of the compound on infectivity of SARS-CoV-2. Virus was incubated with either 50 or 150 µM R-propranolol, 70% ethanol, or medium (untreated control) for 1 h at 37 °C. Remaining infectivity was measured by plaque assay. n=3 independent experiments (b) Time of addition assay with Vero E6 cells infected at MOI 1 and R-propranolol treatments during

the intervals indicated at the X-axis or initiated at the time points indicated after which compound remained present until 16 hpi. Supernatant was harvested at 16 h post infection and extracellular viral RNA was measured by RT-qPCR n=2 independent experiments (c) Supernatant of infected Vero E6 cells at 16 hpi, untreated or treated with 50 µM R-propranolol was analyzed by RT-qPCR and plaque assay. Mean ± SEM are shown.

R-propranolol has broad-spectrum antiviral activity against different coronaviruses

We assessed the activity of R-propranolol against various SARS-CoV-2 variants in viral load reduction assays and found that the delta and omicron variants were inhibited by R-propranolol too (Fig 6A). We then evaluated its effect on different highly pathogenic coronaviruses. The compound also inhibited SARS-CoV replication in Vero E6 cells (**Figure 6b**) and MERS-CoV replication in HuH-7 cells (**Figure 6c**), suggesting it has a broad spectrum activity against coronaviruses.

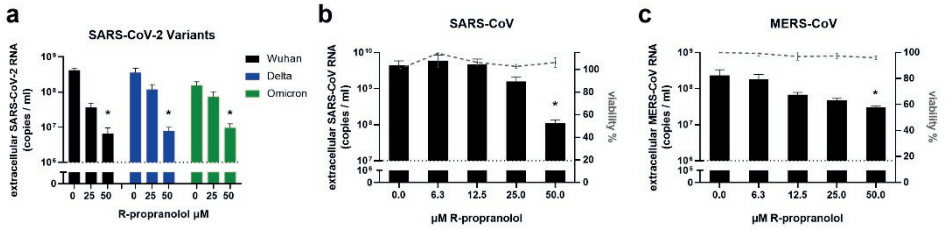

Figure 6: Effect of R-propranolol on replication of SARS-CoV-2 variants, SARS-CoV and MERS-CoV. (a) Viral load reduction assay on Vero E6 cells with SARS-CoV-2 variants. The viral load at 16 hpi was determined by RT-qPCR and cell viability was monitored in parallel. N=2 independent experiments. (b) Viral load reduction assay with SARS-CoV in Vero E6 cells infected at MOI 1. Viral load at 16 hpi was determined by RT-qPCR and cell viability was monitored in parallel. N=3 independent experiments. (c) HuH-7 cells were infected with MERS-CoV (MOI 1) and 16 hpi viral load was determined by RT-qPCR. N=3 independent experiments. Mean ± SEM are shown. Statistical analysis was conducted using two-way ANOVA with a Tukey/Bonferroni post-hoc test. Significant differences are indicated by *P<0.05. Cell viability of uninfected cells treated with compound was determined in parallel using MTS assay and data were normalized to untreated uninfected cells (100 % viability).

Discussion

Despite the unprecedented successes of vaccine development in response to the SARS-CoV-2 pandemic, the demand for safe and effective antiviral drugs reamins. Not only to treat COVID-19 patients but also to better prepare us for future coronavirus outbreaks, as such drugs could be used prophylactically, post-exposure or in outbreak settings when vaccines to new threats are not yet available. Since COVID-19 patients often present with serious

symptoms rather late there is not only a need for drugs that directly inhibit virus replication, but also for therapeutics that target the (pathogenic) host responses to infection. Hallmarks of severe SARS-CoV-2 infection are pulmonary inflammation, tissue damage and microvascular changes in the lung. Pathogenic angiogenesis and upregulation of pro-angiogenic factors like ANGPTL4 have been observed in patients with severe SARS-CoV-2 or influenza virus infections (306). Recently, increased ANGPTL4 plasma levels were associated with higher proportions of ARDS and increased hospital mortality (309). In mice deficient for ANGPTL4, influenza virus infection led to less pulmonary damage (314), suggesting that suppression of the SARS-CoV-2-induced upregulation of ANGPTL4 might be a strategy to counteract the pathogenic angiogenesis that can be caused by SARS-CoV-2 infection. In this study we explored the potential therapeutic effect of R-propranolol on COVID-19 pathophysiology, and uncovered its broad-spectrum antiviral effect against coronaviruses.
The approved drug propranolol is a non-selective β-adrenergic blocker that is mainly used to treat cardiovascular problems. However, it also has a beta-blocker-independent effect on angiogenesis and is therefore used to treat infantile hemangiomas (310). Propranolol consists of the stereoisomers R-propranolol and S-propranolol, of which R-propranolol is devoid of beta blocker activity. R-propranolol was shown to reduce the pro-angiogenic factor ANGPTL4 in a murine hemangioma model, without having beta-blocker activity and thus circumventing potential side effects that could be caused by the beta-blocker activity of S-propranolol. We therefore, also focused our studies on R-propranolol and confirmed the inhibitory effect of this compound on chemically induced *angptl4* expression in lung endothelial cells. Lung endothelial cells were not susceptible to SARS-CoV-2, but treatment of endothelial cells with conditioned medium from SARS-CoV-2-infected epithelial cells caused an increase in *angptl4* expression. This underlines the impact of the epithelium-endothelium crosstalk during infection and the consequences for the microvascular system. *Angptl4* expression was also upregulated in SARS-CoV-2-infected Vero E6 cells and this effect could be suppressed by treatment with R-propranolol. Future studies will need to address the effect of infection and R-propranolol in more advanced (organoid and *in vivo*) models to assess whether the compound could have therapeutic effect on exacerbated angiogenesis.
Besides the effect on expression of virus-induced angiogenic factors, we also observed that R-propranolol inhibits virus replication. Our study for the first time uncovered a direct antiviral effect of R-propranolol that supports previous clinical observations on the apparent (indirect) beneficial effect of propranolol on the outcome of viral infections (315). R-propranolol treatment of infected Vero E6 cells protected them from cytopathic effects with an EC50 of 12 µM, slightly more effective than S-propranolol, which had an EC50 of 15 µM. Treatment of infected cells also led to a significant reduction in extracellular viral RNA

copies with an EC90 of 20 µM and the compound also reduced the viral load by 2 logs in a lung cell line infection model. Finally, we employed primary bronchial epithelial cells cultured at the air-liquid interface as most relevant infection system, as it efficiently reconstitutes the pseudostratified lung epithelium and its infection. In this model R-propranolol also reduced the viral load in the apical wash of the culture without causing any noticeable cytotoxicity.

Furthermore we could show that R-propranolol has broad-spectrum activity against different SARS-CoV-2 variants, including delta and omicron, and it also inhibited other highly pathogenic coronaviruses, i.e. SARS-CoV and MERS-CoV. The compound had no virucidal effect and time of addition assays suggested that it inhibits a post-entry step of the replication cycle. Its broad-spectrum activity and its enhanced activity upon pretreatment suggest that R-propranolol likely inhibits viral replication via one or more host factors. These likely play no role in the attachment or entry of the viral particle, since there was no reduction in viral load when the compound was present only during infection (in the inoculum). R-propranolol reduced the amount of infectious progeny that was released from cells, but did not appear to affect the specific infectivity, suggesting it does not affect infectivity of particles or integrity of the genome (e.g. does not lead to mutations or defects in capping). While we were preparing this manuscript, a preprint was published on the effect of R-propranolol on SARS-CoV-2 and MHV replication, including the observation of an inhibitory effect on MHV replication in a mouse model (316). The findings of this study were in line with our data and the compound was suggested to affect replication complex formation through an effect on phospholipid synthesis, which corroborates our results (in time of addition assays). Previous studies on propranolol-induced changes in gene expression in endothelial cells also included genes involved in lipid and sterol metabolism and ubiquitination (317). Propranolol also has an effect on various other host factors and signalling pathways, including inhibition of the RAS/RAF/ERK and AKT pathways (318, 319). Inhibition of factors involved in these signalling pathways was also shown to affect SARS-CoV-2 replication (320). Therefore, to unravel the compound's mode of action, more in-depth research is required to elucidate which host factor(s) or pathway(s) contribute to the R-propranolol-mediated inhibition of coronavirus replication.

It is also important to keep in mind that most of the studies on the activity of propranolol or its separate stereoisomers have been done in the context of cancer research. Therefore, these findings might not be directly translatable to non-cancer models and need to be investigated in proper infection models. Widespread use of Propranolol renders it a safe and interesting drug to be investigated further, and the use of the enantiomer R-propranolol which has no beta-blocker activity lowers the risk of possible negative side-effects. Its inhibition of virus replication and suppression of detrimental host responses to

infection make R-propranolol an interesting compound for further evaluation in clinical studies.

Materials and Methods

Compounds and Cell Culture

R-(+)-Propranolol hydrochloride, S-(+)-Propranolol hydrochloride and phorbol-12-myristate-13-acetate (PMA) were purchased from MedChemExpress and dissolved in DMSO.

Vero E6 cells and HuH-7 cells were cultured as previously described (321). Human lung cell line H1299-hACE2 will be described elsewhere (Salgado-Benvindo et al, manuscript in preparation). These cells were cultured in Dulbecco's modified Eagle's medium with 4.5 g/l glucose with L-glutamin (DMEM; Lonza, Switzerland), supplemented with 10% fetal calf serum (FCS)(CapriCorn Scientific, USA), 100 U/ml of Penicillin/Streptomycin (P/S) (Sigma-Aldrich) and 1200 µg/ml G418 for selection (InvivoGen). Calu-3 cells (ATCC, HTB-55TM) were cultured in Eagle's minimum essential medium (EMEM, Lonza), supplemented with 9% FCS, 1% non-essential amino acids (NEAA, Sigma-Aldrich), 2 mM L-glutamine (Sigma-Aldrich), 1 mM sodium pyruvate (Sigma-Aldrich) and 100 U/ml of P/S.

Infections of Vero E6 cells, HuH-7 cells, H1299-hACE2 cells and Calu-3 cells were performed in Eagle's minimal essential medium with 25 mM HEPES (EMEM; Lonza) supplemented with 2% FCS, 2mM L-glutamine (Sigma-Aldrich), and 100 U/ml of P/S (referred to as infection medium).

Primary human bronchial epithelial cells (PBEC) were isolated and cultured as previously described (322). Hulec-5a cells were purchased from ATCC and cultured and infected in EGM™-2 MV Microvascular Endothelial Cell Growth Medium-2 BulletKit™. Hulec-5a cells were used between passage 2 and 6. Infections of Hulec-5a cells were done in culture medium, treatment with PMA was done in infection medium.

All cell cultures were maintained at 37 °C in an atmosphere of 5% CO_2.

Virus stocks

All experiments with infectious SARS-CoV, SARS-CoV-2 or MERS-CoV were performed at the LUMC biosafety level 3 facilities. For Vero E6 infections the clinical isolate SARS-CoV-2/Leiden-0002 (isolated at LUMC during the first wave of the Corona pandemic in March 2020 (GenBank: MT510999.1) was used. For H1299-hACE2 and ALI-PBEC infections SARS-CoV-2/Leiden-0008 (isolated at LUMC during the first wave of the Corona pandemic in

March 2020 (GenBank: MT705206.1) was used, as it was not adapted to Vero E6 cells with regard to the spike S1/S2 cleavage site (confirmed by NGS sequencing). SARS-CoV-2 variant BA.1 (Omicron) was obtained from RIVM (strain hCoV-19/Netherlands/NH-RIVM-72291/2021, lineage B.1.1.529), and variant B.1.617 (Delta) was obtained from the University of Leuven. SARS-CoV-2/Leiden-0002 (Passage 3), SARS-CoV-2/Leiden-0008 (Passage 2), SARS-CoV isolate Frankfurt 1 (298) (Passage 4), Omicron (Passage 3) and Delta (Passage 4) variant were grown in Vero E6 cells. MERS-CoV (N3/Jordan) (GenBank: KJ614529.1) (Passage 3) was grown on HuH-7 cells. Virus titers were determined by plaque assay on Vero E6 cells, and for MERS-CoV and on HuH-7 cells, as described before (255).

Endothelial cell infection

Hulec-5a cells were seeded on glass coverslips at a density of $8*10^4$ cells/well in a 12-well plate and infected with SARS-CoV, SARS-CoV-2 or MERS-CoV at a MOI of 5 in 500 µl medium per well. 48 h later cells were fixed and processed as previously described (122). Cells were stained with rabbit polyclonal anti-SARS-CoV nsp4 protein antibody (FGQ4) for SARS-CoV-2 and SARS-CoV, rabbit polyclonal anti-MERS-CoV M protein antibody (R9004) for MERS-CoV and with mouse monoclonal anti-dsRNA antibody (J2). Secondary antibodies used were a Cy3-conjugated donkey anti-rabbit IgG antibody (Jackson ImmunoResearch Laboratories) and an Alexa488-conjugated goat anti-mouse IgG antibody (Invitrogen).

Endothelial cell (drug) treatments

Hulec-5a cells were incubated with conditioned medium from Calu-3 lung epithelial cells (CoM) for 24 h (diluted 1:2 with fresh medium). Intracellular RNA was isolated to quantify *angptl4* expression by RT-qPCR. For CoM, Calu-3 cells were seeded at a density of $2.4*10^5$ cell/well in 6-well plates and infected with SARS-CoV-2 (Leiden-008) at a MOI of 1 for 2 h at 37°C on a rocking platform. The inoculum was removed, cells were washed with PBS three times and 500 µl infection medium was added. At 48 hpi medium was harvested and stored at -80°C.

For treatment with PMA, Hulec-5a cells were seeded at a density of $7*10^3$ cells/well in a 96-well plate. After 24 h medium was changed to infection medium. After 16 h, cells were treated with 100 nM PMA for 6 h. Then R-propranolol was added and cells were incubated for 12 h. Control wells were treated with only PMA, R-propranolol or medium (untreated). Then intracellular RNA was harvested and *angptl4* expression was quantified by RT-qPCR.

Cytopathic effect (CPE) reduction assay

CPE reduction assay was performed as previously described (234). Briefly, Vero E6 cells were seeded in 96-well plates at a density of $5*10^3$ cells per well. The next day, cells were incubated with 2-fold serial dilutions of R- or S-propranolol starting at 50 µM and subsequently infected. 3 days post infection the CellTiter 96 aqueous nonradioactive cell proliferation kit (Promega) was used to measure cell viability of infected (protection) and non-infected cells (assessment of cytotoxicity).

Viral load reduction assays

Viral load reduction assays were performed as previously described (234). Briefly Vero E6 cells were infected with SARS-CoV-2, SARS-CoV-2 variants or SARS-CoV, and HuH-7 cells were infected with MERS-CoV, at a MOI of 1. Pretreatment with R-propranolol was done for 4 h. Alternatively (Figure 2) Vero E6 cells were seeded at a density of $7*10^4$ cells/well in 24-well plates. Cells were pretreated 2 h with 50 µM R-propranolol and infected with SARS-CoV-2 at a MOI of 1. At 16 hpi total intracellular RNA was harvested and viral RNA copies (intracellular & extracellular) and *angptl4* expression were quantified by multiplex RT-qPCR, using PGK1 as reference gene.

Time of Addition Assay

Vero E6 cells were seeded in 24-well cell culture plates at a density of $2*10^4$ cells/well. Cells were incubated with 50 µM of R-Propranolol in 500 µl infection medium at the indicated timepoints. 48h after seeding, cells were infected with $8*10^4$ PFU of virus per well (MOI 1) in 200 µl of medium. Supernatant was harvested at 16 hpi and extracellular viral RNA copies were measured by RT-qPCR (255).

Virucidal effect assay

Vero E6 cells were seeded in 6-well cell culture plates at a density of $3.5*10^5$ cells/well. The next day, virus ($3*10^5$ PFU) was incubated, in a total of 60 µl, at 37 °C with 50 or 150 µM compound, only medium or ethanol (66% end concentration). After incubation for 1 h, 50 µl samples were serially diluted to lower the compound and ethanol concentration to a level that did not inhibit the subsequent plaque assay to determine the remaining infectious virus titer (255).

Viral infection of ALI-PBEC

The apical side of the cells was washed with 200 µl warm PBS for 10 min at 37 °C to remove excess mucus and cellular debris and basal medium was refreshed prior to infection. Cells were infected with 100,000 PFU of SARS-CoV-2 in 200 µl PBS (with or without compound) per insert for 2 h at 37 °C on a rocking platform (estimated multiplicity of infection [MOI] of 0.1). For noninfected (mock) controls the same procedure was performed with only PBS. After removal of the inoculum, the apical side of the cells was washed three times with PBS. At 48 hpi, 200 µl of PBS was added to the apical side of the cells and after incubation for 10 min at 37 °C, supernatant was harvested to quantify the viral load by RT-qPCR.

RNA isolation and RT-qPCR

RNA was isolated either using Tripure isolation reagent (Sigma-Aldrich) or by magnetic bead isolation. Briefly, 20 µl of SpeedBeads™ carboxylate-modified magnetic particles (Merck) and 135 µl of isopropanol were added to 100 µl of supernatant in a 96-well plate. The plate was placed on a magnetic rack for 15 min, then supernatant was removed, and beads were washed one time with 150 µl of isopropanol and then two times with 200 µl of 70% ethanol. The beads were air-dried and, after removal of the plate from the magnetic rack, resuspended in 50 µl RNAse free water for 3 min. The plate was placed back on the magnetic rack for 10 min to collect the eluate containing total RNA. Equine arteritis virus (EAV) RNA in AVL lysis buffer (Qiagen) was spiked into the reagent as an internal control for extracellular RNA samples. The cellular reference gene PGK1 served as a control for intracellular RNA. Primers and probes for EAV and PGK1 and the normalization procedure were described before (255). Viral RNA was quantified by RT-qPCR using TaqMan Fast Virus 1-step master mix (Thermo Fisher Scientific) and as previously described (234). Primers and probes for SARS-CoV-2 and SARS-CoV, as well as a standard curve, were used as described previously (234, 256), and for MERS-CoV with final primer concentrations of 450 nM each and probe concentrations of 200 nM. Angptl4 was quantified using the ANGPTL4 TaqMan® Gene Expression Assay FAM-MGB (ThermoFisher, Catalog No. 4331182, ID Hs01101123_g1).

Author Contributions

Conceptualization, M.T., M.vH., J.A.; methodology, M.T., M.vH.; investigation, M.T. C.S.B, A.L, A.T; resources, D.N, J.A; writing—original draft preparation, M.T, M.vH.; writing—review and editing, M.T, J.A., E.S., M.vH.; visualization, M.T; supervision, E.S., M.vH; project

administration, M.vH.; funding acquisition, M.vH.. All authors have read and agreed to the published version of the manuscript.

Funding

Clarisse Salgado-Benvindo was supported by the Coordination for the Improvement of Higher Education Personnel (CAPES) (Process nr. 88881.171440/2018-01), Ministry of Education, Brazil.

Institutional Review Board Statement: Not applicable

Informed Consent Statement

Informed consent was obtained from all subjects involved in the study. Primary bronchial epithelial cells were isolated from macroscopically normal lung tissue obtained from patients undergoing resection surgery for lung cancer at the Leiden University Medical Center, the Netherlands. Patients from which this lung tissue was derived were enrolled in the biobank via a no-objection system for coded anonymous further use of such tissue (www.coreon.org). However, since 29-11-2020, patients are enrolled in the biobank using active informed consent in accordance with local regulations from the LUMC biobank with approval by the institutional medical ethical committee (B20.042/Ab/ab and B20.042/Kb/kb).

Data Availability Statement

Data is contained within the article

Acknowledgments

We thank Dr. Anne van der Does[2] for advice and help with handling the Hulec-5a cells.

Conflicts of Interest

The authors declare no conflict of interest. The funders had no role in the design of the study; in the collection, analyses, or interpretation of data; in the writing of the manuscript; or in the decision to publish the results.

References

1. Bösmüller H, Matter M, Fend F, Tzankov A. The pulmonary pathology of COVID-19. Virchows Archiv : an international journal of pathology. 2021 Jan;478(1):137-50.
2. Wang P, Luo R, Zhang M, Wang Y, Song T, Tao T, et al. A cross-talk between epithelium and endothelium mediates human alveolar–capillary injury during SARS-CoV-2 infection. Cell Death & Disease. 2020 2020/12/08;11(12):1042.
3. Bordoni V, Mariotti D, Matusali G, Colavita F, Cimini E, Ippolito G, et al. SARS-CoV-2 Infection of Airway Epithelium Triggers Pulmonary Endothelial Cell Activation and Senescence Associated with Type I IFN Production. Cells. 2022 Sep 17;11(18).
4. Solimando AG, Marziliano D, Ribatti D. SARS-CoV-2 and Endothelial Cells: Vascular Changes, Intussusceptive Microvascular Growth and Novel Therapeutic Windows. 2022; Biomedicines 10(9):2242.
5. Ackermann M, Verleden SE, Kuehnel M, Haverich A, Welte T, Laenger F, et al. Pulmonary Vascular Endothelialitis, Thrombosis, and Angiogenesis in Covid-19. 2020; N Engl J. Med 383(2):120-28.
6. Caposio P, Orloff SL, Streblow DN. The role of cytomegalovirus in angiogenesis. Virus Res. 2011 May;157(2):204-11.
7. Hassan M, Selimovic D, El-Khattouti A, Soell M, Ghozlan H, Haikel Y, et al. Hepatitis C virus-mediated angiogenesis: molecular mechanisms and therapeutic strategies. World journal of gastroenterology. 2014 Nov 14;20(42):15467-75.
8. Bhatraju PK, Morrell ED, Stanaway IB, Sathe NA, Srivastava A, Postelnicu R, et al. Angiopoietin-Like4 Is a Novel Marker of COVID-19 Severity. 2023. Critical care explorations. Jan;5(1):e0827.
9. Zhang L, Mai HM, Zheng J, Zheng JW, Wang YA, Qin ZP, et al. Propranolol inhibits angiogenesis via down-regulating the expression of vascular endothelial growth factor in hemangioma derived stem cell. International journal of clinical and experimental pathology. 2014;7(1):48-55.
10. Sasaki M, North PE, Elsey J, Bubley J, Rao S, Jung Y, et al. Propranolol exhibits activity against hemangiomas independent of beta blockade. NPJ Precis Oncol. 2019;3:27-27.
11. Varone F, Sgalla G, Iovene B, Bruni T, Richeldi L. Nintedanib for the treatment of idiopathic pulmonary fibrosis. Expert Opinion on Pharmacotherapy. 2018 2018/01/22;19(2):167-75.
12. Pang J, Xu F, Aondio G, Li Y, Fumagalli A, Lu M, et al. Efficacy and tolerability of bevacizumab in patients with severe Covid-19. Nat Commun. 2021 Feb 5;12(1):814.
13. Li L, Chong Han C, Ng Say Y, Kwok Ka W, Teo Z, Tan Eddie Han P, et al. Angiopoietin-like 4 Increases Pulmonary Tissue Leakiness and Damage during Influenza Pneumonia. Cell Reports. 2015 2015/02/10/;10(5):654-63.
14. Peuschel KE. Some clinical evidence of the hypothesis of an indirect antiviral effect of propranolol through immunoactivation. Med Hypotheses. 2011 2011/05/01/;76(5):689-91.
15. Fang H, Wang Y, Liu L, Cheng K, Li P, Tan Y, et al. A Host-Harbored Metabolic Susceptibility of Coronavirus Enables Broad-Spectrum Targeting. Preprint bioRxiv. 2022:2022.12.07.519404.

16. Stiles J, Amaya C, Pham R, Rowntree RK, Lacaze M, Mulne A, et al. Propranolol treatment of infantile hemangioma endothelial cells: A molecular analysis. Exp Ther Med. 2012 2012/10/01;4(4):594-604.
17. Zhou C, Chen X, Zeng W, Peng C, Huang G, Li X, et al. Propranolol induced G0/G1/S phase arrest and apoptosis in melanoma cells via AKT/MAPK pathway. Oncotarget. 2016 Oct 18;7(42):68314-27.
18. Hu Q, Liao P, Li W, Hu J, Chen C, Zhang Y, et al. Clinical Use of Propranolol Reduces Biomarkers of Proliferation in Gastric Cancer. Frontiers in oncology. 2021;11:628613.
19. Klann K, Bojkova D, Tascher G, Ciesek S, Münch C, Cinatl J. Growth factor receptor signaling inhibition prevents SARS-CoV-2 replication. Molecular Cell. 2020 2020/08/11/.
20. Salgado-Benvindo C, Leijs AA, Thaler M, Tas A, Arbiser JL, Snijder EJ, et al. Honokiol inhibits SARS-CoV-2 replication in cell culture. 2023 Microbiol Spectr.
21. Wang Y, Thaler M, Ninaber DK, van der Does AM, Ogando NS, Beckert H, et al. Impact of human airway epithelial cellular composition on SARS-CoV-2 infection biology. 2023 J. Innate Immun
22. Drosten C, Günther S, Preiser W, Van Der Werf S, Brodt H-R, Becker S, et al. Identification of a novel coronavirus in patients with severe acute respiratory syndrome. New England journal of medicine. 2003;348(20):1967-76.
23. Kovacikova K, Morren BM, Tas A, Albulescu IC, van Rijswijk R, Jarhad DB, et al. 6'-β-Fluoro-Homoaristeromycin and 6'-Fluoro-Homoneplanocin A Are Potent Inhibitors of Chikungunya Virus Replication through Their Direct Effect on Viral Nonstructural Protein 1. Antimicrob Agents Chemother. 2020 Mar 24;64(4).
24. Ogando NS, Dalebout TJ, Zevenhoven-Dobbe JC, Limpens R, van der Meer Y, Caly L, et al. SARS-coronavirus-2 replication in Vero E6 cells: replication kinetics, rapid adaptation and cytopathology. The Journal of general virology. 2020 Sep;101(9):925-40.
25. Salgado-Benvindo C, Thaler M, Tas A, Ogando NS, Bredenbeek PJ, Ninaber DK, et al. Suramin Inhibits SARS-CoV-2 Infection in Cell Culture by Interfering with Early Steps of the Replication Cycle. Antimicrob Agents Chemother. 2020 Jul 22;64(8).
26. Corman VM, Landt O, Kaiser M, Molenkamp R, Meijer A, Chu DK, et al. Detection of 2019 novel coronavirus (2019-nCoV) by real-time RT-PCR. Euro Surveill. 2020 Jan;25(3).

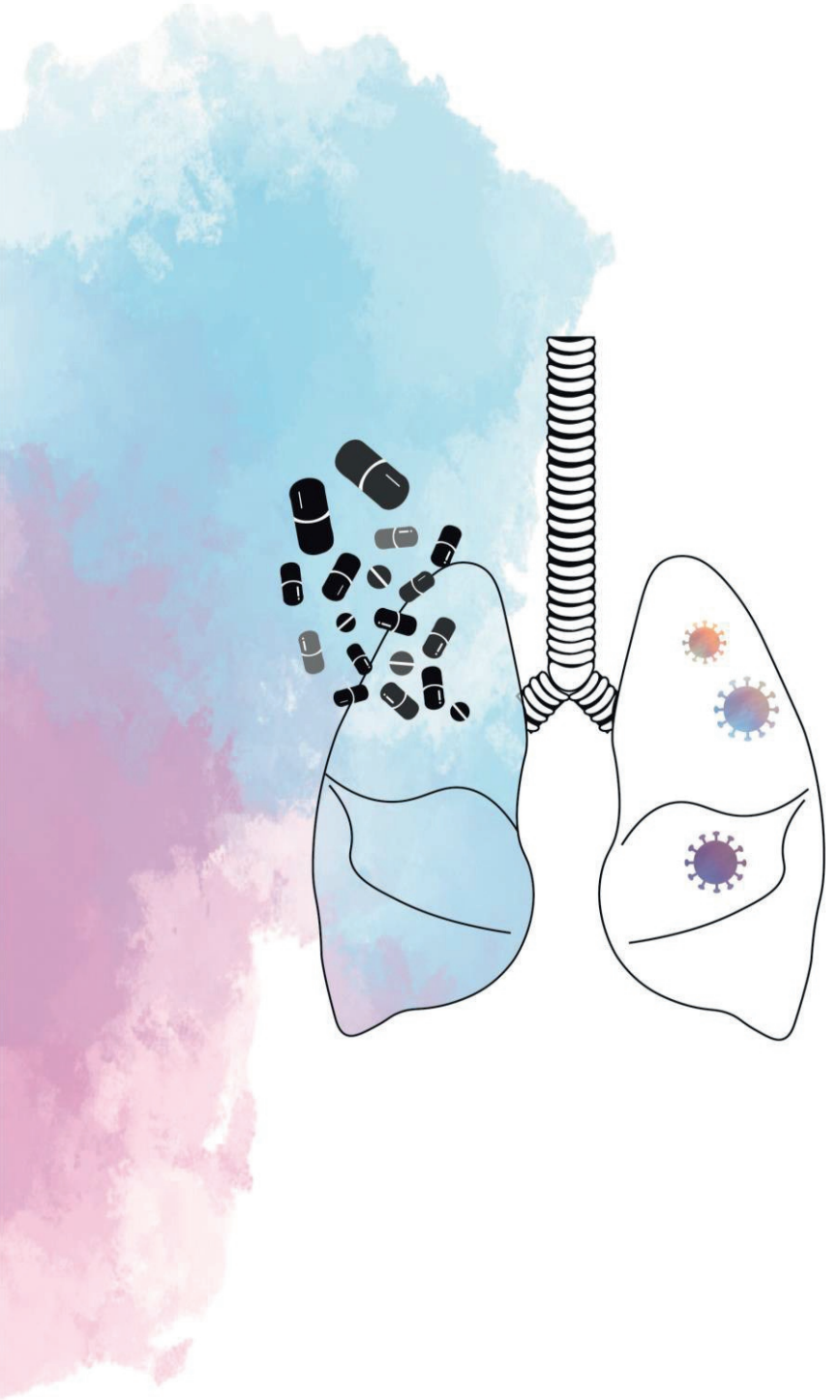

Chapter 5

Epi-cyclophellitol cyclosulfate, a mechanism-based ER α-glucosidase II inhibitor, blocks replication of SARS-CoV-2 and other coronaviruses

Melissa Thaler[1], Tim P. Ofman[2], Ken Kok[2], Jurriaan Heming[2], Elisha Moran[3], Anouk A. Leijs[1], Rian M. C. H. van den Nieuwendijk[2], Richard J. B. H. N. van den Berg[2], Gijs Ruijgrok[2], Zach Armstrong[2], Clarisse Salgado-Benvindo[1], Dennis K. Ninaber[4], Eric J. Snijder[1], Constant A. A. van Boeckel[2], Marta Artola[2], Gideon J. Davies[3], Herman S. Overkleeft[2#], Martijn J. van Hemert[1#]

[1] Leiden University Center for Infectious Diseases (LUCID), Leiden University Medical Center, Leiden, The Netherlands.
[2] Leiden Institute of Chemistry, Leiden University, Leiden, The Netherlands.
[3] Department of Chemistry, University of York, YO10 5DD, York, United Kingdom.
[4] Department of Pulmonology, Leiden University Medical Center, Leiden, The Netherlands.

# These authors share senior authorship

Running Head: Mechanism-based ER α-Glu-II inhibitor blocks coronavirus infection

Under review at Journal ACS Central Science (2024)

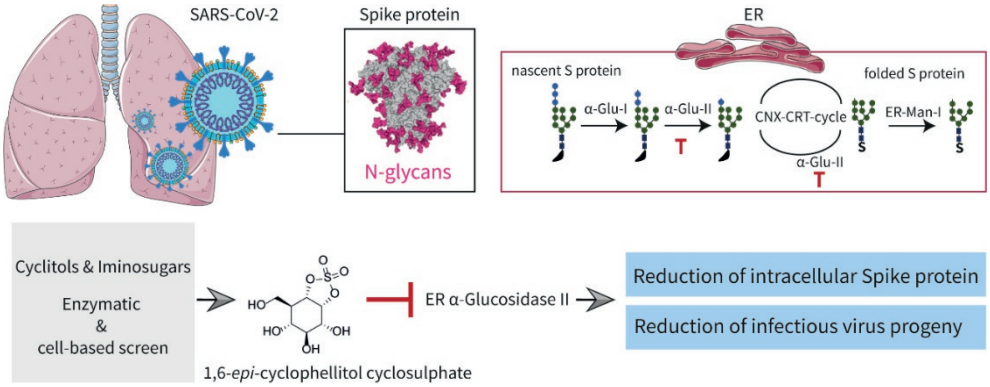

Graphical Abstract: The Figure was partly generated using Servier Medical Art, provided by Servier, licensed under a Creative Commons Attribution 3.0 unported license.

Abstract

The combined inhibition of ER α-glucosidases I and II has been shown to inhibit replication of a broad range of viruses that rely on ER protein quality control. We found, by screening a panel of deoxynojirimycin and cyclitol glycomimetics, that the mechanism-based ER α-glucosidase II inhibitor, 1,6-*epi*-cyclophellitol cyclosulfate, potently blocks SARS-CoV-2 replication in lung epithelial cells, halting intracellular generation of mature Spike protein, reducing production of infectious progeny, and leading to reduced syncytium formation. Through activity-based protein profiling, we confirmed ER α-glucosidase II inhibition in primary airway epithelial cells, grown at the air-liquid interface. 1,6-*Epi*-cyclophellitol cyclosulfate inhibits early pandemic and more recent SARS-CoV-2 variants, as well as SARS-CoV and MERS-CoV. The reported antiviral activity is comparable to the best-in-class described glucosidase inhibitors, all competitive inhibitors also targeting ER α-glucosidase I and other glycoprocessing enzymes not involved in ER protein quality control. We propose selective blocking ER-resident α-glucosidase II in a covalent and irreversible manner as a new strategy in the search for effective antiviral agents targeting SARS-CoV-2 and other viruses that rely on ER protein quality control.

Keywords: glycomimetics, ER-resident α-glucosidase-II, SARS-CoV-2, Spike glycosylation, antiviral, carbohydrate-active enzymes

Introduction

Coronaviruses, like many other virus groups, use the host machinery for co- and post-translational formation and processing of N-linked glycans. N-linked oligosaccharides are crucial for proper protein folding, stability and functioning of many proteins that are part of viral envelopes (323). In the endoplasmic reticulum (ER), α-glucosidases I and II (α-Glu I and α-Glu II) are responsible for trimming the terminal glucose moieties of nascent N-glycans (**Figure 1a**), and the resultant mono-glucosylated N-glycans are subsequently recognized by the ER chaperones calnexin and calreticulin (CNX-CRT cycle) (324, 325), which prevent protein aggregation and assist in polypeptide folding. When a protein fails to fold correctly, glycoprotein glycosyltransferase (UGGT) reconstructs the mono-glucosylated G1M9 N-glycan, enabling another round of refolding attempts facilitated by the CNX-CRT chaperones. Upon proper folding of the protein, the final glucose residue in high mannose-type N-glycans is removed by α-Glu II, leading to further trimming by ER α-mannosidase I (ERMI), after which the N-glycoproteins are routed to the Golgi apparatus for N-glycan maturation and further post-translational modification events en route to their final destination. Glycoproteins that fail to attain their proper conformation undergo mannose trimming orchestrated by the ER degradation-enhancing mannosidase-like proteins (EDEMs) and ultimately are routed toward the ER-associated degradation (ERAD) machinery. Inhibition of ER α-Glu I and II has been shown to interfere with proper processing of nascent proteins through the CNX-CRT cycle, leading to their inappropriate folding, eventual dislocation from the ER and proteasomal degradation (326). This holds true for host and viral N-glycoproteins alike and ER α-Glu I/II inhibition has therefore been considered as a viable strategy for antiviral therapeutics development for several decades (327, 328). Many studies have reported the ability of iminosugars to inhibit replication of various viruses, through the blocking of ER protein quality control via ER α-Glu I/II inhibition (329). Iminosugars are polyhydroxylated glycomimetic alkaloids featuring a basic amine, replacing the sugar ring oxygen, that is thought to interact with glycosidase active site residues that partake in enzymatic glycosidic bond hydrolysis (330, 331). The potential of iminosugars as antivirals was first reported in 1987 (327, 332, 333) in the context of Human Immunodeficiency Virus (HIV), which relies on the host ER machinery for glycoprotein processing (334). These studies revealed that the two iminosugar compounds, deoxynojirimycin and castanospermine, as well as some structural analogues thereof, inhibit ER α-Glu I and II and block the production of HIV infectious progeny *in vitro*. Later studies using a host of structurally diverse iminosugars described blocking replication of a broad range of viruses *in vitro* and *in vivo*, including influenza viruses (335-337), severe acute respiratory syndrome coronavirus (SARS-CoV) (338), dengue virus and the

hemorrhagic fever viruses Marburg and Ebola (339, 340). Interestingly, patients that have N-glycosylation defects due to a congenital disorder, have also reduced susceptibility to infection with enveloped viruses that depend on host glycan processing for their replication (341). Despite promising *in vitro* studies, phase II clinical trials with the iminosugar Celgosivir (a prodrug form of castanospermine) showed no beneficial outcomes when it was used as mono therapy for dengue and hepatitis C virus infections (342, 343). Most recently, a range of competitive α-glucosidase inhibitors have been studied during the search for antivirals against SARS-CoV-2 (344-346). The spike (S) protein of SARS-CoV-2, one of the envelope proteins on the virus surface, is heavily glycosylated with 23 reported N-glycan sites (58). Besides shielding of antibody epitopes (347), and modulating protein structure, N-glycosylation of S protein and its receptor binding domain (RBD) is crucial for virus infectivity, as the S protein drives virus entry by binding to the host receptor ACE2 and mediates fusion between the virus and host cell membrane (23). N-glycans and their modulation through deletion of specific sites on the RBD were reported to be important for conformational stability and accessibility of the RBD for ACE2 binding (59, 348-350). Therefore, the incorporation of non-functional immaturely glycosylated S proteins can reduce the specific infectivity of progeny virions (60, 338). Disruption of the CNX-CRT-mediated glycoprotein processing, by iminosugars specifically, was reported to reduce the incorporation of S protein into SARS-CoV pseudovirus particles (338). In this study, it was suggested that ER α-Glu I/II inhibition could lead to both the degradation of improperly processed S proteins in the ER as well as the incorporation of incompletely glycosylated S proteins into virus particles, thus having a two-pronged mode of action.

Despite the decades of research on iminosugars, no small molecules inhibiting ER α-Glu have proceeded beyond phase II clinical trials (351, 352) as antivirals. With the aim of uncovering alternative inhibitor designs for antiviral drug discovery, and building upon our recent studies on mechanism-based, covalent and irreversible glycosidase inhibition (353-358), we decided to assess a panel of mechanism-based inhibitors, side by side with a set of classical *N*-alkyl iminosugars, for their ability to inhibit SARS-CoV-2 replication through inhibition of ER α-Glu I and II. While performing the same net transformation (hydrolysis of α-glucosidic linkages), ER α-Glu I and II do so with distinct mechanisms. Both enzymes feature a carboxylic acid and a carboxylate containing amino acid in their active site and process their substrate by acid catalysis (330, 331). Both enzymes are therefore amenable to inhibition by a basic, glucose-mimetic iminosugar. In contrast to ER α-Glu I, ER α-Glu II forms a covalent intermediate with its substrate during processing by utilizing one of the carboxylates as nucleophile. This nucleophile can be trapped by glucomimetic cyclitols endowed with an electrophile (epoxide, aziridine or cyclic sulfate). We have shown in the past that 1,6-*epi*-cyclophellitol (**9**, **Figure 1**) as well as its aziridine (**10**) and cyclic sulfate (**11**)

analogues potently and selectively block ER α-Glu II (353). In this study, we screened members of both compound classes, cyclitols and iminosugars, for their inhibition of ER α-Glu II and antiviral activity against SARS-CoV-2. We demonstrate that 1,6-*epi*-cyclophellitol cyclosulfate (**11**) most potently reduces the enzyme activity of α-Glu II, and exerts the best antiviral efficacy against SARS-CoV-2. We also show that this compound blocks replication of all SARS-CoV-2 variants tested, as well as the pathogenic SARS-CoV and MERS-CoV, making it an interesting lead for further exploration towards a new class of antiviral drugs.

Results

Efficacy of glucosidase inhibitors against SARS-CoV-2 correlates with their activity against ER α-glucosidase II

The panel of iminosugars and cyclitols, subject of the here-presented studies, is depicted in **Figure 1b**. With respect to the iminosugars, and to keep in line with literature precedents, we selected *N*-alkyl deoxynojirimycins **1**-**8**. Deoxynojirimycin (DNJ) features the glucopyranose configuration and *N*-alkyl derivatives have been shown to be more effective glucosidase inhibitors compared to non-substituted DNJ (359-361). This includes the benchmark analogue, *N*-butyl-DNJ **1** (Miglustat, Zavesca) which is part of almost all antiviral studies on iminosugars targeting a-Glu I/II. In fact, Miglustat is a clinical drug for the treatment of Gaucher disease and acts as a glucosylceramidase (GCS) inhibitor (362). It also inhibits the human retaining b-glucosidases, GBA1, GBA2 and GBA3, displaying a rather broad activity profile across various glycoprocessing enzymes not involved in ER protein quality control. Besides Miglustat **1**, we included DNJ derivatives **2**-**8** to assess the influence of the hydrophobic *N*-alkyl substituent on antiviral activity. Compound **8** has the L-*ido*-configuration and comprises the C6-epimer (glucopyranose numbering) of DNJ derivative **5**. Compared to **5**, L-*ido*-DNJ **8** is a much weaker ER a-Glu inhibitor, which should be reflected in its antiviral potency. With respect to the cyclitols, we previously published 1,6-*epi*-cyclophellitol **9**, 1,6-*epi*-cyclophellitol aziridine **10** and 1,6-*epi*-cyclophellitol cyclosulfate **11** as potent and selective, mechanism-based, covalent and irreversible retaining a-glucosidase inhibitors (353, 363). Besides inhibiting ER a-Glu II, the single detected off-target (in the context of pharmacological ER protein quality control interference) is the lysosomal a-glucosidase, human acid α-glucosidase GAA. These 1,6-*epi*-cyclophellitol analogues were designed to inhibit retaining a-glucosidases exclusively (so, not inverting ones like a-Glu I), and while epoxide **9** and aziridine **10** partially inhibit the retaining b-glucosidases, GBA1 and

GBA2, cyclosulfate **11** is completely inactive towards these enzymes. We also found that tempering the electrophilicity, as in cyclosulfamidates **17**, **18** and cyclosulfamide **19** yields competitive retaining a-glucosidase inhibitors and to investigate the effect of going from covalent to competitive inhihition within the same compound class we included these compounds in our assays. In addition, we tested a number of structural cyclitol variations. These include 1,2-*epi*-cyclophellitols (**20**-**22**), which may block a-Glu II in a covalent, irreversible manner similar to the 1,6-*epi*-cyclophellitols (364). A number of partially *O*-methylated cyclosulfates (**12**-**16**) were included to assess the effect of polarity, while compounds **23**-**28** were designed to contain alkyl substituents also present in the iminosugar series tested. The synthesis of the iminosugar and cyclitol inhibitors **1**-**11**, **17**-**22**, **25** and **26** have been published previously (353, 359-361, 363, 365). The synthesis of methylated sulfates **12**-**16** and alkyl aziridines **23**, **24**, **27** and **28** can be found in the supporting information (**Scheme S1**-**S5**).

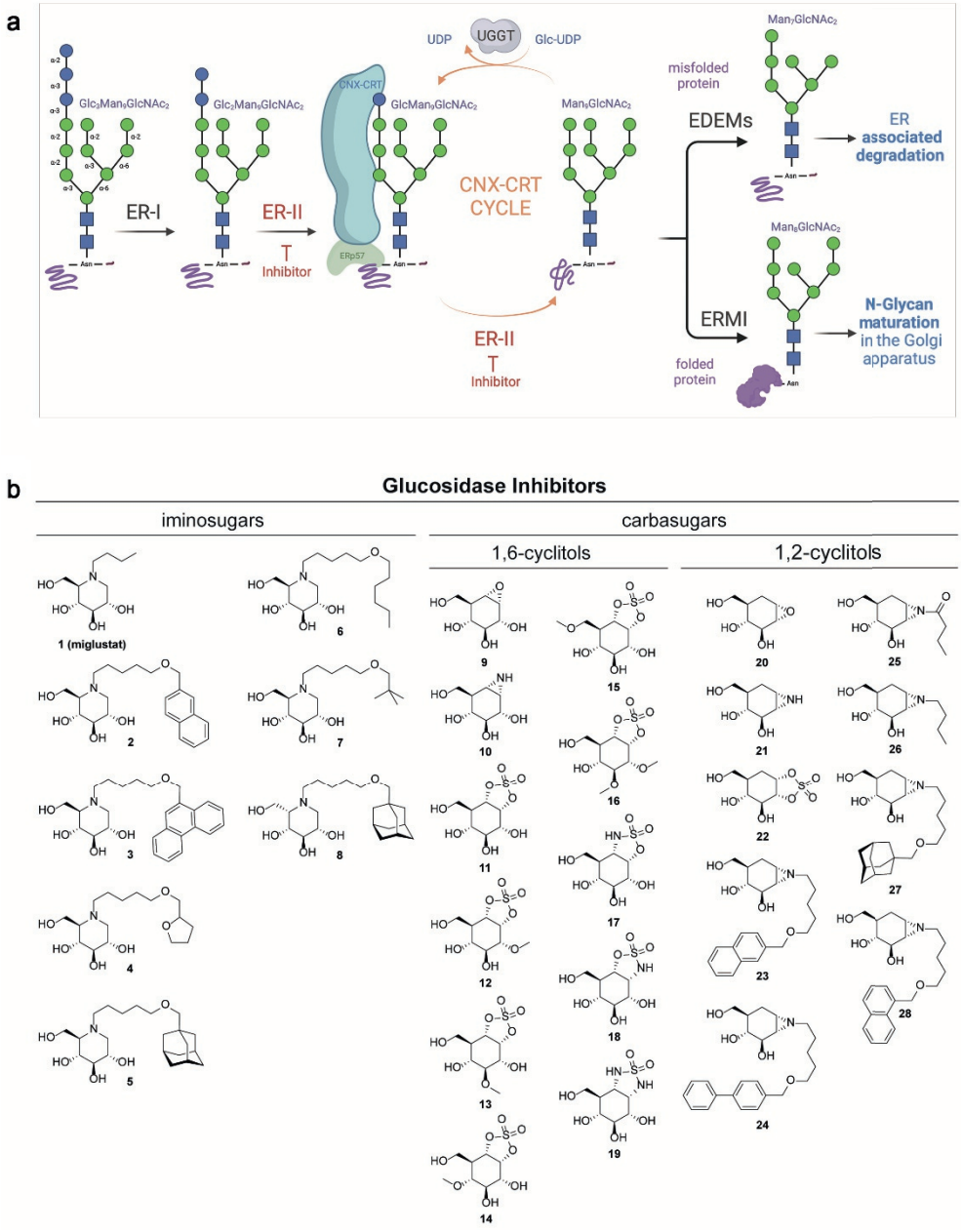

Figure 2: (a) Schematic of N-glycan processing of newly synthesized proteins in the ER lumen. Folding of nascent proteins in the ER is promoted by the calnexin-calreticulin cycle (CNX-CRT cycle), which relies on glycan trimming by ER α-Glu II (ER-II). (b) Focused library of 28 iminosugars and cyclitols subject of the here-presented studies.

The inhibitory effect of all synthesized molecules on the activity of GAA and endoplasmic reticulum α-glucosidase II (ER α-Glu II, GANAB) was determined following *in vitro* enzyme activity methods reported previously (353), using 4-methylumbelliferyl-α-D-glucopyranoside (4-MU-α-Glc) as fluorogenic substrate and measuring the amount of 4-MU-mediated fluorescence (**Figure 2a**, left panel). *N*-alkyldeoxynojirimycins **1**-**8** all inhibited both ER α-Glu II as well as GAA, but with potencies varying from the nanomolar to the micromolar range. *N*-alkyl-iminosugars **2**-**7**, featuring an extended lipophilic *N*-alkyl moiety relative to *N*-butyl-DNJ **1**, inhibited both enzymes rather more potently than this benchmark iminosugar, with **2** showing the highest potency of all iminosugars tested for both ER a-Glu II (IC_{50} = 0.12 μM) and GAA (IC_{50} = 0.19 μM). L-*Ido*-deoxynojirimycin **8** is a much weaker ER a-Glu II inhibitor than its D-*gluco*-isoster **5** (both compounds containing the same adamantane-modified *N*-alkyl chain), and showed no activity against GAA at the measured concentrations. Yet, compound **8** outperformed Miglustat in ER a-Glu II inhibition, revealing the influence of the *N*-alkyl chain in this series of compounds. These results match the literature trend indicating that large, hydrophobic *N*-alkyl appendages positively influence glucosidase inhibitory potency in this class of compound (359-361, 365).

With respect to the cyclitol class of compounds, 1,6-*epi*-cyclophellitol cyclosulfate **11** proved to be the most potent ER α-Glu II inhibitor of all compounds tested, with an IC_{50} value of 0.034 μM. Cyclosulfate **11** was also, and together with naphthyl-iminosugar **2**, the most potent of the GAA inhibitors. Methylation of either of the four hydroxyls (or combinations thereof) in **11**, as in 1,6-*epi*-cyclophellitol cyclosulfates **12**-**16** proved detrimental to inhibitory potency, though 4-*O*-methyl derivative **14** with an IC_{50} value of 8.15 μM for ER α-Glu II and 2.3 μM for GAA still outperformed Miglustat (**1**) as inhibitor of both of these enzymes. Moving from covalent (cyclosulfate, **11**) to competitive (**17**-**19**) cyclitol designs proved detrimental for ER α-Glu II inhibition, although compound **18** retains remarkable (IC_{50} = 2.63 mM) inhibitory activity against GAA. 1,2-*Epi*-cyclitols **20**-**22** turned out to be only moderately active ER α-Glu II inhibitors. In contrast to the 1,6-analogues (**9**-**11**), where the cyclosulfate was more potent compared to the aziridine and epoxide, epoxide **20** was the most potent of this series (364). Interestingly, 1,2-cyclosulfate **22** proved to be a rather potent GAA inhibitor, much more so than epoxide **20** and aziridine **21**, suggesting that conformational aspects (the epoxide and aziridine likely enforcing a half chair conformation with respect to the cyclitol ring where the cyclosulfate will allow a chair-like conformation) are in play for this enzyme. Finally, and in contrast to what was observed for the competitive inhibitor series **1**-**8**, 1,2-cyclophellitol aziridines **23**-**28** bearing an *N*-alkyl chain (and in case of **25** an *N*-acyl one) are much worse inhibitors for both enzymes tested (no significant inhibition up to 100 mM) when compared to the non-substituted aziridine **21**. In all, 1,6-*epi*-cyclophellitol cyclosulfate **11** is the most potent ER α-Glu II inhibitor, with

naphthylated deoxynojirimycin **2** as the most effective of the competitive inhibitors almost on a par with **11**.

To confirm the stabilizing effect of these two compounds on the enzyme, we performed a thermal stability assay with these, as well as with the less potent inhibitors **20**-**22**, on recombinant *M. musculus* α-Glu II, a mouse enzyme with high sequence homology to the human enzyme (**Figure 2b**). ER α-Glu II denaturation as a consequence of heat exposure, as well as the effect of active site-binding inhibitors on the denaturation temperature, can be monitored by a naturally quenched SYPRO orange dye. Upon denaturation of a protein, hydrophobic regions are exposed to which the dye binds, demonstrating a distinct difference in melting temperature (T_m) for each inhibitor compared to the unliganded ER α-Glu II control. *Mm*α-Glu II preincubated with compound **11** or **2** displayed melting temperatures (T_m) of 63.3 °C and 63.5 °C, respectively, whereas the unliganded enzyme denatured at approximately 15 °C lower (T_m = 49.9 °C). In comparison, compounds **21** and **22** gave no (49.5 °C) to marginal (51.7 °C) T_m increases, while epoxide **20**, which had the best efficacy of all 1,2-*epi*-cyclophellitols in the enzyme activity assay, gave a remarkably high T_m of 64.7 °C.

All compounds were then analyzed for their antiviral activity against SARS-CoV-2, in cytopathic effect (CPE) reduction assays, in which Vero E6 cells were pre-treated and infected with SARS-CoV-2 in the presence of various concentrations of compound. Three days post-infection cell viability was measured and EC_{50} values (compound concentration at which 50% of cell viability is reached as compared to the non-treated, infected cells) were determined (**Figure 2a**, right panel). Simultaneously, uninfected cells were treated with the same concentrations of compound to determine the CC_{50} (compound concentration at which cell viability is 50% of that of untreated cells due to cytotoxicity). All iminosugars **1**-**8** protected cells from SARS-CoV-2 infection in this assay, and naphthyl deoxynojirimycin **2**, being the most potent competitive ER α-Glu II inhibitor from the enzyme activity assay, also displayed the highest efficacy of the eight iminosugars assessed in blocking SARS-CoV-2 replication, with an EC_{50} value of 8.3 μM (**Figure 2d**). Similar deoxynojirimycin derivatives were previously reported to have activity against SARS-CoV-2 (346, 366). In contrast, the EC_{50} value in the CPE assay for Miglustat **1** was above 100 μM (**Figure 2c**), which correlates to other studies which found limited antiviral activity for this compound against SARS-CoV-2 (346, 367). 1,6-*Epi*-cyclophellitol cyclosulfate **11**, our most potent ER a-Glu II inhibitor, also proved to be the most potent SARS-CoV-2 replication inhibitor of all compounds tested with an EC_{50} value of 0.57 μM (**Figure 2e**). This matches our general finding that ER α-Glu II inhibitory potency correlates with anti-SARS-CoV-2 replication efficacy (**Figure 2a**). Selective ER α-Glu II inhibition thus appears a promising strategy in the discovery of new antiviral agents. Given that 1,6-*epi*-cyclophellitol cyclosulfate **11** came out as the most potent

compound in both the enzyme inhibition and SARS-CoV-2 CPE assays, and that this compound class, in contrast to that of iminosugars, comprises a new design class, we decided to further profile this inhibitor in more advanced virological assays to study its efficacy and mechanism of action.

a

	Compound	Inhibitory activity against glucosidases (biochemical assay) IC50 GANAB (μM) (ER-Glu-II)	IC50 GAA (μM)	Antiviral activity (CPE assay) EC50 (μM)	CC50 (μM)
Iminosugars	(Miglustat) 1	>100	20.7 ± 7.8	113.5 ± 10.3	>200
	2	1 ± 0.1	0.3 ± 0.07	8.3 ± 1.9	>200
	3	0.7 ± 0.1	0.013 ± 0.02	3.3 ± 0.4	>25
	4	0.8 ± 0.2	2.6 ± 0.2	51.7 ± 3.4	>200
	5	0.7 ± 0.02	1.05 ± 0.05	13.9 ± 8	>100
	6	2.9 ± 0.5	0.78 ± 0.1	11.8 ± 0.8	>200
	7	1.6 ± 0.9	7.7 ± 1.8	22.7 ± 4.3	>200
	8	>100	>100	104 ± 12.4	>200
1,6-cyclitols	9	>100	6.7 ± 0.34	>200	>200
	10	1.5 ± 0.08	0.34 ± 0.1	14 ± 3.2	>200
	11	0.03 ± 0.01	0.06 ± 0.01	0.57 ± 0.13	>200
	12	>100	>100	>200	>200
	13	47.6 ± 0.9	41 ± 1.5	>200	>200
	14	8.2 ± 0.1	2.2 ± 0.1	16.9 ± 2.1	>200
	15	>100	>100	>100	>200
	16	>100	>100	>200	>200
	17	1 ± 0.2	20.2 ± 5.9	45.3 ± 1.5	>200
	18	>100	6.1 ± 1.3	>100	>200
	19	>100	>100	>200	>200
1,2-cyclitols	20	11.3 ± 0.5	32.4 ± 4.6	17.7 ± 1.3	>200
	21	46.2 ± 2.6	>100	67.6 ± 14.8	>200
	22	26.1 ± 3.2	2.6 ± 0.07	>200	>200
	23	>100	>100	64.9 ± 0.8	>200
	24	>100	>100	28.6 ± 0.2	>100
	25	>100	>100	22.3 ± 4.1	>200
	26	>100	>100	91.4 ± 20.6	>200
	27	>100	>100	26.9 ± 1.3	>100
	28	>100	>100	56.7 ± 1.4	>200

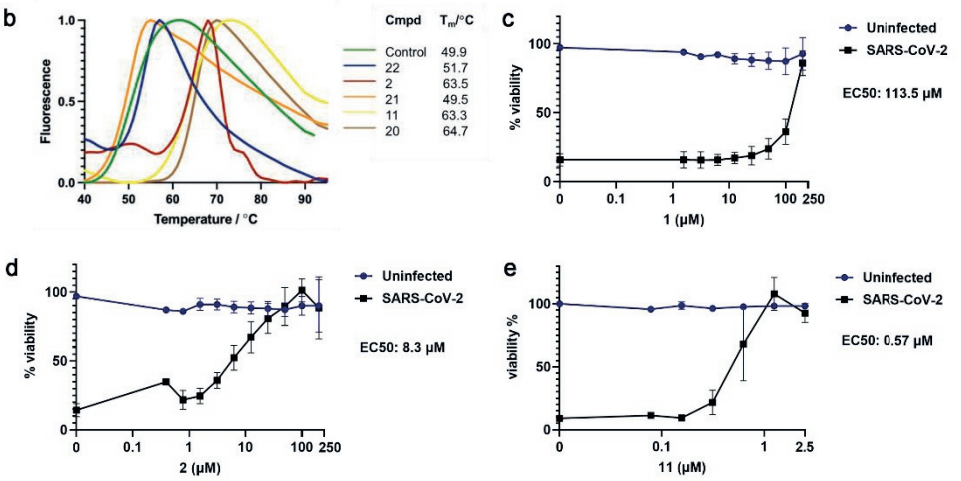

Figure 2: ER α-Glu II inhibitory potency correlates with reduction of SARS-CoV-2 mediated cytopathic effect in cell culture. (a) IC_{50} values of compounds in *in vitro* enzyme activity assays with ER a-Glu-II and GAA, and EC_{50} and CC_{50} values of compounds determined by CPE reduction assays with SARS-CoV-2. (b) Thermal shift profile of preincubated ER-α-Glu II with inhibitors. (c-e) SARS-CoV-2 CPE reduction assay dose-response curves of (c) Miglustat **1**, (d) naphthyl-deoxynojirimycin **2**, and (e) cyclosulfate **11**. n=3 independent experiments. The viability

of uninfected compound-treated cells was established by MTS assay in parallel. Means ± SEM are shown. The 50% inhibitory concentration (EC_{50}) values were determined by non-linear regression with GraphPad Prism 6.

1,6-*Epi*-cyclophellitol cyclosulfate reduces SARS-CoV-2 infectious progeny in cell culture

To investigate further the results from the CPE reduction assays, the effect of the most potent glucosidase inhibitor, 1,6-*epi*-cyclophellitol cyclosulfate **11** was assessed in viral load reduction assays on infected H1299/ACE2 lung epithelial cells. Cells were pre-treated with **11** and infected with SARS-CoV-2 at an MOI of 1. At 16 hours post infection (hpi) supernatant was harvested to quantify the infectious virus titer by plaque assay and extracellular viral RNA copies by RT-qPCR. Treatment of infected H1299/ACE2 lung epithelial cells with **11** resulted in a 100-fold reduction of the infectious progeny virus titer (**Figure 3a**). The inhibitory effect reached a plateau at 1.6 µM, and higher concentrations of **11** did not lead to more inhibition of virus replication. In contrast, Miglustat **1** reduced infectious progeny production only minimally, even at a concentration as high as 100 µM. Cyclosulfate **11** only slightly reduced extracellular viral RNA copy numbers (**Figure 3b**), indicating no effect on viral RNA production. This is in line with the expected mechanism of action of the compound that involves viral (structural) protein maturation, likely resulting in reduced infectivity of progeny virus. We then calculated the specific infectivity (defined as the number of infectious particles per viral RNA copy) of treated and untreated samples for the data in **Figure 3a** and **3b** (**Figure 3C**). Treatment with compound **11** caused a decrease in specific infectivity, suggesting that the infectivity of released particles is affected. None of the treatments caused noticeable cytotoxicity in uninfected treated cells (**Figure 3b**). Similarly, treatment of infected Calu-3 lung epithelial cells with **11** reduced infectious progeny virus titers by ~10-fold, while no reduction in extracellular viral RNA copies was observed (**Figure S1**).

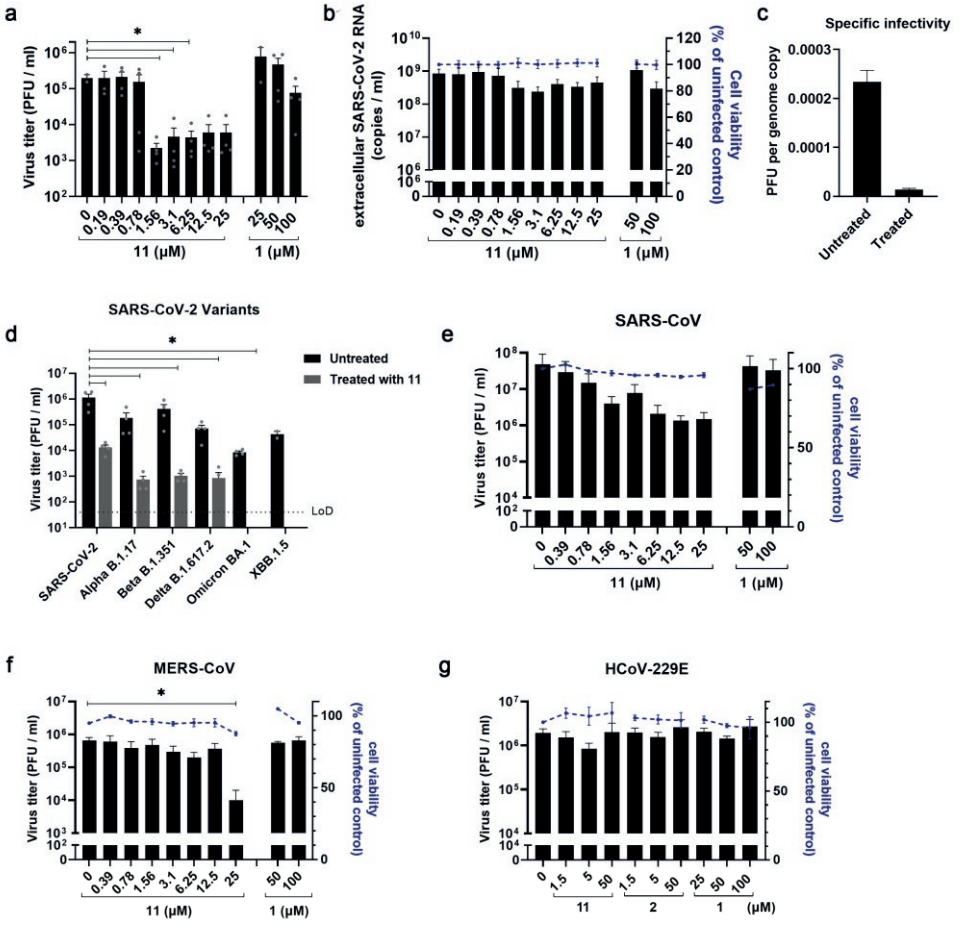

Figure 3: Spectrum of activity of 1,6-*Epi*-cyclophellitol cyclosulfate **11** and iminosugars **1** and **2** against various coronaviruses. (a-b) Viral load reduction assay on H1299/ACE2 cells with SARS-CoV-2 (MOI 1) in the presence of compounds **1** or **11**. (a) Infectious virus titer and (b) extracellular viral RNA copy numbers were quantified by plaque assay and RT-qPCR, respectively. Uninfected compound-treated cells were assessed by MTS assay in parallel to measure cytotoxicity of the compounds. n = 3 independent experiments. Mean ± SEM are shown. (c) The specific infectivity of treated (using 1.5 μM of compound **11**) and untreated samples was calculated by dividing the infectious virus titer (PFU/mL) by the viral RNA copy number (copies/mL). Viral load reduction assays with (d) SARS-CoV-2 variants in H1299/ACE2 cells, (e) SARS-CoV in Vero E6 cells, (f) MERS-CoV in HuH-7 cells, and (g) HCoV-229E in H1299/ACE2 cells (all with MOI 1), and treatment with **1**, **2** or **11**. Supernatant was harvested at 16 hpi to quantify infectious progeny by plaque assay. n = 3 independent experiments. Uninfected compound-treated cells were measured by MTS assay in parallel to assess the cytotoxicity of the compounds. Mean ± SEM are shown. Statistical analysis was conducted using one-way ANOVA and significant differences are indicated by *p<0.05.

1,6-*Epi*-cyclophellitol cyclosulfate inhibits infectious progeny of SARS-CoV-2 variants, SARS-CoV, and MERS-CoV, but not HCoV-229E

To investigate the spectrum of activity against coronaviruses of 1,6-*epi*-cyclophellitol cyclosulfate **11**, its effect on the replication of SARS-CoV-2 variants alpha, beta, delta, omicron BA.1, and XBB.1.5 was tested (**Figure 3d**). As in the above experiments (**Figure 3a**), viral load reduction assays were performed, during which different cell lines were infected with the respective virus in the presence of compound, and at 16 hpi supernatant was harvested to quantify the infectious virus titer by plaque assay. Similar to the antiviral effect on the early pandemic SARS-CoV-2 isolate, treatment of H1299/ACE2 cells that were infected with other variants showed a ~100-fold reduction in infectious virus titer (**Figure 3d**). Viral load reduction assays with SARS-CoV on Vero E6 cells and MERS-CoV on HuH-7 cells showed a significant reduction of infectious progeny upon treatment with increasing concentrations of compound **11** (**Figure 3e** and **3f**), although the efficacy of the compound was slightly lower against SARS-CoV and clearly lower against MERS-CoV. Interestingly, the viral load reduction assay with HCoV-229E on H1299/ACE2 cells did not show any reduction in virus infectivity, upon treatment with either compound **11** or **2** (**Figure 3g**).

1,6-*Epi*-cyclophellitol cyclosulfate strongly reduces α-glucosidase activity and inhibits SARS-CoV-2 in primary human bronchial epithelial cells cultured at the air-liquid interface

We next evaluated the efficacy of 1,6-*epi*-cyclophellitol cyclosulfate **11**, in comparison to our most potent iminosugar, naphthyl-deoxynojirimycin **2**, as well as Miglustat **1** in a more advanced model of primary human bronchial epithelial cells that were cultured at the air-liquid interface (ALI-PBEC), as we described previously (132, 368). Thus, ALI-PBEC cells were infected with SARS-CoV-2 (10^5 PFU per insert; estimated MOI of ~0.1) and treated with compounds on the apical side of the cells for 2 hours. For uninfected controls, PBS was used instead of virus. The compounds were also present in the basal medium during the whole experiment until 48 hpi when samples were harvested. Treatment with 0.5 µM of compound **11** reduced the viral load significantly by up to 100-fold compared to the untreated control (**Figure 4a**). Deoxynojiriomycin derivative **2** reduced SARS-CoV-2 to similar titers, but at higher compound concentrations (10 and 100 µM), while Miglustat **1** had only a slight effect at the highest concentration measured (100 mM) (**Figure 4a**). Measurement of cell death (by LDH release in the supernatant) revealed that none of the compounds tested caused significant cytotoxicity at the highest concentrations (**Figure 4b**).

We also evaluated the reduction of retaining α-glucosidases in the treated ALI-PBEC cell cultures by treatment of the cell lysate at 48 hpi with retaining α-glucosidase activity-based probe **29**, which labels GAA (isoforms at 70 and 76 kDa) and both isoforms of GANAB (∼100 kDa) at pH 7 (369) (**Figure 4d**). In line with the *in vitro* enzyme activity assay results (**Figure 2a**), compound **11** was most efficient in inhibiting ER a-Glu II and GAA at low concentrations (**Figure 4c** and **Figure S2**), suggesting that *in cellulo* ER α-Glu II inhibition potency correlated well with the efficacy to block SARS-CoV-2 replication.

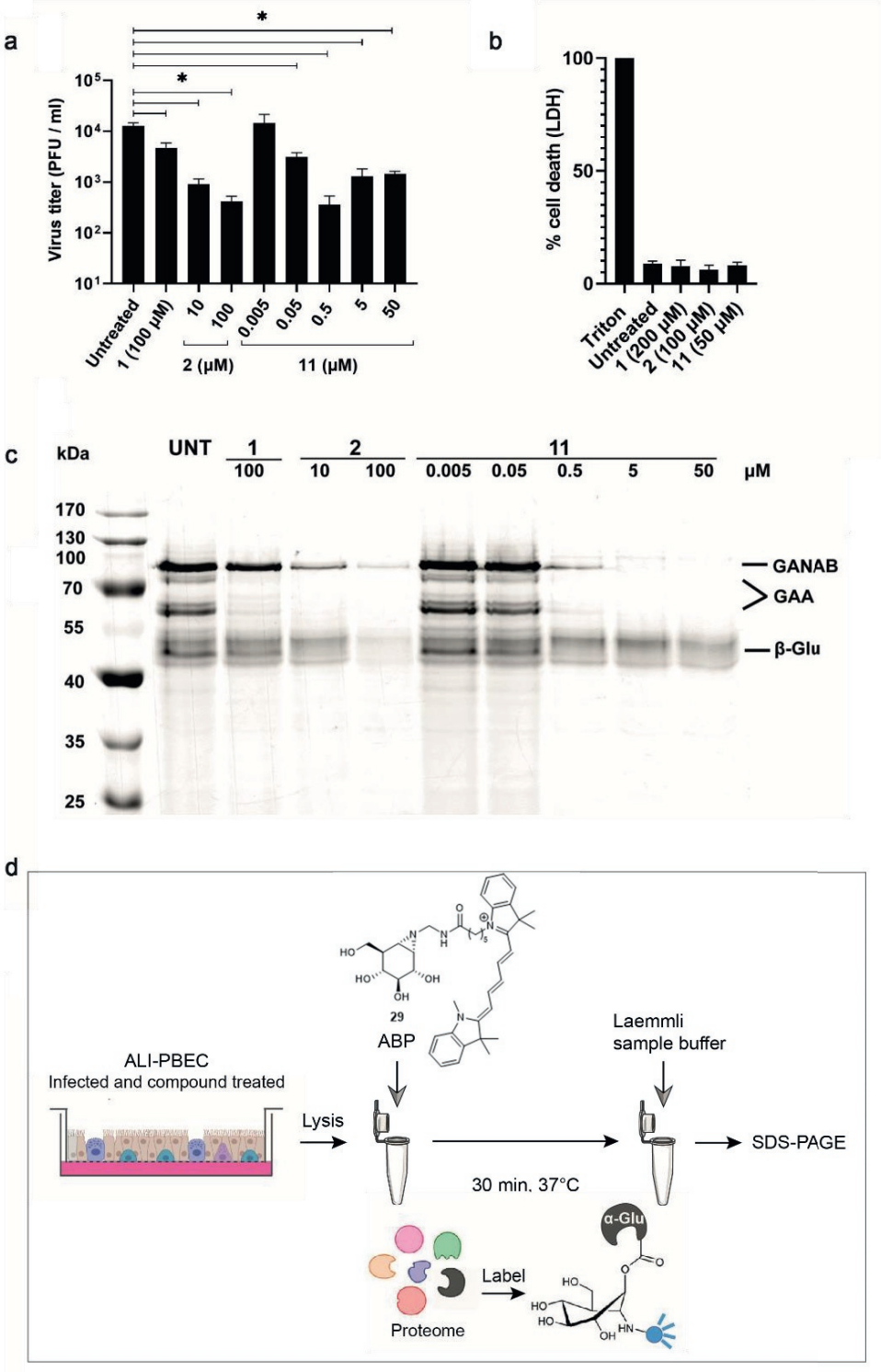
a
Virus titer (PFU / ml)
Untreated
1 (100 µM)
10
100
0.005
0.05
0.5
5
50
2 (µM)
11 (µM)
b
% cell death (LDH)
Triton
Untreated
1 (200 µM)
2 (100 µM)
11 (50 µM)
c
kDa
UNT
1
2
11
µM
170
130
100
70
55
40
35
25
GANAB
GAA
β-Glu
d
ALI-PBEC
Infected and compound treated
Lysis
ABP
29
Laemmli
sample buffer
SDS-PAGE
30 min, 37°C
α-Glu
Label
Proteome

Figure 4: Reduction of SARS-CoV-2 infection in primary bronchial epithelial cells is consistent with inhibition of active ER α-glucosidase II. (a) Viral load reduction assay in ALI-PBEC. Supernatant was harvested at 48 hpi to quantify infectious progeny by plaque assay. n = 3 independent experiments. Mean ± SEM are shown. Statistical analysis was conducted using one-way ANOVA and significant differences are indicated by *p<0.05. (b) The viability of uninfected compound-treated cells was measured by LDH release assay in parallel, to assess cytotoxicity of the compounds. Mean ± SEM are shown. (c) Following compound treatment, cells were lysed and the lysate at pH 7.0 was treated with activity-based probe (ABP) **29** to assess cellular retaining a-glucosidase activities in a competitive activity-based protein profiling experiment. A representative gel of three independent experiments (with two biological replicates/ALI-PBEC inserts each) is shown. (d) Schematic representation of ABP labelling. Part of the figure in (d) was adapted from (369). **Figure S2** shows the Gelcode Blue stained gel of (c), which demonstrated that equal amounts of protein were loaded.

1,6-*Epi*-cyclophellitol cyclosulfate inhibits SARS-CoV-2 replication at a post-entry step of the viral replication cycle

We then investigated the mode of action of 1,6-*epi*-cyclophellitol cyclosulfate **11** by assessing which step in the viral replication cycle is inhibited. First, we assessed whether the compound affects the infectivity of virus particles, that is, has virucidal or neutralizing activity. Therefore, SARS-CoV-2 was incubated with a high concentration of compound **11** (50 µM) for 1 h at 37 °C, and subsequently the infectious virus titer was quantified by plaque assay. Control treatment with 70% ethanol led to full inactivation of the virus, while compound **11** had no effect on the infectious titer (**Figure 5a**). Next, we assessed if treatment early during infection had an effect on virus replication. We infected H1299/ACE2 cells with SARS-CoV-2 at an MOI of 3 and started treatment with compound **11** at 1 hpi. At 2, 3 and 5 hpi, cells were harvested and RT-qPCR was performed to quantify the intracellular viral genome copies. The kinetics of intracellular viral RNA accumulation were similar in untreated and compound **11** treated cells, suggesting the compound had no effect on (early) RNA replication (**Figure 5b**).

To evaluate whether compound **11** has an effect on host proteins (for instance, ACE2) involved in viral entry, we treated monolayers of H1299/ACE2 cells with compound **11** either 48 or 2 h before infection, during infection (0-1 h), or starting from 1 h post-infection (hpi). The cell monolayers were infeed with ~20 PFU of SARS-CoV-2 and after 1 h the inoculum was replaced with an overlay. In one well (Post Infection) the overlay contained compound **11**. Remdesivir, a viral RNA synthesis inhibitor, was added to the overlay of another well, as a positive control for blocking virus replication in the cell. At 3 dpi cells were fixed and stained with crystal violet. Pre-treatment of the cells with compound **11**, or treatment only during infection had no effect on the number of plaques that developed or

their morphology. Only the presence of compound **11** after infection prevented the formation of plaques, similar to treatment with remdesivir treatment (**Figure 5c and 5d**). This result suggests that the antiviral effect of **11** is not through modulating expression or functioning of host proteins (such as the ACE2 receptor) that are essential for viral attachment to, or entry into, the host cell.

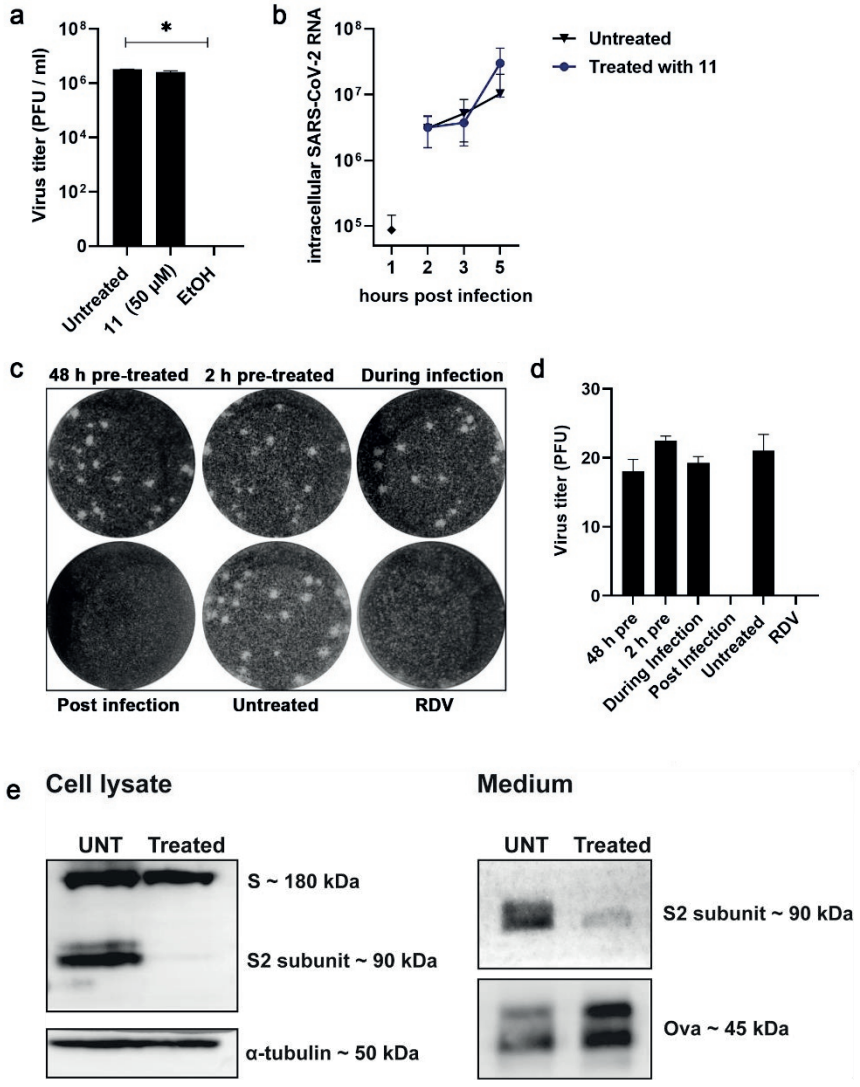

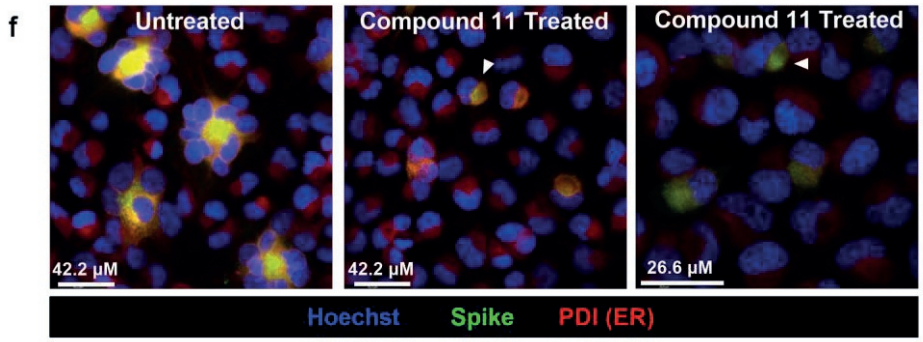

Figure 5: 1,6-*Epi*-cyclophellitol cyclosulfate **11** inhibits SARS-CoV-2 replication and syncytium formation by reducing intracellular spike protein levels and processing. (a) Virucidal activity assay in which SARS-CoV-2 was incubated with compound **11** or 70% ethanol (as control) for 1 h at RT, and (remaining) infectious progeny was quantified by plaque assay. n = 2 independent experiments. Mean ± SEM are shown. Statistical analysis was conducted using one-way ANOVA and significant differences are indicated by **p*<0.05. (b) H1299/ACE2 cells were infected with SARS-CoV-2 (MOI 3) and treated with **11** from 1 hpi until harvesting at the indicated time points. Intracellular viral RNA copies were quantified by RT-qPCR. n = 3 independent experiments. (c, d) Plaque reduction assay was performed with 1 h infection and incubation for 3 days until cells were fixed and stained with crystal violet. Cells were treated with 5 µM of compound **11**, either before infection (pre-treatment), during infection, or after infection (post infection) in the overlay. Treatment with RDV in the overlay was used as a control. n = 2 independent experiments. Means ± SEM are shown. (e) Western Blot analysis of viral S protein in the medium and cell lysates of untreated (UNT) or compound **11** treated (2 µM) H1299/ACE2 cells that were infected with SARS-CoV-2 (MOI 2) and analyzed at 10 hpi using an S2-specific antibody. The medium was spiked with ovalbumin (Ova) as a recovery control and was concentrated, before a sample corresponding to ~250 µL of the original medium volume was analyzed. α-tubulin was used as a loading control for cell lysates. (f) H1299/ACE2 cells were infected with SARS-CoV-2 (MOI 0.1), fixed at 10 hpi, and the viral S protein and ER marker PDI were visualized by immunofluorescence microscopy. Cells were stained with human anti-SARS-CoV-2 S protein antibody (green), mouse anti-PDI antibody for ER staining (red), and Hoechst for visualizing nuclei(blue). White arrows indicate co-localization of S with PDI. Images are representative of n = 2 independent experiments.

1,6-*Epi*-cyclophellitol cyclosulfate inhibits SARS-CoV-2 replication through effects on intracellular S protein maturation and infectivity of viral progeny

From the above-described experiments it became evident that treatment with 1,6-*epi*-cyclophellitol cyclosulfate **11** led to a reduction in virus infectivity, but not to a reduction in the number of viral genome copies (**Figure 3**), and that inhibition was not through an effect on the receptor or virus binding and entry, but at a post-entry step other than RNA replication (**Figure 5a-d**). Therefore, we suspected an effect on the S protein. As shown in **Figure 4**, compound **11** effciently inhibited ER α-Glu II, which is crucial for the processing of N-glycosylated viral proteins such as S. To assess the effect of α-Glu II inhibition on S protein

production/maturation, we performed viral load reduction assays on H1299/ACE2 cells. Cells were infected with SARS-CoV-2 (MOI of 2) and treated with 2 µM of compound **11** or cell culture medium. At 10 hpi medium and cell lysate were harvested to analyze S protein levels by Western blotting with an S2-specific antibody. Treatment with compound **11** led to a minor reduction in the amount of full-length S protein in the cell lysate and to the almost complete disappearance of the ~90 kDa S2 fragment, a product of proteolytic (furin) cleavage of mature S protein in the Golgi apparatus. This indicated that treatment with **11** impaired maturation of the S protein in the ER, leading to reduced trafficking to the Golgi (**Figure 5e**). The amount of (processed) S2 was also strongly reduced in the medium of compound-treated cells, suggesting the compound impaired biogenesis of particles or their S protein content (**Figure 5e**).

Next, we set out to analyze the effect of compound **11** treatment on the level and localization of the S protein in infected cells, and formation of syncytia, which are large multinucleated cells resulting from the interaction of S protein on the surface of infected cells with ACE2 receptors on neighbouring cells, which triggers cell fusion. To this end, SARS-CoV-2-infected H1299/ACE2 cells (MOI 0.1) were treated with 5 µM of compound **11** or cell culture medium as control, and at 10 hpi cells were fixed and analyzed by immunofluorescence staining for the viral S protein and the ER marker protein disulfide isomerase (**Figure 5f**). We observed a reduction in the amount of S protein in infected cells that were treated with compound **11** and the co-localization of S protein with the ER marker, which suggests (partial) retention of S proteins in the ER. Treatment also led to reduced syncytium formation compared to untreated infected cells, likely due to impaired maturation, and subsequent impaired trafficking of S protein to the plasma membrane.

Discussion

In this study we have assessed the ER α-Glu II inhibitory potency and anti-SARS-CoV-2 activity of selected members (28 compounds in total) of two classes of glycomimetics: iminosugars and cyclitol analogues, and to what extent these two effects correlate. Deoxynojirimycin-type iminosugars as competitive inhibitors have been studied for almost four decades as candidate-antivirals for pathogenic viruses that rely on ER-protein quality control, and in recent years have also been explored as anti-SARS-CoV-2 agents (336, 337, 340, 346, 370, 371). In contrast, cyclophellitol-type mechanism-based inhibitors have not been considered for this purpose. The results described here support the hypothesis that mechanism-based inactivation of ER α-Glu II may lead to effective new antiviral agents to treat infections with the numerous viruses that rely on host protein glycosylation for

replication. In particular, 1,6-*epi*-cyclophellitol cyclosulfate **11**, the most potent ER α-Glu II inhibitor of the tested compounds, also blocked viral replication most effectively. Further investigations revealed that the antiviral effect is not due to effects on (glycosylation or quantity of) host cell factors that play a role in virus binding and entry into the host cell, or replication of the viral genome, suggesting it does not (noticeably) target the SARS-CoV-2 non-structural proteins. The antiviral effect is on blocking N-glycosylation of the S protein, the most heavily N-glycosylated SARS-CoV-2 protein, which plays crucial roles in virus binding and entry. The absence of cleaved S2 fragment in compound treated cells, indicates that impairing processing of S protein at the ER led to reduced trafficking of S to the Golgi and prevention of (furin) cleavage of the S1/S2 site, ultimately leading to less mature S protein for incorporation into infectious virus particles. Thus, cyclosulfate **11** acts on protein N-glycosylation/ER protein quality control, just as the N-alkyl deoxynojirimycin derivatives tested by us and others, but, in addition compound **11** is much more selective compared to the iminosugars (353). Considering the mechanistic mode of action of inverting and retaining glucosidases, compound **11** inhibits retaining a-glucosidases exclusively over inverting a-glucosidases; with in the context of this work the lysosomal retaining a-glucosidase, GAA, as the single off-target. Deoxynojirimycin-type iminosugars in contrast also block inverting a-glucosidases including ER a-Glu I. The finding that blocking ER a-Glu II alone is sufficient (at least in the assays reported here) for halting SARS-CoV-2 replication may therefore be beneficial for situations in which ER inhibiting a-Glu I has adverse effects. Iminosugars have often also other human glycoprocessing enzymes as off-target. *N*-butyldeoxynojirimycin **1** (Miglustat) is applied in the clinic for the treatment of Gaucher disease where it acts as glucosylceramide synthase inhibitor (362, 372). It also inhibits the three human retaining b-glucosidases, GBA1, GBA2, GBA3 (373). None of these enzymes play a role in SARS-CoV-2 infections, and their inhibition may lead to adverse effects as well. Such adverse effects in contrast are not to be expected from 1,6-*epi*-cyclophellitol cyclosulfate **11**, which does not inhibit any of these enzymes (GCS, GBA1, GBA2, GBA3) as we have shown before (353). Arguably, adverse effects as elicited by **11** may be the result of inhibition of the lysosomal a-glucosidase, GAA, however this enzyme is also inhibited by the iminosugars (374). We therefore conclude that compound **11**, which in contrast to the iminosugars is non-basic, thus not charged at physiological conditions, may be a good starting point for the development of new antiviral agents for the treatment of infections by SARS-CoV-2 and other (emerging) viruses that require ER-protein quality control for replication.

Methods

Compounds and cell lines

Inhibitors were synthesized at the department of bio-organic synthesis at the Leiden Institute of Chemistry. The synthesis of the cyclitol and iminosugar inhibitors **9**–**11, 17, 18**–**22, 25, 26, and 1**–**8** have been published previously (353, 359-361, 363, 365). The synthesis of methylated sulfates **12**–**16** and alkyl aziridines **23**, **24**, **27** and **28** can be found in the supporting information (**Scheme S1 – S5**). Lyophilized compounds were diluted in DMSO prior to use. Remdesivir, which was used as compound control in different assays, was purchased from Sigma-Aldrich and dissolved in DMSO.
Vero E6 cells and HuH-7 cells were cultured as previously described (375). Human lung cell line H1299/ACE2 is described elsewhere (376). These cells were cultured in Dulbecco's modified Eagle's medium with 4.5 g/L glucose with L-glutamine (DMEM; Lonza, Basel, Switzerland) supplemented with 10% fetal calf serum (FCS) (CapriCorn Scientific, Ebsdorfergrund, Germany), 100 U/mL of Penicillin/Streptomycin (P/S) (Sigma-Aldrich, St. Louis, MO, USA), and 1200 µg/mL G418 for selection (InvivoGen, San Diego, CA, USA). Infections of Vero E6 cells, HuH-7 cells, and H1299/ACE2 cells were performed in Eagle's minimal essential medium with 25 mM HEPES (EMEM; Lonza) supplemented with 2% FCS, 2 mM L-glutamine (Sigma-Aldrich), and 100 U/mL of P/S. Primary human bronchial epithelial cells (PBEC) were isolated and cultured as previously described (377). All cell cultures were maintained at 37 °C in an atmosphere of 5% CO_2.

Virus stocks

All experiments with infectious SARS-CoV, SARS-CoV-2, or MERS-CoV were performed at the LUMC biosafety level 3 facilities. The clinical isolate SARS-CoV-2/Leiden-0008 (isolated at LUMC during the first wave of the Corona pandemic in March 2020 (GenBank: MT705206.1) was used for H1299/ACE2 and ALI-PBEC infections. This virus stock was not adapted to Vero E6 cells with regard to the spike S1/S2 cleavage site (confirmed by NGS). For CPE assays in Vero E6 cells SARS-CoV-2/Leiden0002 was used (GenBank: MT510999.1). SARS-CoV-2 variant B.1.1.7 (A), variant B.1.351 (Beta), and variant B.1.617 (Delta) were obtained from the University of Leuven. SARS-CoV-2 variant BA.1 (Omicron) was obtained from RIVM (strain hCoV-19/Netherlands/NH-RIVM-72291/2021, lineage B.1.1.529, GenBank: OR427989.1) and variant XBB.1.5 was isolated from a patient sample at LUMC. SARS-CoV-2/Leiden-0008 (Passage 2), SARS-CoV-2/Leiden0002 and SARS-CoV isolate Frankfurt 1 (298) (Passage 4) were grown on Vero E6 cells. Alpha (Passage 4), Beta (Passage

4), Delta (Passage 4), Omicron BA.1 and XBB.1.5 (P3) variants were grown on Calu-3 cells. MERS-CoV (N3/Jordan) (GenBank: KJ614529.1) (Passage 3) and HCoV-229E were grown on HuH-7 cells. Virus titers were determined by plaque assay on Vero E6 cells, and for MERS-CoV and HcoV-229E on HuH-7 cells, as described before (255).

In vitro GAA and GANAB enzyme activity assay

Inhibition of the enzymes GAA and GANAB by the compounds was tested *in vitro* as described previously (353). Briefly, enzymes were preincubated with a range of inhibitor concentrations for 30 min at 37°C. The residual activity of the enzymes was then measured by adding the 4-MU–Glc substrate mixture at their corresponding optimal pH. Reactions were quenched with 1 M NaOH–glycine (pH 10.3) upon completion, and 4-MU fluorescence was measured with an LS55 fluorescence spectrophotometer (PerkinElmer) (λEX 366 nm; λEM 445 nm). IC50 values reported are the mean values from three technical replicates.

Cytopathic Effect (CPE) reduction assay

CPE reduction assays were performed as previously described (375). Briefly, Vero E6 cells were seeded in 96-well plates at a density of $5*10^3$ cells per well. The next day, cells were infected with SARS-CoV-2/Leiden0002 in the presence of 2-fold serial dilutions of compound. 4 days post infection the CellTiter 96 aqueous nonradioactive cell proliferation kit (Promega) was used to measure the cell viability of infected (protection) and non-infected cells (assessment of cytotoxicity). EC_{50} values reported are the mean values from three independent experiments and were calculated using GraphPad Prism 6.

Expression of Mmα-Glu-II

The two subunits of *M. musculus* α-glucosidase II ganab and prkcsh were subcloned into separate vectors (pOPING and pOPINGS for ganab and prkcsh respectively) and codon optimized for mammalian expression by Genscript. Each vector was transformed into DH5α (Thermofisher) cells by heat shock. Cultures of each subunit were grown at 37 °C in LB, and the amplified DNA was purified using the PureLink™ HiPure plasmid filter Maxiprep kit (Invitrogen) obtaining 750 μg of DNA for both constructs. The isolated DNA was co-transfected into a 600 mL suspension of 293-F cells following the Freestyle 293 Expression system protocol (ThermoFisher) and harvested after 4 days at 37°C, 8% CO_2, at 135 rpm.

Purification of ER α-Glu-II

Cells were pelleted at 200 *g*, for 20 minutes at 4 °C and the clarified media was then further centrifuged for 20 minutes, at 5000 *g* at 4 °C. The clarified media was loaded onto a pre-equilibrated 5 mL HisTrap excel column (Cytiva) with binding buffer (1x PBS, 20 mM imidazole, 5% glycerol w/v) and eluted using a buffer gradient 0-100% of elution buffer (1x PBS, 500 mM imidazole, 5% glycerol w/v) over 20 CVs. Fractions containing *Mm*α-Glu-II were concentrated and loaded onto size exclusion S200 column (Cytiva), which was pre-equilibrated with HEPES buffer (20 mM HEPES pH 7.5 and 150 mM NaCl). The *Mm*α-Glu-II containing fractions were pooled and a trypsinolysis was performed using sequencing grade modified trypsin (Promega), supplemented with 2 mM $CaCl_2$ for 4 hours at a ratio of 1:100 (trypsin: *Mm*α-Glu-II). The size exclusion was repeated and the resulting *Mm*α-Glu-II was pooled and concentrated to 8 mg/mL.

Thermal shift assays

Triplicate reactions of 10 μM *Mm*α-Glu-II unliganded control and 10 μM *Mm*α-Glu-II with 50 μM inhibitor were prepared to a final volume of 30 μL with buffer (20 mM HEPES pH 7.5 and 150 mM NaCl). Before the assay, 20x SYPRO orange dye was added to each reaction mixture. The assay was performed using the Stratagene Mx3005P qPCR machine where the SYPRO orange dye was excited at λ_{ex} 517 nm and monitored at 585 nm with 2 °C min^{-1} increases from 25 °C – 95 °C. Readings were averaged to produce a thermal stability curve with fluorescence plotted against temperature and the T_m estimated from the midpoint.

Viral load reduction assays

For SARS-CoV-2 (variants) and HCoV-229E infections, H1299/ACE2 cells were seeded in 96-well plates at a density of 10^4 cells per well and the next day infected at MOI 1. Infections with SARS-CoV-2 were incubated at 37 °C, and infections with HCoV-229E at 33 °C. For SARS-CoV or MERS-CoV infections (MOI 1), Vero E6 or HuH-7 cells were seeded in 96-well plates at a density of $2*10^4$ cells per well. Cells were incubated at 37 °C. After removal of the inoculum at 1 hpi, cells were washed three times with warm PBS or medium after which they were incubated in infection medium (EMEM). Supernatant samples were harvested at 16 hpi and infectious virus titers were determined by plaque assay, and viral RNA copy numbers by RT-qPCR. In parallel, the cytotoxicity of compound treatment was measured on uninfected cells by the CellTiter 96 aqueous nonradioactive cell proliferation kit.

Immunofluorescence staining

For immunofluorescence imaging of viral spike protein H1299/ACE2 cells were seeded onto glass cover slips in 24-well plates at a density of $1.6*10^5$ cells per well. Thenext day they were infected with SARS-CoV-2/Leiden0008 (MOI 0.1) in Opti-MEM reduced serum medium (Thermo Fisher Scientific). At 16 hpi, cells were fixed with 3% warm paraformaldehyde. Immunofluorescent staining of viral spike protein was done using human anti-spike antibody P52 (gift from King's college) and goat-α-human IgG Alexa 488 antibody (Thermo Fisher Scientific). Staining of endoplasmic reticulum was done using mouse anti-PDI antibody (Fuller)(378), and donkey-α-mouse Cy3 antibody (Jackson).

Western Blot

For western blot analysis, H1299/ACE2 cells were seeded in 6-well plates at a density of $6.5*10^5$ cells per well and the next day infected with SARS-CoV-2/Leiden0008 at an MOI of 2. At 10 hpi supernatant was harvested and 4000 µL medium was spiked with ovalbumin (internal recovery control), and concentrated to 150 µL using Amicon Ultra-0.5 centrifugal filter units (Merck), according to the manufacturer's instruction. An equal amount of Laemmli buffer was added and samples were heated at 95 °C for 5 min. Samples were analyzed by SDS-PAGE (10% gel, 30 min at 90 V, then 50 min at 120 V) and subsequently blotted for 30 min in a semi-dry blotting system (Bio-Rad). The membrane was blocked with 1% casein in PBST for 1 h at RT, before incubation with primary antibodies overnight at 4 °C. Spike proteins were detected using SARS/SARS-CoV-2 spike protein S2-specific mAb 1A9 (Invitrogen) as primary antibody. The loading control tubulin was detected with mouse-anti-α-tubulin antibody B-5-1-2 (abcam) and spiked ovalbumin was detected with mouse ovalbumin mAb 1D3D5 (ThermoFischer). The next day the membrane was washed three times for 5 min with PBST, and then incubated in 0.5% casein in PBST with a secondary goat-α-mouse-HRP antibody (P0447, Dako) for 1 h at RT. After washing again three times, the membrane was incubated in Clarity Western ECL Substrate (Bio-Rad) for 2 minutes and imaged with the Uvitec Alliance Q9 advanced imager.

RNA isolation and RT-qPCR

RNA was isolated by magnetic bead isolation, as described in (368). Equine arteritis virus (EAV) in AVL lysis buffer (Qiagen) was spiked into the isolation reagent as an internal control for extracellular RNA samples. RT-qPCR was performed using TaqMan Fast Virus 1-step master mix (Thermo Fisher Scientific) and as previously described (234). The cellular

reference gene PGK1 served as a control for intracellular RNA. Primers and probes for EAV and PGK1 and the normalization procedure were described before (255). Primers and probes for SARS-CoV-2, as well as a standard curve, were used as described previously (234, 256).

Plaque Assay

To quantify infectious virus titers, plaque assays were done on Vero E6 cells (SARS-CoV-2 and variants, SARS-CoV), H1299/ACE2 (HCoV-229E) or HuH-7 (MERS-CoV). For SARS-CoV-2 and variants, $2x10^4$ cells/well were seeded in a 96-well plate, and serial dilutions of samples were inoculated for 1 h at 37 °C on a rocking platform. Inoculums were removed and 100 µL of methylcellulose overlay was added. Cells were incubated for 4 days until fixation and crystal violet staining. Alternatively, plaque assays for SARS-CoV-2 and variants were done in 6-well plates, with avicel overlay and 3 days incubation. HCoV-229E samples were quantified in 12-well plates, using avicel overlay and incubating for 4 days. MERS-CoV samples were quantified in 12-well plates with avicel overlay or 96-well plates with methylcellulose overlay for 3 days.

Infection of ALI-PBEC and activity-based probe labelling

ALI-PBEC were pre-treated with compound in the basal medium for 3 hours. Cells were infected with 100 000 PFU of SARS-CoV-2/Leiden0008 per insert (estimated MOI of 0.1) with compounds present in the inoculum. After 2 hours at 37 °C on a rocking platform, the inoculum was removed and cells were washed three times with warm PBS. Compounds stayed present in the basal medium until 48 h post infection. At 48 hpi the viral load was determined by plaque assay on a 200 µL apical wash (PBS incubated on the apical side of the inserts for 10 min at 37 °C). For assessing cytotoxicity with the CyQuant LDH cytotoxicity assay (Thermo Fisher Scientific), 10 µL of apical wash was diluted 5x with 40 µL PBS. 25 µL of this dilution was added to 25 µL assay reagent and incubated for 30 min at RT in the dark. The plate was fixed and measured at a wavelength of 490 nM (Envision reader, Perkin Elmer). For the activity-based probe labelling, the inserts were washed one more time with PBS and processed as described previously (369). Briefly, cells were lysed with 60 µL of potassium phosphate buffer per insert. A fluorescently-labelled Probe (JJB383) was diluted in McIlvaine buffer (pH 7) to a 10 µM stock and incubated for 5 min on ice. For labelling of the cell lysate, 10 µL of lysate was added to 10 µL of McIlvaine buffer and 5 µL of probe. The lysate was incubated for 30 min at 37 °C, before addition of 10 µL of Laemmli sample buffer (4x). Samples were heated at 95 °C for 5 min and separated in a 10% SDS-PAGE gel.

Fluorescence was measured at a wavelength of 625 nm (Cy5) with a Uvitec Alliance Q9 imager (BioSPX). After imaging, the gels were stained with GelCode Blue stain reagent (Thermo Fisher Scientific) and visualized using a Uvitec Essential V6 system to check for equal loading.

Plaque reduction assay

H1299/ACE2 cells were seeded in a 6-well plate at a density of 1.3*10^5 cells/well (20 % confluency), 96 h prior to infection. Cells were treated with 5 µM of compound **11** either 48 or 2 h before infection, or during the 1 h infection in the inoculum. The monolayers were infected with ~20 PFU of SARS-CoV-2/Leiden0008. In the post infection treatment, the compound (or RDV) was added to the avicel overlay. Cells were incubated for 4 days at 37 °C before fixation and crystal violet staining.

Acknowledgements

The authors are grateful for funding from the European Research Council (ERC-2020-SyG-951231 Carbocentre, to GJD and HSO). GJD is funded by the Royal Society Ken Murray research Professorship. ZA thanks the NWO for support through the Veni grant: VI.Veni.212.173. CSB was supported by the Coordination for the Improvement of Higher Education Personnel (CAPES) (Process nr. 88881.171440/2018-01), Ministry of Education, Brazil.
Figure 1 was created with BioRender.com.

Supplementary Material

Supplementary material can be accessed in an online repository (figshare). Please find the (private) link to access it below:
https://figshare.com/s/fb980aa325353f631af7

References

1. Feng T, Zhang J, Chen Z, Pan W, Chen Z, Yan Y, Dai J. 2022. Glycosylation of viral proteins: Implication in virus–host interaction and virulence. Virulence 13:670-683.
2. O'Keefe S, Roebuck QP, Nakagome I, Hirono S, Kato A, Nash R, High S. 2019. Characterizing the selectivity of ER α-glucosidase inhibitors. Glycobiology 29:530-542.
3. Hebert DN, Foellmer B, Helenius A. 1995. Glucose trimming and reglucosylation determine glycoprotein association with calnexin in the endoplasmic reticulum. Cell 81:425-33.
4. Kostova Z, Wolf DH. 2003. For whom the bell tolls: protein quality control of the endoplasmic reticulum and the ubiquitin–proteasome connection. EMBO J. 22:2309-2317.
5. Gruters RA, Neefjes JJ, Tersmette M, de Goede RE, Tulp A, Huisman HG, Miedema F, Ploegh HL. 1987. Interference with HIV-induced syncytium formation and viral infectivity by inhibitors of trimming glucosidase. Nature 330:74-7.
6. Fuhrmann U, Bause E, Ploegh H. 1985. Inhibitors of oligosaccharide processing. Biochimica et Biophysica Acta (BBA) - Gene Structure and Expression 825:95-110.
7. Chang J, Block TM, Guo J-T. 2013. Antiviral therapies targeting host ER alpha-glucosidases: Current status and future directions. Antiviral Research 99:251-260.
8. Koshland Jr. DE. 1953. Stereochemistry and the mechanism of enzymatic reactions 28:416-436. Biological Reviews
9. Koshland DE. 1958. Application of a Theory of Enzyme Specificity to Protein Synthesis. Proc Natl Acad Sci U S A 44:98-104.
10. Walker BD, Kowalski M, Goh WC, Kozarsky K, Krieger M, Rosen C, Rohrschneider L, Haseltine WA, Sodroski J. 1987. Inhibition of human immunodeficiency virus syncytium formation and virus replication by castanospermine. Proc Natl Acad Sci U S A 84:8120-4.
11. Fleet GW, Karpas A, Dwek RA, Fellows LE, Tyms AS, Petursson S, Namgoong SK, Ramsden NG, Smith PW, Son JC, et al. 1988. Inhibition of HIV replication by amino-sugar derivatives. FEBS Lett 237:128-32.
12. Montagnier L, Clavel F, Krust B, Chamaret S, Rey F, Barré-Sinoussi F, Chermann JC. 1985. Identification and antigenicity of the major envelope glycoprotein of lymphadenopathy-associated virus. Virology 144:283-9.
13. Warfield KL, Barnard DL, Enterlein SG, Smee DF, Khaliq M, Sampath A, Callahan MV, Ramstedt U, Day CW. 2016. The Iminosugar UV-4 is a Broad Inhibitor of Influenza A and B Viruses ex Vivo and in Mice. Viruses 8:71.
14. Stavale EJ, Vu H, Sampath A, Ramstedt U, Warfield KL. 2015. In vivo therapeutic protection against influenza A (H1N1) oseltamivir-sensitive and resistant viruses by the iminosugar UV-4. PLoS One 10:e0121662.
15. Warfield KL, Alonzi DS, Hill JC, Caputo AT, Roversi P, Kiappes JL, Sheets N, Duchars M, Dwek RA, Biggins J, Barnard D, Shresta S, Treston AM, Zitzmann N. 2020. Targeting Endoplasmic Reticulum α-Glucosidase I with a Single-Dose Iminosugar Treatment Protects against Lethal Influenza and Dengue Virus Infections. J Med Chem 63:4205-4214.
16. Fukushi M, Yoshinaka Y, Matsuoka Y, Hatakeyama S, Ishizaka Y, Kirikae T, Sasazuki T, Miyoshi-Akiyama T. 2012. Monitoring of S Protein Maturation in the Endoplasmic Reticulum by Calnexin Is Important for the Infectivity of Severe Acute Respiratory Syndrome Coronavirus. J Virolog. 86:11745-11753.
17. Chang J, Warren TK, Zhao X, Gill T, Guo F, Wang L, Comunale MA, Du Y, Alonzi DS, Yu W, Ye H, Liu F, Guo J-T, Mehta A, Cuconati A, Butters TD, Bavari S, Xu X, Block TM. 2013. Small molecule inhibitors of ER α-glucosidases are active against multiple hemorrhagic fever viruses. Antiviral Research 98:432-440.

18. Perry ST, Buck MD, Plummer EM, Penmasta RA, Batra H, Stavale EJ, Warfield KL, Dwek RA, Butters TD, Alonzi DS, Lada SM, King K, Klose B, Ramstedt U, Shresta S. 2013. An iminosugar with potent inhibition of dengue virus infection in vivo. Antiviral Res 98:35-43.
19. Sadat MA, Moir S, Chun T-W, Lusso P, Kaplan G, Wolfe L, Memoli MJ, He M, Vega H, Kim LJY, Huang Y, Hussein N, Nievas E, Mitchell R, Garofalo M, Louie A, Ireland DC, Grunes C, Cimbro R, Patel V, Holzapfel G, Salahuddin D, Bristol T, Adams D, Marciano BE, Hegde M, Li Y, Calvo KR, Stoddard J, Justement JS, Jacques J, Long Priel DA, Murray D, Sun P, Kuhns DB, Boerkoel CF, Chiorini JA, Di Pasquale G, Verthelyi D, Rosenzweig SD. 2014. Glycosylation, Hypogammaglobulinemia, and Resistance to Viral Infections. N Engl J. Med 370:1615-1625.
20. Sung C, Wei Y, Watanabe S, Lee HS, Khoo YM, Fan L, Rathore AP, Chan KW, Choy MM, Kamaraj US, Sessions OM, Aw P, de Sessions PF, Lee B, Connolly JE, Hibberd ML, Vijaykrishna D, Wijaya L, Ooi EE, Low JG, Vasudevan SG. 2016. Extended Evaluation of Virological, Immunological and Pharmacokinetic Endpoints of CELADEN: A Randomized, Placebo-Controlled Trial of Celgosivir in Dengue Fever Patients. PLoS Negl Trop Dis 10:e0004851.
21. Durantel D. 2009. Celgosivir, an alpha-glucosidase I inhibitor for the potential treatment of HCV infection. Curr Opin Investig Drugs 10:860-70.
22. Clarke EC, Nofchissey RA, Ye C, Bradfute SB. 2021. The iminosugars celgosivir, castanospermine and UV-4 inhibit SARS-CoV-2 replication. Glycobiology 31:378-384.
23. Karade SS, Hill ML, Kiappes JL, Manne R, Aakula B, Zitzmann N, Warfield KL, Treston AM, Mariuzza RA. 2021. N-Substituted Valiolamine Derivatives as Potent Inhibitors of Endoplasmic Reticulum α-Glucosidases I and II with Antiviral Activity. Journal of Medicinal Chemistry
24. Ferjancic Z, Bihelovic F, Vulovic B, Matovic R, Trmcic M, Jankovic A, Pavlovic M, Djurkovic F, Prodanovic R, Djurdjevic Djelmas A, Kalicanin N, Zlatovic M, Sladic D, Vallet T, Vignuzzi M, Saicic RN. 2024. Development of iminosugar-based glycosidase inhibitors as drug candidates for SARS-CoV-2 virus via molecular modelling and in vitro studies. J Enzyme Inhib Med Chem 39:2289007.
25. Gong Y, Qin S, Dai L, Tian Z. 2021. The glycosylation in SARS-CoV-2 and its receptor ACE2. Signal Transduction and Targeted Therapy 6:396.
26. Grant OC, Montgomery D, Ito K, Woods RJ. 2020. Analysis of the SARS-CoV-2 spike protein glycan shield reveals implications for immune recognition. Sci Rep 10:14991.
27. Jackson CB, Farzan M, Chen B, Choe H. 2022. Mechanisms of SARS-CoV-2 entry into cells. Nature Reviews Molecular Cell Biology 23:3-20.
28. Bouwman KM, Tomris I, Turner HL, van der Woude R, Shamorkina TM, Bosman GP, Rockx B, Herfst S, Snijder J, Haagmans BL, Ward AB, Boons G-J, de Vries RP. 2021. Multimerization- and glycosylation-dependent receptor binding of SARS-CoV-2 spike proteins. PLOS Pathogens 17:e1009282.
29. Henderson R, Edwards RJ, Mansouri K, Janowska K, Stalls V, Kopp M, Haynes BF, Acharya P. 2020. Glycans on the SARS-CoV-2 Spike Control the Receptor Binding Domain Conformation. Preprint bioRxiv.
30. Huang H-C, Lai Y-J, Liao C-C, Wang F-Y, Huang K-B, Lee IJ, Chou W-C, Wang S-H, Wang L-H, Hsu J-M, Sun C-P, Kuo C-T, Wang J, Hsiao T-C, Yang P-J, Lee T-A, Huang W, Li F-A, Shen C-Y, Lin Y-L, Tao M-H, Li C-W. 2021. Targeting conserved N-glycosylation blocks SARS-CoV-2 variant infection in vitro. eBioMedicine 74:103712.
31. Casalino L, Gaieb Z, Goldsmith JA, Hjorth CK, Dommer AC, Harbison AM, Fogarty CA, Barros EP, Taylor BC, McLellan JS, Fadda E, Amaro RE. 2020. Beyond Shielding: The Roles of Glycans in the SARS-CoV-2 Spike Protein. ACS Cent Sci 6:1722-1734.
32. Casas-Sanchez A, Romero-Ramirez A, Hargreaves E, Ellis CC, Grajeda BI, Estevao IL, Patterson EI, Hughes GL, Almeida IC, Zech T, Acosta-Serrano Á. 2022. Inhibition of Protein N-Glycosylation Blocks SARS-CoV-2 Infection. mBio 13:e03718-21.

33. Watanabe S, Chan KW-K, Dow G, Ooi EE, Low JG, Vasudevan SG. 2016. Optimizing celgosivir therapy in mouse models of dengue virus infection of serotypes 1 and 2: The search for a window for potential therapeutic efficacy. Antiviral Research 127:10-19.
34. Roussel HM. 1996. A randomized, double-blind active-controlled, dose-ranging study of safety and efficacy of chronically administered MDL 28,574A in the treatment of HIV-infected patients. NLM identifier: NCT00002151.
35. Artola M, Wu L, Ferraz MJ, Kuo C-L, Raich L, Breen IZ, Offen WA, Codée JDC, van der Marel GA, Rovira C, Aerts JMFG, Davies GJ, Overkleeft HS. 2017. 1,6-Cyclophellitol Cyclosulfates: A New Class of Irreversible Glycosidase Inhibitor. ACS Central Science 3:784-793.
36. Schröder SP, Petracca R, Minnee H, Artola M, Aerts JMFG, Codée JDC, van der Marel GA, Overkleeft HS. 2016. A Divergent Synthesis of l-arabino- and d-xylo-Configured Cyclophellitol Epoxides and Aziridines. Eur. J. Org. Chem. 2016:4787-4794.
37. Jiang J, Artola M, Beenakker TJM, Schröder SP, Petracca R, de Boer C, Aerts JMFG, van der Marel GA, Codée JDC, Overkleeft HS. 2016. The Synthesis of Cyclophellitol-Aziridine and Its Configurational and Functional Isomers. Eur. J. Inorg. Chem. 2016:3671-3678.
38. Willems LI, Jiang J, Li K-Y, Witte MD, Kallemeijn WW, Beenakker TJN, Schröder SP, Aerts JMFG, van der Marel GA, Codée JDC, Overkleeft HS. 2014. From Covalent Glycosidase Inhibitors to Activity-Based Glycosidase Probes. Chem. Eur. J., 20:10864-10872.
39. de Boer C, McGregor NGS, Peterse E, Schröder SP, Florea BI, Jiang J, Reijngoud J, Ram AFJ, van Wezel GP, van der Marel GA, Codée JDC, Overkleeft HS, Davies GJ. 2020. Glycosylated cyclophellitol-derived activity-based probes and inhibitors for cellulases. RSC Chemical Biology 1:148-155.
40. Schröder SP, van de Sande JW, Kallemeijn WW, Kuo C-L, Artola M, van Rooden EJ, Jiang J, Beenakker TJM, Florea BI, Offen WA, Davies GJ, Minnaard AJ, Aerts JMFG, Codée JDC, van der Marel GA, Overkleeft HS. 2017. Towards broad spectrum activity-based glycosidase probes: synthesis and evaluation of deoxygenated cyclophellitol aziridines. Chemical Communications 53:12528-12531.
41. Wennekes T, Meijer AJ, Groen AK, Boot RG, Groener JE, van Eijk M, Ottenhoff R, Bijl N, Ghauharali K, Song H, O'Shea TJ, Liu H, Yew N, Copeland D, van den Berg RJ, van der Marel GA, Overkleeft HS, Aerts JM. 2010. Dual-Action Lipophilic Iminosugar Improves Glycemic Control in Obese Rodents by Reduction of Visceral Glycosphingolipids and Buffering of Carbohydrate Assimilation. Journal of Medicinal Chemistry 53:689-698.
42. Ghisaidoobe A, Bikker P, de Bruijn ACJ, Godschalk FD, Rogaar E, Guijt MC, Hagens P, Halma JM, van't Hart SM, Luitjens SB, van Rixel VHS, Wijzenbroek M, Zweegers T, Donker-Koopman WE, Strijland A, Boot R, van der Marel G, Overkleeft HS, Aerts JMFG, van den Berg RJBHN. 2011. Identification of Potent and Selective Glucosylceramide Synthase Inhibitors from a Library of N-Alkylated Iminosugars. ACS Medicinal Chemistry Letters 2:119-123.
43. Ghisaidoobe AT, van den Berg RJBHN, Butt SS, Strijland A, Donker-Koopman WE, Scheij S, van den Nieuwendijk AMCH, Koomen G-J, van Loevezijn A, Leemhuis M, Wennekes T, van der Stelt M, van der Marel GA, van Boeckel CAA, Aerts JMFG, Overkleeft HS. 2014. Identification and Development of Biphenyl Substituted Iminosugars as Improved Dual Glucosylceramide Synthase/Neutral Glucosylceramidase Inhibitors. Journal of Medicinal Chemistry 57:9096-9104.
44. Ficicioglu C. 2008. Review of miglustat for clinical management in Gaucher disease type 1. Ther Clin Risk Manag 4:425-31.
45. Kok K, Kuo C-L, Katzy RE, Lelieveld LT, Wu L, Roig-Zamboni V, van der Marel GA, Codée JDC, Sulzenbacher G, Davies GJ, Overkleeft HS, Aerts JMFG, Artola M. 2022. 1,6-epi-Cyclophellitol Cyclosulfamidate Is a Bona Fide Lysosomal α-Glucosidase Stabilizer for the Treatment of Pompe Disease. Journal of the American Chemical Society 144:14819-14827.

46. Ofman TP, Heming JJA, Nin-Hill A, Küllmer F, Steneker R, Klein A, Moran E, Bennett M, Ruijgrok G, Kok K, Armstrong ZWB, Aerts JMFG, van der Marel GA, Rovira C, Davies GJ, Artola M, Codée JDC, Overkleeft HS. 2024. Conformational and Electronic Variations in 1,2- and 1,6-Cyclophellitols and Their Impact on Retaining α-Glucosidase Inhibition. submitted to Chem Eur J.
47. Lahav D, Liu B, van den Berg RJBHN, van den Nieuwendijk AMCH, Wennekes T, Ghisaidoobe AT, Breen I, Ferraz MJ, Kuo C-L, Wu L, Geurink PP, Ovaa H, van der Marel GA, van der Stelt M, Boot RG, Davies GJ, Aerts JMFG, Overkleeft HS. 2017. A Fluorescence Polarization Activity-Based Protein Profiling Assay in the Discovery of Potent, Selective Inhibitors for Human Nonlysosomal Glucosylceramidase. Journal of the American Chemical Society 139:14192-14197.
48. Karade SS, Franco EJ, Rojas AC, Hanrahan KC, Kolesnikov A, Yu W, MacKerell AD, Jr., Hill DC, Weber DJ, Brown AN, Treston AM, Mariuzza RA. 2023. Structure-Based Design of Potent Iminosugar Inhibitors of Endoplasmic Reticulum α-Glucosidase I with Anti-SARS-CoV-2 Activity. Journal of Medicinal Chemistry 66:2744-2760.
49. Rajasekharan S, Milan Bonotto R, Nascimento Alves L, Kazungu Y, Poggianella M, Martinez-Orellana P, Skoko N, Polez S, Marcello A. 2021. Inhibitors of Protein Glycosylation Are Active against the Coronavirus Severe Acute Respiratory Syndrome Coronavirus SARS-CoV-2. Viruses 13.
50. Thaler M, Wang Y, van der Does AM, Faiz A, Ninaber DK, Ogando NS, Beckert H, Taube C, Salgado-Benvindo C, Snijder EJ, Bredenbeek PJ, Hiemstra PS, van Hemert MJ. 2023. Impact of Changes in Human Airway Epithelial Cellular Composition and Differentiation on SARS-CoV-2 Infection Biology. Journal of Innate Immunity 15:562-580.
51. Thaler M, Salgado-Benvindo C, Leijs A, Tas A, Ninaber DK, Arbiser JL, Snijder EJ, van Hemert MJ. 2023. R-Propranolol Has Broad-Spectrum Anti-Coronavirus Activity and Suppresses Factors Involved in Pathogenic Angiogenesis. Int J Mol Sci 24.
52. Jiang J, Kuo C-L, Wu L, Franke C, Kallemeijn WW, Florea BI, van Meel E, van der Marel GA, Codée JDC, Boot RG, Davies GJ, Overkleeft HS, Aerts JMFG. 2016. Detection of Active Mammalian GH31 α-Glucosidases in Health and Disease Using In-Class, Broad-Spectrum Activity-Based Probes. ACS Central Science 2:351-358.
53. Warfield KL, Plummer EM, Sayce AC, Alonzi DS, Tang W, Tyrrell BE, Hill ML, Caputo AT, Killingbeck SS, Beatty PR, Harris E, Iwaki R, Kinami K, Ide D, Kiappes JL, Kato A, Buck MD, King K, Eddy W, Khaliq M, Sampath A, Treston AM, Dwek RA, Enterlein SG, Miller JL, Zitzmann N, Ramstedt U, Shresta S. 2016. Inhibition of endoplasmic reticulum glucosidases is required for in vitro and in vivo dengue antiviral activity by the iminosugar UV-4. Antiviral Res 129:93-98.
54. Fukushi M, Yoshinaka Y, Matsuoka Y, Hatakeyama S, Ishizaka Y, Kirikae T, Sasazuki T, Miyoshi-Akiyama T. 2012. Monitoring of S protein maturation in the endoplasmic reticulum by calnexin is important for the infectivity of severe acute respiratory syndrome coronavirus. J Virol 86:11745-53.
55. Elstein D, Hollak C, Aerts JMFG, van Weely S, Maas M, Cox TM, Lachmann RH, Hrebicek M, Platt FM, Butters TD, Dwek RA, Zimran A. 2004. Sustained therapeutic effects of oral miglustat (Zavesca, N-butyldeoxynojirimycin, OGT 918) in type I Gaucher disease. J Inherit Metab Dis. 27:757-766.
56. Kiappes JL, Hill ML, Alonzi DS, Miller JL, Iwaki R, Sayce AC, Caputo AT, Kato A, Zitzmann N. 2018. ToP-DNJ, a Selective Inhibitor of Endoplasmic Reticulum α-Glucosidase II Exhibiting Antiflaviviral Activity. ACS Chem Biol 13:60-65.
57. Fiege L, Duran I, Marquardt T. 2023. Improved Enzyme Replacement Therapy with Cipaglucosidase Alfa/Miglustat in Infantile Pompe Disease. Pharmaceuticals (Basel) 16.

58. Salgado-Benvindo C, Leijs AA, Thaler M, Tas A, Arbiser JL, Snijder EJ, van Hemert MJ. 2023. Honokiol Inhibits SARS-CoV-2 Replication in Cell Culture at a Post-Entry Step. Microbiol Spectr 11:e0327322.
59. Salgado-Benvindo C, Tas A, Zevenhoven-Dobbe JC, van der Meer Y, Sidorov IA, Leijs AA, Gelderloos AT, van Kasteren PB, Snijder EJ, van Hemert MJ. 2024. Characterization of SARS-CoV-2 replication in human H1299/ACE2 cells: a versatile and practical infection model for antiviral research and beyond. submitted to Antiviral Research
60. Ninaber DK, van der Does AM, Hiemstra PS. 2023. Isolating Bronchial Epithelial Cells from Resected Lung Tissue for Biobanking and Establishing Well-Differentiated Air-Liquid Interface Cultures. J Vis Exp.
61. Drosten C, Günther S, Preiser W, Van Der Werf S, Brodt H-R, Becker S, Rabenau H, Panning M, Kolesnikova L, Fouchier RA. 2003. Identification of a novel coronavirus in patients with severe acute respiratory syndrome. New England journal of medicine 348:1967-1976.
62. Kovacikova K, Morren BM, Tas A, Albulescu IC, van Rijswijk R, Jarhad DB, Shin YS, Jang MH, Kim G, Lee HW, Jeong LS, Snijder EJ, van Hemert MJ. 2020. 6'-β-Fluoro-Homoaristeromycin and 6'-Fluoro-Homoneplanocin A Are Potent Inhibitors of Chikungunya Virus Replication through Their Direct Effect on Viral Nonstructural Protein 1. Antimicrob Agents Chemother 64.
63. Vaux D, Tooze J, Fuller S. 1990. Identification by anti-idiotype antibodies of an intracellular membrane protein that recognizes a mammalian endoplasmic reticulum retention signal. Nature 345:495-502.
64. Salgado-Benvindo C, Thaler M, Tas A, Ogando NS, Bredenbeek PJ, Ninaber DK, Wang Y, Hiemstra PS, Snijder EJ, van Hemert MJ. 2020. Suramin Inhibits SARS-CoV-2 Infection in Cell Culture by Interfering with Early Steps of the Replication Cycle. Antimicrob Agents Chemother 64.
65. Corman VM, Landt O, Kaiser M, Molenkamp R, Meijer A, Chu DK, Bleicker T, Brunink S, Schneider J, Schmidt ML, Mulders DG, Haagmans BL, van der Veer B, van den Brink S, Wijsman L, Goderski G, Romette JL, Ellis J, Zambon M, Peiris M, Goossens H, Reusken C, Koopmans MP, Drosten C. 2020. Detection of 2019 novel coronavirus (2019-nCoV) by real-time RT-PCR. Euro Surveill 25.

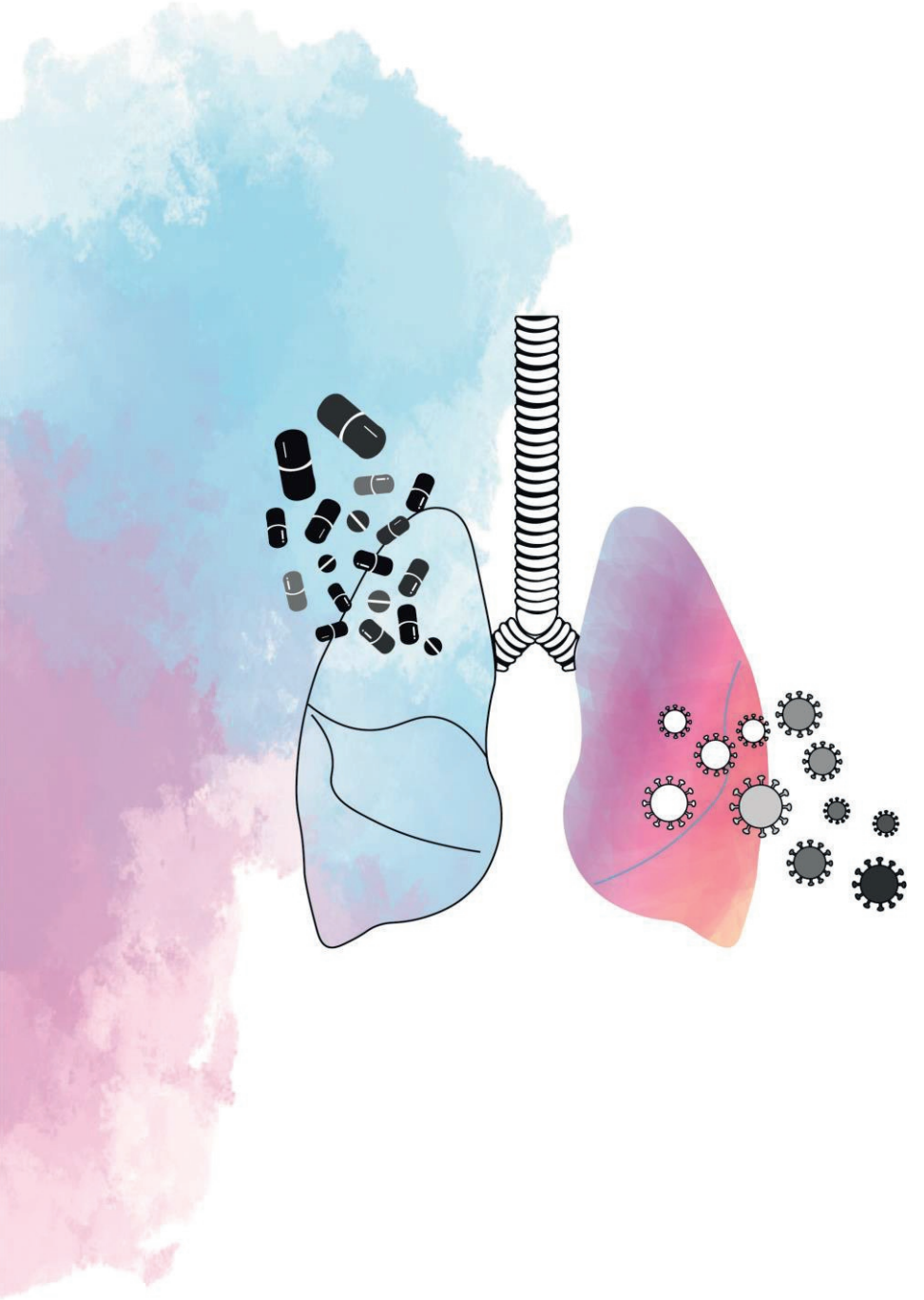

Chapter 6

Summary and General Discussion

Introduction

December 2019 marked the beginning of an unprecedented pandemic, with an enormous impact on health, society and economy worldwide. During the next four years, intensive research efforts have enhanced our understanding of many aspects of SARS-CoV-2 replication, pathogenicity and epidemiology, contributing to the rapid development of effective vaccines and antiviral drugs. Undoubtedly, decades of prior research on coronaviruses helped to understand and combat SARS-CoV-2 at such an unprecedented speed. Still, there are many aspects of SARS-CoV-2 and its associated disease COVID-19 that are not fully understood. Many healthy individuals will experience asymptomatic infections (1-3). If symptoms occur, they are primarily of a respiratory nature and can range from mild to severe, resulting in life-threatening pneumonia in a fraction of patients (4). However, the virus can also cause damage to other organs, like the cardiovascular, gastrointestinal, or nervous system, rendering COVID-19 a multisystemic disease. COVID-19 is unique in that it can cause acute olfactory dysfunction (anosmia), a loss of smell or taste that occurs more frequently than reported for other viruses, with the underlying mechanism remaining unclear (5, 6). Another phenomenon that is not fully understood, is post-COVID syndrome (also known as “long COVID”), a term used to describe a plethora of possibly debilitating symptoms that persist or arise after the acute infection, and can last for months or years. The development of post-COVID syndrome is associated with all disease severity, ages or vaccination status (7-10). Although the rapid development of vaccines and antiviral therapies was successful and helped to curb the pandemic, SARS-CoV-2 has now become endemic in the human population, with new variants continuously evolving (11) and causing periodic spikes in infection rates (12). Although the World Health Organization has declared the pandemic no longer a public health emergency, the evolution of SARS-CoV-2 and the emergence of new variants with possible changes in virulence continues to be monitored (12, 13). Omicron descendants, which are now, in early 2024, the dominant circulating strains, have increased transmission fitness (14, 15), changed their cell entry routes compared to early pandemic variants (16), and also cause olfactory dysfunction less frequently (17). New variants also show some level of evasion to natural or vaccine-induced immunity against earlier variants (16, 18, 19). In response, vaccines were updated (20). Continuous monitoring of SARS-CoV-2 evolution, as well as research and surveillance to detect zoonotic transmission of novel coronaviruses from their abundant animal reservoirs, will be crucial to detect new threats early on. While vaccines are efficient in curbing an outbreak of a known virus or new virus variants, by protecting a naïve population or reducing reinfections, their development takes time, and the demand for safe and effective antiviral drugs remains, for prophylaxis or treatment of early patients. Particularly broad-

spectrum antivirals would enable a faster response to combat (re-) emerging viruses, especially in an outbreak situation. Ideally, they would be stockpiled and made available quickly in the early phase of an outbreak. When vaccines are not yet available, such drugs could also be used prophylactically pre- or post-exposure. Furthermore, with COVID-19, patients often present with serious symptoms rather late, so there is not only a need for drugs that directly inhibit virus replication, but also for therapeutics that target the (pathogenic) host responses to infection, as well as treat post-COVID syndrome. One major challenge of all antiviral therapeutic approaches is the translation of drug efficacy and safety in preclinical models into clinical development. The use of advanced human cell culture models, that are more biologically relevant than immortalized cells and recapitulate the human tissue complexity, can help overcome this limitation.

The research projects described in this thesis, aimed to contribute to combatting SARS-CoV-2, and to increase our preparedness for the next emerging coronavirus. Besides screening for antiviral compounds, SARS-CoV-2 infection was characterized in an advanced infection model of human primary airway epithelial cells cultured at the air-liquid interface (HAE-ALI), aiming to better understand infection biology, epithelial host responses and the effect of antiviral drugs. Furthermore, SARS-CoV-2 and other coronavirus infections of HAE-ALI cultures revealed differences in host responses to high- and low-pathogenic coronaviruses.

Understanding coronaviruses through studying infection of advanced cell culture models (Chapters 2 and 3)

At the start of the SARS-CoV-2 pandemic, many researchers rushed to develop cell culture models in order to culture the virus and study its replication. Initially, the Vero E6 cell line was often used for studying SARS-CoV-2 and antiviral drug testing, but later the use of these cells was found to have some specific drawbacks. Besides the fact that they are African green monkey kidney cells and not representative of the human lung epithelium, they do not elicit an interferon immune response (21) and express high levels of an efflux transporter protein, which leads to increased cellular export of molecules like antiviral compounds, thus potentially obscuring efficacious compounds (22). The latter can be avoided by adding efflux inhibitors to the cell culture medium. Another disadvantage of using Vero E6 cells is the rapid acquisition of adaptive changes in the S protein of SARS-CoV-2. The SARS-CoV-2 S protein contains a furin cleavage site between the S1 and S2 domains, which plays a role in the high infection efficiency of SARS-CoV-2 (23). Upon passaging of (early pandemic variants of) SARS-CoV-2 in Vero E6 cells, several research groups reported that SARS-CoV-2 lost the furin cleavage site, resulting in drastic phenotypic changes (24, 25)

that improved viral fitness in Vero E6 cells, but reduced pathogenic properties *in vivo* (26). This is only one example that emphasizes that the choice of the right cell culture system for propagating and studying SARS-CoV-2 is crucial (24). Cell lines and organoids representing the liver, intestinal system, heart, brain, or kidney, have also been used (27-29), which might be relevant to study the implications of SARS-CoV-2 infections outside the respiratory tract. As the respiratory system is the entry point and primary target organ for SARS-CoV-2, the availability of *in vitro* infection models that represent the lung epithelium was crucial. Most frequently, conventional cell culture was used, with immortalized lung cell lines, like cancer-derived Calu-3 cell lines, immortalized human bronchial epithelial cells (30), or cell lines that are non-permissive but were modified to express higher levels of ACE2, like A549 or H1299 lung cancer-derived cells (31). More advanced cell culture infection models like human primary airway epithelial cells, cultured at the air-liquid interface (HAE-ALI), and organoids were also developed. Additionally, there are advances in the development and use of precision-cut lung slices or lung-on-a-chip models (32) that add further relevant infection models to the SARS-CoV-2 toolbox. The use of such advanced cell culture models has clear ethical and economic advantages over the use of animal models, and working with them is also less labour intensive and faster (33). At the same time, advanced models that use primary human epithelial cells better recapitulate the lung epithelium and the human tissue complexity (34), as opposed to monocellular laboratory-adapted immortalized or tumour cell lines.

Chapter 2 describes the characterization and optimization of SARS-CoV-2 infection in in-house produced ALI cultures of well-differentiated HAE cells. Using donor cells isolated from different anatomical locations, we found that ALI cultures of bronchial cells displayed increased SARS-CoV-2 infection compared to cultures of tracheal origin. The trachea and bronchi are at the beginning of the lower respiratory tract and contain similar cell types, mainly ciliated, goblet, club, and basal cells (35). Others have also found differences in infection based on the location in the respiratory system. Human nasal epithelial cells and upper airway cells *in vitro* were reported to be more permissive to infection than lower airway cells (36). High levels of virus replication in the upper airway could be linked to transmission efficiency, while high infection rates in the distal airway region of the alveoli is associated with severe disease symptoms and lung tissue damage, which was shown in non-human primate models as well as in deceased patients (37, 38). Single-cell sequencing data also revealed that a hyperinflammatory phenotype was enhanced in the bronchi compared to the nasopharynx (39). The difference in susceptibility between airway regions can be explained by the presence of susceptible cells containing the virus entry receptor and other co-factors. Ciliated cells, but also goblet or club cells are the main target cells of SARS-CoV-2 (40-43), as confirmed by our studies described in **Chapter 2**. Recently, a study analyzing

lung tissue from deceased patients with acute infection also confirmed ciliated cells as the main target cell type in the bronchial epithelium (38). Accordingly, our bronchial epithelial cell cultures, in which we observed higher viral infection, contained more ciliated cells than the cultures using cells derived from the trachea. A longer culture time also changed the cellular composition towards the presence of more susceptible cells and our transcriptome analysis revealed an increase in TMPRSS2 and CTSL expression, both host proteases facilitating virus entry into the cell, and expressed on ciliated cells (44). They are also both targets of antiviral drugs currently investigated for SARS-CoV-2 (**Table 1**). Besides the influence of the presence of ciliated cells (and virus entry factors) on viral infection, our study indicates a complex interplay of factors, in which the presence of goblet cells plays a role, as treatment with a γ-secretase inhibitor (DAPT), which shifts the epithelial differentiation entirely toward ciliated cells, did not increase virus replication compared to untreated cells. IL-13 treatment skewed differentiation towards more goblet cells, but with ciliated cells still present, resulting in (slightly) higher levels of infection compared to untreated cultures. Despite ciliated cells being the main target, there might be other factors in play, like the presence of the mucus that is secreted by goblet cells (45). Contrary to our results, one study showed a reduction in virus replication after IL-13 treatment (46), but in that study cell cultures were only treated for 48 hours, while our cultures were treated for two weeks to achieve differences in the cellular composition of the epithelium. Another study showed the upregulation of TMPRSS2 and downregulation of ACE2 expression by IL-13, however, this study focused on a different airway location, i.e. the nasal epithelium of children (47). Furthermore, that study and others also showed that ACE2 is an infection-mediated interferon-upregulated gene, which highlights the impact of virus infection itself on the expression of pro-viral factors like ACE2 and susceptibility of the epithelium (39). Allergic asthma, a disease associated with IL-13-induced changes in epithelial cell composition, was suggested to leave patients more vulnerable to a severe COVID-19 outcome, although reports are not always concordant (48, 49). Also chronic obstructive pulmonary disease (COPD) induces altered epithelial cellular composition, and was found to be a risk factor for severe COVID-19 (50). Our findings, that changes in epithelium cell composition (especially with ciliated and goblet cells of the mucociliary system) can impact the susceptibility to SARS-CoV-2, therefore could have implications for the disease outcome in patients with chronic lung diseases. Knowledge about the susceptibility of cells and the kinetics of virus replication and spread is important to understand virus transmission, pathogenesis, and evolution. A recent study showed that the SARS-CoV-2 variant Omicron BA.5, compared to its predecessors Omicron BA.1 and BA.2, more efficiently enters human lung cells and replicates better in the upper and lower respiratory tract of animal models (51). This indicates that it is not certain that continued subvariant evolution will only lead

to viruses that are less pathogenic, and that studying the replication kinetics and properties of new variants in advanced infection models remains crucial, to monitor risks.

To decipher the factors that determine replication kinetics and virulence, comparative studies (in advanced infection models) of different coronaviruses can provide valuable information. SARS-CoV and MERS-CoV are both highly pathogenic, but they use different cell-entry factors (52, 53), which can affect host cell tropism. A common cold coronavirus (NL63), causing only mild respiratory symptoms, utilizes the same ACE2 receptor (54) as the highly pathogenic SARS-CoV and SARS-CoV-2. This demonstrates that the determinants of pathogenicity are more complex than receptor use/cell tropism alone. Therefore, comparisons of host cell responses to high- and low-pathogenic coronaviruses in relevant infection models can help to understand the host and viral factors that truly play a role in pathogenesis.

Chapter 3 describes the differences in the host transcriptional response of HAE-ALI cultures to various coronaviruses. Although SARS-CoV-2 has been intensively studied since the start of the pandemic, only a limited number of comparative studies was done to learn from the differences and similarities between this pandemic virus and other human coronaviruses (55-60). One study utilized nasal epithelial cells cultured at the ALI and focussed on the infection kinetics and cell tropism of pathogenic and common cold coronaviruses, but did not investigate host responses (55). Some studies identified transcriptome changes induced by infection with pathogenic coronaviruses, but did not include common cold viruses (56, 57, 59), or combined already available datasets from different studies (57, 60). One of these studies employed a meta-analysis of available datasets for SARS-CoV and MERS-CoV from different studies (that used different cell culture models) and utilized the Calu-3 lung cancer cell line to compare differentially expressed genes in SARS-CoV, MERS-CoV and SARS-CoV-2 infections, but did not find major differences (57). Based on their analyses of common dysregulated pathways, they also performed a screen for potential drugs. In another study, analysis of the global transcriptomes of the cell lines Calu-3 and A549hACE2, infected with SARS-CoV-2, showed varying responses, underlining the impact of the choice of cell culture model on experimental results (61). Another study employed a biologically more relevant cell line of primary human lung epithelial cells and found differences in the responses to MERS-CoV and SARS-CoV-2 infection, mainly concerning immune-response-related genes. The study also reported an increased number of differentially expressed genes in MERS-CoV-infected cells compared to cells infected with SARS-CoV-2 (56).

In our study, we directly compared different high- and low-pathogenic coronaviruses side-by-side in the same advanced infection model, as the HAE-ALI cultures are susceptible to all human coronaviruses (**Chapter 3**). Our study corroborated the previously reported suppression or delay of an interferon response in cells infected with pathogenic

coronaviruses (61-63), but not with common cold coronaviruses (64), which highlights the relevance of the HAE-ALI cultures as a model for the *in vivo* situation. Interferon lambda (IFN-λ) was significantly higher expressed in cultures infected with HCoV-229E and HCoV-OC43, compared to highly pathogenic coronaviruses. Mucosal epithelial cells produce predominantly IFN-λ, which plays a crucial role in the antiviral defence against infections (65). IFN-λ treatment of HAE-ALI infected with SARS-CoV-2 led to a reduction in virus replication, confirming that suppression of interferon responses by pathogenic coronaviruses like SARS-CoV-2 favours their replication. The observation of decreased IFN-λ in critically-ill COVID-19 patients, and beneficial effects of treatment with pegylated IFN-λ in a mouse model (66) and in clinical trials (67, 68), supports this observation (69). We further identified differences in the transcriptional host response to infection with SARS-CoV-2 compared to the other coronaviruses SARS-CoV, MERS-CoV and HCoV-229E. Specifically, for SARS-CoV-2, we observed the down-regulation of a set of immediate early response genes related to the JNK/AP-1 pathway and NR4A1 expression. The results from our experimental infections were further supported by analysing available datasets from experimental and clinical studies (70-74). The AP-1 transcription factor, for example, regulates a range of cellular processes associated with apoptosis or inflammatory responses and was previously reported to be activated by SARS-CoV and HCoV-229E (75, 76). The role of NR4A1 in coronavirus biology has remained mostly unexplored so far. This protein is a master regulator of the stress response, is involved in regulating apoptosis and inflammation, and is associated with the immediate early response genes (77, 78). Suppression of the activity of this protein and associated pathways by SARS-CoV-2 may benefit the virus by evading innate immunity or other host responses, and may prevent the host cells from keeping early replication in check. The complexity of the JNK/AP-1 pathway, the exact implications of its up- or downregulation and its role in viral infection require further in-depth studies. For example, it remains to be investigated if the observed downregulation of the transcription factors is directly mediated by SARS-CoV-2 infection, and, if yes, which viral protein(s) is responsible. Proteomics studies could be used to validate our transcriptomics results and provide more information on how the observed changes in the transcriptome translate into changes in protein expression or modulation of pathways. Although we could confirm that the results from our *in vitro* (transcriptomics) studies were in line with clinical datasets, the question remains if and how these transcriptional changes play a role in pathogenesis *in vivo*. Despite the fact that we did not elucidate the exact role of NR4A1 in coronavirus replication, it appears an interesting target for follow-up studies and possibly for therapeutic strategies, as we found that an NR4A1 antagonist reduced replication of SARS-CoV-2 and MERS-CoV. This emphasizes the significance of studying

coronavirus biology to identify new potential host targets for the advancement of drug development.

Targeting coronaviruses through host-directed antiviral strategies (Chapters 4 and 5)

With the SARS-CoV-2 pandemic, there was a surge in antiviral drug discovery efforts, as scientists and clinicians raced to combat the virus and its associated disease, utilizing repurposing strategies as well as the development of new drugs. As mentioned in **Chapter 1**, currently there are only four drug therapies approved to treat COVID-19 in Europe (additionally, molnupiravir has still EUA by the FDA). Two of these are the direct-acting inhibitors of virus replication ritonavir-boosted nirmatrelvir (Paxlovid) and remdesivir (Veklury) (79, 80). The other two approved therapies concern the host-directed tocilizumab (IL-6 receptor antagonist) and baricitinib (JAK kinase inhibitor), which modulate the innate immune response and suppress a hyperinflammatory response (81-83). Approved anti-SARS-CoV-2 monoclonal antibodies, that target the S protein, are conditionally recommended or not authorized, as the dominant Omicron subvariants are not expected to be susceptible (84-86). Furthermore, other immunomodulatory drugs, like the corticosteroid dexamethasone, were found to reduce mortality by inhibiting hyperinflammation in critically-ill patients (87, 88). Therefore, host-directed strategies have been successful in tackling COVID-19 pathogenesis. So far, there are no host-directed antivirals (HDAs) that inhibit SARS-CoV-2 replication, although efforts to identify them are ongoing, as described below. HDAs that target host factors that are important for the replication of various (corona)viruses are especially interesting antiviral drug candidates as they have the potential to have broad-spectrum antiviral activity and thus would be beneficial to combat a newly emerging virus in an outbreak situation. **Chapters 4 and 5** describe two different classes of host-directed antiviral molecules, which both efficiently reduce the replication of SARS-CoV-2 and other coronaviruses.

Chapter 4 describes propranolol, a drug that is approved for various medical conditions, including cardiovascular problems and hemangioma, which is a benign tumor that develops through dysregulated blood vessel formation (89, 90). Propranolol is a mix of two stereoisomers, R- and S-Propranolol. R-propranolol was reported to lack the beta-blocker activity of its S-stereoisomer and therefore might induce fewer side effects in patients (91), which is why we investigated R-propranolol. We initially evaluated R-propranolol for its ability to inhibit proangiogenic (transcription) factors, reported in the context of hemangioma research (91), because the list of pathologies described for COVID-19 includes

vascular disease, associated with endothelial dysfunction and pathological angiogenesis in the lungs of patients (92). In a recent study, increased expression of biomarkers involved in angiogenesis was observed in COVID-19 patients, compared to influenza patients or control groups (93). Factors like vascular endothelial growth factor (VEGF), VEGF receptor 1, matrix metalloproteinase 2 (MMP-2), hypoxia-inducible factor 1 α (HIF-1α), angiopoietin 2 (Ang-2), TGF-β, angiopoietin-like proteins, and others are mentioned as biomarkers in COVID-19. Another proangiogenic factor, angiopoietin like 4 (ANGPLT4), is described in the literature as a key player in angiogenesis, often with a detrimental role in respiratory virus infections like Influenza (94). Very recently, increased plasma concentrations of ANGPTL4 in COVID-19 patients were correlated with an increased rate of ARDS and mortality (95). In our project, using Hulec-5a human lung endothelial cells, we confirmed increased expression of *angptl4*, when we mimicked the endothelium-epithelium environment during infection. We did so by treatment of Hulec-5a with conditioned medium from Calu-3 lung epithelial cells, as Hulec-5a are not susceptible to SARS-CoV-2 infection (96). Another study utilized a more advanced setup of alveolar epithelial cells at the ALI with endothelial cells co-cultured on the other side of the membrane (96), a design that represents the epithelial-endothelial crosstalk even better. Treatment of Hulec-5a cells, which were chemically induced to express *angptl4*, with R-propranolol led to a reduction of *angptl4* expression compared to untreated cells, confirming the anti-angiogenic properties of R-propranolol (91). Besides the suppression of the proangiogenic factor, we also discovered an antiviral effect of R-Propranolol, which we observed also in experiments with SARS-CoV, MERS-CoV, and the SARS-CoV-2 variants delta and omicron. Prior to this project, only some clinical evidence of a potential antiviral effect of propranolol had been published, suggesting activity against herpes simplex or influenza virus (97). Confirmation of a potential broad-spectrum activity of R-propranolol would need further evaluation in clinical studies. Another study, which is available as preprint, observed antiviral activity of propranolol against SARS-CoV-2, mouse hepatitis virus, Dengue virus, and Zika virus, and suggested that the compound affects replication complex formation through an effect on phospholipid synthesis (98). Propranolol also has an effect on various other host factors and signalling pathways, including inhibition of the RAS/RAF/ERK and AKT pathways (99, 100). Inhibition of factors involved in these signalling pathways was also shown to affect SARS-CoV-2 replication (101). Propranolol was also suggested to have immunomodulatory effects, although through its effect on the sympathetic nerve system by beta-blocker activity (102). Due to R-propranolol's (potential) broad-spectrum antiviral activity it is likely that propranolol exerts its antiviral activity through targeting host factors that play a role in virus infection, but more in-depth research is required to elucidate the underlying mechanisms, and to establish if there are multiple angles of activity and if this depends on the virus. RNA sequencing

analysis of host transcriptional changes could be a starting point for further investigation. The dual-activity of R-propranolol to act as potent (broad-spectrum) antiviral and possibly limit proangiogenic responses, which could play a role in reducing lung pathology in COVID-19 patients or those suffering from other serious respiratory virus infections, makes it an interesting candidate to investigate further and elucidate the mode of actions. In an ideal situation, certain risk groups of patients could be tested for biomarkers, like those for pathogenic angiogenesis, to predict the severity of the disease, allowing the early initiation of appropriate (preventative) treatment. The suitability of the use of such biomarkers is currently being assessed (103) and drugs to prevent endothelial dysfunction through anti-angiogenic action, like the VEGF inhibitor bevacizumab, are being evaluated for the treatment of COVID-19 lung pathologies in clinical trials (104). In our project, it would have contributed additional supportive information to also evaluate the effect of R-propranolol on VEGF for comparison with bevacizumab. Furthermore, future studies will need to address the effect of R-propranolol in more advanced models (organoids or *in vivo*), to recapitulate the pathogenesis of angiogenesis and see if the compound has a therapeutic effect on exacerbated endothelial dysfunction. Finally, existing pharmacological knowledge of propranolol and its two stereoisomers could aid in the development of R-propranolol as a repurposed antiviral drug.

Chapter 5 describes another class of host-directed antiviral compounds: glucosidase inhibitors. SARS-CoV-2, like other viruses, uses the host machinery for post-translational modifications of their proteins, including glycan processing in the endoplasmic reticulum (ER), which is involved in proper protein folding (105, 106). The surface of the most prominent SARS-CoV-2 structural protein, the Spike (S) protein, is covered with N-glycans, which are important for protein stability and function (107, 108). Using small molecule drugs, which inhibit α-glucosidase enzymes I and II in the ER (ER α-Glu I/II), prevents the production of viral glycoproteins and blocks replication of viruses that rely on the ER-protein quality control (105). Decades of research on iminosugars, a class of glucosidase inhibitors, reported the inhibition of a number of viruses (109-112), including most recently SARS-CoV-2 (113-115), however none have proceeded beyond phase II clinical trials as antivirals (116, 117). We screened a collection of iminosugars and another class of glucosidase inhibitors, cyclitols. We identified 1,6-*epi*-cyclophellitol cyclosulfate as the most potent and selective inhibitor of ER a-Glu II (118), and with the highest antiviral activity against SARS-CoV-2. Selective inhibition of ER a-Glu II by 1,6-*epi*-cyclophellitol cyclosulfate prevents the production of SARS-CoV-2 infectious virus particles through blocking of S protein N-glycosylation, and not through blocking of viral entry into the host cell or replication of the viral genome. Compared to the selective activity of 1,6-*epi*-cyclophellitol cyclosulfate against ER a-Glu II (with the lysosomal retaining a-glucosidase, GAA reported as the only off-

target effect) (118), iminosugars also target ER-α Glu I and other human glycoprocessing enzymes (119, 120), possibly leading to adverse effects. For example, for Hepatitis A virus infection, treatment with iminosugars was suggested to enhance virus entry, through inhibition of β-glucosidases which interferes with ganglioside degradation (121). Notably, it would add to our study to have an enzyme activity assay to assess the specific inhibition of ER α-Glu I by the compounds and confirm ER α-Glu II-selectivity of 1,6-*epi*-cyclophellitol cyclosulfate. Furthermore, as reported in a phase II clinical trial with an iminosugar compound (122), toxicity has to be evaluated in long term treatment. In that study, there was no concern about short term or emergency treatment, as the concentrations that are necessary for antiviral activity, appear to affect viral glycoproteins more than cellular glycoproteins. Also in our study, we did not observe toxicity, even at high concentrations of compounds used, that is, at least in short term treatment *in vitro*. Furthermore, we observe a potency limitation for 1,6-epi-cyclophellitol cyclosulfate, i.e. the antiviral activity reaches a plateau when higher concentrations of compound are used. The maximum antiviral effect is already reached at 0.5 µM, a concentration at which also an almost full inhibition of ER α-glucosidase II activity was observed. This could be a result of proteins escaping the glucosidase machinery in the ER through an endo-mannosidase dependent mechanism that acts in the Golgi (123, 124). Mechanistically, this escape route may account for the inability of glucosidase inhibitors to completely inhibit viral glycoprotein production. Further studies should determine whether other enzymes can complement the inhibition of ER α-glucosidase II. In one study combination of glucosidase I/II inhibitor and endo-mannosidase inhibitor indeed reduced virus replication (124). Glucosidase inhibitors in general do not exert activity in the initial infection, but are effective at reducing spread and therefore have potential as drug candidates that can be used later in infection, or used in combination therapy with other antivirals. Their broad-spectrum activity against various viruses make them interesting candidates in HDA strategies that could be employed during an outbreak with a new virus when urgent treatment options are needed. The selective blocking of ER α-Glu II, linked to potent antiviral activity, presents a new strategy in the search for effective antiviral compounds targeting SARS-CoV-2 and other viruses that rely on ER-protein quality control for replication.

Importance of advanced cell culture models in drug research

Animal-free models are increasingly implemented in (bio)medical research, driven by ethical concerns, advancements in innovations and increased funding support. To optimize the evaluation of drug candidates and shorten the way from pre-clinical research to clinical

trials, the use of the right *in vitro* cell culture model is crucial. Besides ethical advantages, animal-free drug-testing models cost less and are less labour-intensive, thus saving time and manpower. Compared to the use of animal models, studying new drugs in a system that closely mimics the human tissue complexity and physiology might even be more reliable in predicting human responses. Organoids, organ-on-chip models, or ALI cultures derived from primary human cells better mimic the characteristics of infections *in vivo*, host responses, or drug effects compared to some conventional cell culture models, based on the use of immortalized or cancer-derived cell lines and lacking tissue complexity (34, 70, 125). Currently, tests in animal models are still required before moving therapies or vaccinations into clinical trials with humans, but innovation in animal-free science moves fast. Only in 1998, scientists were able to isolate and culture human embryonic stem cells for the first time, and later, in 2007, induced pluripotent stem cell research followed, which really started 3D organoid research (126). Since then 3D models using human cells have become a standard tool in many fields like infectious disease modelling and drug discovery, to evaluate the efficacy and toxicity of a drug (127). One study reported on an extensive high-throughput drug screen in lung and colonic organoids (128). Recently, another study evaluated the efficacy and toxicity of reference antiviral drugs, which either succeeded or failed in late stage clinical trials, in human small intestine organoids and showed the reliability of the organoid model (129). In 2010, the first lung-on-chip model was described (130). Organ-on-chip models include microfluidics, allowing for a continuous exchange of used and fresh culture medium and nutrients, or introducing mechanical stimulation, like stretching in the case of simulation of the lung epithelium (131). A lung-on-chip model constituting epithelium and endothelium could successfully be infected by SARS-CoV-2 and used for treatment with an IL-6 receptor antagonist (132). Most frequently used in SARS-CoV-2 research and preclinical drug discovery were primary human airway epithelial cells that are differentiated at the air-liquid interface (HAE-ALI). These cultures are more accessible and less elaborate than organ-on-chip models, while recapitulating the pseudostratified epithelium of the human lung (133). Technological advances, like bioprinting, will automate the generation of such cultures in a reproducible and high-throughput fashion (134). Like organ-on-chip models, HAE-ALI cultures also provide the option of adding endothelial cells or immune cells, thus moving closer to simulating human tissue complexity (96, 135). Other advantages of using advanced lung cell culture models are that the number of experimental animals can be reduced, and that more relevant research results can be obtained with better reliability in predicting human responses. One study reviewed molecular screens of host factors that are important for coronavirus infection and reported high variability in the findings when different cell lines were used (136). Especially, results obtained with the often used Vero E6 cells do not always translate

to the situation in the lung epithelium *in vivo*. Chloroquine, ivermectin, or favipiravir are examples of repurposed drugs that showed promising results when tested on Vero cells (137) but had no benefits for patients suffering from COVID-19 (138-140). Later it was shown that these drugs do not protect human lung cells from SARS-CoV-2 infection (138, 141, 142). The same scenario occurred for the tyrosine kinase inhibitor imatinib (143). This illustrates the importance of using appropriate cell culture models for antiviral drug screening, or additional evaluation in preferably primary human cells, already at the stage of pre-clinical research, to decrease the resources and development time and also shorten the time until failure (**Figure 1**). Using primary human cell models therefore bridges the gap between *in vitro* and *in vivo* studies; especially now that the FDA Modernization Act 2.0 permits incorporation of results from pre-clinical *in vitro* studies and allows alternatives to animal testing (144, 145). These regulatory changes, alongside the development of advanced human cell culture models *in vitro*, are changing the landscape of drug development. Although the final evaluation of drug candidates still needs to be done in human clinical trials, the use of advanced cell culture models can shorten the way from pre-clinical to clinical development and increase the probability of success.

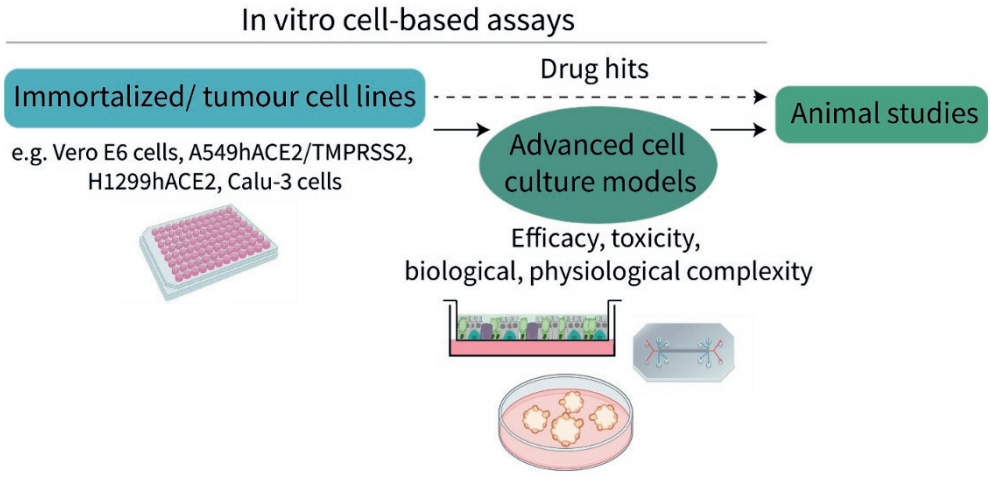

Figure 1: Advanced cell culture models for infection and drug testing, that recapitulate human tissue complexity and provide reliable predictive data on drug efficacy and toxicity have an important role in increasing efficiency in the drug development pipeline, by increasing the success rate of a drug to progress from the pre-clinical to the clinical phase. These models will also aid in reducing the number of animal experiments.

Current and future landscape in SARS-CoV-2 host-directed antiviral drug development

Many factors have to be taken into account in the context of antiviral drug development, both for the assessment of repurposed drugs and the development of new potential therapies. The whole drug development pipeline is time-consuming and cost-intensive (146). That is why the idea of repurposing already studied or approved drugs is appealing, especially in the context of a new outbreak, where time is crucial. The use of artificial intelligence (AI) will accelerate drug discovery, as it can scale up the target and hit identification process (147). Lead optimization efforts benefit from the information that AI-based models can predict, which can for example be pharmacokinetic (adsorption, distribution, metabolism, excretion) or toxicity properties (148). AI tools can further be used for the prediction of synergistic drug combinations. Of course, new technology also creates new challenges. The combination of new technologies like AI with human expertise is crucial, to assure input of good-quality, standardized data and confidence in interpreting results. In recent years, advances in AI made it possible for pharmaceutical companies and university research laboratories to collaborate and share their data about small-molecule drugs to enable more accurate predictive machine learning-based drug discovery models (149, 150). Through these collaborations, already available proprietary data, which would otherwise remain classified, could be shared by collecting it in a decentralized database.
For the treatment of SARS-CoV-2, target-based development of new antivirals has yielded effective drugs. The most successful SARS-CoV-2 antiviral to date, nirmatrelvir (Paxlovid), directly targets the viral main protease (80). The fast development of nirmatrelvir was made possible through pre-existing knowledge about the SARS-CoV main protease and inhibitors (drug candidates) against it (151). Thus, repurposing strategies in drug development should not only encompass approved drugs, but should also leverage scientific knowledge and existing antiviral compounds that did not (yet) reach advanced (clinical) stages in drug development. Although repurposing efforts for treating SARS-CoV-2 infections had limited success, there is still great potential in collecting knowledge about clinically relevant drugs, providing this knowledge preferably in open-access databases to make it available for future research. Meanwhile, other inhibitors that target the main protease of SARS-CoV-2 are being investigated, like masitinib (152) or ensitrelvir (marketed as Xocova), which received emergency approval in Japan at the end of 2022 (153). The drug showed very promising results in a phase II clinical trial, but is further evaluated in phase III clinical trials before authorization outside of Japan. Direct-acting drugs like these, with high specificity against a viral protein that is well conserved among coronaviruses, will likely retain their efficacy against new circulating variants and subvariants (154). However, persistent infections in

patients treated with direct-acting drugs can lead to resistance development, as was reported in various studies for the protease inhibitors (155, 156), as well as remdesivir (157, 158). Therefore, monitoring for new resistant variants is important, as well as the development of next generation protease inhibitors (155). Furthermore, combination therapy, the use of more than one drug, can be employed to reduce the risk of resistance development (159).

Given the systemic and long-term pathology that can be caused by SARS-CoV-2 infection, researchers are challenged with the task of developing drugs that not only inhibit virus replication and treat acute symptoms, but also protect from tissue damage and hyperinflammation. Clinicians are faced with the challenge to get the timing right when treating patients with DAAs to reduce viral load, or with anti-inflammatory drugs when the disease is more advanced (139). Treatment with protease inhibitors, for example, needs to start during the early stage of infection. Therapies to control pathological host responses and prevent disease progression in the lung or other organs, or alleviate long-term consequences of COVID-19 are at least equally important, as well as treatment to restore functionality of damaged organs or tissues. Combination therapy, besides having the potential to reduce virus resistance development and increase antiviral efficacy, could be used to target virus replication and pathological responses at the same time (159). For example, combination of remdesivir and baricitinib was found to improve recovery time in hospitalized patient compared to remdesivir mono-therapy (160). An ongoing study also investigates the use of a combination of a direct antiviral drug, the main protease inhibitor masitinib (152), and the immunomodulatory drug isoquercetin (161) (**Table 1**). Now, as we have moved past the SARS-CoV-2 pandemic being an acute threat to public health, research efforts are also switching to find therapies to treat long-term consequences of infection, like post-COVID syndrome, and lung pathologies, like fibrosis (162, 163). Researchers are aiming to bridge the gap between elucidating the molecular processes during infection and understanding clinical outcomes. Immune-modulatory drugs are crucial in the treatment of severe COVID-19, like the approved drugs tocilizumab or baricitinib, which are host-targeting and reduce the hyperinflammation that can follow SARS-CoV-2 infection (82, 83). Besides many pre-clinical studies reporting on potential candidates for host-targeting therapies, a number of these treatments are currently also evaluated in clinical trials. Following up on a review (164), a search of clinicaltrials.gov in December 2023 for interventional host-targeting therapies, yielded a list of potential drugs that either aim to inhibit virus replication or treat SARS-CoV-2 induced pathologies through targeting host factors (**Table 1**). SARS-CoV-2 neutralizing monoclonal antibody therapies, of which there are now eleven marketed and many more investigated in clinical trials (165), were not included in **Table 1**. The search was limited to active trials for interventional therapies, and

therefore the table also does not include trials that are not yet recruiting or are currently recruiting, like US trials for the protease inhibitor ensitrelvir. Notably, some of the inhibitors have the potential to act as broad-spectrum antivirals, like for example serine protease inhibitors that affect the cleavage of viral surface glycoproteins and inhibit virus entry (166). Also kinase inhibitors to treat the pathologies that follow virus infection, like hyperinflammation or lung fibrosis (163), have the potential to be applicable for a broader range of virus infections. The landscape of antiviral treatment of COVID-19 is rapidly changing, with hundreds of trials currently active or recruiting participants, and therefore **Table 1** merely provides a snapshot summary of the current situation and a look into the future of COVID-19 therapy development**.**

Table 1. Host-directed antivirals evaluated in clinical trials

Drug	**Target**	**Effect**	**Clinical trial**	**Clinical trial reference**
Meplazumab	CD147 receptor	Inhibition of virus entry (167)	Phase III	NCT05679479
SLV213	Cathepsin	Inhibition of virus entry (168)	Phase II	NCT04843787
Nafamostat mesylate	Transmembrane serine protease 2 (TMPRSS2)	Inhibition of virus entry (169)	Phase II and III	NCT04352400
Upamostat	Serine proteases	Inhibition of virus entry (166)	Phase II	NCT05954286
Plitidepsin	Host-translation cofactor eEF1A	Inhibition of virus replication (170)	Phase II	NCT05705167
TXA127, TRV027;	*Renin-Angiotensin-Aldosteron-System*	Reduction of fibrosis (171)	Phase II and III;	NCT04924660
Fostamatinib	*Spleen tyrosine kinase*	Reduction of thrombosis (172)	Phase II and III	NCT05593770
EB05	TLR4	Reduction of TLR-4 mediated IL-6 release / hyperinflammation	Phase II and III	NCT04401475
LAU-7b	Fatty acid metabolism	Inhibition of lipogenesis (173)	Phase II and III	NCT04417257

Imatinib	Abl tyrosine kinase	Inhibition of hyperinflammation (174)	Phase III	NCT04394416
Isoquercetin (in combination with masitinib)	Oxidation-Inflammation response	Inhibition of hyperinflammation (161)	Phase II	NCT04622865
Nintedanib	Tyrosine kinase	Inhibition of lung fibrosis (163)	Phase IV	NCT04619680

The website clinicaltrials.gov was searched for drug candidates that are currently in active clinical trials for the treatment of COVID-19 and are interventional and targeting host factors (December 2023). Drugs were listed only if there is a known or proposed mode of action.

Concluding remarks

Decades of coronavirus research and intense efforts to curb the SARS-CoV-2 outbreak have led us to understand many aspects of the viral replication cycle and pathogenicity. This thesis highlights some of my work, in collaboration with many others, in the context of anti-coronavirus drug research. The ultimate goal, of course, would be a broad-spectrum antiviral drug targeting all current highly-pathogenic coronaviruses (and future ones), or a universal vaccine, which seems to be an even more challenging task, given the rapid evolution of SARS-CoV-2 subvariants and their escape from previously developed immunity. However, with efficient development platforms in place, such as mRNA vaccine development platforms or portfolios of known antivirals ready for further development, the response time to a newly emerging disease can be reduced. Furthermore, the implementation of advanced cell culture models/animal-free models to validate drug candidates is an extra step that can increase the success rate from pre-clinical to clinical research. Continuous monitoring of SARS-CoV-2 and ongoing efforts in adapting vaccines and developing antivirals are crucial to combat new subvariants. The accumulated knowledge about coronavirus biology as well as public health infection prevention methods hopefully leaves us better prepared for any new epidemic or pandemic.

References

1. Guan WJ, Ni ZY, Hu Y, Liang WH, Ou CQ, He JX, Liu L, Shan H, Lei CL, Hui DSC, Du B, Li LJ, Zeng G, Yuen KY, Chen RC, Tang CL, Wang T, Chen PY, Xiang J, Li SY, Wang JL, Liang ZJ, Peng YX, Wei L, Liu Y, Hu YH, Peng P, Wang JM, Liu JY, Chen Z, Li G, Zheng ZJ, Qiu SQ, Luo J, Ye CJ, Zhu SY, Zhong NS. 2020. Clinical Characteristics of Coronavirus Disease 2019 in China. N Engl J Med 382:1708-1720.
2. Diarra M, Ndiaye R, Barry A, Talla C, Diagne MM, Dia N, Faye J, Sarr FD, Gaye A, Diallo A, Cisse M, Dieng I, Fall G, Tall A, Faye O, Faye O, Sall AA, Loucoubar C. 2023. Analysis of contact tracing data showed contribution of asymptomatic and non-severe infections to the maintenance of SARS-CoV-2 transmission in Senegal. Scientific Reports 13:9121.
3. El-Ghitany EM, Hashish MH, Farghaly AG, Omran EA, Osman NA, Fekry MM. 2022. Asymptomatic versus symptomatic SARS-CoV-2 infection: a cross-sectional seroprevalence study. Trop Med Health 50:98.
4. Lamers MM, Haagmans BL. 2022. SARS-CoV-2 pathogenesis. Nature Reviews Microbiology 20:270-284.
5. Butowt R, Bilinska K, von Bartheld CS. 2023. Olfactory dysfunction in COVID-19: new insights into the underlying mechanisms. Trends Neurosci 46:75-90.
6. Haehner A, Marquardt B, Kardashi R, de With K, Rößler S, Landis BN, Welge-Luessen A, Hummel T. 2022. SARS-CoV-2 Leads to Significantly More Severe Olfactory Loss than Other Seasonal Cold Viruses. Life (Basel) 12.
7. Davis HE, McCorkell L, Vogel JM, Topol EJ. 2023. Long COVID: major findings, mechanisms and recommendations. Nat Rev Microbiol 21:133-146.
8. Pérez-González A, Araújo-Ameijeiras A, Fernández-Villar A, Crespo M, Poveda E, Cabrera JJ, del Campo V, de Araujo BG, Gómez C, Leiro V, Longueira MR, López-Domínguez A, Ramón Lorenzo J, Marcos M, Teresa Pérez M, Patiño L, Pérez S, Pérez-Fernández S, Ramos C, Regueiro B, Retresas C, Rivera T, Souto O, Taboada I, Teijeira S, Torres M, Val V, Viéitez I, the Cohort C-otGSHRI. 2022. Long COVID in hospitalized and non-hospitalized patients in a large cohort in Northwest Spain, a prospective cohort study. Scientific Reports 12:3369.
9. Chevinsky JR, Tao G, Lavery AM, Kukielka EA, Click ES, Malec D, Kompaniyets L, Bruce BB, Yusuf H, Goodman AB, Dixon MG, Nakao JH, Datta SD, MacKenzie WR, Kadri SS, Saydah S, Giovanni JE, Gundlapalli AV. 2021. Late Conditions Diagnosed 1-4 Months Following an Initial Coronavirus Disease 2019 (COVID-19) Encounter: A Matched-Cohort Study Using Inpatient and Outpatient Administrative Data-United States, 1 March-30 June 2020. Clin Infect Dis 73:S5-s16.
10. Ayoubkhani D, Bosworth ML, King S, Pouwels KB, Glickman M, Nafilyan V, Zaccardi F, Khunti K, Alwan NA, Walker AS. 2022. Risk of Long COVID in People Infected With Severe Acute Respiratory Syndrome Coronavirus 2 After 2 Doses of a Coronavirus Disease 2019 Vaccine: Community-Based, Matched Cohort Study. Open Forum Infectious Diseases 9.
11. Looi M-K. 2023. Covid-19: WHO adds JN.1 as new variant of interest. BMJ 383:p2975.
12. World Health Organization (WHO). 2023. WHO Coronavirus (COVID-19) dashboard > Cases [Dashboard]. datawhoint, https://datawhoint/dashboards/covid19/cases, accessed February 2024.
13. World Health Organization (WHO). 2023. Statement on the fifteenth meeting of the IHR (2005) Emergency Committee on the COVID-19 pandemic. Geneva: WHO.
14. Cui Z, Liu P, Wang N, Wang L, Fan K, Zhu Q, Wang K, Chen R, Feng R, Jia Z, Yang M, Xu G, Zhu B, Fu W, Chu T, Feng L, Wang Y, Pei X, Yang P, Xie XS, Cao L, Cao Y, Wang X. 2022. Structural and functional characterizations of infectivity and immune evasion of SARS-CoV-2 Omicron. Cell 185:860-871.e13.

15. Uriu K, Ito J, Kosugi Y, Tanaka YL, Mugita Y, Guo Z, Hinay AA, Putri O, Kim Y, Shimizu R, Begum MSTM, Jonathan M, Saito A, Ikeda T, Sato K. 2023. Transmissibility, infectivity, and immune evasion of the SARS-CoV-2 BA.2.86 variant. The Lancet Infectious Diseases 23:e460-e461.
16. Willett BJ, Grove J, MacLean OA, Wilkie C, De Lorenzo G, Furnon W, Cantoni D, Scott S, Logan N, Ashraf S, Manali M, Szemiel A, Cowton V, Vink E, Harvey WT, Davis C, Asamaphan P, Smollett K, Tong L, Orton R, Hughes J, Holland P, Silva V, Pascall DJ, Puxty K, da Silva Filipe A, Yebra G, Shaaban S, Holden MTG, Pinto RM, Gunson R, Templeton K, Murcia PR, Patel AH, Klenerman P, Dunachie S, Dunachie S, Klenerman P, Barnes E, Brown A, Adele S, Kronsteiner B, Murray SM, Abraham P, Deeks A, Ansari MA, de Silva T, Turtle L, Moore S, Austin J, et al. 2022. SARS-CoV-2 Omicron is an immune escape variant with an altered cell entry pathway. Nature Microbiology 7:1161-1179.
17. von Bartheld CS, Wang L. 2023. Prevalence of Olfactory Dysfunction with the Omicron Variant of SARS-CoV-2: A Systematic Review and Meta-Analysis. Cells 12.
18. Kurhade C, Zou J, Xia H, Liu M, Chang HC, Ren P, Xie X, Shi PY. 2023. Low neutralization of SARS-CoV-2 Omicron BA.2.75.2, BQ.1.1 and XBB.1 by parental mRNA vaccine or a BA.5 bivalent booster. Nat Med 29:344-347.
19. Yang S, Yu Y, Xu Y, Jian F, Song W, Yisimayi A, Wang P, Wang J, Liu J, Yu L, Niu X, Wang J, Wang Y, Shao F, Jin R, Wang Y, Cao Y. 2024. Fast evolution of SARS-CoV-2 BA.2.86 to JN.1 under heavy immune pressure. The Lancet Infectious Diseases 24:e70-e72.
20. Firouzabadi N, Ghasemiyeh P, Moradishooli F, Mohammadi-Samani S. 2023. Update on the effectiveness of COVID-19 vaccines on different variants of SARS-CoV-2. Int Immunopharmacol 117:109968.
21. Emeny JM, Morgan MJ. 1979. Regulation of the Interferon System: Evidence that Vero Cells have a Genetic Defect in Interferon Production. J Gen Virol. 43:247-252.
22. Zhu Y, Binder J, Yurgelonis I, Rai DK, Lazarro S, Costales C, Kobylarz K, McMonagle P, Steppan CM, Aschenbrenner L, Anderson AS, Cardin RD. 2022. Generation of a VeroE6 Pgp gene knock out cell line and its use in SARS-CoV-2 antiviral study. Antiviral Res 208:105429.
23. Örd M, Faustova I, Loog M. 2020. The sequence at Spike S1/S2 site enables cleavage by furin and phospho-regulation in SARS-CoV2 but not in SARS-CoV1 or MERS-CoV. Scientific Reports 10:16944.
24. Ogando NS, Dalebout TJ, Zevenhoven-Dobbe JC, Limpens R, van der Meer Y, Caly L, Druce J, de Vries JJC, Kikkert M, Bárcena M, Sidorov I, Snijder EJ. 2020. SARS-coronavirus-2 replication in Vero E6 cells: replication kinetics, rapid adaptation and cytopathology. J Gen Virol 101:925-940.
25. Davidson AD, Williamson MK, Lewis S, Shoemark D, Carroll MW, Heesom KJ, Zambon M, Ellis J, Lewis PA, Hiscox JA, Matthews DA. 2020. Characterisation of the transcriptome and proteome of SARS-CoV-2 reveals a cell passage induced in-frame deletion of the furin-like cleavage site from the spike glycoprotein. Genome Medicine 12:68.
26. Johnson BA, Xie X, Bailey AL, Kalveram B, Lokugamage KG, Muruato A, Zou J, Zhang X, Juelich T, Smith JK, Zhang L, Bopp N, Schindewolf C, Vu M, Vanderheiden A, Winkler ES, Swetnam D, Plante JA, Aguilar P, Plante KS, Popov V, Lee B, Weaver SC, Suthar MS, Routh AL, Ren P, Ku Z, An Z, Debbink K, Diamond MS, Shi P-Y, Freiberg AN, Menachery VD. 2021. Loss of furin cleavage site attenuates SARS-CoV-2 pathogenesis. Nature 591:293-299.
27. Pellegrini L, Albecka A, Mallery DL, Kellner MJ, Paul D, Carter AP, James LC, Lancaster MA. 2020. SARS-CoV-2 Infects the Brain Choroid Plexus and Disrupts the Blood-CSF Barrier in Human Brain Organoids. Cell Stem Cell 27:951-961.e5.
28. Yang L, Han Y, Nilsson-Payant BE, Gupta V, Wang P, Duan X, Tang X, Zhu J, Zhao Z, Jaffré F, Zhang T, Kim TW, Harschnitz O, Redmond D, Houghton S, Liu C, Naji A, Ciceri G, Guttikonda S, Bram Y, Nguyen DT, Cioffi M, Chandar V, Hoagland DA, Huang Y, Xiang J, Wang H, Lyden D, Borczuk A, Chen HJ, Studer L, Pan FC, Ho DD, tenOever BR, Evans T, Schwartz RE, Chen S.

2020. A Human Pluripotent Stem Cell-based Platform to Study SARS-CoV-2 Tropism and Model Virus Infection in Human Cells and Organoids. Cell Stem Cell 27:125-136.e7.
29. Zhao X, Li C, Liu X, Chiu MC, Wang D, Wei Y, Chu H, Cai JP, Hau-Yee Chan I, Kak-Yuen Wong K, Fuk-Woo Chan J, Kai-Wang To K, Yuen KY, Zhou J. 2021. Human Intestinal Organoids Recapitulate Enteric Infections of Enterovirus and Coronavirus. Stem Cell Reports 16:493-504.
30. Liao Y, Li X, Mou T, Zhou X, Li D, Wang L, Zhang Y, Dong X, Zheng H, Guo L, Liang Y, Jiang G, Fan S, Xu X, Xie Z, Chen H, Liu L, Li Q. 2020. Distinct infection process of SARS-CoV-2 in human bronchial epithelial cell lines. J Med Virol 92:2830-2838.
31. Heinen N, Klöhn M, Steinmann E, Pfaender S. 2021. In Vitro Lung Models and Their Application to Study SARS-CoV-2 Pathogenesis and Disease. Viruses 13.
32. Wang Y, Wang P, Qin J. 2022. Human Organoids and Organs-on-Chips for Addressing COVID-19 Challenges. Adv Sci (Weinh) 9:e2105187.
33. Bestion E, Halfon P, Mezouar S, Mège JL. 2022. Cell and Animal Models for SARS-CoV-2 Research. Viruses 14.
34. Dvorak A, Tilley AE, Shaykhiev R, Wang R, Crystal RG. 2011. Do airway epithelium air-liquid cultures represent the in vivo airway epithelium transcriptome? Am J Respir Cell Mol Biol 44:465-73.
35. Hewitt RJ, Lloyd CM. 2021. Regulation of immune responses by the airway epithelial cell landscape. Nature Reviews Immunology 21:347-362.
36. Hou YJ, Okuda K, Edwards CE, Martinez DR, Asakura T, Dinnon KH, Kato T, Lee RE, Yount BL, Mascenik TM, Chen G, Olivier KN, Ghio A, Tse LV, Leist SR, Gralinski LE, Schäfer A, Dang H, Gilmore R, Nakano S, Sun L, Fulcher ML, Livraghi-Butrico A, Nicely NI, Cameron M, Cameron C, Kelvin DJ, de Silva A, Margolis DM, Markmann A, Bartelt L, Zumwalt R, Martinez FJ, Salvatore SP, Borczuk A, Tata PR, Sontake V, Kimple A, Jaspers I, O'Neal WK, Randell SH, Boucher RC, Baric RS. 2020. SARS-CoV-2 Reverse Genetics Reveals a Variable Infection Gradient in the Respiratory Tract. Cell 182:429-446.e14.
37. Rockx B, Kuiken T, Herfst S, Bestebroer T, Lamers MM, Oude Munnink BB, de Meulder D, van Amerongen G, van den Brand J, Okba NMA, Schipper D, van Run P, Leijten L, Sikkema R, Verschoor E, Verstrepen B, Bogers W, Langermans J, Drosten C, Fentener van Vlissingen M, Fouchier R, de Swart R, Koopmans M, Haagmans BL. 2020. Comparative pathogenesis of COVID-19, MERS, and SARS in a nonhuman primate model. Science (New York, NY)
38. Van Slambrouck J, Khan M, Verbeken E, Choi S, Geudens V, Vanluyten C, Feys S, Vanhulle E, Wollants E, Vermeire K, De Fays C, Aversa L, Kaes J, Van Raemdonck D, Vos R, Vanaudenaerde B, De Hertogh G, Wauters E, Wauters J, Ceulemans LJ, Mombaerts P. 2023. Visualising SARS-CoV-2 infection of the lung in deceased COVID-19 patients. eBioMedicine 92.
39. Chua RL, Lukassen S, Trump S, Hennig BP, Wendisch D, Pott F, Debnath O, Thürmann L, Kurth F, Völker MT, Kazmierski J, Timmermann B, Twardziok S, Schneider S, Machleidt F, Müller-Redetzky H, Maier M, Krannich A, Schmidt S, Balzer F, Liebig J, Loske J, Suttorp N, Eils J, Ishaque N, Liebert UG, von Kalle C, Hocke A, Witzenrath M, Goffinet C, Drosten C, Laudi S, Lehmann I, Conrad C, Sander L-E, Eils R. 2020. COVID-19 severity correlates with airway epithelium–immune cell interactions identified by single-cell analysis. Nature Biotechnology 38:970-979.
40. Zhu N, Wang W, Liu Z, Liang C, Wang W, Ye F, Huang B, Zhao L, Wang H, Zhou W, Deng Y, Mao L, Su C, Qiang G, Jiang T, Zhao J, Wu G, Song J, Tan W. 2020. Morphogenesis and cytopathic effect of SARS-CoV-2 infection in human airway epithelial cells. Nature Communications 11:3910.
41. Thaler M, Wang Y, van der Does AM, Faiz A, Ninaber DK, Ogando NS, Beckert H, Taube C, Salgado-Benvindo C, Snijder EJ, Bredenbeek PJ, Hiemstra PS, van Hemert MJ. 2023. Impact

of Changes in Human Airway Epithelial Cellular Composition and Differentiation on SARS-CoV-2 Infection Biology. Journal of Innate Immunity 15:562-580.

42. Ziegler CGK, Allon SJ, Nyquist SK, Mbano IM, Miao VN, Tzouanas CN, Cao Y, Yousif AS, Bals J, Hauser BM, Feldman J, Muus C, Wadsworth MH, II, Kazer SW, Hughes TK, Doran B, Gatter GJ, Vukovic M, Taliaferro F, Mead BE, Guo Z, Wang JP, Gras D, Plaisant M, Ansari M, Angelidis I, Adler H, Sucre JMS, Taylor CJ, Lin B, Waghray A, Mitsialis V, Dwyer DF, Buchheit KM, Boyce JA, Barrett NA, Laidlaw TM, Carroll SL, Colonna L, Tkachev V, Peterson CW, Yu A, Zheng HB, Gideon HP, Winchell CG, Lin PL, Bingle CD, Snapper SB, Kropski JA, Theis FJ, et al. 2020. SARS-CoV-2 Receptor ACE2 Is an Interferon-Stimulated Gene in Human Airway Epithelial Cells and Is Detected in Specific Cell Subsets across Tissues. Cell 181:1016-1035.e19.
43. Ahn JH, Kim J, Hong SP, Choi SY, Yang MJ, Ju YS, Kim YT, Kim HM, Rahman MDT, Chung MK, Hong SD, Bae H, Lee CS, Koh GY. 2021. Nasal ciliated cells are primary targets for SARS-CoV-2 replication in the early stage of COVID-19. J Clin Invest 131.
44. Ravindra NG, Alfajaro MM, Gasque V, Huston NC, Wan H, Szigeti-Buck K, Yasumoto Y, Greaney AM, Habet V, Chow RD, Chen JS, Wei J, Filler RB, Wang B, Wang G, Niklason LE, Montgomery RR, Eisenbarth SC, Chen S, Williams A, Iwasaki A, Horvath TL, Foxman EF, Pierce RW, Pyle AM, van Dijk D, Wilen CB. 2021. Single-cell longitudinal analysis of SARS-CoV-2 infection in human airway epithelium identifies target cells, alterations in gene expression, and cell state changes. PLoS Biol 19:e3001143.
45. Rogers D. 1994. Airway goblet cells: responsive and adaptable front-line defenders. Eur Respir J. 7:1690-1706.
46. Bonser LR, Eckalbar WL, Rodriguez L, Shen J, Koh KD, Ghias K, Zlock LT, Christenson S, Woodruff PG, Finkbeiner WE, Erle DJ. 2022. The Type 2 Asthma Mediator IL-13 Inhibits Severe Acute Respiratory Syndrome Coronavirus 2 Infection of Bronchial Epithelium. Am J Respir Cell Mol Biol. 66:391-401.
47. Sajuthi SP, DeFord P, Li Y, Jackson ND, Montgomery MT, Everman JL, Rios CL, Pruesse E, Nolin JD, Plender EG, Wechsler ME, Mak ACY, Eng C, Salazar S, Medina V, Wohlford EM, Huntsman S, Nickerson DA, Germer S, Zody MC, Abecasis G, Kang HM, Rice KM, Kumar R, Oh S, Rodriguez-Santana J, Burchard EG, Seibold MA. 2020. Type 2 and interferon inflammation regulate SARS-CoV-2 entry factor expression in the airway epithelium. Nature Communications 11:5139.
48. Conway FM, Bloom CI, Shah PL. 2022. Susceptibility of Patients with Airway Disease to SARS-CoV-2 Infection. Am J Respir Crit Care Med 206:696-703.
49. Eger K, Bel EH. 2021. Asthma and COVID-19: do we finally have answers? Eur Respir J 57:2004451.
50. Bloom CI, Drake TM, Docherty AB, Lipworth BJ, Johnston SL, Nguyen-Van-Tam JS, Carson G, Dunning J, Harrison EM, Baillie JK, Semple MG, Cullinan P, Openshaw PJM. 2021. Risk of adverse outcomes in patients with underlying respiratory conditions admitted to hospital with COVID-19: a national, multicentre prospective cohort study using the ISARIC WHO Clinical Characterisation Protocol UK. Lancet Respir Med 9:699-711.
51. Hoffmann M, Wong L-YR, Arora P, Zhang L, Rocha C, Odle A, Nehlmeier I, Kempf A, Richter A, Halwe NJ, Schön J, Ulrich L, Hoffmann D, Beer M, Drosten C, Perlman S, Pöhlmann S. 2023. Omicron subvariant BA.5 efficiently infects lung cells. Nature Communications 14:3500.
52. Li W, Moore MJ, Vasilieva N, Sui J, Wong SK, Berne MA, Somasundaran M, Sullivan JL, Luzuriaga K, Greenough TC, Choe H, Farzan M. 2003. Angiotensin-converting enzyme 2 is a functional receptor for the SARS coronavirus. Nature 426:450-4.
53. Wang N, Shi X, Jiang L, Zhang S, Wang D, Tong P, Guo D, Fu L, Cui Y, Liu X, Arledge KC, Chen YH, Zhang L, Wang X. 2013. Structure of MERS-CoV spike receptor-binding domain complexed with human receptor DPP4. Cell Res 23:986-93.

54. Hofmann H, Pyrc K, van der Hoek L, Geier M, Berkhout B, Pöhlmann S. 2005. Human coronavirus NL63 employs the severe acute respiratory syndrome coronavirus receptor for cellular entry. Proc Natl Acad Sci U S A 102:7988-93.
55. Otter Clayton J, Fausto A, Tan Li H, Khosla Alisha S, Cohen Noam A, Weiss Susan R. 2023. Infection of primary nasal epithelial cells differentiates among lethal and seasonal human coronaviruses. Proc Natl Acad Sci U S A 120:e2218083120.
56. Jang Y, Seo SH. 2020. Gene expression pattern differences in primary human pulmonary epithelial cells infected with MERS-CoV or SARS-CoV-2. Arch Virol 165:2205-2211.
57. Krishnamoorthy P, Raj AS, Roy S, Kumar NS, Kumar H. 2021. Comparative transcriptome analysis of SARS-CoV, MERS-CoV, and SARS-CoV-2 to identify potential pathways for drug repurposing. Computers in Biology and Medicine 128:104123.
58. Coden ME, Loffredo LF, Abdala-Valencia H, Berdnikovs S. 2021. Comparative Study of SARS-CoV-2, SARS-CoV-1, MERS-CoV, HCoV-229E and Influenza Host Gene Expression in Asthma: Importance of Sex, Disease Severity, and Epithelial Heterogeneity. Viruses 13:1081.
59. Sun J, Ye F, Wu A, Yang R, Pan M, Sheng J, Zhu W, Mao L, Wang M, Xia Z, Huang B, Tan W, Jiang T. 2020. Comparative Transcriptome Analysis Reveals the Intensive Early Stage Responses of Host Cells to SARS-CoV-2 Infection. Front Microbiol
60. Jha PK, Vijay A, Halu A, Uchida S, Aikawa M. 2020. Gene Expression Profiling Reveals the Shared and Distinct Transcriptional Signatures in Human Lung Epithelial Cells Infected With SARS-CoV-2, MERS-CoV, or SARS-CoV: Potential Implications in Cardiovascular Complications of COVID-19. Front Cardiovasc Med 7:623012.
61. Blanco-Melo D, Nilsson-Payant BE, Liu W-C, Uhl S, Hoagland D, Møller R, Jordan TX, Oishi K, Panis M, Sachs D, Wang TT, Schwartz RE, Lim JK, Albrecht RA, tenOever BR. 2020. Imbalanced Host Response to SARS-CoV-2 Drives Development of COVID-19. Cell 181:1036-1045.e9.
62. Chang CY, Liu HM, Chang MF, Chang SC. 2020. Middle East Respiratory Syndrome Coronavirus Nucleocapsid Protein Suppresses Type I and Type III Interferon Induction by Targeting RIG-I Signaling. J Virol 94.
63. Frieman M, Ratia K, Johnston RE, Mesecar AD, Baric RS. 2009. Severe acute respiratory syndrome coronavirus papain-like protease ubiquitin-like domain and catalytic domain regulate antagonism of IRF3 and NF-kappaB signaling. J Virol 83:6689-705.
64. Duncan JKS, Xu D, Licursi M, Joyce MA, Saffran HA, Liu K, Gohda J, Tyrrell DL, Kawaguchi Y, Hirasawa K. 2023. Interferon regulatory factor 3 mediates effective antiviral responses to human coronavirus 229E and OC43 infection. Front Immunol 14:930086.
65. Andreakos E, Salagianni M, Galani IE, Koltsida O. 2017. Interferon-λs: Front-Line Guardians of Immunity and Homeostasis in the Respiratory Tract. Front. Immunol.
66. Dinnon KH, Leist SR, Schäfer A, Edwards CE, Martinez DR, Montgomery SA, West A, Yount BL, Hou YJ, Adams LE, Gully KL, Brown AJ, Huang E, Bryant MD, Choong IC, Glenn JS, Gralinski LE, Sheahan TP, Baric RS. 2020. A mouse-adapted model of SARS-CoV-2 to test COVID-19 countermeasures. Nature 586:560-566.
67. Feld JJ, Kandel C, Biondi MJ, Kozak RA, Zahoor MA, Lemieux C, Borgia SM, Boggild AK, Powis J, McCready J, Tan DHS, Chan T, Coburn B, Kumar D, Humar A, Chan A, O'Neil B, Noureldin S, Booth J, Hong R, Smookler D, Aleyadeh W, Patel A, Barber B, Casey J, Hiebert R, Mistry H, Choong I, Hislop C, Santer DM, Lorne Tyrrell D, Glenn JS, Gehring AJ, Janssen HLA, Hansen BE. 2021. Peginterferon lambda for the treatment of outpatients with COVID-19: a phase 2, placebo-controlled randomised trial. Lancet Respir Med 9:498-510.
68. Reis G, Moreira Silva EAS, Medeiros Silva DC, Thabane L, Campos VHS, Ferreira TS, Santos CVQ, Nogueira AMR, Almeida APFG, Savassi LCM, Figueiredo-Neto AD, Dias ACF, Freire Júnior AM, Bitarães C, Milagres AC, Callegari ED, Simplicio MIC, Ribeiro LB, Oliveira R, Harari O, Wilson LA, Forrest JI, Ruton H, Sprague S, McKay P, Guo CM, Limbrick-Oldfield EH, Kanters

S, Guyatt GH, Rayner CR, Kandel C, Biondi MJ, Kozak R, Hansen B, Zahoor MA, Arora P, Hislop C, Choong I, Feld JJ, Mills EJ, Glenn JS. 2023. Early Treatment with Pegylated Interferon Lambda for Covid-19. N Engl J Med 388:518-528.

69. Oleinik LA, Madonov PG, Pykhtina MB. 2023. Potential of Interferon Lambda as an Inhibitor of SARS-CoV-2. Molecular Biology 57:291-298.
70. Vanderheiden A, Ralfs P, Chirkova T, Upadhyay AA, Zimmerman MG, Bedoya S, Aoued H, Tharp GM, Pellegrini KL, Manfredi C, Sorscher E, Mainou B, Lobby JL, Kohlmeier JE, Lowen AC, Shi P-Y, Menachery VD, Anderson LJ, Grakoui A, Bosinger SE, Suthar MS. 2020. Type I and Type III Interferons Restrict SARS-CoV-2 Infection of Human Airway Epithelial Cultures. Journal of Virology 94:e00985-20.
71. Mulay A, Konda B, Garcia G, Yao C, Beil S, Villalba JM, Koziol C, Sen C, Purkayastha A, Kolls JK, Pociask DA, Pessina P, de Aja JS, Garcia-de-Alba C, Kim CF, Gomperts B, Arumugaswami V, Stripp BR. 2021. SARS-CoV-2 infection of primary human lung epithelium for COVID-19 modeling and drug discovery. Cell Reports 35:109055.
72. Subramaniyan B, Larabee JL, Bodas M, Moore AR, Burgett AWG, Myers DA, Georgescu C, Wren JD, Papin JF, Walters MS. 2021. Characterization of the SARS-CoV-2 Host Response in Primary Human Airway Epithelial Cells from Aged Individuals. Viruses 13:1603.
73. Johansen MD, Mahbub RM, Idrees S, Nguyen DH, Miemczyk S, Pathinayake P, Nichol K, Hansbro NG, Gearing LJ, Hertzog PJ, Gallego-Ortega D, Britton WJ, Saunders BM, Wark PA, Faiz A, Hansbro PM. 2022. Increased SARS-CoV-2 Infection, Protease, and Inflammatory Responses in Chronic Obstructive Pulmonary Disease Primary Bronchial Epithelial Cells Defined with Single-Cell RNA Sequencing. Am J Respir Crit Care Med 206:712-729.
74. Melms JC, Biermann J, Huang H, Wang Y, Nair A, Tagore S, Katsyv I, Rendeiro AF, Amin AD, Schapiro D, Frangieh CJ, Luoma AM, Filliol A, Fang Y, Ravichandran H, Clausi MG, Alba GA, Rogava M, Chen SW, Ho P, Montoro DT, Kornberg AE, Han AS, Bakhoum MF, Anandasabapathy N, Suárez-Fariñas M, Bakhoum SF, Bram Y, Borczuk A, Guo XV, Lefkowitch JH, Marboe C, Lagana SM, Del Portillo A, Zorn E, Markowitz GS, Schwabe RF, Schwartz RE, Elemento O, Saqi A, Hibshoosh H, Que J, Izar B. 2021. A molecular single-cell lung atlas of lethal COVID-19. Nature
75. Yoshikawa T, Hill TE, Yoshikawa N, Popov VL, Galindo CL, Garner HR, Peters CJ, Tseng C-TK. 2010. Dynamic innate immune responses of human bronchial epithelial cells to severe acute respiratory syndrome-associated coronavirus infection. PloS one 5:e8729-e8729.
76. Yuan L, Fung TS, He J, Chen RA, Liu DX. 2022. Modulation of viral replication, apoptosis and antiviral response by induction and mutual regulation of EGR and AP-1 family genes during coronavirus infection. Emerg Microbes Infect 11:1717-1729.
77. Guo H, Golczer G, Wittner BS, Langenbucher A, Zachariah M, Dubash TD, Hong X, Comaills V, Burr R, Ebright RY, Horwitz E, Vuille JA, Hajizadeh S, Wiley DF, Reeves BA, Zhang JM, Niederhoffer KL, Lu C, Wesley B, Ho U, Nieman LT, Toner M, Vasudevan S, Zou L, Mostoslavsky R, Maheswaran S, Lawrence MS, Haber DA. 2021. NR4A1 regulates expression of immediate early genes, suppressing replication stress in cancer. Mol Cell 81:4041-4058.e15.
78. Zhang L, Wang Q, Liu W, Liu F, Ji A, Li Y. 2018. The Orphan Nuclear Receptor 4A1: A Potential New Therapeutic Target for Metabolic Diseases. J Diabetes Res 2018:9363461.
79. Beigel JH, Tomashek KM, Dodd LE, Mehta AK, Zingman BS, Kalil AC, Hohmann E, Chu HY, Luetkemeyer A, Kline S, Lopez de Castilla D, Finberg RW, Dierberg K, Tapson V, Hsieh L, Patterson TF, Paredes R, Sweeney DA, Short WR, Touloumi G, Lye DC, Ohmagari N, Oh M-d, Ruiz-Palacios GM, Benfield T, Fätkenheuer G, Kortepeter MG, Atmar RL, Creech CB, Lundgren J, Babiker AG, Pett S, Neaton JD, Burgess TH, Bonnett T, Green M, Makowski M, Osinusi A, Nayak S, Lane HC. 2020. Remdesivir for the Treatment of Covid-19 — Final Report. N Engl J Med 383:1813-1826.

80. Harris E. 2023. FDA Grants Full Approval to Paxlovid, COVID-19 Antiviral Treatment. Jama 329:2118.
81. Toussi SS, Hammond JL, Gerstenberger BS, Anderson AS. 2023. Therapeutics for COVID-19. Nature Microbiology 8:771-786.
82. Sebba A. 2008. Tocilizumab: the first interleukin-6-receptor inhibitor. Am J Health Syst Pharm 65:1413-8.
83. Kubo S, Nakayamada S, Sakata K, Kitanaga Y, Ma X, Lee S, Ishii A, Yamagata K, Nakano K, Tanaka Y. 2018. Janus Kinase Inhibitor Baricitinib Modulates Human Innate and Adaptive Immune System. Front Immunol
84. Food and Drug Administration. 2023. Fact sheet for healthcare providers: Emergency Use Authorization for Evusheld (tixagevimab co-packaged with cilgavimab). Available at: https://wwwfdagov/media/154701/download.
85. Food and Drug Administration. 2022. Fact sheet for healthcare providers: Emergency Use Authorization (EUA) of sotrovimab. Available at: https://wwwfdagov/media/149534/download.
86. European Medicines Agency (EMA). 2022. ETF statement on the loss of activity of anti-spike protein monoclonal antibodies due to emerging SARS-CoV-2 variants of concern. https://wwwemaeuropaeu/en/documents/public-statement/etf-statement-loss-activity-anti-spike-protein-monoclonal-antibodies-due-emerging-sars-cov-2-variants-concern_enpdf.
87. Ferreto LED, Bortoloti DS, Fortes PCN, Follador F, Arruda G, Ximenez JP, Wendt GW. 2021. Dexamethasone for treating SARS-CoV-2 infection: a systematic review and meta-analysis. Sao Paulo Med J 139:657-661.
88. The WHO Rapid Evidence Appraisal for COVID-19 Therapies Working Group. 2020. Association Between Administration of Systemic Corticosteroids and Mortality Among Critically Ill Patients With COVID-19: A Meta-analysis. JAMA 324:1330-1341.
89. Stiles J, Amaya C, Pham R, Rowntree RK, Lacaze M, Mulne A, Bischoff J, Kokta V, Boucheron LE, Mitchell DC, Bryan BA. 2012. Propranolol treatment of infantile hemangioma endothelial cells: A molecular analysis. Exp Ther Med 4:594-604.
90. Léauté-Labrèze C, Hoeger P, Mazereeuw-Hautier J, Guibaud L, Baselga E, Posiunas G, Phillips RJ, Caceres H, Lopez Gutierrez JC, Ballona R, Friedlander SF, Powell J, Perek D, Metz B, Barbarot S, Maruani A, Szalai ZZ, Krol A, Boccara O, Foelster-Holst R, Febrer Bosch MI, Su J, Buckova H, Torrelo A, Cambazard F, Grantzow R, Wargon O, Wyrzykowski D, Roessler J, Bernabeu-Wittel J, Valencia AM, Przewratil P, Glick S, Pope E, Birchall N, Benjamin L, Mancini AJ, Vabres P, Souteyrand P, Frieden IJ, Berul CI, Mehta CR, Prey S, Boralevi F, Morgan CC, Heritier S, Delarue A, Voisard JJ. 2015. A randomized, controlled trial of oral propranolol in infantile hemangioma. N Engl J Med 372:735-46.
91. Sasaki M, North PE, Elsey J, Bubley J, Rao S, Jung Y, Wu S, Zou M-H, Pollack BP, Kumar J, Singh H, Arbiser JL. 2019. Propranolol exhibits activity against hemangiomas independent of beta blockade. NPJ precision oncology 3:27-27.
92. Ackermann M, Verleden SE, Kuehnel M, Haverich A, Welte T, Laenger F, Vanstapel A, Werlein C, Stark H, Tzankov A, Li WW, Li VW, Mentzer SJ, Jonigk D. 2020. Pulmonary Vascular Endothelialitis, Thrombosis, and Angiogenesis in Covid-19. N Engl J Med 383:120-128.
93. Miggiolaro A, da Silva FPG, Wiedmer DB, Godoy TM, Borges NH, Piper GW, Oricil AGG, Klein CK, Hlatchuk EC, Dagostini JCH, Collete M, Arantes MP, D'Amico RC, Dutra AA, de Azevedo MLV, de Noronha L. 2023. COVID-19 and Pulmonary Angiogenesis: The Possible Role of Hypoxia and Hyperinflammation in the Overexpression of Proteins Involved in Alveolar Vascular Dysfunction. Viruses 15.
94. Li L, Chong Han C, Ng Say Y, Kwok Ka W, Teo Z, Tan Eddie Han P, Choo Chee C, Seet Ju E, Choi Hyung W, Buist Martin L, Chow Vincent Tak K, Tan Nguan S. 2015. Angiopoietin-like 4

Increases Pulmonary Tissue Leakiness and Damage during Influenza Pneumonia. Cell Reports 10:654-663.

95. Bhatraju PK, Morrell ED, Stanaway IB, Sathe NA, Srivastava A, Postelnicu R, Green R, Andrews A, Gonzalez M, Kratochvil CJ, Kumar VK, Hsiang TY, Gale M, Jr., Anesi GL, Wyles D, Broadhurst MJ, Brett-Major D, Mukherjee V, Sevransky JE, Landsittel D, Hung C, Altemeier WA, Gharib SA, Uyeki TM, Cobb JP, Liebler JM, Crosslin DR, Jarvik GP, Segal LN, Evans L, Mikacenic C, Wurfel MM. 2023. Angiopoietin-Like4 Is a Novel Marker of COVID-19 Severity. Crit Care Explor 5:e0827.
96. Wang P, Luo R, Zhang M, Wang Y, Song T, Tao T, Li Z, Jin L, Zheng H, Chen W, Zhao M, Zheng Y, Qin J. 2020. A cross-talk between epithelium and endothelium mediates human alveolar–capillary injury during SARS-CoV-2 infection. Cell Death & Disease 11:1042.
97. Peuschel KE. 2011. Some clinical evidence of the hypothesis of an indirect antiviral effect of propranolol through immunoactivation. Medical Hypotheses 76:689-691.
98. Fang H, Wang Y, Liu L, Cheng K, Li P, Tan Y, Hao X, Mei M, Xu X, Yao Y, Zan F, Wu L, Zhu Y, Xu B, Huang D, Wang C, Tan X, Qian Z, Chen X-W. 2022. A Host-Harbored Metabolic Susceptibility of Coronavirus Enables Broad-Spectrum Targeting. bioRxiv
99. Hu Q, Liao P, Li W, Hu J, Chen C, Zhang Y, Wang Y, Chen L, Song K, Liu J, Zhang W, Li Q, McLeod HL, He Y. 2021. Clinical Use of Propranolol Reduces Biomarkers of Proliferation in Gastric Cancer. Front Oncol 11:628613.
100. Zhou C, Chen X, Zeng W, Peng C, Huang G, Li X, Ouyang Z, Luo Y, Xu X, Xu B, Wang W, He R, Zhang X, Zhang L, Liu J, Knepper TC, He Y, McLeod HL. 2016. Propranolol induced G0/G1/S phase arrest and apoptosis in melanoma cells via AKT/MAPK pathway. Oncotarget 7:68314-68327.
101. Klann K, Bojkova D, Tascher G, Ciesek S, Münch C, Cinatl J. 2020. Growth factor receptor signaling inhibition prevents SARS-CoV-2 replication. Molecular Cell
102. Maisel AS, Murray D, Lotz M, Rearden A, Irwin M, Michel MC. 1991. Propranolol treatment affects parameters of human immunity. Immunopharmacology 22:157-164.
103. Josuttis D, Schwedler C, Heymann G, Gümbel D, Schmittner MD, Kruse M, Hoppe B. 2023. Vascular Endothelial Growth Factor as Potential Biomarker for COVID-19 Severity. J Intensive Care Med 38:1165-1173.
104. Pang J, Xu F, Aondio G, Li Y, Fumagalli A, Lu M, Valmadre G, Wei J, Bian Y, Canesi M, Damiani G, Zhang Y, Yu D, Chen J, Ji X, Sui W, Wang B, Wu S, Kovacs A, Revera M, Wang H, Jing X, Zhang Y, Chen Y, Cao Y. 2021. Efficacy and tolerability of bevacizumab in patients with severe Covid-19. Nat Commun 12:814.
105. Feng T, Zhang J, Chen Z, Pan W, Chen Z, Yan Y, Dai J. 2022. Glycosylation of viral proteins: Implication in virus–host interaction and virulence. Virulence 13:670-683.
106. Shajahan A, Pepi LE, Rouhani DS, Heiss C, Azadi P. 2021. Glycosylation of SARS-CoV-2: structural and functional insights. Anal Bioanal Chem 413:7179-7193.
107. Bouwman KM, Tomris I, Turner HL, van der Woude R, Shamorkina TM, Bosman GP, Rockx B, Herfst S, Snijder J, Haagmans BL, Ward AB, Boons G-J, de Vries RP. 2021. Multimerization- and glycosylation-dependent receptor binding of SARS-CoV-2 spike proteins. PLOS Pathogens 17:e1009282.
108. Huang H-C, Lai Y-J, Liao C-C, Wang F-Y, Huang K-B, Lee IJ, Chou W-C, Wang S-H, Wang L-H, Hsu J-M, Sun C-P, Kuo C-T, Wang J, Hsiao T-C, Yang P-J, Lee T-A, Huang W, Li F-A, Shen C-Y, Lin Y-L, Tao M-H, Li C-W. 2021. Targeting conserved N-glycosylation blocks SARS-CoV-2 variant infection in vitro. eBioMedicine 74:103712.
109. Perry ST, Buck MD, Plummer EM, Penmasta RA, Batra H, Stavale EJ, Warfield KL, Dwek RA, Butters TD, Alonzi DS, Lada SM, King K, Klose B, Ramstedt U, Shresta S. 2013. An iminosugar with potent inhibition of dengue virus infection in vivo. Antiviral Res 98:35-43.

110. Warfield KL, Alonzi DS, Hill JC, Caputo AT, Roversi P, Kiappes JL, Sheets N, Duchars M, Dwek RA, Biggins J, Barnard D, Shresta S, Treston AM, Zitzmann N. 2020. Targeting Endoplasmic Reticulum α-Glucosidase I with a Single-Dose Iminosugar Treatment Protects against Lethal Influenza and Dengue Virus Infections. J Med Chem 63:4205-4214.
111. Chang J, Warren TK, Zhao X, Gill T, Guo F, Wang L, Comunale MA, Du Y, Alonzi DS, Yu W, Ye H, Liu F, Guo J-T, Mehta A, Cuconati A, Butters TD, Bavari S, Xu X, Block TM. 2013. Small molecule inhibitors of ER α-glucosidases are active against multiple hemorrhagic fever viruses. Antiviral Research 98:432-440.
112. Fukushi M, Yoshinaka Y, Matsuoka Y, Hatakeyama S, Ishizaka Y, Kirikae T, Sasazuki T, Miyoshi-Akiyama T. 2012. Monitoring of S Protein Maturation in the Endoplasmic Reticulum by Calnexin Is Important for the Infectivity of Severe Acute Respiratory Syndrome Coronavirus. J Virol. 86:11745-11753.
113. Ferjancic Z, Bihelovic F, Vulovic B, Matovic R, Trmcic M, Jankovic A, Pavlovic M, Djurkovic F, Prodanovic R, Djurdjevic Djelmas A, Kalicanin N, Zlatovic M, Sladic D, Vallet T, Vignuzzi M, Saicic RN. 2024. Development of iminosugar-based glycosidase inhibitors as drug candidates for SARS-CoV-2 virus via molecular modelling and in vitro studies. J Enzyme Inhib Med Chem 39:2289007.
114. Clarke EC, Nofchissey RA, Ye C, Bradfute SB. 2021. The iminosugars celgosivir, castanospermine and UV-4 inhibit SARS-CoV-2 replication. Glycobiology 31:378-384.
115. Karade SS, Franco EJ, Rojas AC, Hanrahan KC, Kolesnikov A, Yu W, MacKerell AD, Jr., Hill DC, Weber DJ, Brown AN, Treston AM, Mariuzza RA. 2023. Structure-Based Design of Potent Iminosugar Inhibitors of Endoplasmic Reticulum α-Glucosidase I with Anti-SARS-CoV-2 Activity. Journal of Medicinal Chemistry 66:2744-2760.
116. Roussel HM. 1996. A randomized, double-blind active-controlled, dose-ranging study of safety and efficacy of chronically administered MDL 28,574A in the treatment of HIV-infected patients. NLM identifier: NCT00002151.
117. Watanabe S, Chan KW-K, Dow G, Ooi EE, Low JG, Vasudevan SG. 2016. Optimizing celgosivir therapy in mouse models of dengue virus infection of serotypes 1 and 2: The search for a window for potential therapeutic efficacy. Antiviral Research 127:10-19.
118. Artola M, Wu L, Ferraz MJ, Kuo C-L, Raich L, Breen IZ, Offen WA, Codée JDC, van der Marel GA, Rovira C, Aerts JMFG, Davies GJ, Overkleeft HS. 2017. 1,6-Cyclophellitol Cyclosulfates: A New Class of Irreversible Glycosidase Inhibitor. ACS Central Science 3:784-793.
119. Elstein D, Hollak C, Aerts JMFG, van Weely S, Maas M, Cox TM, Lachmann RH, Hrebicek M, Platt FM, Butters TD, Dwek RA, Zimran A. 2004. Sustained therapeutic effects of oral miglustat (Zavesca, N-butyldeoxynojirimycin, OGT 918) in type I Gaucher disease. J Inherit Metab Dis. 27:757-766.
120. Kiappes JL, Hill ML, Alonzi DS, Miller JL, Iwaki R, Sayce AC, Caputo AT, Kato A, Zitzmann N. 2018. ToP-DNJ, a Selective Inhibitor of Endoplasmic Reticulum α-Glucosidase II Exhibiting Antiflaviviral Activity. ACS Chem Biol 13:60-65.
121. Misumi I, Li Z, Sun L, Das A, Shiota T, Cullen J, Zhang Q, Whitmire JK, Lemon SM. 2021. Iminosugar Glucosidase Inhibitors Reduce Hepatic Inflammation in Hepatitis A Virus-Infected Ifnar1-/- Mice. Journal of Virology 95:10.1128/jvi.00058-21.
122. Durantel D. 2009. Celgosivir, an alpha-glucosidase I inhibitor for the potential treatment of HCV infection. Curr Opin Investig Drugs 10:860-70.
123. Stanley P MK, Lewis NE, et al. 2022. N-Glycans. In: Varki A, Cummings RD, Esko JD, et al, Essentials of Glycobiology 4th edition Cold Spring Harbor (NY): Cold Spring Harbor Laboratory Press; Chapter 9
124. Sobala Ł F, Fernandes PZ, Hakki Z, Thompson AJ, Howe JD, Hill M, Zitzmann N, Davies S, Stamataki Z, Butters TD, Alonzi DS, Williams SJ, Davies GJ. 2020. Structure of human endo-

α-1,2-mannosidase (MANEA), an antiviral host-glycosylation target. Proc Natl Acad Sci U S A 117:29595-29601.
125. Pizzorno A, Padey B, Julien T, Trouillet-Assant S, Traversier A, Errazuriz-Cerda E, Fouret J, Dubois J, Gaymard A, Lescure FX, Dulière V, Brun P, Constant S, Poissy J, Lina B, Yazdanpanah Y, Terrier O, Rosa-Calatrava M. 2020. Characterization and Treatment of SARS-CoV-2 in Nasal and Bronchial Human Airway Epithelia. Cell Rep Med 1:100059.
126. Corrò C, Novellasdemunt L, Li VSW. 2020. A brief history of organoids. 319:C151-C165.
127. Moysidou C-M, Barberio C, Owens RM. 2021. Advances in Engineering Human Tissue Models. Front Bioeng Biotechnol Jan 28;8:620962. PMID: 33585419; PMCID: PMC7877542.
128. Han Y, Duan X, Yang L, Nilsson-Payant BE, Wang P, Duan F, Tang X, Yaron TM, Zhang T, Uhl S, Bram Y, Richardson C, Zhu J, Zhao Z, Redmond D, Houghton S, Nguyen D-HT, Xu D, Wang X, Jessurun J, Borczuk A, Huang Y, Johnson JL, Liu Y, Xiang J, Wang H, Cantley LC, tenOever BR, Ho DD, Pan FC, Evans T, Chen HJ, Schwartz RE, Chen S. 2021. Identification of SARS-CoV-2 inhibitors using lung and colonic organoids. Nature 589:270-275.
129. Masmoudi F, Santos-Ferreira N, Pajkrt D, Wolthers KC, DeGroot J, Vlaming MLH, Rocha-Pereira J, Buti L. 2023. Evaluation of 3D Human Intestinal Organoids as a Platform for EV-A71 Antiviral Drug Discovery. Cells 12.
130. Huh D, Matthews BD, Mammoto A, Montoya-Zavala M, Hsin HY, Ingber DE. 2010. Reconstituting organ-level lung functions on a chip. Science 328:1662-8.
131. Ronaldson-Bouchard K, Vunjak-Novakovic G. 2018. Organs-on-a-Chip: A Fast Track for Engineered Human Tissues in Drug Development. Cell Stem Cell 22:310-324.
132. Thacker VV, Sharma K, Dhar N, Mancini GF, Sordet-Dessimoz J, McKinney JD. 2021. Rapid endotheliitis and vascular damage characterize SARS-CoV-2 infection in a human lung-on-chip model. EMBO Rep 22:e52744.
133. Hiemstra PS, Tetley TD, Janes SM. 2019. Airway and alveolar epithelial cells in culture. European Respiratory Journal 54:1900742.
134. Horváth L, Umehara Y, Jud C, Blank F, Petri-Fink A, Rothen-Rutishauser B. 2015. Engineering an in vitro air-blood barrier by 3D bioprinting. Scientific Reports 5:7974.
135. Barreto-Duran E, Szczepański A, Gałuszka-Bulaga A, Surmiak M, Siedlar M, Sanak M, Rajfur Z, Milewska A, Lenart M, Pyrć K. 2022. The interplay between the airway epithelium and tissue macrophages during the SARS-CoV-2 infection. Front Immunol
136. Rebendenne A, Roy P, Bonaventure B, Chaves Valadão AL, Desmarets L, Rouillé Y, Tauziet M, Arnaud-Arnould M, Giovanni D, Lee Y, DeWeirdt P, Hegde M, Garcia de Gracia F, McKellar J, Wencker M, Dubuisson J, Belouzard S, Moncorgé O, Doench JG, Goujon C. 2021. Bidirectional genome-wide CRISPR screens reveal host factors regulating SARS-CoV-2, MERS-CoV and seasonal coronaviruses. BioRxiv:2021.05.19.444823.
137. Wang M, Cao R, Zhang L, Yang X, Liu J, Xu M, Shi Z, Hu Z, Zhong W, Xiao G. 2020. Remdesivir and chloroquine effectively inhibit the recently emerged novel coronavirus (2019-nCoV) in vitro. Cell Research 30:269-271.
138. Hoffmann M, Mösbauer K, Hofmann-Winkler H, Kaul A, Kleine-Weber H, Krüger N, Gassen NC, Müller MA, Drosten C, Pöhlmann S. 2020. Chloroquine does not inhibit infection of human lung cells with SARS-CoV-2. Nature 585:588-590.
139. Li G, Hilgenfeld R, Whitley R, De Clercq E. 2023. Therapeutic strategies for COVID-19: progress and lessons learned. Nature Reviews Drug Discovery 22:449-475.
140. Golan Y, Campos JAS, Woolson R, Cilla D, Hanabergh R, Gonzales-Rojas Y, Lopez R, Finberg R, Balboni A. 2023. Favipiravir in Patients With Early Mild-to-moderate Coronavirus Disease 2019 (COVID-19): A Randomized Controlled Trial. Clin Infect Dis 76:e10-e17.
141. Dinesh Kumar N, Ter Ellen BM, Bouma EM, Troost B, van de Pol DPI, van der Ende-Metselaar HH, van Gosliga D, Apperloo L, Carpaij OA, van den Berge M, Nawijn MC, Stienstra Y, Rodenhuis-Zybert IA, Smit JM. 2022. Moxidectin and Ivermectin Inhibit SARS-CoV-2

Replication in Vero E6 Cells but Not in Human Primary Bronchial Epithelial Cells. Antimicrob Agents Chemother 66:e0154321.
142. Tomita Y, Takeda M, Matsuyama S. 2021. The Anti-Influenza Virus Drug Favipiravir Has Little Effect on Replication of SARS-CoV-2 in Cultured Cells. Antimicrob Agents Chemoter. 65:10.1128/aac.00020-21.
143. Touret F, Driouich JS, Cochin M, Petit PR, Gilles M, Barthélémy K, Moureau G, Mahon FX, Malvy D, Solas C, de Lamballerie X, Nougairède A. 2021. Preclinical evaluation of Imatinib does not support its use as an antiviral drug against SARS-CoV-2. Antiviral Res 193:105137.
144. Han JJ. 2023. FDA Modernization Act 2.0 allows for alternatives to animal testing. Artif Organs. 47:449-450.
145. Owens RM. 2023. Advanced tissue engineering for in vitro drug safety testing. MRS Communications 13:685-694.
146. Brown DG, Wobst HJ. 2021. A Decade of FDA-Approved Drugs (2010–2019): Trends and Future Directions. Journal of Medicinal Chemistry 64:2312-2338.
147. Tiwari PC, Pal R, Chaudhary MJ, Nath R. 2023. Artificial intelligence revolutionizing drug development: Exploring opportunities and challenges. Drug Dev Res 84(8):1652-1663.
148. Vijayan RSK, Kihlberg J, Cross JB, Poongavanam V. 2022. Enhancing preclinical drug discovery with artificial intelligence. Drug Discovery Today 27:967-984.
149. Innovative Medicines Initiative EH, EFPIA 2024. MELLODY. https://wwwimieuropaeu/projects-results/project-factsheets/melloddy.
150. Minnich AJ, McLoughlin K, Tse M, Deng J, Weber A, Murad N, Madej BD, Ramsundar B, Rush T, Calad-Thomson S, Brase J, Allen JE. 2020. AMPL: A Data-Driven Modeling Pipeline for Drug Discovery. Journal of Chemical Information and Modeling 60:1955-1968.
151. Hoffman RL, Kania RS, Brothers MA, Davies JF, Ferre RA, Gajiwala KS, He M, Hogan RJ, Kozminski K, Li LY, Lockner JW, Lou J, Marra MT, Mitchell LJ, Jr., Murray BW, Nieman JA, Noell S, Planken SP, Rowe T, Ryan K, Smith GJ, 3rd, Solowiej JE, Steppan CM, Taggart B. 2020. Discovery of Ketone-Based Covalent Inhibitors of Coronavirus 3CL Proteases for the Potential Therapeutic Treatment of COVID-19. J Med Chem 63:12725-12747.
152. Durojaye OA, Okoro NO, Odiba AS, Nwanguma BC. 2023. MasitinibL shows promise as a drug-like analog of masitinib that elicits comparable SARS-Cov-2 3CLpro inhibition with low kinase preference. Scientific Reports 13:6972.
153. Mukae H, Yotsuyanagi H, Ohmagari N, Doi Y, Sakaguchi H, Sonoyama T, Ichihashi G, Sanaki T, Baba K, Tsuge Y, Uehara T. 2023. Efficacy and Safety of Ensitrelvir in Patients With Mild-to-Moderate Coronavirus Disease 2019: The Phase 2b Part of a Randomized, Placebo-Controlled, Phase 2/3 Study. Clin Infect Dis 76:1403-1411.
154. Cho J, Shin Y, Yang JS, Kim JW, Kim KC, Lee JY. 2023. Evaluation of antiviral drugs against newly emerged SARS-CoV-2 Omicron subvariants. Antiviral Res 214:105609.
155. Duan Y, Zhou H, Liu X, Iketani S, Lin M, Zhang X, Bian Q, Wang H, Sun H, Hong SJ, Culbertson B, Mohri H, Luck MI, Zhu Y, Liu X, Lu Y, Yang X, Yang K, Sabo Y, Chavez A, Goff SP, Rao Z, Ho DD, Yang H. 2023. Molecular mechanisms of SARS-CoV-2 resistance to nirmatrelvir. Nature 622:376-382.
156. Kiso M, Yamayoshi S, Iida S, Furusawa Y, Hirata Y, Uraki R, Imai M, Suzuki T, Kawaoka Y. 2023. In vitro and in vivo characterization of SARS-CoV-2 resistance to ensitrelvir. Nat Commun 14:4231.
157. Hogan JI, Duerr R, Dimartino D, Marier C, Hochman SE, Mehta S, Wang G, Heguy A. 2023. Remdesivir Resistance in Transplant Recipients With Persistent Coronavirus Disease 2019. Clin Infect Dis 76:342-345.
158. Gandhi S, Klein J, Robertson AJ, Peña-Hernández MA, Lin MJ, Roychoudhury P, Lu P, Fournier J, Ferguson D, Mohamed Bakhash SAK, Catherine Muenker M, Srivathsan A, Wunder EA, Jr., Kerantzas N, Wang W, Lindenbach B, Pyle A, Wilen CB, Ogbuagu O, Greninger AL, Iwasaki A,

Schulz WL, Ko AI. 2022. De novo emergence of a remdesivir resistance mutation during treatment of persistent SARS-CoV-2 infection in an immunocompromised patient: a case report. Nat Commun 13:1547.

159. Akinbolade S, Coughlan D, Fairbairn R, McConkey G, Powell H, Ogunbayo D, Craig D. 2022. Combination therapies for COVID-19: An overview of the clinical trials landscape. Br J Clin Pharmacol 88:1590-1597.
160. Kalil AC, Patterson TF, Mehta AK, Tomashek KM, Wolfe CR, Ghazaryan V, Marconi VC, Ruiz-Palacios GM, Hsieh L, Kline S, Tapson V, Iovine NM, Jain MK, Sweeney DA, El Sahly HM, Branche AR, Regalado Pineda J, Lye DC, Sandkovsky U, Luetkemeyer AF, Cohen SH, Finberg RW, Jackson PEH, Taiwo B, Paules CI, Arguinchona H, Erdmann N, Ahuja N, Frank M, Oh MD, Kim ES, Tan SY, Mularski RA, Nielsen H, Ponce PO, Taylor BS, Larson L, Rouphael NG, Saklawi Y, Cantos VD, Ko ER, Engemann JJ, Amin AN, Watanabe M, Billings J, Elie MC, Davey RT, Burgess TH, Ferreira J, Green M, et al. 2021. Baricitinib plus Remdesivir for Hospitalized Adults with Covid-19. N Engl J Med 384:795-807.
161. Mbikay M, Chrétien M. 2022. Isoquercetin as an Anti-Covid-19 Medication: A Potential to Realize. Front Pharmcacol.
162. Yong SJ. 2021. Long COVID or post-COVID-19 syndrome: putative pathophysiology, risk factors, and treatments. Infect Dis (Lond) 53:737-754.
163. Umemura Y, Mitsuyama Y, Minami K, Nishida T, Watanabe A, Okada N, Yamakawa K, Nochioka K, Fujimi S. 2021. Efficacy and safety of nintedanib for pulmonary fibrosis in severe pneumonia induced by COVID-19: An interventional study. Int J Infect Dis 108:454-460.
164. Săndulescu O, Apostolescu CG, Preoțescu LL, Streinu-Cercel A, Săndulescu M. 2023. Therapeutic developments for SARS-CoV-2 infection—Molecular mechanisms of action of antivirals and strategies for mitigating resistance in emerging variants in clinical practice. Front Microbiol.
165. Taylor PC, Adams AC, Hufford MM, de la Torre I, Winthrop K, Gottlieb RL. 2021. Neutralizing monoclonal antibodies for treatment of COVID-19. Nature Reviews Immunology 21:382-393.
166. Plasse TF, Fathi R, Fehrmann C, McComsey GA. Upamostat: a serine protease inhibitor for antiviral, gastrointestinal, and anticancer indications. Expert Opinion on Investigational Drugs
167. Bian H, Chen L, Zheng Z-H, Sun X-X, Geng J-J, Chen R, Wang K, Yang X, Chen S-R, Chen S-Y, Xie R-H, Zhang K, Miao J-L, Jia J-F, Tang H, Liu S-S, Shi H-W, Yang Y, Chen X-C, Malhotra V, Nasir N, Khanum I, Mahmood F, Hamid S, Stadnik CMB, Itinose K, de Oliveira CCC, Dusilek C, Rivabem L, Cavalcante AJW, Lopes SS, Saporito WF, Fucci FJC, Simon-Campos JA, Wang L, Liu L-N, Wang Q-Y, Wei D, Zhang Z, Chen Z-N, Zhu P. 2023. Meplazumab in hospitalized adults with severe COVID-19 (DEFLECT): a multicenter, seamless phase 2/3, randomized, third-party double-blind clinical trial. Signal Transduction and Targeted Therapy 8:46.
168. Mellott DM, Tseng C-T, Drelich A, Fajtová P, Chenna BC, Kostomiris DH, Hsu J, Zhu J, Taylor ZW, Kocurek KI, Tat V, Katzfuss A, Li L, Giardini MA, Skinner D, Hirata K, Yoon MC, Beck S, Carlin AF, Clark AE, Beretta L, Maneval D, Hook V, Frueh F, Hurst BL, Wang H, Raushel FM, O'Donoghue AJ, de Siqueira-Neto JL, Meek TD, McKerrow JH. 2021. A Clinical-Stage Cysteine Protease Inhibitor blocks SARS-CoV-2 Infection of Human and Monkey Cells. ACS Chemical Biology 16:642-650.
169. Sonawane KD, Barale SS, Dhanavade MJ, Waghmare SR, Nadaf NH, Kamble SA, Mohammed AA, Makandar AM, Fandilolu PM, Dound AS, Naik NM, More VB. 2021. Structural insights and inhibition mechanism of TMPRSS2 by experimentally known inhibitors Camostat mesylate, Nafamostat and Bromhexine hydrochloride to control SARS-coronavirus-2: A molecular modeling approach. Inform Med Unlocked 24:100597.

170. White KM, Rosales R, Yildiz S, Kehrer T, Miorin L, Moreno E, Jangra S, Uccellini MB, Rathnasinghe R, Coughlan L, Martinez-Romero C, Batra J, Rojc A, Bouhaddou M, Fabius JM, Obernier K, Dejosez M, Guillén MJ, Losada A, Avilés P, Schotsaert M, Zwaka T, Vignuzzi M, Shokat KM, Krogan NJ, García-Sastre A. 2021. Plitidepsin has potent preclinical efficacy against SARS-CoV-2 by targeting the host protein eEF1A. Science 371:926-931.

171. Kuriakose J, Montezano AC, Touyz RM. 2021. ACE2/Ang-(1-7)/Mas1 axis and the vascular system: vasoprotection to COVID-19-associated vascular disease. Clin Sci (Lond) 135:387-407.

172. Wigerblad G, Warner SA, Ramos-Benitez MJ, Kardava L, Tian X, Miao R, Reger R, Chakraborty M, Wong S, Kanthi Y, Suffredini AF, Dell'Orso S, Brooks S, King C, Shlobin O, Nathan SD, Cohen J, Moir S, Childs RW, Kaplan MJ, Chertow DS, Strich JR. 2023. Spleen tyrosine kinase inhibition restores myeloid homeostasis in COVID-19. Sci Adv 9:eade8272.

173. Youssef M, De Sanctis JB, Shah J, Dumut DC, Hajduch M, Petrof BJ, Radzioch D. 2020. Age-Dependent Progression in Lung Pathophysiology can be Prevented by Restoring Fatty Acid and Ceramide Imbalance in Cystic Fibrosis. Lung 198:459-469.

174. Mulgaonkar N, Wang H, Mallawarachchi S, Růžek D, Martina B, Fernando S. 2023. In silico and in vitro evaluation of imatinib as an inhibitor for SARS-CoV-2. Journal of Biomolecular Structure and Dynamics 41:3052-3061.

Appendix

Nederlandse Samenvatting

English Summary

List of Publications

Curriculum Vitae

Nederlandse Samenvatting

Van de zeven coronavirussen die mensen infecteren, zijn er vier gewone verkoudheidsvirussen die slechts milde symptomen veroorzaken bij gezonde individuen, terwijl SARS-CoV, MERS-CoV en SARS-CoV-2 ernstige ziekte en dodelijke longontstekingen kunnen veroorzaken. De uitbraak van SARS-CoV-2 in 2019 en de snelle wereldwijde verspreiding ervan hebben de noodzaak van een snelle reactie op nieuw opkomende virussen en de beschikbaarheid van effectieve therapieën duidelijk gemaakt. Hoewel vaccins tegen SARS-CoV-2 met ongekende snelheid zijn ontwikkeld, zouden vroeg in de pandemie patiënten hebben geprofiteerd van de beschikbaarheid antivirale middelen. Het ademhalingsstelsel is het eerste toegangspunt voor coronavirussen. Hier worden epitheelcellen geïnfecteerd, welke tevens de eerste verdedigingsbarrière vormen. Als geavanceerd experimenteel model zijn primaire humane luchtwegepitheelcellen die gekweekt en gedifferentieerd worden aan de lucht-vloeistofinterface (HAE-ALI) beter in staat het menselijke longepitheel na te bootsen dan in monolaag gekweekte cellijnen.
In dit proefschrift worden vier onderzoeksprojecten beschreven die zijn uitgevoerd tijdens het promotietraject en zich voornamelijk richtten op SARS-CoV-2. **Hoofdstuk 1** geeft een inleiding op het algemene onderzoeksthema van de coronavirusbiologie en de ontdekking van antivirale geneesmiddelen, en het gebruik van HAE-ALI om beide te bestuderen. **Hoofdstuk 2** beschrijft de karakterisering van SARS-CoV-2-infectie in HAE-ALI. Veranderingen in de cellulaire samenstelling, veroorzaakt door de kweektijd of medicamenteuze behandeling, beïnvloedden de virusreplicatie, en dit correleerde met de aanwezigheid van de belangrijkste vatbare cellen, nl. trilhaarcellen en slijmcellen, evenals de expressie van eiwitten die verantwoordelijk zijn voor virus infectie. Verder werd het belang van de samenstelling van het epitheel in de kweken vastgesteld, waarbij bleek dat slijmcellen waarschijnlijk een ondersteunende rol spelen bij infectie. De bevindingen dragen bij aan ons begrip van de verschillen in gevoeligheid voor SARS-CoV-2-infectie tussen individuen en het effect van de anatomische locatie in het ademhalingsstelsel en chronische longziekten die het epitheel aantasten op de infectie. **Hoofdstuk 3** beschrijft een vergelijkende studie waarin SARS-CoV, MERS-CoV en SARS-CoV-2, vergeleken worden met twee gewone verkoudheids-coronavirussen. In het HAE-ALI-celkweekmodel werden verschillen in de epitheliale transcriptionele respons tijdens de coronavirusinfectie vastgesteld. RNA-sequentiegegevens wezen op een beperkte expressie van interferongenen bij infecties met SARS-CoV, MERS-CoV en SARS-CoV-2, terwijl de gewone verkoudheids-coronavirussen een sterkere interferon respons veroorzaakten. Uniek voor de SARS-CoV-2-infectie was het ontbreken van de expressie van een reeks vroege genen (early immediate genes) die tot expressie komen als reactie op stressoren zoals infectie. In

vervolgstudies gebaseerd op deze bevinding en gericht op 1 van de betreffende genen, NR4A1, werd een remmer geïdentificeerd die de replicatie van SARS-CoV-2 en MERS-CoV blokkeert. **Hoofdstukken 4** en **5** beschrijven twee antivirale middelen die de replicatie van SARS-CoV-2 en andere coronavirussen efficiënt blokkeren. De eerste, R-Propranolol, maakt deel uit van een geneesmiddel dat is goedgekeurd voor de behandeling van hemangiomen (goedaardige vasculaire tumoren), naast verschillende andere medische aandoeningen zoals hart- en vaatziekten. R-propranolol bleek een pro-angiogene factor te verminderen, die recentelijk in verband is gebracht met een verhoogd aantal ernstige longpathologieën bij COVID-19. Daarom zou dit medicijn interessant kunnen zijn om verder te onderzoeken als gastheer-gerichte therapie om vasculaire schade bij COVID-19 te verminderen, welke wordt veroorzaakt door endotheliale disfunctie en pathologische angiogenese. Bovendien werd een krachtig virusremmend effect van R-propranolol waargenomen tegen SARS-CoV-2 en andere coronavirussen. Hierdoor heeft het medicijn een interessante tweeledige activiteit: remming van de virusreplicatie en tegengaan van gastheer processen die pathologische angiogenese veroorzaken. **Hoofdstuk 5** beschrijft een klasse van gastheergerichte antivirale middelen, glucosidaseremmers, die alfa-glucosidase enzymen remmen die zich in het endoplasmatisch reticulum (ER) bevinden en belangrijk zijn voor de eiwitvouwing en kwaliteitscontrole daarop. Veel virussen, waaronder coronavirussen, maken gebruik van de eiwitkwaliteitscontrole van de gastheer in het ER voor de productie van hun glycoproteïnen (eiwitten met suikergroepen). Voor SARS-CoV-2 is met name het spike-eiwit, dat cruciaal is voor de hechting van het virus en de infectie van de gastheercel, sterk geglycosyleerd en afhankelijk van de juiste verwerking in het ER en het Golgi-apparaat. Verschillende verbindingen werden getest, behorend tot twee klassen, de iminosuikers en cyclitolen. Hoewel iminosuikers al decennialang worden bestudeerd als mogelijke antivirale middelen, werd 1,6-epi-cyclophellitol cyclosulfaat geïdentificeerd als veelbelovende kandidaat van een nieuwe klasse glucosidaseremmers, vanwege zijn hoge specificiteit voor ER alfa-glucosidase II en krachtige antivirale werkzaamheid. Remming van ER alfa-glucosidasen leidde tot een vermindering van de productie/maturatie van spike-eiwit en bijgevolg tot een verminderde productie van infectieuze virusdeeltjes. Naast SARS-CoV-2 blokkeert 1,6-epi-cyclophellitol cyclosulfaat ook de productie van infectieuze SARS-CoV- en in mindere mate MERS-CoV deeltjes, waardoor deze klasse van verbindingen veelbelovende breedspectrum antivirale moleculen zijn. In het laatste hoofdstuk worden de belangrijkste bevindingen van de onderzoeksprojecten besproken, mede in de context van recent gepubliceerde studies. Bovendien wordt de huidige stand van zaken van de gastheergerichte antivirale therapie voor SARS-CoV-2 besproken en worden de voordelen van het gebruik van de meest relevante en geavanceerde celkweekmodellen bij de ontwikkeling van antivirale geneesmiddelen besproken.

English Summary

Coronaviruses comprise seven human viruses, some of them the common cold viruses, only causing mild symptoms in healthy individuals, while SARS-CoV, MERS-CoV, and SARS-CoV-2 can potentially cause severe disease and deadly pneumonia. The outbreak of SARS-CoV-2 in 2019 and its rapid worldwide spread has made apparent the need for a fast response to newly emerging viruses and to have effective therapies available. Although vaccines against SARS-CoV-2 were developed at an unprecedented speed, early patients would have benefitted from antiviral drugs. The respiratory tract is the first entry point for coronaviruses, where epithelial cells are infected and also represent the first barrier of defense. Primary human airway epithelial cells that are cultured and differentiated at the air-liquid interface (HAE-ALI) represent an advanced cell culture model recapitulating the human lung epithelium better than mono-cell cultures.

In this thesis, four research projects conducted during the PhD track, are described and discussed, which focussed mainly on SARS-CoV-2. **Chapter 1** gives an introduction to the overall research topic of coronavirus biology and antiviral drug discovery, and the use of HAE-ALI to study both. **Chapter 2** describes the characterization of SARS-CoV-2 infection in HAE-ALI. Changes in the cellular composition, caused by culture time or drug treatment, impacted virus replication, and this correlated with the presence of the main susceptible cells, ciliated cells and goblet cells, as well as expression of virus cell-entry factors. Furthermore, the importance of having a diverse epithelium in the cultures was identified, where likely goblet cells play a supportive role in infection. The findings contribute to the understanding of the variable susceptibility to SARS-CoV-2 infection between individuals and across anatomical locations in the respiratory tract, and possibly in chronic lung diseases affecting the epithelium. **Chapter 3** then aimed to conduct a comparative study between SARS-CoV, MERS-CoV, and SARS-CoV-2, and two common cold coronaviruses. We employed the HAE-ALI cell culture model to decipher differences in the epithelial transcriptional response upon coronavirus infection. RNA sequencing data showed limited expression of interferon genes in infections with SARS-CoV, MERS-CoV, and SARS-CoV-2, as opposed to the common cold coronaviruses, which corroborated previous studies showing suppression of interferon responses by the these three coronaviruses. Furthermore, SARS-CoV-2 infection uniquely lacked the expression of a set of immediate early genes, which are expressed in response to stressors like infection. By utilizing the findings about one of these genes, NR4A1, an inhibitor was identified that blocks SARS-CoV-2 and MERS-CoV replication. **Chapters 4 and 5** describe two antiviral drugs that efficiently block the replication of SARS-CoV-2 and other coronaviruses. The first, R-Propranolol, is part of a drug that is approved for the treatment of hemangioma (benign vascular tumor), besides various

medical conditions like cardiovascular diseases. R-Propranolol was shown to reduce a pro-angiogenic factor, which was recently reported to be associated with an increased rate of severe lung pathology in COVID-19. Therefore, this drug could be an interesting candidate to investigate further as host-directed therapy to reduce vascular damage in COVID-19, caused by endothelial dysfunction and pathological angiogenesis. Additionally, a potent antiviral effect of R-Propranolol against SARS-CoV-2 and other coronaviruses was observed, which makes the drug an interesting antiviral with two potential angles of activity. **Chapter 5** describes a class of host-directed antivirals, glucosidase inhibitors, which inhibit endoplasmic reticulum (ER) resident alpha-glucosidases, important for protein folding in the ER and quality control. Many viruses, including coronaviruses, use the host's ER protein quality control machinery for their glycoproteins. For SARS-CoV-2, especially the spike protein, which is crucial for virus attachment and entry into the host cell, is heavily glycosylated and dependent on processing in the ER and Golgi. Several compounds were tested, belonging to two classes, iminosugars and cyclitols. While iminosugars have been studied for decades as potential antiviral drugs, we identified 1,6-*epi*-cyclophellitol cyclosulfate, a candidate of a new class of glucosidase inhibitors, as superior due to its high specificity for ER alpha-glucosidase II and potent antiviral efficacy. Inhibition of ER alpha-glucosidases led to a reduction in spike protein generation and subsequently to a reduced production of infectious virus particles. In addition to SARS-CoV-2, 1,6-*epi*-cyclophellitol cyclosulfate also blocks the production of SARS-CoV and MERS-CoV progeny, rendering this class of compounds promising broad-spectrum antivirals. In the final chapter, the main findings of the research projects are discussed in the context of recently published studies. Furthermore, the current landscape of SARS-CoV-2 host-directed antiviral therapy and the benefits of using the most relevant cell culture models in antiviral drug discovery are discussed.

List of Publications (in chronological order)

- Cyclic sulphate inhibitor of ER α-glucosidase inhibits replication of SARS-CoV-2 and other coronaviruses
  M. Thaler, T. P. Ofman, K. Kok, J. J.A. Heming, El. Moran, A. A. Leijs, A. M. C. H. van den Nieuwendijk, R. J. B. H. N. van den Berg, G. Ruijgrok, Z. Armstrong, C. Salgado-Benvindo, D. K. Ninaber, E. J. Snijder, C. A. A. van Boeckel, M. Artola, G. J. Davies, H. S. Overkleeft#, M. J. van Hemert# *Under review at ACS Central Science*

- SARS-CoV-2-infected human airway epithelial cell cultures uniquely lack interferon and immediate early gene responses caused by other coronaviruses
  M. Thaler*, Y. Wang*, C. Salgado-Benvindo, N. Ly, A. A. Leijs, D. K. Ninaber, P. Hansbro, F. Boedijono, M. J. van Hemert, P. S. Hiemstra, A. M. van der Does#, A. Faiz#, Clinical and Translational Immunology 2024 Apr 15;13(4):e1503. doi: 10.1002/cti2.1503.

- Honokiol Inhibits SARS-CoV-2 Replication in Cell Culture at a Post-Entry Step
  C. Salgado-Benvindo, A. Leijs, **M. Thaler**, A. Tas, J. L. Arbiser, E. J. Snijder, M. J. van Hemert, Microbiology Spectrum. 2023 May 4; Vol. 11, No.3. doi:10.1128/spectrum.03273-22

- Impact of changes in human airway epithelial cellular composition and differentiation on SARS-CoV-2 infection biology
  M. Thaler*, Y. Wang*, D. K. Ninaber, A. M. van der Does, N. S. Ogando, H. Beckert, C. Taube, C. Salgado-Benvindo, E. J. Snijder, P. J. Bredenbeek, P. S. Hiemstra#, M. J. van Hemert#, Journal of Innate Immunity. 2023 Mar 25;15(1):562-580. doi: 10.1159/000530374.

- R-Propranolol Has Broad-Spectrum Anti-Coronavirus Activity and Suppresses Factors Involved in Pathogenic Angiogenesis
  M. Thaler, C. Salgado-Benvindo, A. Leijs, A. Tas, D. K. Ninaber, J. L. Arbiser, E. J. Snijder, M. J. van Hemert#, International Journal of Molecular Sciences. 2023 Feb 27;24(5):4588. doi: 10.3390/ijms24054588.

- SARS-CoV-2-specific CD4+ and CD8+ T cell responses can originate from cross-reactive CMV-specific T cells
  C.R. Pothast, R.C. Dijkland, **M. Thaler**, R.S. Hagedoorn, M.G.D. Kester, A.K. Wouters, P.S. Hiemstra, M.J. van Hemert, S. Gras, J.H.F. Falkenburg, M.H.M. Heemskerk, Elife. 2022 Nov 21;11:e82050. doi: 10.7554/eLife.82050.

- Suramin Inhibits SARS-CoV-2 Infection in Cell Culture by Interfering with Early Steps of the Replication Cycle.
  C. Salgado-Benvindo *, **M. Thaler***, A. Tas, N.S. Ogando, P.J. Bredenbeek, D.K. Ninaber, Y. Wang, P.S. Hiemstra, E.J. Snijder, M.J. van Hemert. Antimicrob Agents Chemother. 2020 Jul 22;64(8):e00900-20. doi:10.1128/AAC.00900-20.

- A piRNA-lncRNA regulatory network initiates responder and trailer piRNA formation during mosquito embryonic development.
  V. Betting, J. Joosten, R. Halbach, **M. Thaler**, P. Miesen, R.P. van Rij. RNA. 2021 Oct;27(10):1155-1172. doi: 10.1261/rna.078876.121. Epub 2021 Jul 1.

- Impact of flavivirus vaccine-induced immunity on primary Zika virus antibody response in humans
  S. Malafa, I. Medits, J.H. Aberle, S.W. Aberle, D. Haslwanter, G. Tsouchnikas, S. Wölfel, K.L. Huber, E. Percivalle, P. Cherpillod, **M. Thaler**, L. Roßbacher, M. Kundi, F.X. Heinz, K. Stiasny, PLoS Negl Trop Dis. 2020 Feb 4;14(2):e0008034. doi: 10.1371/journal.pntd.0008034.

- Effect of previous heterologous flavivirus vaccinations on human antibody responses in tick-borne encephalitis and dengue virus infections.
  L. Roßbacher, S. Malafa, K. Huber, **M. Thaler**, S. Aberle, J. Aberle, F.X. Heinz, K. Stiasny, Journal of medical Virology, 2023 Nov;95(11):e29245. doi: 10.1002/jmv.29245.

** and # contributed equally*

Curriculum Vitae

Melissa Thaler was born on 13 June 1994 in Klagenfurt am Wörthersee, Austria. In 2012 she moved to Vienna to study Biology at the University of Vienna. In 2015 she obtained her Bachelor degree in Biology, with specialization in Ecology. She continued with her Master's study in Molecular Microbiology, Microbial Ecology and Immunobiology at the University of Vienna, with specialization in Molecular Microbiology. In July 2016 she took part in the Biotechnology Summerschool at the University of Kent, Canterbury, the United Kingdom. In 2017 she performed an Erasmus Internship with Prof. Dr. Ronald van Rij, under the supervision of Dr. Rebecca Halbach, at the Radboud Institute for Molecular Life Sciences in Nijmegen, the Netherlands. From August 2017 until December 2018 she worked with Prof. Dr. Karin Stiasny at the Center for Virology at the Medical University of Vienna, where she conducted research for her Master thesis entitled "Generation and characterization of Zika and dengue virus antigens". In June 2019 she started her PhD research at the Medical Microbiology Department, Leiden University Medical Center (LUMC), the Netherlands, under the supervision of Dr. Martijn J. van Hemert and Prof. Dr. Eric J. Snijder. Initially, her PhD project was aimed towards accelerating academic drug development against emerging arboviruses. With the beginning of the SARS-CoV-2 pandemic, she switched projects to study drug development against coronaviruses. She also collaborated closely with then PhD candidate Ying Wang, Prof. Dr. Pieter S. Hiemstra and Dr. Anne M. van der Does from the PulmoScience Laboratory of the Department of Pulmonology, LUMC, on a number of projects.